


Fall 12-2014

## Molecular Probes for the Detection of Zn<sup>2+</sup> and Fe<sup>3+</sup> Ions

Erendra Manandhar  
*University of Southern Mississippi*

Follow this and additional works at: <https://aquila.usm.edu/dissertations>

 Part of the [Inorganic Chemistry Commons](#), [Organic Chemistry Commons](#), and the [Other Chemistry Commons](#)

---

### Recommended Citation

Manandhar, Erendra, "Molecular Probes for the Detection of Zn<sup>2+</sup> and Fe<sup>3+</sup> Ions" (2014). *Dissertations*. 43.  
<https://aquila.usm.edu/dissertations/43>

This Dissertation is brought to you for free and open access by The Aquila Digital Community. It has been accepted for inclusion in Dissertations by an authorized administrator of The Aquila Digital Community. For more information, please contact [Joshua.Cromwell@usm.edu](mailto:Joshua.Cromwell@usm.edu).

The University of Southern Mississippi

MOLECULAR PROBES FOR THE DETECTION OF Zn<sup>2+</sup> AND Fe<sup>3+</sup> IONS

by

Erendra Manandhar

Abstract of a Dissertation  
Submitted to the Graduate School  
of The University of Southern Mississippi  
in Partial Fulfillment of the Requirements  
for the Degree of Doctor of Philosophy

December 2014

## ABSTRACT

### MOLECULAR PROBES FOR THE DETECTION OF Zn<sup>2+</sup> AND Fe<sup>3+</sup> IONS

by Erendra Manandhar

December 2014

A number of molecular probes have been designed and synthesized for the detection of Zn<sup>2+</sup> and Fe<sup>3+</sup> ions. Two types of functional groups have been incorporated into the molecular scaffolds to utilize different fluorescent mechanisms. The first class of receptors contains a pyrene moiety. These molecular probes use the excimer mechanism for the detection of Zn<sup>2+</sup> ion. The probes work well in an organic solvent with a detection limit of 20 nM (one ppb). Alternatives are made to make them water soluble, but this proved to be difficult. An interesting ion-induced self-assembly system will also be discussed.

The second class of molecules is based on the “Off-On” mechanism. The rhodamine dyes are used in these molecular probes. This system is found to be selective for Fe<sup>3+</sup> ions in a mixed organic/aqueous system. A protocol has also been developed to distinguish between Fe<sup>3+</sup> and Al<sup>3+</sup> ions. One of the rhodamine dyes has also been shown to detect Fe<sup>3+</sup> ion in bacteria.

COPYRIGHT BY  
ERENDRA MANANDHAR  
2014

The University of Southern Mississippi

MOLECULAR PROBES FOR THE DETECTION OF  $Zn^{2+}$  AND  $Fe^{3+}$  IONS

by

Erendra Manandhar

A Dissertation  
Submitted to the Graduate School  
of The University of Southern Mississippi  
in Partial Fulfillment of the Requirements  
for the Degree of Doctor of Philosophy

Approved:

Dr. Karl J. Wallace

Committee Chair

Dr. Douglas Masterson

Dr. Wujian Miao

Dr. Vijay Rangachari

Dr. Matthew Donahue

Dr. Karen Coats

Dean of the Graduate School

December 2014

## ACKNOWLEDGMENTS

I would like to express my sincere gratitude to my supervisor, Dr. Karl J. Wallace, for his continuous guidance, support, and encouragement during the course of my Ph.D. study as well as his supramolecular knowledge and experience that I have gained from working underneath him. I have been fortunate to have him as an advisor who gave me the freedom to explore on my own. I could not have imagined having a better advisor and mentor for my Ph.D. study. I would also like to extend thanks to my committee members: Drs. Masterson, Miao, Rangachari, Donohue, and Alvin A. Holder for their guidance, insightful comments, and suggestions. I would like to thank our collaborators: Drs. Cragg from the School of Pharmacy and Biomolecular Science, University of Brighton, UK for helpful molecular modeling calculations, Elsari from the Department of Biological Science, The University of Southern Mississippi for cell imaging experiment, and Frank R. Fronczek from the Department of Chemistry, Louisiana State University for getting crystal structures. I would like to thank the Department of Chemistry and Biochemistry at The University of Southern Mississippi and the National Science Foundation for financial support for my Ph.D. studies.

I would also like to thank my group members: Dr. Jones, J. Hugh Broome, Aaron Davis, and Jason Clements and my friends: Suman Parajuli, Sajan Lal Shyaula, Ajaya Ram Shrestha, Mahesh Bhatt, Lekth Nath Gautam, Suman Maharjan, Sanjay Shrestha, and Gyan Sundar Sahukhal.

Lastly, I would like to thank my family members (my mom and sister), especially my wife, Sanjeebani Manandhar, and two daughters, Esha and Eva, for their endless patience, love, support, and understanding during my graduate studies.

## TABLE OF CONTENTS

ABSTRACT .....	ii
ACKNOWLEDGMENTS .....	iii
LIST OF TABLES .....	vii
LIST OF ILLUSTRATIONS .....	ix
LIST OF SCHEMES.....	xx
LIST OF ABBREVIATIONS.....	xxiii
CHAPTER	
I. GENERAL INRODUCTION.....	1
Significance of target analytes	
Current techniques for the detection of Zn <sup>2+</sup> and Fe <sup>3+</sup> ions	
Optical spectroscopy	
Chemosensors	
Fluorescent mechanism for ion sensing	
Summary	
Hypothesis	
II. PYRENE MOLECULAR TWEEZERS FOR DETECTION OF Zn <sup>2+</sup> ION .....	40
Introduction	
Synthesis of molecular probes 2.6a and 2.6b	
Job's plot studies of molecular probes 2.6a and 2.6b	
Optical studies of the molecular probes 2.6a and 2.6b	
1D and 2D NMR studies of molecular probe 2.6b	
Molecular modeling's studies of molecular probes 2.6a and 2.6b	
IR studies of molecular probe 2.6b	
Sensitivity of molecular probes 2.6a and 2.6b	
Reversibility of molecular probe 2.6b	
Protocol to determine concentration of Zn <sup>2+</sup> ion in aqueous sample	
Summary	
Experimental	
General procedures for the synthesis	
III. SIMULTANEOUS CATION AND ANION INDUCED SELF-ASSEMBLY.....	82

Introduction  
 Synthesis of molecular probe 3.6  
 Job's plot study of molecular probe 3.6  
 X-ray crystallographic study of molecular probe 3.6  
 Optical studies of the molecular probe 3.6  
<sup>1</sup>H NMR study of molecular probe 3.6  
 2D NMR studies of molecular probe 3.6  
 Molecular modeling's studies of molecular probe 3.6  
 Friedal Craft acylation protocol  
 Summary  
 Experimental  
 General procedures for the synthesis

IV. SUGAR FUNCTIONALIZED MOLECULAR PROBE FOR Fe<sup>3+</sup> ION.....123

Introduction  
 Synthesis of molecular probe 4.7  
 Job's plot study of molecular probe 4.7  
 Optical studies of the molecular probe 4.7  
<sup>1</sup>H NMR study of molecular probe 4.7  
 Electrogenated chemiluminescence (ECl) studies of molecular probe 4.7  
 Summary  
 Experimental  
 General procedure for ECl experiment to determine binding stoichiometry  
 General procedure for the synthesis

V. RHODAMINE BASED MOLECULAR PROBES FOR DETECTION OF Fe<sup>3+</sup> AND Al<sup>3+</sup> IONS .....153

Introduction  
 Synthesis of molecular probes 5.11, 5.12, and 5.13  
 X-ray crystallographic study of molecular probes 5.11 and 5.12  
 Job's plot study of molecular probes 5.12 and 5.13  
 pH study on the molecular probes 5.12 and 5.13  
 Optical studies of the molecular probe 5.11, 5.12, and 5.13  
<sup>1</sup>H NMR studies of molecular probes 5.11, 5.12, and 5.13  
<sup>13</sup>C NMR studies of molecular probes 5.11 and 5.12  
 2D NMR studies of molecular probes 5.11 and 5.12  
 IR study of molecular probe 5.12  
 Reversibility of molecular probes 5.11, 5.12, and 5.13  
 Detection limit of molecular probes 5.12 and 5.13  
 Protocols to distinguish Fe<sup>3+</sup> and Al<sup>3+</sup> ions  
 Protocol to distinguish Fe<sup>3+</sup> and Al<sup>3+</sup> ions using ferrozine  
 Protocol to distinguish Fe<sup>3+</sup> and Al<sup>3+</sup> ions using 1, 10 phenanthroline



Cell imaging studies of molecular probe 5.12 in Vero cells  
 Cell imaging studies of molecular probe 5.12 in bacterial cells  
 Summary  
 Experimental  
 General procedure for the synthesis  
 Protocol for bacterial cell imaging  
 Protocol for Vero cell line imaging

VI. RHODAMINE BASED TWEEZERS FOR DETECTION OF Fe<sup>3+</sup>  
 AND Al<sup>3+</sup> IONS.....226

Introduction  
 Synthesis of molecular probes 6.6a, 6.6b, and 6.7  
 X-ray crystallographic study of molecular probes 6.7  
 Job's plot study of molecular probes 6.6a, 6.6b, and 6.7  
 pH studies on the molecular probes 6.6a, 6.6b, and 6.7  
 Optical studies of the molecular probes 6.6a, 6.6b, and 6.7  
 Reversibility of molecular probes 6.6a, 6.6b, and 6.7  
 Detection limit of molecular probes 6.6 and 6.6b  
 Summary  
 Experimental  
 General procedures for the synthesis

VII. CONCLUSION.....255

Conclusion of Chapters II, III, and IV  
 Conclusion of Chapters V and VI

REFERENCES .....257

## LIST OF TABLES

Table	
1.1	Advantages and disadvantages of different techniques for detection of metal ions .....5
1.2	Advantages and disadvantages of UV-Vis, fluorescence, and chemiluminescence .....10
2.1	Association constant ( $K_{11}$ ) between receptors 2.6a and 2.6b and $ZnX_2$ in $CH_3CN$ .....56
2.2	Data for $Zn^{2+}$ binding calibration curve (***) point ignored in calibration curve due to solubility) .....72
2.3	Molar absorptivity for compounds <i>ortho</i> -2.6a and <i>meta</i> -2.6b in $CH_3CN$ ( $M^{-1}cm^{-1}$ ) .....75
2.4	Key interactions in angstroms (Å) and degrees (°).....77
3.1	Binding constants ( $K_{21}$ & $K_{11}$ ) determined by fluorescence titrations for the interactions between compound 3.6 and $Zn^{2+}$ salts. The binding constant for TBAX ( $X=Cl^-$ , $Br^-$ , $I^-$ , $NO_3^-$ ) were also determined, but their values were magnitudes smaller than the $Zn^{2+}$ salts .....99
3.2	Binding constants ( $K_{21}$ & $K_{11}$ ) determined by $^1H$ NMR titrations for the interactions between compound 3.6 and $Zn^{2+}$ salts. The binding constant for TBAX ( $X=Cl^-$ , $Br^-$ , $I^-$ , $NO_3^-$ ) were also determined, but their values were magnitudes smaller than the $Zn^{2+}$ salts .....107
3.3	X-H and X-H...halide distances in angstroms (Å) .....115
4.1	Molecular logic gate table.....126
4.2	Change in chemical shift of compound 4.7 after addition of one equivalent of $Al(ClO_4)_3$ in $CD_3CN$ .....141
4.3	Volume and concentration used for ECL experiment for calculating binding stoichiometry.....149
5.1	Binding constants ( $K_{11}$ ) calculated for UV-Vis titration of 5.12 and 5.13 with $Fe(ClO_4)_3$ and $Al(ClO_4)_3$ using Benesi-Hildbrand and HypSpec program .....176

5.2	Binding constants ( $K_{11}$ ) calculated for fluorescence titration of 5.12 and 5.13 with $\text{Fe}(\text{ClO}_4)_3$ and $\text{Al}(\text{ClO}_4)_3$ using Benesi-Hildbrand and HypSpec program .....	181
5.3	Change in $^1\text{H}$ NMR chemical shift of compound 5.12 (10 mM) after addition of five equivalents of $\text{Al}(\text{ClO}_4)_3$ in $\text{CD}_3\text{CN}$ .....	186
5.4	Change in $^{13}\text{C}$ NMR chemical shift of compound 5.12 (10 mM) after addition of five equivalents of $\text{Al}(\text{ClO}_4)_3$ in $\text{CD}_3\text{CN}$ .....	191
6.1	Binding constant ( $K_{11}$ ) calculated for UV-Vis titrations of 6.6a, 6.6b, and 6.7 (50 $\mu\text{M}$ ) with $\text{Fe}(\text{ClO}_4)_3$ and $\text{Al}(\text{ClO}_4)_3$ (5 mM) in 1:1 (EtOH: $\text{H}_2\text{O}$ ) using Benesi-Hildbrand and HypSpec program .....	239
6.2	Binding constant ( $K_{11}$ ) calculated for fluorescence titrations of 6.6a, 6.6b, and 6.7 with $\text{Fe}(\text{ClO}_4)_3$ and $\text{Al}(\text{ClO}_4)_3$ using Benesi-Hildbrand and HypSpec program .....	247

## LIST OF ILLUSTRATIONS

### Figure

1.1	Biological roles of divalent $Zn^{2+}$ ions and its associated diseases .....	2
1.2	Biological roles of $Fe^{3+}$ ions and its associated diseases .....	3
1.3	Simplified Jablonski diagram. The sequence of events leading to fluorescence and phosphorescence are shown. $S_0$ is the ground state; $S_1$ and $S_2$ are excited singlet states; $T_1$ is an excited triplet state. 0, 1, 2 represent vibration levels. straight lines represent transition involving photons, dotted lines represent vibrational or thermal transitions .....	9
1.4	Fluorophore/chromophore-spacer-receptor probe .....	13
1.5	Different sensing motifs commonly used in design of chemosensors, highlighting the absorbance, emission and excitation wavelength.....	13
1.6	(A) Emission spectra of pyrene, and its excimer. As the concentration decreases (6 mM to 0.09 M) the excimer band at 490 nm loses intensity, and (B) the emission spectrum of monomer and excimer .....	16
1.7	Potential energy diagrams for (A) pyrene excimer formation $M-M^*$ in the absence of ground state dimerization, and (B) for the GSD excimer, showing the $E_d$ , and $E_s$ .....	16
1.8	The rhodamine motif, the xanthene unit is highlighted in (Red) and numbering system utilized in IUPAC .....	17
1.9	Absorption spectra of dilute solutions of rhodamine B (10 $\mu$ M). Absorption band one=1.0 M KCl, 0.03 M $NH_3$ ; Absorption band two=1.0 M KCl, 4 mM HCl; Absorption band three= 5.0 M HCl; Absorption band four= concd. $H_2SO_4$ ; Absorption band five=benzene .....	19
1.10	The rhodamine B species that exist under different pH conditions .....	19
1.11	Common binding motifs utilized in receptors design .....	22
1.12	Principle of cation recognition by fluorescent PET sensors .....	24
1.13	Spectral displacements of PCT sensors resulting from interaction of a bound cation with an electron-donating or electron-withdrawing group.....	27
1.14	Structures of compounds 1.2, 1.3a, and 1.3b .....	28

1.15	Schematic of FRET process.....	35
2.1	Cartoons showing binding of guest species by molecular cleft.....	40
2.2	Structure for compound 2.1 and 2.2.....	42
2.3	Job's plot of compound 2.6a (A) and 2.6b (B) with Zn(ClO <sub>4</sub> ) <sub>2</sub> obtained by fluorescence measurements in CH <sub>3</sub> CN. The total concentration is 100, and 50 μM for experiment with 2.6a, and 2.6b, respectively, where X ≈ 0.5 (1:1 ligand:metal ratio). The red lines are for visual interpretation only .....	50
2.4	The excimer emission of compound 2.6a and 2.6b in CH <sub>3</sub> CN (5 μM, λ <sub>ex</sub> = 325 nm) .....	52
2.5	Fluorescence intensity of 2.6a and 2.6b (5 μM) upon addition of ten equivalent of metal chlorides and perchlorates at 405 nm (CH <sub>3</sub> CN, λ <sub>ex</sub> = 325 nm) .....	52
2.6	The fluorescence spectrum of compound 2.6a (5 μM, λ <sub>ex</sub> = 325 nm) upon incremental additions (up to ten equiv.) of Zn(ClO <sub>4</sub> ) <sub>2</sub> in CH <sub>3</sub> CN (A) and its binding isotherm (B) .....	53
2.7	Binding isotherms for the fluorescence titration of compound 2.6a with Zn(ClO <sub>4</sub> ) <sub>2</sub> at 380, 420, and 505 nm from HypSpec program.....	53
2.8	The fluorescence spectrum of compound 2.6b (5 μM, λ <sub>ex</sub> = 325 nm) upon incremental additions (up to ten equiv.) of Zn(ClO <sub>4</sub> ) <sub>2</sub> in CH <sub>3</sub> CN (A) and its binding isotherm (B) .....	54
2.9	Binding isotherm for the fluorescence titration of compound 2.6b with Zn(ClO <sub>4</sub> ) <sub>2</sub> 378, 420, and 505 nm from HypSpec program.....	54
2.10	Fluorescence intensity of 2.6a and 2.6b (5 μM) upon addition of ten equivalents of various anions of Zn <sup>2+</sup> salts (CH <sub>3</sub> CN, λ <sub>ex</sub> = 325 nm).....	55
2.11	Fluorescence titrations (CH <sub>3</sub> CN, λ <sub>ex</sub> = 325 nm) between 2.6b and Zn(ClO <sub>4</sub> ) <sub>2</sub> in 1% H <sub>2</sub> O .....	57
2.12	<sup>1</sup> H NMR complete spectrum of free receptor 2.6b (bottom), and upon the addition of five equivalents of Zn <sup>2+</sup> ion in a mixture of 1:1 (CD <sub>3</sub> Cl:CD <sub>3</sub> CN) (top).....	59
2.13	(A) rOe signals (B) numbering system, and (C) 2D ROESY of 2.6b in a mixture of CDCl <sub>3</sub> :CD <sub>3</sub> CN (1:1).....	61
2.14	(A) Numbering system and rOe signals (B) ROESY spectrum of	

2.6b after addition of five equivalents of Zn <sup>2+</sup> ions in a mixture of CDCl <sub>3</sub> :CD <sub>3</sub> CN (1:1) .....	62
2.15 ROESY expanded spectrum (aromatic region) of 2.6b after addition of five equivalents of Zn <sup>2+</sup> ions in a mixture of CDCl <sub>3</sub> :CD <sub>3</sub> CN (1:1) .....	63
2.16 DFT fully optimized structures of (A) 2.6a, (B) [Zn.(2.6a)] (ClO <sub>4</sub> ) <sub>2</sub> , (C) 2.6b, and (D) [Zn.(2.6b)](ClO <sub>4</sub> ) <sub>2</sub> .....	65
2.17 ATR-IR data of 2.6b on the addition of Zn(ClO <sub>4</sub> ) <sub>2</sub> .....	68
2.18 Calibration curve used to calculate the LoD for Zn <sup>2+</sup> ion (blue diamond) and Ca <sup>2+</sup> ion (red triangle) with 2.6b.....	70
2.19 Calibration curve used to calculate the LoD for Zn <sup>2+</sup> with 2.6a.....	70
2.20 Reversibility test. The effect of sequential addition of 1, 10-phenanthroline, and Zn(II) to compound 2.6b ([ <i>meta</i> ]=5 μM, [Zn <sup>2+</sup> ]= 500 μM, 1,10-phen = 500 μM, CH <sub>3</sub> CN, λ <sub>ex</sub> = 325 nm) .....	71
2.21 Calibration curve generated from fluorescence data of 2.6b (5 μM, λ <sub>ex</sub> =325 nm, CH <sub>3</sub> CN) and [Zn(2.6b)] <sup>2+</sup> complexes demonstrating a linear response.....	73
3.1 Job's plot of compound 3.6 with ZnCl <sub>2</sub> obtained by fluorescence measurements in CH <sub>3</sub> CN. The total concentration of compound 3.6 and ZnCl <sub>2</sub> is 6.48×10 <sup>-4</sup> M where X ≈ 0.33 (2:1 ligand:metal ratio). The red lines are for visual interpretation only.....	92
3.2 (A) Monomer emission of compound 3.6 in CH <sub>3</sub> CN (λ <sub>ex</sub> =340 nm), and (B) crystal packing in 3.6 showing hydrogen bonding. C-H (triazole)···CO (carbonyl)=2.457 Å, CH <sub>2</sub> (benzene)···CO (carbonyl)=2.394 Å, N-H (amide)···N (triazole) = 2.082 Å .....	93
3.3 (A) Fluorescence selectivity chart, and (B) bar chart of compound 3.6 (6.5 × 10 <sup>-4</sup> M and λ <sub>ex</sub> = 355 nm) in CH <sub>3</sub> CN upon the addition of ten equivalents of different metal ions as their Cl <sup>-</sup> salts (*NO <sub>3</sub> <sup>-</sup> salt) .....	96
3.4 (A) Fluorescence spectra of compound 3.6 (6.5 × 10 <sup>-4</sup> M and λ <sub>ex</sub> = 355 nm) upon addition of ten equivalents of F <sup>-</sup> , I <sup>-</sup> , CN <sup>-</sup> , SO <sub>4</sub> <sup>2-</sup> , PO <sub>4</sub> <sup>3-</sup> , and CH <sub>3</sub> COO <sup>-</sup> (B) Cl <sup>-</sup> , Br <sup>-</sup> , BF <sub>4</sub> <sup>-</sup> , ClO <sub>4</sub> <sup>-</sup> , and NO <sub>3</sub> <sup>-</sup> , of zinc in CH <sub>3</sub> CN .....	97
3.5 Fluorescence titration of compound 3.6 (6.5 × 10 <sup>-4</sup> M and λ <sub>ex</sub> = 355 nm) with ZnCl <sub>2</sub> in CH <sub>3</sub> CN. (A) Fluorescence spectra and (B) binding isotherm.....	98

3.6	Fluorescence titration of compound 3.6 ( $6.5 \times 10^{-4}$ M and $\lambda_{\text{ex}} = 355$ nm) with $\text{Zn}(\text{NO}_3)_2$ in $\text{CH}_3\text{CN}$ . (A) fluorescence spectra and (B) binding isotherm.....	98
3.7	Fluorescence titration of compound 3.6 ( $6.5 \times 10^{-4}$ M and $\lambda_{\text{ex}} = 355$ nm) with TBACl in $\text{CH}_3\text{CN}$ . (A) fluorescence spectra and (B) binding isotherm.....	99
3.8	$^1\text{H}$ NMR assignments that are followed in the NMR titration experiments in $\text{CD}_3\text{CN}$ . The chemical shifts values of A, B, C, and D in the free ligand 3.6 are $\delta$ 7.46 , 4.74, 7.85, and 5.56 ppm, respectively) .....	101
3.9	Partial $^1\text{H}$ NMR Stack plot: Addition of $\text{ZnCl}_2$ with compound 3.6 (10 mM) in $\text{CD}_3\text{CN}$ (aromatic region only).....	103
3.10	$^1\text{H}$ NMR Stack plot: Addition of $\text{ZnCl}_2$ with compound 3.6 (10 mM) in $\text{CD}_3\text{CN}$ for aromatic protons .....	103
3.11	$^1\text{H}$ NMR Stack plot: Addition of $\text{ZnCl}_2$ with compound 3.6 (10 mM) in $\text{CD}_3\text{CN}$ for $\text{CH}_2$ protons attached to amide group ( $\delta$ 4.74 ppm) and for $\text{CH}_2$ protons attached to benzene group ( $\delta$ 5.56 ppm) .....	104
3.12	Partial $^1\text{H}$ NMR Stack plot: Addition of $\text{Zn}(\text{NO}_3)_2$ with compound 3.6 (10 mM) in $\text{CD}_3\text{CN}$ (aromatic region only).....	104
3.13	Partial $^1\text{H}$ NMR Stack plot: Addition of $\text{TBANO}_3$ with compound 3.6 (10 mM) in $\text{CD}_3\text{CN}$ (aromatic region only).....	105
3.14	$^1\text{H}$ NMR binding isotherms of compound 3.6 (10 mM) plus the addition of $\text{ZnCl}_2$ .....	105
3.15	$^1\text{H}$ NMR binding isotherms of compound 3.6 (10 mM) plus the addition of $\text{Zn}(\text{NO}_3)_2$ .....	106
3.16	$^1\text{H}$ NMR binding isotherms of compound 3.6 (10 mM) plus the addition of $\text{TBANO}_3$ .....	106
3.17	Correlation of protons labelled as (a), (b), (c), (d), and (e) seen in the 2D ROESY of free ligand (3.6) in $\text{CD}_3\text{CN}$ .....	108
3.18	gROSEY of compound 3.6 (10 mM) in $\text{CD}_3\text{CN}$ . Calculated distances (a) 2.585 Å, (b) 2.592 Å, (c) 2.861 Å, (d) 2.805 Å, and (e) 2.404 Å from molecular modelling structures (Figure 3.23).....	109
3.19	Correlation of protons labelled as (a), (b), (c), (d), (e), and (f) seen in the 2D ROESY of complex $[\text{ZnCl}_2(3.6)_2]$ in $\text{CD}_3\text{CN}$ .....	109

3.20	gROSEY of complex $[\text{ZnCl}_2(3.6)_2]$ in $\text{CD}_3\text{CN}$ : Calculated distances (a) 2.386 Å (b) 2.336 Å (c) 2.983 Å (d) 2.738 Å (e) 2.471 Å, and (f) 2.96 from molecular modelling structures (Figure 3.22).....	110
3.21	Relative energies of the geometric and optical isomers, for $[\text{ZnX}_2(3.6)_2]$ ( $\text{X} = \text{F}^-$ , $\text{Cl}^-$ and $\text{NO}_3^-$ ) .....	112
3.22	DFT fully optimised structure of $[\text{ZnCl}_2(3.6)_2]$ . Calculated pyrene distance 4.4 Å and angle $4.91^\circ$ .....	114
3.23	(A) Molecular models of compound 3.6, (B) <i>syn</i> $[\text{Zn}(\text{NO}_3)_2(3.6)_2]$ , and (C) <i>syn</i> $[\text{ZnF}_2(3.6)_2]$ .....	115
3.24	Fluorescence chart for protocol one.....	118
3.25	Fluorescence chart for protocol two .....	119
4.1	The symbolic representation of the INHIBIT logic gate function .....	127
4.2	Job's plot of compound 4.7 with $\text{Fe}(\text{ClO}_4)_3$ obtained by fluorescence measurement. The total concentration of compound 4.7 and $\text{Fe}(\text{ClO}_4)_3$ is $1 \times 10^{-4} \text{ M}$ in $\text{CH}_3\text{CN}$ .....	132
4.3	Bar chart of compound 4.7 ( $10 \mu \text{ M}$ and $\lambda_{\text{ex}} = 340 \text{ nm}$ ) in $\text{CH}_3\text{CN}$ upon the addition of 1.5 equivalents of different metal ions as their $\text{ClO}_4^-$ salts (* $\text{Cl}^-$ salt).....	134
4.4	Fluorescence titration of compound 4.7 ( $10 \mu \text{ M}$ ) with $\text{Fe}(\text{ClO}_4)_3$ ( $100 \mu \text{ M}$ ) in $\text{CH}_3\text{CN}$ . Fluorescence spectrum (A) and (B) its binding isotherm. $\lambda_{\text{ex}} = 340 \text{ nm}$ .....	135
4.5	Binding isotherm of fluorescence titration of compound 4.7 with $\text{Fe}(\text{ClO}_4)_3$ from HypSpec program.....	135
4.6	Fluorescence titration of compound 4.7 ( $10 \mu \text{ M}$ ) with $\text{Fe}(\text{ClO}_4)_3$ ( $100 \mu \text{ M}$ ) in $\text{CH}_3\text{CN}$ . Fluorescence spectrum (A) and (B) its binding isotherm. $\lambda_{\text{ex}} = 340 \text{ nm}$ .....	135
4.7	Fluorescence titration of compound 4.7 ( $10 \mu \text{ M}$ ) with $\text{TBACl}$ ( $100 \mu \text{ M}$ ) in $\text{CH}_3\text{CN}$ . Fluorescence spectrum (A) and (B) its binding isotherm. $\lambda_{\text{ex}} = 340 \text{ nm}$ .....	136
4.8	Bar chart of compound 4.7 ( $10 \mu \text{ M}$ and $\lambda_{\text{ex}} = 340 \text{ nm}$ ) in $\text{CH}_3\text{CN}$ upon the addition of 1.5 equivalents of different anions of iron.....	137
4.9	$^1\text{H}$ NMR assignments that are followed in the NMR titration experiments	



	in CD <sub>3</sub> CN. The chemical shifts values of A, B, C, and D in the free ligand 4.7 are $\delta$ 7.54, 4.76, 7.92, and 3.12 ppm, respectively.....	138
4.10	Partial <sup>1</sup> H NMR stack plot: Addition of Al(ClO <sub>4</sub> ) <sub>3</sub> to compound 4.7 in CD <sub>3</sub> CN (aromatic regions only).....	140
4.11	Partial <sup>1</sup> H NMR stack plot: Addition of Al(ClO <sub>4</sub> ) <sub>3</sub> to compound 4.7 in CD <sub>3</sub> CN (sugar group only) .....	140
4.12	<sup>1</sup> H NMR binding isotherm of amide proton (A) and –OCH <sub>3</sub> (attached to carbon number 20) group of sugar of compound 4.7 upon addition of Al(ClO <sub>4</sub> ) <sub>3</sub> .....	141
4.13	ECL response of 50 $\mu$ M 4.7 (black) and after addition of one equivalent of 500 $\mu$ M Fe(ClO <sub>4</sub> ) <sub>3</sub> (red) with a 0.02 M TPrA and 0.1M TBAP in CH <sub>3</sub> CN at a 2 mm Pt electrode with a scan rate of 100 mV/S .....	145
4.14	ECL plot vs different mole ratio of ligand 4.7 to Fe(ClO <sub>4</sub> ) <sub>3</sub> .....	145
4.15	Bar chart of electrogenerated chemiluminescence of 4.7 with one equivalent of different metal ions in CH <sub>3</sub> CN (4.7= 50 $\mu$ M, TBAP= 0.1 M, TPrA= 20 mM) .....	146
4.16	Proposed ECL mechanism for the compound 4.7 .....	146
5.1	Structures for compounds 5.2 and 5.3 synthesized using rhodamine 6G .....	157
5.2	X-ray crystal structures of (A) compounds 5.12, (B) its crystal packing, and (C) crystal structure of compound 5.11 .....	165
5.3	Job's plot of compound 5.12 with Fe(ClO <sub>4</sub> ) <sub>3</sub> obtained by fluorescence measurements in 1:1 (EtOH:H <sub>2</sub> O). The total concentration of compound 5.12 and Fe(ClO <sub>4</sub> ) <sub>3</sub> is 100 $\mu$ M where $X \approx 0.55$ (1:1 ligand:metal ratio). The red lines are for visual interpretation only .....	167
5.4	Job's plot of compound 5.12 with Al(ClO <sub>4</sub> ) <sub>3</sub> obtained by fluorescence measurements in 1:1 (EtOH:H <sub>2</sub> O). The total concentration of compound 5.12 and Al(ClO <sub>4</sub> ) <sub>3</sub> is 100 $\mu$ M where $X \approx 0.55$ (1:1 ligand:metal ratio). The red lines are for visual interpretation only .....	167
5.5	pH profile of compound 5.12 (20 $\mu$ M) with pH from 1-14 (bottom black circle) and upon the addition of five equivalents of Fe <sup>3+</sup> ions (upper red diamond) and Al <sup>3+</sup> ions (middle purple triangle) in EtOH :H <sub>2</sub> O.....	169
5.6	UV-Vis selectivity chart of compound 5.12 (100 $\mu$ M) in 1:1(EtOH:H <sub>2</sub> O),	

	pH =7.1, upon the addition of one equivalent of metal ions as their $\text{ClO}_4^-$ salts (* $\text{Cl}^-$ salt).....	171
5.7	Comparison of UV-Vis selectivity chart of compound 5.11 (benzene), 5.12 (pyridine), and 5.13 (sugar) (10 $\mu\text{M}$ ) in 1:1 (EtOH:H <sub>2</sub> O), pH =7.1, upon the addition of one equivalent of $\text{Fe}^{3+}$ and $\text{Al}^{3+}$ ions as their $\text{ClO}_4^-$ salts.....	171
5.8	(A) UV-Vis spectrum of compound 5.12 (50 $\mu\text{M}$ ) upon addition of $\text{Fe}(\text{ClO}_4)_3$ , (B) its binding isotherm in 1:1 (EtOH:H <sub>2</sub> O), pH =7.1, (C) Binding isotherm for HypSpec program, and (D) Benesi-Hildbrand plot .....	173
5.9	(A) UV-Vis spectrum of compound 5.12 (50 $\mu\text{M}$ ) upon addition of $\text{Al}(\text{ClO}_4)_3$ , (B) its binding isotherm in 1:1 (EtOH:H <sub>2</sub> O), pH =7.1, (C) binding isotherm for HypSpec program, and (D) Benesi-Hildbrand plot.....	174
5.10	Fluorescence selectivity chart of compound 5.8 (10 $\mu\text{M}$ ) in 1:1 (EtOH:H <sub>2</sub> O), pH =7.1, upon the addition of metal ions (five equivalents) as their $\text{ClO}_4^-$ salts (* $\text{Cl}^-$ salt) $\lambda_{\text{ex}}=550$ nm .....	177
5.11	Comparison of fluorescence selectivity chart of compound 5.11 (benzene), 5.12 (pyridine), and 5.13 (sugar) (10 $\mu\text{M}$ ) in 1:1 (EtOH:H <sub>2</sub> O), pH =7.1, upon the addition of five equivalents of $\text{Fe}^{3+}$ and $\text{Al}^{3+}$ ions as their $\text{ClO}_4^-$ salts ( $\lambda_{\text{ex}}=550$ nm) .....	178
5.12	(A) Fluorescence spectrum of compound 5.12 (20 $\mu\text{M}$ ) upon addition of $\text{Fe}(\text{ClO}_4)_3$ , (B) binding isotherm in 1:1 (EtOH:H <sub>2</sub> O), pH=7.1, (C) binding isotherm from HypSpec program, and (D) Benesi-Hildbrand plot.....	179
5.13	(A) Fluorescence spectrum of compound 5.12 (20 $\mu\text{M}$ ) upon addition of $\text{Al}(\text{ClO}_4)_3$ , (B) binding isotherm in 1:1 (EtOH:H <sub>2</sub> O), pH =7.1, (C) binding isotherm from Hyp Spec program, and (D) Benesi-Hildbrand plot.....	180
5.14	<sup>1</sup> H NMR assignments that are followed in the NMR titration experiments in CD <sub>3</sub> CN. The chemical shifts values of A, B, and C in the free ligand 5.12 are $\delta$ 4.32, 7.19, and 5.36 ppm, respectively.....	182
5.15	Partial <sup>1</sup> H NMR stack plot: Addition of $\text{Al}(\text{ClO}_4)_3$ with compound 5.12 (10 mM) in CD <sub>3</sub> CN (aromatic region only).....	185
5.16	<sup>1</sup> H NMR Stack plot: Addition of $\text{Al}(\text{ClO}_4)_3$ with compound 5.12 (10 mM) in CD <sub>3</sub> CN for CH <sub>2</sub> protons attached to lactam (A) at $\delta$ 4.32 ppm, and for CH <sub>2</sub> protons attached to pyridine (C) at $\delta$ 5.36 ppm.....	185
5.17	<sup>1</sup> H NMR Binding isotherms of compound 5.12 (10 mM) for the protons (A), (B), and (C) after the addition of $\text{Al}(\text{ClO}_4)_3$ from HypNMR program .....	187

5.18	Cartoons showing the proposed binding mechanism of metal ion by compounds 5.11 (A) and 5.12 (B) .....	188
5.19	<sup>13</sup> C NMR spectrum of free ligand 5.12 (10 mM) in CD <sub>3</sub> CN (Figure 5.13).....	190
5.20	<sup>13</sup> C NMR spectrum of complex of ligand 5.12 (10 mM) with five equivalents Al(ClO <sub>4</sub> ) <sub>3</sub> in CD <sub>3</sub> CN.....	191
5.21	Cartoon showing the pendent arm becomes far from the xanthene ring after coordination of metal ion.....	193
5.22	Correlation of protons labelled as A, B, and C seen in the 2D ROESY of free ligand (5.12) in CD <sub>3</sub> CN .....	194
5.23	ROSEY of compound 5.12 (10 mM) in CD <sub>3</sub> CN. Calculated distances (A) 3.25 Å, (B) 3.07 Å, and (C) 4.82 Å.....	194
5.24	Proposed structures of complex [Al(5.12)] <sup>3+</sup> .....	195
5.25	ROSEY of complex of compound 5.12 (10 mM) with five equivalents Al(ClO <sub>4</sub> ) <sub>3</sub> in CD <sub>3</sub> CN. The cross peak labelled as (A), (B), and (C) were absent in the complex.....	195
5.26	ATR-IR data of compound 5.12 on the addition of Fe(ClO <sub>4</sub> ) <sub>3</sub> .....	197
5.27	Reversibility test: [5.12] =10 µM; Fe (III) =100 µM; DFB=100 µM in EtOH: H <sub>2</sub> O (1:1) .....	199
5.28	Reversibility test: [5.12] =10 µM; Al (III) =100 µM; DFB=100 µM in EtOH: H <sub>2</sub> O (1:1) .....	199
5.29	Fluorescence chart of 5.12 (10 µM) with 100 µM Fe(ClO <sub>4</sub> ) <sub>3</sub> used to calculate LoD .....	200
5.30	Calibration curve used to calculate the LoD for Fe <sup>3+</sup> with 5.12 .....	201
5.31	(A) UV-Vis spectrum of ferrozine (50 µM), its complex with Fe <sup>2+</sup> (0.5 mM) and Fe <sup>3+</sup> (0.5 mM) ions in 1:1 (EtOH:H <sub>2</sub> O) and (B) its UV-Vis absorbance from 350-750 nm .....	204
5.32	Ferrozine protocol with Fe(ClO <sub>4</sub> ) <sub>3</sub> in 1:1( EtOH: H <sub>2</sub> O). (A) UV-Vis absorbance of 5.12 (100 µM) on addition of Fe(ClO <sub>4</sub> ) <sub>3</sub> (1 mM), sodium ascorbate (10 mM), and ferrozine (1 mM), and (B) absorbance with increasing time interval.....	206
5.33	Ferrozine protocol with Fe(ClO <sub>4</sub> ) <sub>3</sub> in 1:1( EtOH: H <sub>2</sub> O). (A) UV-Vis	

	absorbance of 5.12 (100 $\mu\text{M}$ ) on addition of $\text{Al}(\text{ClO}_4)_3$ (1 mM), sodium ascorbate (10 mM), and ferrozine (1 mM), and (B) absorbance with increasing time interval.....	207
5.34	Ferrozine protocol with 1:3 ( $\text{Fe}(\text{ClO}_4)_3$ ): $\text{Al}(\text{ClO}_4)_3$ in 1:1 ( EtOH: $\text{H}_2\text{O}$ ). (A) UV-Vis absorbance of 5.12 (100 $\mu\text{M}$ ) on addition of 1:3 ( $\text{Fe}(\text{ClO}_4)_3$ ): $\text{Al}(\text{ClO}_4)_3$ (1 mM), sodiuam ascorbate (10 mM), and ferrozine (1 mM), and (B) absorbance with increasing time interval.....	208
5.35	(A) UV-Vis spectrum of 1,10-phenanthroline (50 $\mu\text{M}$ ), its complex with $\text{Fe}^{2+}$ (0.5 mM) and $\text{Fe}^{3+}$ (0.5 mM) ions in 1:1 (EtOH: $\text{H}_2\text{O}$ ) and (B) its UV-Vis absorbance from 330-630 nm.....	209
5.36	1, 10-phenanthroline protocol with $\text{Fe}(\text{ClO}_4)_3$ in 1:1 ( EtOH: $\text{H}_2\text{O}$ ). (A) UV-Vis absorbance of 5.12 (100 $\mu\text{M}$ ) on addition of $\text{Fe}(\text{ClO}_4)_3$ (1mM), sodium ascorbate (10 mM), and 1, 10-phenanthroline (1 mM), and (B) absorbance with increasing time interval .....	211
5.37	1, 10-phenanthroline protocol with $\text{Al}(\text{ClO}_4)_3$ in 1:1( EtOH: $\text{H}_2\text{O}$ ). (A) UV-Vis absorbance of 5.12 (100 $\mu\text{M}$ ) on addition of $\text{Al}(\text{ClO}_4)_3$ (1 mM), sodium ascorbate (10 mM), and 1, 10-phenanthroline (1 mM), and (B) absorbance with increasing time interval.....	212
5.38	1, 10-phenanthroline protocol with 1:1 ( $\text{Fe}(\text{ClO}_4)_3$ ): $\text{Al}(\text{ClO}_4)_3$ in 1:1 (EtOH: $\text{H}_2\text{O}$ ). (A) UV-Vis absorbance of 5.12 (100 $\mu\text{M}$ ) on addition of 1:1 ( $\text{Fe}(\text{ClO}_4)_3$ ): $\text{Al}(\text{ClO}_4)_3$ (1 mM), sodium ascorbate (10 mM), and 1, 10-phenanthroline (1 mM), and (B) absorbance with increasing time interval .....	212
5.39	Confocal microscopy for detecting intracellular free iron using probe 5.12. Phase contrast images (A and C) and fluorecence images (B and D) of Vero cells. The upper panel is negative control, and the lower panel is the test with an additional iron.....	215
5.40	Confocal microscopy for detecting intracellular free iron using probe 5.12. Phase contrast images (A and C) and fluorecence images (B and D) of gram positive bacterium, <i>Staphylococcus aureus</i> . The upper panel is negative control, and the lower panel is the test with an additional iron.....	217
5.41	Fluorescence of baterial cells showing enhancement upon addition of additional $\text{FeCl}_3$ or $\text{Fe}(\text{ClO}_4)_3$ .....	218
6.1	Structure of model compound 6.1 and molecular cleft 6.2.....	227
6.2	X-ray crystal structure of compound 6.7 .....	234

6.3	Job's plot of compound 6.6b with $\text{Fe}(\text{ClO}_4)_3$ obtained by fluorescence measurements in 1:1 (EtOH : $\text{H}_2\text{O}$ ). The total concentration of 6.6b and $\text{Fe}(\text{ClO}_4)_3$ is 100 $\mu\text{M}$ where $X \approx 0.5$ (1:1 ligand:metal ratio). The red lines are for visual interpretation only.....	235
6.4	pH profile of compound 6.6b (20 $\mu\text{M}$ ) with pH from 1-14 (bottom green circle) and upon the addition of five equivalents of $\text{Fe}(\text{III})$ ( upper red diamond) in 1:1 (EtOH: $\text{H}_2\text{O}$ ).....	236
6.5	UV-Vis selectivity chart of compound 6.6b (100 $\mu\text{M}$ ) in 1:1 (EtOH: $\text{H}_2\text{O}$ ), at pH =7.1, upon the addition of one equivalents of metal ions as their $\text{ClO}_4^-$ salts (* $\text{Cl}^-$ salt) .....	238
6.6	Comparison of UV-Vis selectivity chart of compounds 6.6a, 6.6b, and 6.7 (100 $\mu\text{M}$ ) in 1:1 (EtOH: $\text{H}_2\text{O}$ ), pH 7.1, upon addition of one equivalents of $\text{Fe}^{3+}$ and $\text{Al}^{3+}$ ions as their $\text{ClO}_4^-$ salts .....	238
6.7	(A) UV-Vis spectrum of compound 6.6b (50 $\mu\text{M}$ ) upon addition of $\text{Fe}(\text{ClO}_4)_3$ , (B) its binding isotherm in 1:1 (EtOH: $\text{H}_2\text{O}$ ), pH =7.1 (C) binding isotherm for HypSpec program, and (D) Benesi-Hildbrand plot.....	240
6.8	(A) UV-Vis spectrum of compound 6.6b (50 $\mu\text{M}$ ) upon addition of $\text{Al}(\text{ClO}_4)_3$ , (B) its binding isotherm in 1:1 (EtOH: $\text{H}_2\text{O}$ ), pH =7.1, (C) binding isotherm for HypSpec program, and (D) Benesi-Hildbrand plot.....	241
6.9	Fluorescence selectivity chart of compound 6.6b (10 $\mu\text{M}$ ) in 1:1 (EtOH: $\text{H}_2\text{O}$ ), at pH =7.1, upon the addition of metal ions (five equivalents) as their $\text{ClO}_4^-$ salts (* $\text{Cl}^-$ salt). $\lambda_{\text{ex}}=550$ nm.....	243
6.10	Comparison of UV-Vis selectivity chart of compounds 6.6a, 6.6b, and 6.7 (10 $\mu\text{M}$ ) in 1:1 (EtOH: $\text{H}_2\text{O}$ ), pH = 7.1, upon addition of one equivalents of $\text{Fe}^{3+}$ and $\text{Al}^{3+}$ ions as their $\text{ClO}_4^-$ salts.....	243
6.11	(A) Fluorescence spectrum of compound 6.6b (20 $\mu\text{M}$ ) upon addition of $\text{Fe}(\text{ClO}_4)_3$ , (B) its binding isotherm in 1:1 (EtOH: $\text{H}_2\text{O}$ ), pH =7.1, (C) binding isotherm for HypSpec program, and (D) Benesi-Hildbrand plot.....	245
6.12	(A) Fluorescence spectrum of compound 6.6b (20 $\mu\text{M}$ ) upon addition of $\text{Al}(\text{ClO}_4)_3$ , (B) its binding isotherm in 1:1 (EtOH: $\text{H}_2\text{O}$ ), pH =7.1, (C) binding isotherm for HypSpec program, and (D) Benesi-Hildbrand plot.....	246
6.13	Reversibility test: [6.6b] =10 $\mu\text{M}$ ; $\text{Fe}(\text{III})$ =100 $\mu\text{M}$ ; DFB=100 $\mu\text{M}$ in EtOH: $\text{H}_2\text{O}$ (1:1) .....	248
6.14	Fluorescence chart of 6.6b (20 $\mu\text{M}$ ) with $\text{Fe}(\text{ClO}_4)_3$ (50 $\mu\text{M}$ ) used to calculate L.o.D in 1:1 (EtOH: $\text{H}_2\text{O}$ ).....	249

6.15	Calibration curve used to calculate the LoD for Fe <sup>3+</sup> ion with 6.6b .....	250
------	--	-----

## LIST OF SCHEMES

Scheme	
1.1	Generation of free radicals such as hydroxyl radicals <i>via</i> Fenton's reaction .....3
1.2	Spirolactam ring-opening process of rhodamine derivatives.....20
1.3	Cu (I)-catalysed azide-alkyne cycloaddition to afford a 1,4-substituted 1,2,3-triazole.....22
1.4	Proposed binding of compound 1.1 with Al <sup>3+</sup> ion .....25
1.5	Proposed structure for binding Zn <sup>2+</sup> ions by compound 1.4.....30
1.6	Proposed structure for binding Hg <sup>2+</sup> ions by compound 1.5 .....31
1.7	Proposed structure for binding Ni <sup>2+</sup> by compound 1.6.....32
1.8	Proposed structure for binding Al <sup>3+</sup> ion by compound 1.7.....34
1.9	Proposed binding of compound 1.8 with Fe <sup>3+</sup> ion .....37
2.1	Proposed binding mechanism of 2.2 with Hg <sup>2+</sup> ion in CH <sub>3</sub> CN-H <sub>2</sub> O (80:20, v/v).....42
2.2	Proposed binding mechanism of 2.3 with Cr <sup>3+</sup> ion in Tris HNO <sub>3</sub> buffered solution (pH 7.0). Detection limit was calculated to be 4 × 10 <sup>-8</sup> M (2 ppb) for Cr <sup>3+</sup> ions .....44
2.3	Conformation change of receptor 2.4 on addition of Ag <sup>+</sup> ion in a 10 μM concentration, DMSO:HEPES solution (pH 7.4, 1:1, v/v) .....45
2.4	Synthesis of molecular receptor 2.6a and 2.6b .....48
3.1	The proposed binding mode of compound 3.1 with the P <sub>4</sub> O <sub>7</sub> <sup>4-</sup> .....84
3.2	Proposed binding mode of compound 3.2 with Cu <sup>2+</sup> ion.....85
3.3	A chelation-enhanced quenching sensor complex formation of [Hg(3.3) <sub>2</sub> ] <sup>2+</sup> in pH 7.4 HEPES buffer solution.....87
3.4	The proposed binding mode of 3.4 with Ag <sup>+</sup> ion.....89
3.5	Synthesis of molecular receptor 3.6.....91

3.6	Preparation of 1-(2,4 dihydroxyphenyl)ethanone <i>via</i> a Friedel-Crafts acylation .....	116
4.1	Proposed binding mechanism of 4.1 and 4.2 with Hg <sup>2+</sup> ion based on computation calculation .....	124
4.2	Proposed binding mechanism of 4.3 with F <sup>-</sup> ion based upon DFT calculations .....	126
4.3	Proposed binding mechanism of 4.4a and 4.4b with Cu <sup>2+</sup> ion.....	128
4.4	Synthesis of molecular probe 4.7.....	131
4.5	Proposed binding mechanism of compound 4.7 with Fe <sup>3+</sup> ion.....	137
5.1	Proposed binding mode of 5.1 with Fe <sup>3+</sup> ion .....	156
5.2	Proposed binding mode of Fe <sup>3+</sup> ion by compound 5.2 .....	157
5.3	Proposed structure for binding Pt <sup>2+</sup> ion by rhodamine 6G based compound 5.4.....	158
5.4	A proposed structure of the ternary complex between [Au (5.5)] <sup>+</sup> and cysteine .....	160
5.5	Proposed structure for binding Hg <sup>2+</sup> ion by compound 5.6 .....	161
5.6	Synthesis of molecular probes 5.11, 5.12, and 5.13 .....	164
5.7	Proposed binding mode of compound 5.12 with Fe <sup>3+</sup> /Al <sup>3+</sup> ion .....	188
5.8	Structures of ferrozine and its complex with Fe <sup>2+</sup> ion (counter ion Na <sup>+</sup> ) .....	203
5.9	Representation of protocol using ferrozine to distinguish Fe <sup>3+</sup> and Al <sup>3+</sup> ions .....	205
5.10	Structures of 1,10-phenanthroline and its complex with Fe <sup>2+</sup> ion .....	209
5.11	Representation of protocol using 1, 10-phenanthroline to distinguish Fe <sup>3+</sup> and Al <sup>3+</sup> ions .....	210
6.1	Proposed structure for binding Hg <sup>2+</sup> ion by compound 6.2 .....	228
6.2	Proposed structure for binding Cu <sup>2+</sup> /Fe <sup>3+</sup> ions by compound 6.3.....	230
6.3	Synthesis of molecular probes 6.6a, 6.6b, and 6.7.....	233



6.4	Proposed binding mode of compound 6.6b with Fe <sup>3+</sup> ion on the basis of UV-Vis and fluorescence results (S = solvent).....	247
-----	---	-----

## LIST OF ABBREVIATIONS

<i>PPB</i>	Parts Per Billion
<i>PPT</i>	Parts Per Trillion
<i>AAS</i>	Atomic Absorption Spectrometry
<i>AES</i>	Atomic Emission Spectroscopy
<i>ICP-MS</i>	Inductively Coupled Plasma Mass Spectrometry
<i>CL</i>	Chemiluminescence
<i>UV-Vis</i>	Ultraviolet Visible
<i>PET</i>	Photoinduced Electron Transfer
<i>CHEF</i>	Chelation Enhanced Fluorescence
<i>CHEQ</i>	Chelation Enhanced Quenching
<i>PCT</i>	Photoinduced Charge Transfer
<i>FRET</i>	Fluorescence Resonance Energy Transfer
<i>HOMO</i>	Highest Occupied Molecular Orbital
<i>LUMO</i>	Lowest Unoccupied Molecular Orbital
<i>TPEN</i>	N, N, N', N'-Tetrakis(2-pyridylmethyl) Ethylenediamine
<i>HEPES</i>	4-(2-Hydroxyethyl)-1-piperazineethanesulfonic acid
<i>ICT</i>	Internal Charge Transfer
<i>DMSO</i>	Dimethyl Sulfoxide
<i>DFT</i>	Density Functional Theory
<i>TDDFT</i>	Time-dependent Density Functional Theory
<i>ATR-IR</i>	Attenuated Total Reflectance-Infrared

<i>NMR</i>	Nuclear Magnetic Resonance
<i>ESI</i>	Electro Spray Ionization
<i>COSY</i>	Correlation Spectroscopy
<i>HMQC</i>	Heteronuclear Multiple Quantum Coherence
<i>HMBC</i>	Heteronuclear Multiple Bond Coherence
<i>TOCSY</i>	Total Correlation Spectroscopy
<i>ROESY</i>	Rotating Frame Overhauser Effect Spectroscopy
<i>NOE</i>	Nuclear Overhauser Effect
<i>LOD</i>	Limit of Detection
<i>WHO</i>	World Health Organization
<i>EPA</i>	Environmental Protection Agency
<i>TBACl</i>	Tetrabutyl Ammonium Chloride
<i>TBANO<sub>3</sub></i>	Tetrabutyl Ammonium Nitrate
<i>TBAF</i>	Tetrabutyl Ammonium Fluoride
<i>ECL</i>	Electrogenerated Chemiluminescence
<i>DPA</i>	9,10-Diphenylanthracene
<i>TMPD</i>	<i>N, N, N, N'</i> -tetramethyl- <i>p</i> -phenylenediamine
<i>An</i>	Anthracene
<i>TBAP</i>	Tetrabutyl Ammonium Perchlorate
TPrA	Tri Propyl Amine
<i>CV</i>	Cyclic Voltammetry
<i>MTT</i>	(3-(4,5-Dimethylthiazole-2-yl)-2,5-Diphenyltetrazolium

<i>EDC</i>	1-Ethyl-3-(3-Diethylaminopropyl) Carbodiimide
<i>TBAI</i>	Terabutyl Ammonium Iodate
<i>DIPEA</i>	N,N-Diisopropylethylamine
<i>DMF</i>	Dimethyl Formamide
<i>BME</i>	Basal Media
<i>DFB</i>	Deferoxamine

## CHAPTER I

### GENERAL INTRODUCTION

#### Significance of Target Analytes

The selective detection of  $\text{Zn}^{2+}$  and  $\text{Fe}^{3+}$  ions is an area of current interest. They play important roles in many biological and environmental processes.<sup>1,2</sup> The following sections highlight the importance of these metal ions and their relevance to the dissertation.

#### *Biological importance of $\text{Zn}^{2+}$ ion*

The  $\text{Zn}^{2+}$  ion is the second most abundant transition metal in the human body after iron.<sup>3</sup> There is total of two to three grams of  $\text{Zn}^{2+}$  ions in an adult human body. It occurs as a divalent cation known to play diverse roles in biological processes (Figure 1.1).<sup>4</sup> More than 90% of the  $\text{Zn}^{2+}$  ions found in the body are classified as static and they play structural or catalytic roles in transcription factors, proteins (e.g., zinc finger proteins which bind specifically to DNA sequences), and enzymes (for example: lactase dehydrogenase, Copper or zinc superoxide dismutase).<sup>4-7</sup> In addition to these tightly bound  $\text{Zn}^{2+}$  ions by proteins and enzymes, labile pools of  $\text{Zn}^{2+}$  ions are present throughout the brain and central nervous system where they are largely localized within the vesicles of zinc-dependent glutamatergic neurons. It is believed that the concentration of  $\text{Zn}^{2+}$  ion found in the nerve tissues is in the range of 0.1-0.5 mM.<sup>8,9</sup> Within the brain tissue,  $\text{Zn}^{2+}$  ion is concentrated in the hippocampus, amygdala, neocortex, and olfactory bulb regions.<sup>10</sup> However, the precise role of this labile zinc pool needs to be explored.<sup>11</sup>

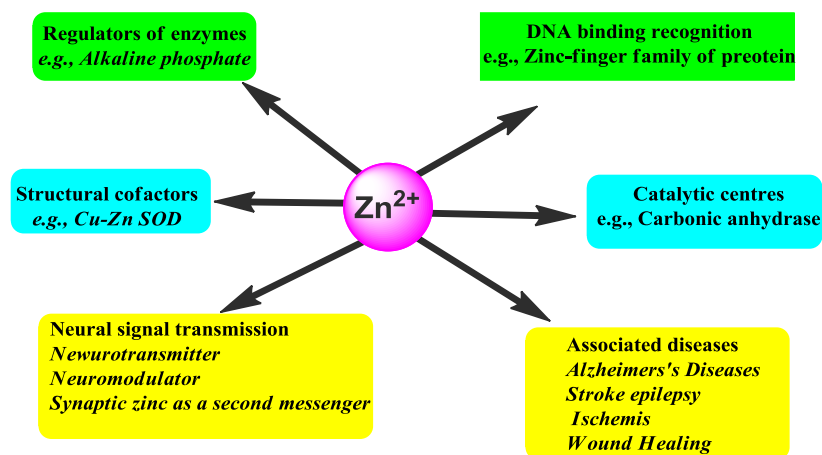


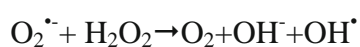
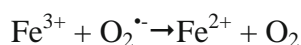
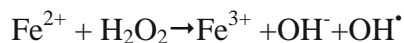
Figure 1.1. Biological roles of divalent  $Zn^{2+}$  ions and its associated diseases.<sup>9</sup>

Although  $Zn^{2+}$  ions plays a vital role in many biological processes, it has been linked with a number of diseases such as types I and II diabetes,<sup>12</sup> Parkinson's disease,<sup>13</sup> Alzheimer's diseases,<sup>14</sup> and epilepsy.<sup>12, 15, 16</sup> Zinc is now recognized as an important factor in the regulation of apoptosis.<sup>17</sup> The problem with the detection of free  $Zn^{2+}$  ions in the cell is the low abundance in the nanomolar range. Another challenge in detecting  $Zn^{2+}$  ion is the electronic configuration of  $Zn^{2+}$  ( $d^{10}$ ) leading to difficulties in monitoring  $Zn^{2+}$  ions directly. Therefore, there is a real need to develop other spectroscopic means for detection of  $Zn^{2+}$  ions.<sup>18</sup>

#### Biological importance of $Fe^{3+}$ ion

Iron is another essential element and plays a major role in many biochemical processes at the cellular level such as oxygen metabolism, electron transfer, and DNA and RNA synthesis (Figure 1.2).<sup>19</sup> Like the  $Zn^{2+}$  ion, most iron present in a biological system is tied up within a number of enzymes and proteins either for structural purposes or as a part of a catalytic site.<sup>20</sup> However, a minor fraction of iron (generally called labile iron pools) is bound to some organic anions (phosphates, citrates, carbonates, and carboxylates), polyfunctional ligands (polypeptides and siderophores), and surface

components of membranes (phospholipids head groups).<sup>19</sup> Both  $\text{Fe}^{2+}$  and  $\text{Fe}^{3+}$  ions are present in labile iron and can undergo a redox cycle in the presence of molecular oxygen. The labile iron is a source for the metabolic reaction that occurs within the cell and is a site for the generation of highly reactive oxygen species such as hydroxy radicals *via* the Fenton reaction ( Scheme 1.1).<sup>21, 22</sup>



*Scheme 1.1.* Generation of free radicals such as hydroxyl radicals *via* Fenton's reaction.<sup>21</sup>

The highly reactive radicals can interact with most of the biological materials including sugars, lipids, proteins, and nucleic acids resulting in peroxidative tissue damage.<sup>23</sup> The reactive oxygen species (ROS) has been suspected to play a key role in the pathogenesis of neurodegenerative diseases such as Alzheimer's,<sup>24</sup> Huntington's<sup>25</sup> and Parkinson diseases.<sup>26, 27</sup> Similarly, deficiency of  $\text{Fe}^{3+}$  ion is well known to cause anaemia, kidney and liver damages, diabetes, and heart diseases. But the labile bioiron is chelatable and therefore amenable for detection by metal sensing devices.<sup>28</sup>

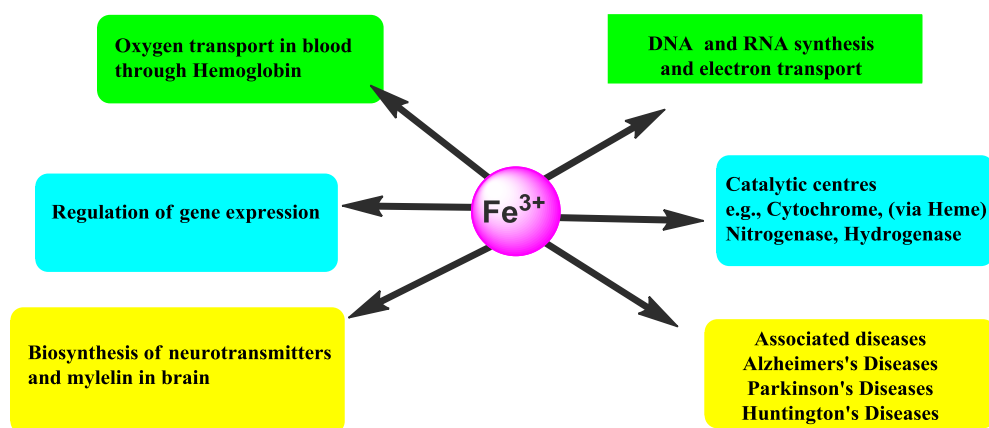


*Figure 1.2.* Biological roles of  $\text{Fe}^{3+}$  ions and its associated diseases.<sup>2</sup>

### *Environmental importance of Zn<sup>2+</sup> and Fe<sup>3+</sup> ions*

Several industrial processes such as coal burning, gold-mining, cement manufacturer, and smelting of iron introduce heavy metals such as iron and zinc in mineral forms into the environment.<sup>1,29</sup> These metal ions are also introduced into the environment by naturally occurring phenomena such as oceanic and volcanic emissions. Both of these processes can be problematic for environmental waste and pollution problems.<sup>30</sup> Soils may become contaminated with the zinc from these processes. Zinc then reduces the soil microbial activity resulting in a phototoxic effect, leading to reduce crop yields in agriculture.<sup>1</sup> The levels of zinc greater than 500 ppm in soil affects the plant's ability to absorb other essential metals such as iron and manganese.<sup>29</sup>

Iron (in the form of Fe<sup>3+</sup>) is present in low concentrations in sea water because of its poor solubility. The total dissolved concentration of iron in sea water at pH 8.2 is 0.76 nM, and the fraction of iron found as Fe<sup>3+</sup> ion is two percent.<sup>31</sup> This concentration is too low for microorganism growth: ideally the concentration should exceed 0.1 μM, magnitudes larger than actual iron availability.<sup>32</sup> Thus, the low solubility of iron in sea water affects the growth of phytoplankton which in turn affects the ecosystem, carbon cycle, and fisherie's productivity.<sup>33,34</sup> Uncontrolled growths of a number of harmful algal species such as *Alexandrium tamarense* in the sea are due to the higher concentration of Fe<sup>3+</sup> ions.<sup>35,36</sup>

### **Current Techniques for the Detection of Zn<sup>2+</sup> and Fe<sup>3+</sup> Ions**

A number of techniques are available for the detection of Zn<sup>2+</sup> and Fe<sup>3+</sup> ions. Each technique has its advantages and disadvantages which are summarized in the Table 1.1.



Table 1.1

*Advantages and disadvantages of different techniques for detection of metal ions*

Techniques	Advantages	Disadvantages
Atomic absorption spectrometry <sup>37</sup>	<ol style="list-style-type: none"> <li>1) Instrument is relatively simple and inexpensive.</li> <li>2) Widely used technique for the quantitative determination of metals at trace levels.</li> <li>3) Detection limit 0.1 to 100 ppm (parts per million).</li> <li>4) Rapid analysis is possible.</li> </ol>	<ol style="list-style-type: none"> <li>1) Limited to metal and metalloids.</li> <li>2) Sample preparation is tedious and time consuming.</li> <li>3) Sample is destroyed during analysis.</li> <li>4) Measured one element at time.</li> <li>5) Provide no information on the chemical form of the metals.</li> </ol>
Atomic Emission Spectroscopy (Flame photometry) <sup>38</sup>	<ol style="list-style-type: none"> <li>1) Simple and inexpensive.</li> <li>2) Useful for low ionization metals such as alkali and alkaline earth metals.</li> <li>3) Qualitative determination is also possible as each element emits its own characteristic line spectrum such as (<math>K^+</math>=violet at 766 nm, <math>Li^+</math>=red at 670 nm, <math>Ca^{2+}</math>=orange at 622 nm).</li> <li>4) Sensitivity is in ppm range.</li> </ol>	<ol style="list-style-type: none"> <li>1) Required a large amount of samples.</li> <li>2) Intensity of emission is very sensitive to changes in flame temperature.</li> <li>3) Affects analysis by purity, fuel, and oxidant flow rates, solution viscosity and contaminants in the samples.</li> <li>4) The elements such as carbon, hydrogen and halides cannot be detected due to its non-radiating nature.</li> <li>5) Difficult to obtain the accurate result of ions with higher concentration.</li> </ol>

Table 1.1 (continued).

Techniques	Advantages	Disadvantages
Inductively coupled plasma mass spectroscopy (ICP-MS) <sup>39</sup>	<ol style="list-style-type: none"> <li>1) Performs multi-element analysis.</li> <li>2) The high temperature and homogeneity of the source: it offers better signal stability and greater analytical precision.</li> <li>3) Sensitivity is in ppb range (parts per billion).</li> </ol>	<ol style="list-style-type: none"> <li>1) Very expensive.</li> <li>2) Solids must require dissolution before analysis.</li> <li>3) Instrumentation is complex and requires high operator's skill.</li> <li>4) Cannot detect halogens and noble gases.</li> <li>5) Additive interferences caused by ionized molecular species may occur.</li> </ol>
Voltammetry techniques <sup>40</sup>	<ol style="list-style-type: none"> <li>1) Portable, inexpensive, selective, and sample preparation is easy.</li> <li>2) Anodic stripping voltammetry, in particular, is most widely used for trace metal determination and has practical detection limit in ppt.</li> </ol>	<ol style="list-style-type: none"> <li>1) Samples must be oxidizable or reducible in the range where the solvent and electrodes are electrochemically inert.</li> <li>2) Provides very little or no information on species identity.</li> <li>3) Unsuitable for light metals (Na, K, and Al) and inorganic elements (S, Br).</li> </ol>
X-ray fluorescent spectroscopy <sup>41</sup>	<ol style="list-style-type: none"> <li>1) Non-destructive and applicable to very small samples.</li> <li>2) Applicable to both solid and liquid samples.</li> <li>3) Simultaneous multielement determinations are possible.</li> <li>4) Rapid analysis are possible.</li> <li>5) Detection limit is 10-100 ppm.</li> </ol>	<ol style="list-style-type: none"> <li>1) Instruments are often large, complicated and costly.</li> <li>2) The sensitivity is limited by matrix absorption, secondary fluorescence and scattering of the particles.</li> </ol>

The methods described are often sophisticated, cumbersome, and impractical for on-site testing. These instruments are often expensive to run; however, they can detect in the ppb (parts per billion) and ppt (parts per trillion) range which make them very sensitive. Therefore, the development of less expensive methods that utilize smaller, more portable instruments for the sensitive detection of trace elements is desirable for example, optical spectroscopy, which is a very attractive approach.

### Optical Spectroscopy

There is a continuous need for an analytical method to be simple, faster, and reliable for the detection of metal ions. Optical spectroscopy is of particular interest as it provides the basis for sensitive and inexpensive methods for detection. Optical spectroscopy is a group of spectroscopic analytical techniques that measures the intensity and wavelength of radiation absorbed and/or emitted by the sample. Optical spectroscopy includes both absorption spectroscopy and luminescence (photoluminescence and chemiluminescence) spectroscopy. Luminescence covers several techniques that involve the emission of radiation by either atoms or molecules, but varies in the manner in which the emission is induced. The theory behind optical spectroscopy can be highlighted with a Jablonski diagram (Figure 1.3).<sup>38</sup>

#### *Jablonski diagram*

Once a molecule absorbs energy in the form of electromagnetic radiation, it is excited from ground state ( $S_0$ ) to one of the higher electronically excited states ( $S_1$ ,  $S_2$ , and  $S_3$ ) (Figure 1.3). The absorption process is fast and occurs in the range of  $10^{-14}$ - $10^{-16}$  s. The molecule in the higher excited state quickly loses its excess vibrational energy in the form of heat to surrounding and reach the lowest vibration level of the first electronic

state ( $S_1$ ). This process is known as “internal conversion.” This occurs between the electronic states that have the same spin multiplicity, from singlet to singlet or triplet to triplet states. Internal conversion from  $S_1$  to  $S_0$  is often not possible because of large energy gaps between those two electronic states. Once the molecule is in the first electronic state, it can return by many ways to the ground state. The emission of photons from the first electronic state ( $S_1$ ) to ground state ( $S_0$ ) is called fluorescence. It generally occurs in the range of  $10^{-8}$ - $10^{-10}$  s. and emits at higher wavelength than absorption spectrum due to the loss in energy by internal conversion and vibrational relaxation. The difference between the maximum of the first absorbance band to the maximum of the fluorescence is called the Stokes shift. The first electronic state can change to a triplet excited state through intersystem crossing when they have relatively close energy. The emission of light from this triplet excited state to ground state is called phosphorescence. The relaxation time for phosphorescence is in the second time period, a lot slower than the fluorescence.<sup>42</sup>

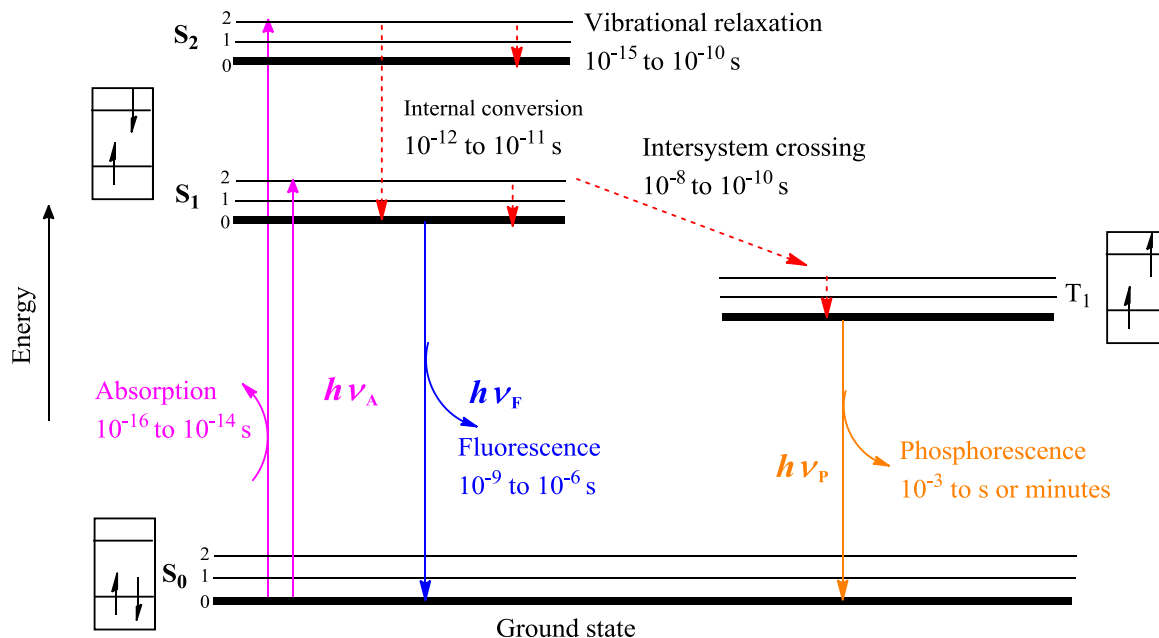


*Figure 1.3.* Simplified Jablonski diagram. The sequence of events leading to fluorescence and phosphorescence are shown.  $S_0$  is the ground state,  $S_1$  and  $S_2$  are excited singlet states;  $T_1$  is an excited triplet state. 0, 1, 2 represent vibration levels. Straight lines represent transition involving photons, dotted lines represent vibrational or thermal transitions.<sup>43</sup>

### *Chemiluminescence (CL)*

Another technique is when the excitation source is produced from a chemical reaction. When this happens, the process is called chemiluminescence. CL involves both chemical reaction and a luminescence process. One important requirement for CL is that the reaction must be exothermic to produce sufficient energy to produce the electronically excited state. Therefore, most CL reactions use oxygen, hydrogen peroxide, or similar reactive species as potential oxidants. Some useful reagents for solution phase CL are luminol, acridinium esters, aryl oxalates, dioxetanes, and tris(2,2'-bipyridyl)ruthenium (III) or  $\text{Ru}(\text{bpy})_3^{3+}$ .<sup>44-47</sup>

The advantages and disadvantages of the three techniques (UV-Vis, fluorescence, and chemiluminescence) are discussed below in Table 1.2.

Table 1.2

*Advantages and disadvantages of UV-Vis, fluorescence, and chemiluminescence*

Techniques	Advantages	Disadvantages
UV-Vis absorption <sup>38, 48</sup>	<ol style="list-style-type: none"> <li>1) Simple, portable, and inexpensive.</li> <li>2) Most organic molecules absorb UV-Vis light.</li> <li>3) Quantitative (Beer's law).</li> <li>4) Nondestructive, and naked eye detection of analytes.</li> <li>5) Rapid analysis is possible.</li> </ol>	<ol style="list-style-type: none"> <li>1) Mixture of molecules can be a problem due to overlap of absorption bands.</li> <li>2) Spectra are not highly specific for particular molecules.</li> <li>3) Sensitivity is low (can detect only up to micro molar concentration).</li> <li>4) Must follow Beer Lambert law.</li> <li>5) Light scattering can limit the precision of measurement.</li> </ol>
Fluorescence <sup>38, 42</sup>	<ol style="list-style-type: none"> <li>1) More sensitive than UV-Vis absorption (can detect pico, femto or even to a molecular level).</li> <li>2) Simple, portable, and inexpensive.</li> <li>3) Non destructive.</li> <li>4) More specific than UV-Vis absorption (only fluorescent molecule detected).</li> <li>5) Applicable to remote analysis using fibroptics or laser sources (e.g., atmospheric remote sensing).</li> <li>6) Selection of emission and excitation wavelength allows selectivity control.</li> <li>7) Adjustment of source intensity allows sensitivity control.</li> <li>8) Rapid analysis is possible</li> <li>9) Information content of measurement is high (Polarization, decay times as well as spectral data).</li> </ol>	<ol style="list-style-type: none"> <li>1) Samples containing mixture of substances cannot be analyzed.</li> <li>2) Very few molecules are naturally luminescent.</li> <li>3) More complicated equipment required compared to UV-Vis absorption.</li> <li>4) Accuracy and precision are generally lower than those of UV-Vis.</li> <li>5) Highly susceptible to multiplicative, and additive interferences unless specialized techniques are used.</li> </ol>

Table 1.2 (continued).

Techniques	Advantages	Disadvantages
Fluorescence <sup>38, 42</sup>	<ol style="list-style-type: none"> <li>10) More sensitive than UV-Vis absorption (can detect pico, femto or even to a molecular level).</li> <li>11) Simple, portable and inexpensive.</li> <li>12) Non destructive.</li> <li>13) More specific than UV-Vis absorption (only fluorescent molecule detected).</li> <li>14) Applicable to remote analysis using fiberoptics or laser sources (e.g., atmospheric remote sensing).</li> <li>15) Selection of emission and excitation wavelength allows selectivity control.</li> <li>16) Adjustment of source intensity allows sensitivity control.</li> <li>17) Rapid analysis is possible</li> <li>18) Information content of measurement is high (Polarization, decay times as well as spectral data).</li> </ol>	<ol style="list-style-type: none"> <li>6) Samples containing mixture of substances cannot be analyzed.</li> <li>7) Very few molecules are naturally luminescent</li> <li>8) More complicated equipment required compared to UV-Vis absorption.</li> <li>9) Accuracy, and precision are generally lower than those of UV-Vis. Highly susceptible to multiplicative, and additive interferences unless specialized techniques are used.</li> </ol>
Chemiluminescence <sup>44-47</sup>	<ol style="list-style-type: none"> <li>1) Simple, rapid, and inexpensive.</li> <li>2) Highly sensitive, and detection limit in the range of pico to femto molar concentration.</li> <li>3) No external source is required for excitation as compared to UV-Vis, and fluorescence.</li> <li>4) No scattering or background photoluminescence signal.</li> </ol>	<ol style="list-style-type: none"> <li>1) Limited to relatively few analytes.</li> <li>2) Lack of selectivity (a CL reagent may yield significant emission not for just one unique analyte) is major problem.</li> <li>3) Sensitive to temperature, solvent, ionic strength, pH, and other species present in the system.</li> </ol>

Table 1.2 (continued).

Techniques	Advantages	Disadvantages
Chemiluminescence	5) No problems related to instability of the external source. Reduction of interferences due to a nonselective excitation process, and simple instrumentation.	4) The reaction is destructive for both analyte and CL reagent. 5) Reagents and solvents must be of highest purity as the impurities can cause a nonspecific background signal that degrades assay sensitivity 5) Not applicable for remote sensing as in fluorescence. 6) Cannot be used for multicomponent determinations on mixture of analytes without a separation step.

#### Chemosensors

Chemosensors are molecular devices that transform chemical information into measurable signals in the presence of target analyte.<sup>49</sup> Since the two different processes occur during an analyte detection i.e., molecular recognition and signal transduction, chemosensors are usually designed based on the “classic” reporting unit-spacer-receptor principle (Figure 1.4).<sup>50</sup> The receptor is responsible for the binding of an analyte, while the reporting unit e.g., chromophore or fluorophore changes its properties upon coordination with the analyte. The spacer can establish the geometry of the system and tune the electronic interaction between the two active moieties. The three components in the “classical” chemosensor are all key in the design of successful molecular probes.



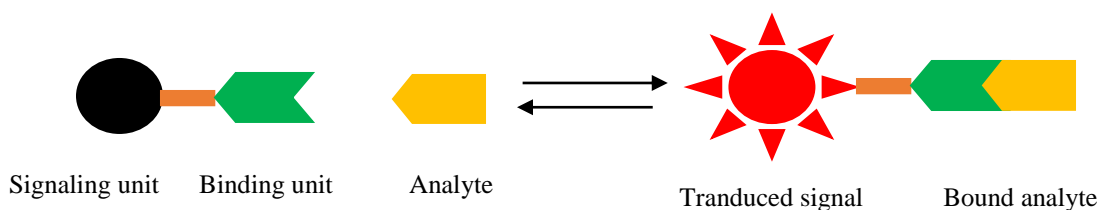


Figure 1.4. Fluorophore/chromophore-spacer-receptor probe.

### The sensing motif

This functional group produces a change in spectroscopic signal upon the detection of an analyte. A sensing motif is typically a fluorophore or chromophore that is highly conjugated and is rigid and planar. Common fluorophores or/and chromophores used as sensing motifs include pyrene, rhodamine, fluorescein, and coumarin whose structure, the maximum absorbance and emission are shown in Figure 1.5.

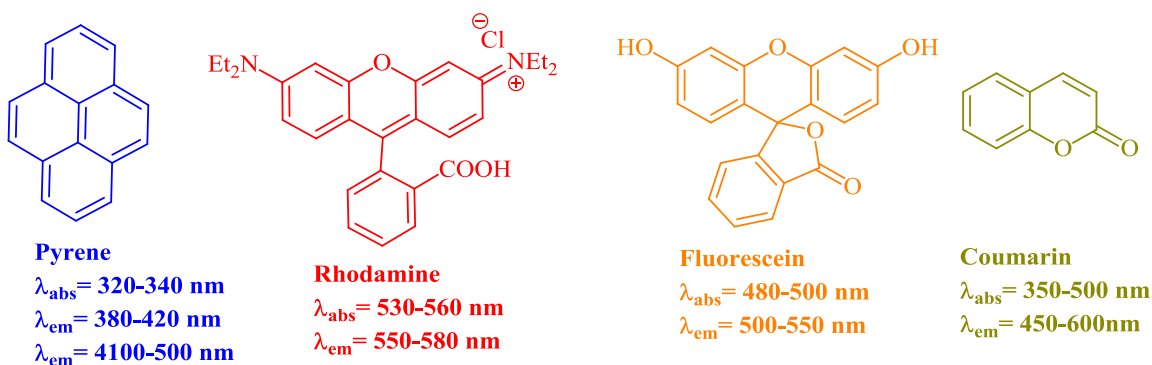


Figure 1.5. Different sensing motifs commonly used in design of chemosensors, highlighting the absorbance, emission, and excitation wavelength.

### Optical properties of pyrene

Pyrene is one of the most commonly used fluorogenic probes in the design of chemosensors. This is due to pyrene's unique properties which are extremely sensitive to the polarity of local environment.<sup>51, 52</sup> Pyrene has three strong UV-Vis absorbance bands at 338, 323, and 340 nm, and the fluorescence monomer emission is seen between 380 nm and 420 nm. In addition to the monomer emission, pyrene can form excimers (see

below) generally located between 410-480 nm depending on the distance between pyrene moieties, through which structural information can be analyzed.<sup>53</sup> This monomer-excimer equilibrium has been used as a sensing principle in several pyrene-based receptors to study the conformation changes in host-guest recognition.<sup>54-56</sup>

An excimer, as defined by Berk, is a dimer that is associated in the excited state but dissociated in the ground state.<sup>57</sup> This is a non-radioactive process which can occur between non-covalent molecular complexes, forming either an exciplex or excimer, between different molecules or the same molecule, respectively. The absorption/emission band associated with the excimer/exciplex will occur at a longer wavelength that is significantly different, often a rather broad featureless transition over a wide range of wavelengths (Figure 1.6).<sup>58</sup> To be more specific, there are two different types of excimers: dynamic ( $E_d$ ) and static ( $E_s$ ). Dynamic excimer ( $E_d$ ) is the dimeric molecular photo association which results from the collision of a molecule in its lowest singlet excited state with an identical molecule in the ground state (Figure 1.7A). The lifetime of  $M^*$  (excited state monomer) is relatively long to allow its diffusive encounter with  $M$  (ground state monomer). Static excimer results from the excitation of a ground state van der Waals dimer (ground state dimer)  $M \cdots M$  formed by  $\pi$ - $\pi$  stacking or hydrophobic interaction in water. The two molecular components of dynamic excimers are free to fully overlap in comparison to static excimers which are maintained together by other interactions which may not maximize their overlap. Hence static excimer has lower stabilization energy than dynamic excimer and occurs at higher energy than dynamic excimer (Figure 1.7B).<sup>59, 60</sup> The static and dynamic excimers can be differentiated by two ways. The first one is an excitation experiment in which the excitation spectra of the

system under study will be broadened and bathochromically shifted in the  $E_s$  state. This is not seen in the  $E_d$  state, i.e., the excitation spectrum for a dynamic excimer will be the same as the monomer maximum emission wavelength. The second is time resolved experiment in which the time-dependent excimer emission profile shows a rising profile for a dynamic system but not for static excimer. The radiative lifetime of the monomer and excimer of pyrene were found to be 680 and 690 nanoseconds, respectively.<sup>61, 62</sup>

One important factor that needs to be considered while working with the pyrene based sensors is concentration, especially if one is investigating conformational changes induced by guest binding. The excimer must be formed through intramolecular interaction rather than intermolecular interaction between the pyrene units of different molecules. When the concentration of the solution is significantly high (millimolar to molar), a false positive can be observed as the excimer emission band, possibly due to the interaction between two adjacent molecules in the solution rather than the host-guest complex. This can be easily ruled out by carrying out dilution experiments. However, if excimer formation is seen at very low concentrations, for example nanomolar, this can lead to highly sensitive molecular receptors and detect analytes at low concentrations.<sup>53</sup>

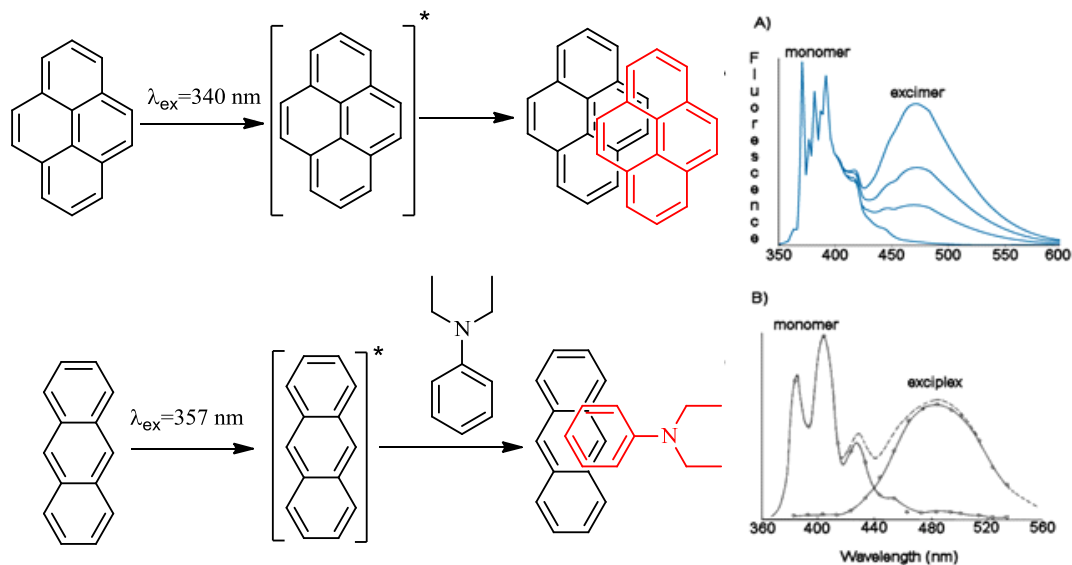


Figure 1.6. (A) Emission spectra of pyrene, and its excimer. As the concentration decreases (6 mM to 0.09 M) the excimer band at 490 nm loses intensity, and (B) the emission spectrum of monomer, and exciplex.<sup>53</sup>

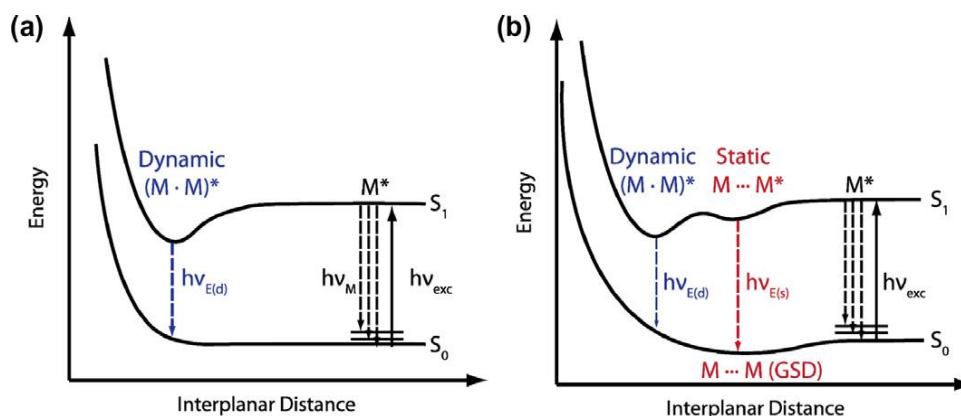
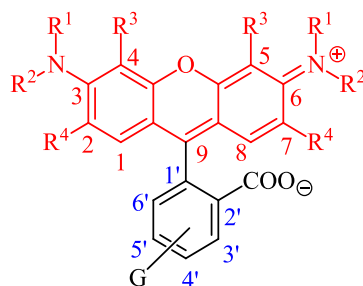


Figure 1.7. Potential energy diagrams for (A) pyrene excimer formation  $M-M^*$  in the absence of ground state dimerization, and (B) for the GSD excimer, showing the  $E_d$  and  $E_s$ . "Reprinted with permission from Winnik, F. M., Photophysics of preassociated pyrenes in aqueous polymer solutions and in other organized media. *Chem. Rev.* **1993**, 93, 587-614. Copyright 1993 American Chemical Society."

### Optical properties of rhodamine

Rhodamine belongs to the family of xanthene (highlighted in red color in Figure 1.8) and has excellent photophysical properties, which displays absorption and emission bands in the visible region of electromagnetic spectrum (550- 600 nm). Rhodamine

derivatives have high extinction coefficient ( $1.2 \times 10^5 \text{ M}^{-1} \text{ cm}^{-1}$ ), high fluorescence quantum yield ( $\Phi=0.53$  for cationic form and 0.70 for zwitterionic form in EtOH), and high photo stability against light. Different substitutions patterns on the xanthen ring lead to different photophysical behavior.<sup>63</sup> The fluorescence quantum yields of rhodamine 6G and rhodamine 101 are identical, close to unity and nearly temperature and solvent independent.<sup>64</sup> The main difference between the two dyes is in the substitution of the amino group. Rhodamine 101 has the nitrogen atoms rigidly linked to the xanthen ring whereas rhodamine 6G has free amine nitrogen secondary substituents with only one alky group. In contrast, in rhodamine B with two alky groups at each nitrogen atoms, the fluorescence quantum yields depends on the temperature, viscosity, and solvent polarity. At low temperature, its fluorescence quantum yields is close to unity as for rhodamine 6G and rhodamine 101.<sup>65</sup> The fundamental reason behind this variation is not well understood. Different mechanisms have been proposed to explain the photo physic of rhodamine B such as amino group rotation hindered by solvent viscosity, amino NH vibration, and the formation of twisted intramolecular charge transfer state.<sup>66</sup>



*Figure 1.8.* The rhodamine motif, the xanthen unit is highlighted in (Red) and numbering system utilized in IUPAC.<sup>67</sup>

*pH effect on the rhodamine molecule*

The pH at which rhodamine probes can operate is a very important factor, together with polarity.<sup>67</sup> The absorption spectra of very dilute solutions of rhodamine B as a function of acidity is shown in Figure 1.9.<sup>68</sup> Absorption band one is indicative of the zwitterionic form of rhodamine B and is believed to exist between pH 4-13 (Figure 1.10). The lactone ring opens in polar solvents (alcohol, acetone, or water to form a zwitterion  $R^+$ ). Absorption band two represents the cationic form of rhodamine B and is believed to exist between pH 1-3. The carboxyl anion of zwitterion  $R^+$  is protonated when the pH is lowered to 3. Absorption band two is almost identical to absorption band one but shifted by 3 m $\mu$  to longer wavelength. It is possible to protonate the tertiary nitrogen atoms below pH 1 to form structure  $RH_2^{2+}$ . This additional proton hinders the resonance in one ring which forms an orange color and is represented by absorption band three (Figure 1.9). Concentrated sulphuric acid can protonate the second nitrogen atom giving structure  $RH_3^{3+}$ . It is represented by absorption band four and has yellow color. Absorption band five is the colorless solution of rhodamine in non-polar solvents like benzene and ether (Figure 1.10), typical of aromatic benzene system.

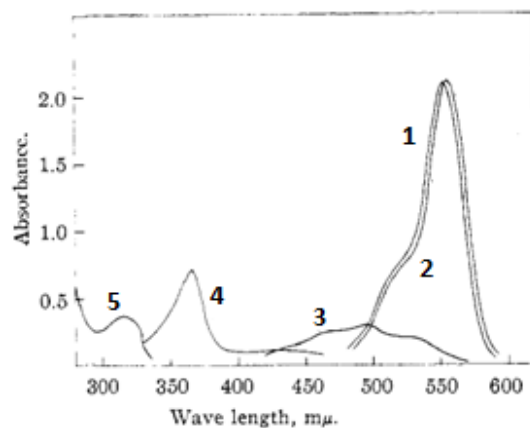


Figure 1.9. Absorption spectra of dilute solutions of rhodamine B (10  $\mu\text{M}$ ). Absorption band one=1.0 M KCl, 0.03 M  $\text{NH}_3$ ; Absorption band two=1.0M KCl, 4 mM HCl; Absorption band three= 5.0 M HCl; Absorption band four= concd.  $\text{H}_2\text{SO}_4$ ; Absorption band five= benzene. "Reprinted with permission from Ramette, R. W.; Sandell, E. B., Rhodamine B equilibria. *J. Am. Chem. Soc.* **1956**, 78, 4872-8. Copyright 1956 American Chemical Society."

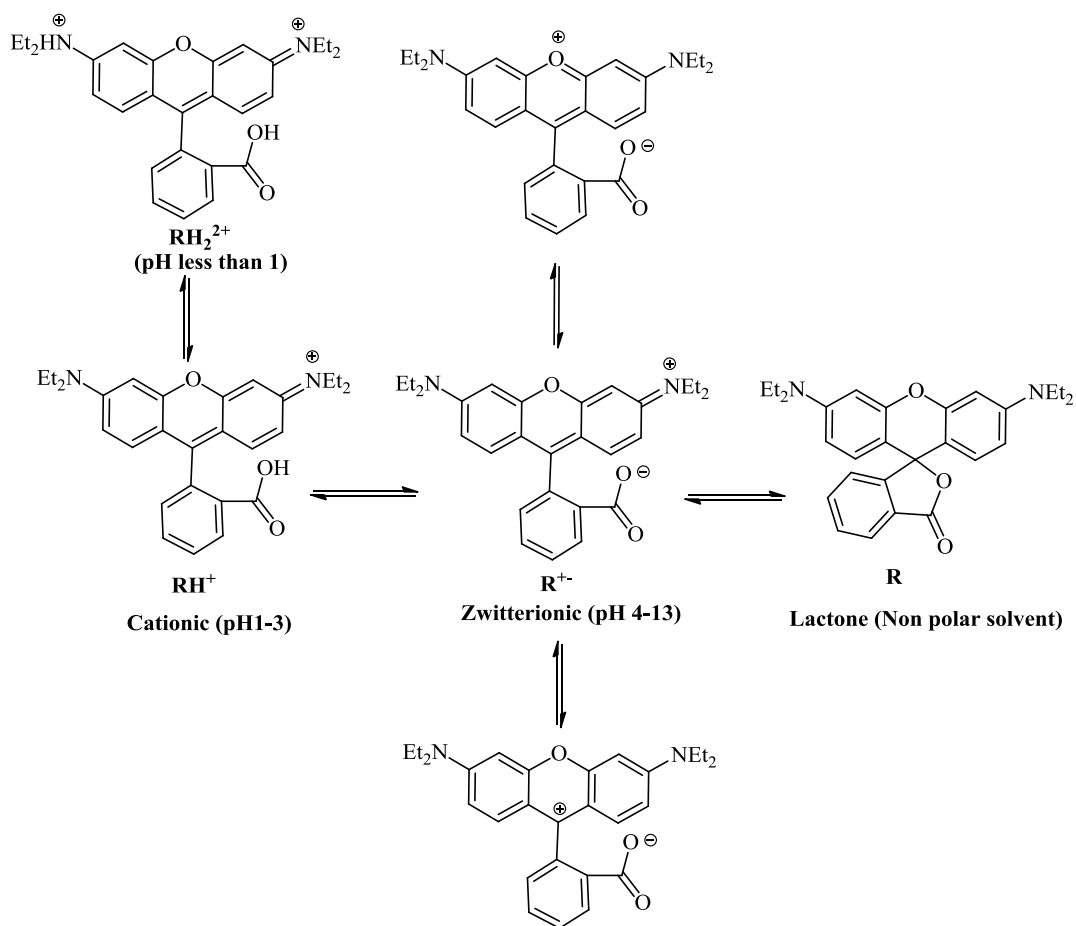
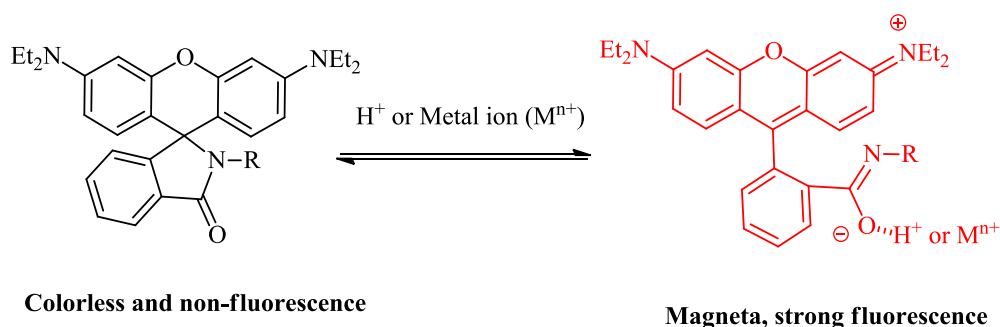


Figure 1.10. The rhodamine B species that exist under different pH conditions.<sup>67, 68</sup>

### Mechanism for rhodamine-based chemosensor

All of the chemosensors that incorporate the rhodamine spirolactam molecule are non-fluorescent and colorless because of the lack of conjugation in the closed ring forms. The spirolactam ring opens upon binding with suitable metal ions or in the solution of strong acid (pH 1-3) as previously discussed (Figures 1.9 and 1.10). The ring opening brings back the conjugation to the system producing a strong fluorescence emission and a pink color (Scheme 1.2).<sup>69</sup> Therefore, this motif can be used as an “Off-On” fluorescent sensor.



Scheme 1.2. Spirolactam ring-opening process of rhodamine derivatives.<sup>69</sup>

### Receptors (A binding site)

The binding site is the part of chemosensor that will coordinate to the metal ion. It is a region of the molecule that has the correct size, shape, geometry, and complimentary functionalities to interact with the other molecule through both non-covalent interaction and coordinate covalent bonds. The nature of binding site depends upon the analyte of choice, i.e., a cation, anion, or neutral species. The binding site has to be complimentary to the “guest” species but be able to bind ions efficiently with a high degree of thermodynamic stability which usually depends upon the characteristics of the ions such as ionic radius, charge density, coordination number, oxidation states, and polarizability. In summary, binding sites of the molecular probe must be complementary to the guest in



terms of size, shape, and chemical properties to have “strong” and selective binding. For example, a classical example is the crown ether which has oxygen atoms (e.g., [18] crown-6) that can coordinate to the alkali metal ion (e.g.,  $K^+$ ) more strongly ( $\log K = 6.08$  in  $CH_3OH$ ) than the azamacrocycles (e.g., diaza [18] crown-6) which have softer nitrogen atoms ( $\log K = 2.04$  in  $CH_3OH$ ).<sup>70</sup> A chemosensor with two or more binding sites connected by covalent bonds forms a more stable complex than with the similar system that are not connected due to the chelate effect.<sup>70, 71</sup> The stability of host guest can further be enhanced by preorganising the host molecules. It is defined as the host having a series of binding sites which do not require a significant conformational change to bind a guest to form more stable complex. Examples of preorganized hosts are mostly cyclic in nature for example crown ethers, cryptands, and cavitands (Figure 1.11).<sup>70, 72</sup>

#### *Cation binding motifs*

The Lewis basic nature of an atom is an effective way to coordinate metal ions. Crown ethers, aza crowns, cryptands, and imines contain nitrogen and oxygen atoms which are used to coordinate metal ions. For examples, triazole and schiff base are used as cation binding sites for coordination of metal ions (Figure 1.11).

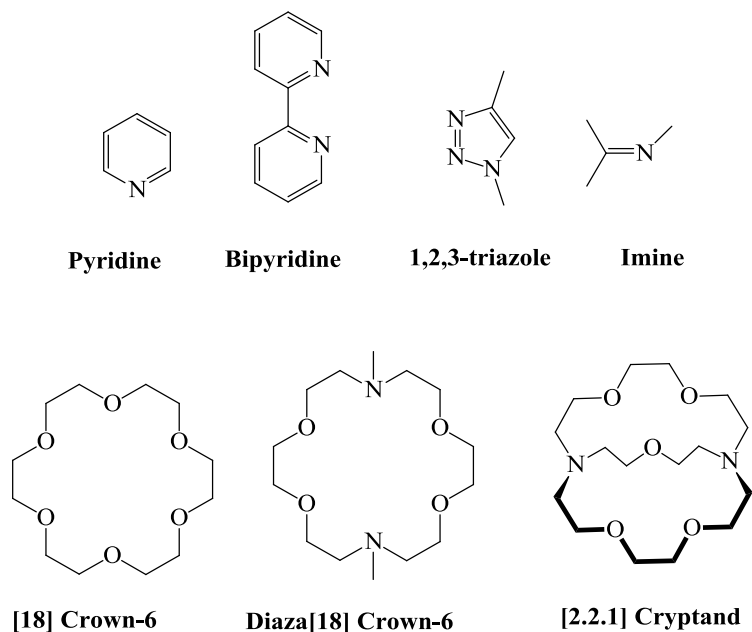
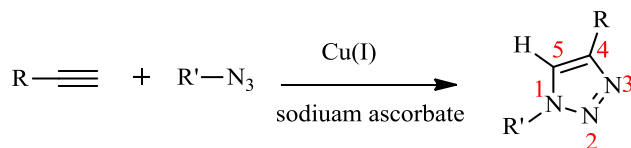


Figure 1.11. Common binding motifs utilized in receptors design.<sup>73</sup>

### The triazole motifs

The triazole functional group has been used as a cation binding site in number of chemosensors.<sup>74</sup> It is often synthesized from an azide functional group and alkyne using the so called “Click” reaction (Scheme 1.3).<sup>75</sup> Additionally, the “Click” reaction is an efficient way to connect a fluorophore group and receptors in favorable geometry.<sup>76</sup> It has molecular dimensions and planarity similar to the amide bond and coordinative properties similar to substituted imidazole.<sup>77-79</sup> The basicity of nitrogen at third position is suitable for binding metals, for example  $Zn^{2+}$  ions. It has also been shown that the proton attached to carbon 5 (Scheme 1.3) can act as an effective hydrogen bond donor for anions.<sup>80-82</sup>



Scheme 1.3. Cu (I)-catalysed azide-alkyne cycloaddition to afford a 1,4-substituted 1,2,3-triazole.<sup>83</sup>

## Fluorescent Mechanism for Ion Sensing

Now the scene has been laid out concerning the design of the molecular probe that incorporates a fluorophore. The final part is to introduce the types of fluorescence mechanism that are used for the molecular probes. There are several mechanisms that are well known to play an important part in sensing. These include:

- Photoinduced Electron Transfer (PET): This includes CHEF, CHEQ, and heavy atom effect.
- Photoinduced Charge Transfer (PCT)
- “On or Off” excimer emission
- Fluorescence resonance energy transfer (FRET)

### *Photoinduced Electron Transfer (PET) Mechanism*

In this mechanism, the metal ion receptor acts as an electron donor while the fluorophore acts as an electron acceptor. Upon excitation by photon, an electron of the fluorophore is promoted from highest occupied molecular orbital (HOMO) to the lowest unoccupied molecular orbital (LUMO) which enables PET from the HOMO of the donor (binding sites) to that of the fluorophore, causing fluorescence quenching of the latter. But after binding the target analyte (metal ion, anion, or neutral species), HOMO of donor becomes lower in energy than the fluorophores moiety and the PET process is no longer possible, and the chemosensor begins to fluoresce. In other words, enhancement of fluorescence takes place upon binding with the analyte.<sup>84</sup> Many fluorescent sensors utilize this mechanism (Figure 1.12).<sup>85</sup> In the case of metal ion binding, this effect is called chelation-enhanced fluorescence (CHEF).<sup>86, 87</sup>

However, the coordination of metal ions such as  $\text{Fe}^{3+}$ ,  $\text{Cr}^{3+}$ ,  $\text{Cu}^{2+}$ ,  $\text{Hg}^{2+}$ , and  $\text{Pb}^{2+}$  ions does not induce CHEF but quenches the fluorescence. This is known as a chelation-enhanced quenching effect (CHEQ).<sup>88, 89</sup> There are many ways in which metals can quench the fluorescence. The metal ions such as  $\text{Hg}^{2+}$  and  $\text{Pb}^{2+}$  ions, due to spin-orbit coupling, can enhance the intersystem crossing from the excited state to the corresponding excited triplet state, known as the heavy atom effect, whereby the fluorescence is quenched by non-radiative decay.<sup>90</sup> While the quenching of fluorescence by redox active species such as  $\text{Fe}^{3+}$  and  $\text{Cu}^{2+}$  ions can be a consequence of their empty *d*-orbitals which can accept an electron donated by the excited fluorophore.<sup>88, 91</sup>

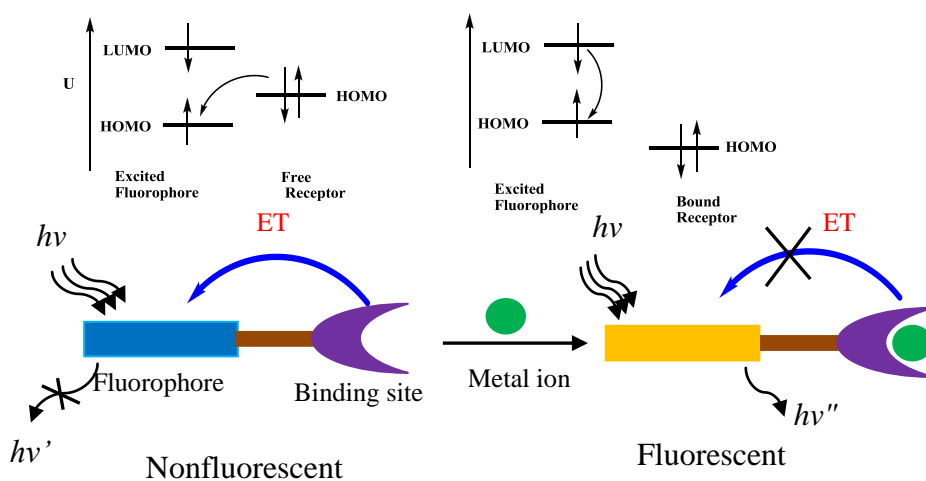
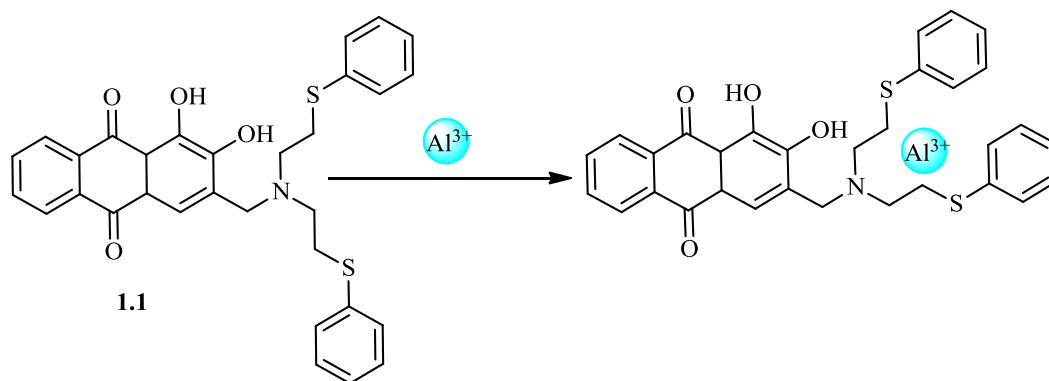


Figure 1.12. Principle of cation recognition by fluorescent PET sensors.<sup>84</sup>

Zheng et al. report a PET-based chemosensor (1.1) for  $\text{Al}^{3+}$  ions by using 1,2-dihydroxyanthraquinone as the fluorophore and a conjugated N,N-bis(2-phenylthioethyl)amine as the chelating unit.<sup>92</sup> Compound **1.1** exhibited a maximum absorbance band at 446 nm in EtOH:H<sub>2</sub>O (1:1, v/v). Upon addition of 2.5 equivalents of  $\text{Al}^{3+}$  ions, absorbance bands at 395 and 600 nm decreased, but an increase at 504 nm was

seen with three clear isobestic points at 446, 579, and 650 nm. The isobestic point implies the conversion of the free compound **1.1** to a single  $\text{Al}^{3+}$  species, means that there are two distinct species in equilibrium. Compound **1.1** shows no fluorescence emission over the entire pH window. This is because the PET derived from the sulfur donor to the fluorophore is always switched on even the PET process from a nitrogen donor was blocked by protonation or intramolecular hydrogen bonding in lower to neutral pH. While under basic condition, the PET from both the nitrogen and sulfur donate the electron density to the fluorophore which was subsequently switched on due to deprotonation of the phenyl hydroxyl group leading to a complete quenching of the fluorescence. Upon binding of  $\text{Al}^{3+}$  ion, a significant fluorescence enhancement which turns on the signal with ratios over 100-fold was achieved by the inhibition of the PET mechanism from both the sulfur and nitrogen donors to the fluorophore. The response of **1.1** to the other metal ions was also studied ( $\text{Ag}^+$ ,  $\text{Ca}^{2+}$ ,  $\text{Cd}^{2+}$ ,  $\text{Co}^{2+}$ ,  $\text{Cr}^{3+}$ ,  $\text{Cu}^{2+}$ ,  $\text{Fe}^{3+}$ ,  $\text{Hg}^{2+}$ ,  $\text{K}^+$ ,  $\text{Mg}^{2+}$ ,  $\text{Na}^+$ ,  $\text{NH}_4^+$ ,  $\text{Ni}^{2+}$ , and  $\text{Zn}^{2+}$ ), but no fluorescence emission was seen. The association constant ( $K_{11}$ ) of **1.1** with  $\text{Al}^{3+}$  ion was calculated to be  $8.8 \times 10^3 \text{ M}^{-1}$  by nonlinear least-square analysis with a detection limit of  $5.0 \times 10^{-7} \text{ M}$  (13 ppb) (Scheme 1.4).



*Scheme 1.4.* Proposed binding of compound **1.1** with  $\text{Al}^{3+}$  ion.<sup>92</sup>

### *Photoinduced Charge Transfer (PCT) Mechanism*

When both electron donating and electron withdrawing groups are present in the same fluorophore, intramolecular charge transfer takes place from donor to the acceptor upon excitation of light. This makes the change in the dipole moment, and its effect is seen as a bathochromic (red direction) or hypsochromic (blue direction) shift in the absorption and emission bands of the spectra, and there are changes in the extinction parameters too. Thus, close interaction of donor or acceptor moiety with cation or anion will change the photo physical-properties of the fluorophore. Coordination of an electron donor group with a cation decrease its electron donating character which results in the reduction of conjugation causing a blue shift of the absorption spectrum together with a decrease of the molar absorptivity. Conversely, coordination of electron withdrawing group with cation enhances its electron-withdrawing character resulting in a red shift of the absorption band and increase in molar absorptivity.<sup>93, 94</sup> In principle, the fluorescence spectra are shifted in the same direction as those of the absorption spectra. In addition to these shifts, changes in quantum yields and lifetimes are often observed. All of these photophysical effects are obviously dependent on the charge, and the size of the cation and selectivity of these effects are expected (Figure 1.13).<sup>95</sup>

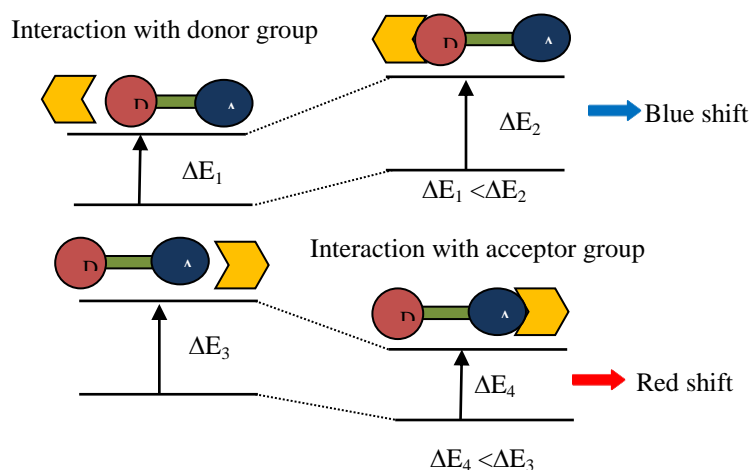


Figure 1.13. Spectral displacements of PCT sensors resulting from interaction of a bound cation with an electron-donating or electron-withdrawing group.<sup>96</sup>

Nagano et al. have designed and synthesized fluorescent molecule (**1.2**) for sensing  $\text{Zn}^{2+}$  ion by using 4-amino-1,8-naphthalimide as a fluorophore and a  $\text{N}_3\text{N}'_3$ -tetrakis(2-pyridylmethyl) ethylenediamine (TPEN) derivative as a  $\text{Zn}^{2+}$  ion binding site.<sup>97</sup> Compound **1.2** is the first  $\text{Zn}^{2+}$  ion sensitive off–on fluorescent sensor based on the internal charge transfer (ICT) mechanism on a 4-amino-1,8 naphthalimide. Compound **1.2** showed a one major absorption band at 437 nm, and no fluorescence emission was seen at 507 nm ( $\Phi=0.039$ ) in HEPES buffer (100 mM, pH 7.4). The addition of  $\text{Zn}^{2+}$  ions to **1.2** gives a green fluorescence at 507 nm ( $\Phi=0.942$ ) and characteristic absorption band at 380 nm. The addition of one equivalent of  $\text{Zn}^{2+}$  ions increases the fluorescence emission intensity of **1.2** (5 mm) by more than 20 times with a blue shift of 57 nm. The fluorescence emission of compound **1.2** was not changed between pH of 3-9 indicating that the fluorescence increment of **1.2** upon addition of  $\text{Zn}^{2+}$  ions was not due to PET mechanism but instead by an ICT mechanism. This ICT mechanism is further confirmed by the low quantum yield of  $[\text{Zn}(\mathbf{1.3a})]^{2+}$  ( $\Phi=0.016$ ) and  $[\text{Zn}(\mathbf{1.3b})]^{2+}$  ( $\Phi=0.392$ ) which

have different electron donating substituent's at the fourth position of 1,8-naphthalimide. Compound **1.2** showed high selectivity for  $\text{Zn}^{2+}$  ion over other metal ions ( $\text{Na}^+$ ,  $\text{K}^+$ ,  $\text{Ca}^{2+}$ ,  $\text{Mg}^{2+}$ ,  $\text{Mn}^{2+}$ ,  $\text{Fe}^{2+}$ ,  $\text{Fe}^{3+}$ ,  $\text{Co}^{2+}$ ,  $\text{Ni}^{2+}$ , and  $\text{Cu}^{2+}$ ). However,  $\text{Cd}^{2+}$  ion did show a small spectroscopic response, presumably due to the similar chemistry as  $\text{Zn}^{2+}$  ions. The dissociation constant,  $K_{11}$ , for  $\text{Zn}^{2+}$  ion was calculated to be 1.1 nM at pH 7.4 in a high salt environment (100 mM HEPES buffer,  $I = 0.1$  M ( $\text{NaNO}_3$ )). The biological application of **1.2** was also investigated in cultured HeLa cells. The HeLa cells were incubated with compound **1.2** only showed a fluorescence signal which could possibly be due to the solvatochromic properties of **1.2**. The intracellular fluorescence was increased on addition of a  $\text{Zn}^{2+}$  ion and zinc-selective ionophore, pyrithione (2-mercaptopyridine N-oxide, 5 mM) to the medium and decreased on addition of the cell-membrane-permeable chelator TPEN (100  $\mu\text{M}$ ). Thus, compound **1.2** can be used to reversibly monitor changes in intracellular ionic  $\text{Zn}^{2+}$  ion.

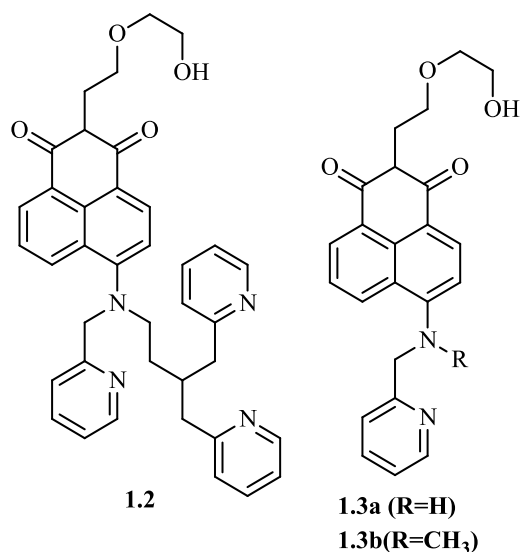


Figure 1.14. Structures of compounds **1.2**, **1.3a**, and **1.3b**.<sup>97</sup>



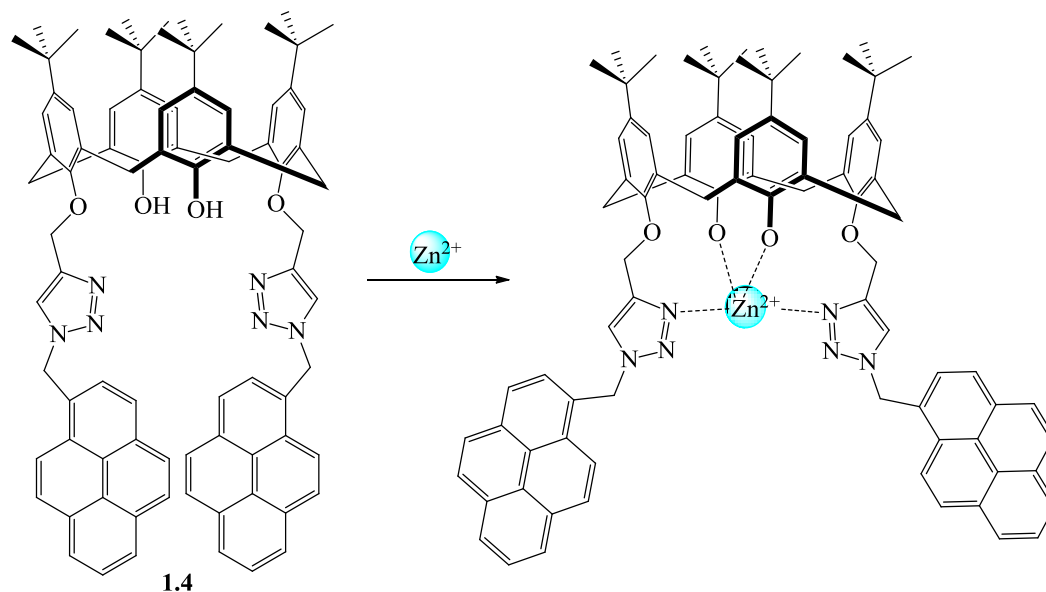
*“On or Off” excimer emission*

When a molecular receptor incorporates a pyrene or anthracene group, a structureless broad band known as excimer is formed at longer wavelengths in addition to a monomer emission due to close interaction of its excited state with ground state which has been previously discussed (Figures 1.6 and 1.7). An excimer may also form from an excited monomer if the interaction takes place within the lifetime period of the latter. Thus, excimers are possible to form by relatively long-lived monomer excited states. The ratio of the fluorescence intensities correspond to monomer and excimer emission on molecular mobility and microviscosity. When a molecular receptor contains two fluorophores whose mutual distance is affected by cation/anion coordination, recognition of this cation/anion can be monitored by the monomer/excimer fluorescence-intensity ratio. Cation binding may favor or hinder excimer formation. In any case, such a ratiometric method can allow self-calibration measurement and is of great interest for practical applications.<sup>84</sup>

Kim et al. have developed fluorescent chemosensor **1.4** for  $\text{Cd}^{2+}$  and  $\text{Zn}^{2+}$  ions by modifying the bottom rim of a calix[4]arene with a 1,2,3-triazole using click chemistry.<sup>98</sup> Compound **1.4** (6  $\mu\text{M}$ ) shows both monomer and excimer emissions at 395 nm and 476 nm, respectively, upon excitation at 343 nm in  $\text{CH}_3\text{CN}$ . The changes in fluorescence were studied by adding perchlorate salts of metal ions such as  $\text{Li}^+$ ,  $\text{Na}^+$ ,  $\text{K}^+$ ,  $\text{Rb}^+$ ,  $\text{Cs}^+$ ,  $\text{Mg}^{2+}$ ,  $\text{Ba}^{2+}$ ,  $\text{Ca}^{2+}$ ,  $\text{Sr}^{2+}$ ,  $\text{Ag}^+$ ,  $\text{Cu}^{2+}$ ,  $\text{Zn}^{2+}$ ,  $\text{Cd}^{2+}$ ,  $\text{Hg}^{2+}$ , and  $\text{Pb}^{2+}$ . Addition of  $\text{Zn}^{2+}$  or  $\text{Cd}^{2+}$  ions enhanced the monomer emission but reduced excimer emission in the ratiometric manner showing two triazole units as efficient metal ion binding sites. The calculated binding constant was  $K_{11} = 5.2 \times 10^4$  and  $1.7 \times 10^4 \text{ M}^{-1}$  for  $\text{Cd}^{2+}$ , and  $\text{Zn}^{2+}$  ions,

respectively. The quantum yield of compound **1.4**,  $[\text{Cd}(\mathbf{1.4})]^{2+}$ , and  $[\text{Zn}(\mathbf{1.4})]^{2+}$  referenced to anthracene, were determined to be 0.229, 0.267, and 0.258, respectively.<sup>99</sup>

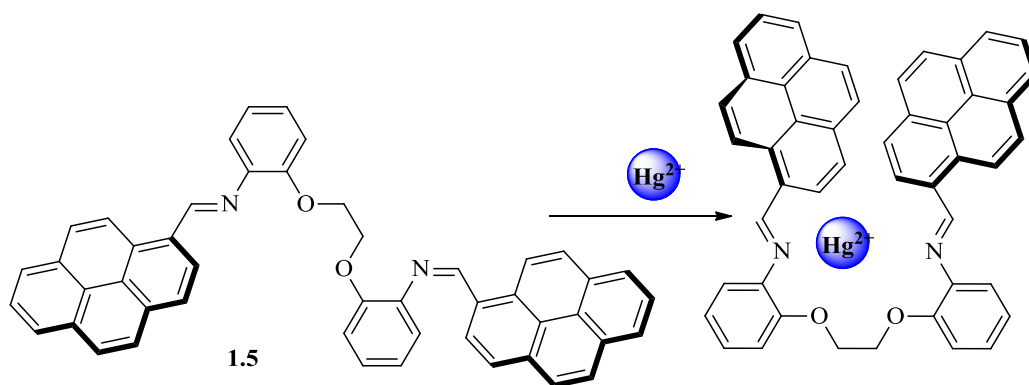
A model compound with only one pyrene was also prepared but did not show any significant spectral change which confirms that the excimer formation is due to a intramolecular formation as opposed to intermolecular formation (Scheme 1.5).



*Scheme 1.5.* Proposed structure for binding  $\text{Zn}^{2+}$  ions by compound **1.4**.<sup>98</sup>

A pyrene-based derivative bearing an azadiene group **1.5** was synthesized by Yao and co-workers as a ratiometric chemosensors for  $\text{Hg}^{2+}$  ion in aqueous  $\text{CH}_3\text{CN}$  solution.<sup>100</sup> Compound **1.5** shows three pyrene absorption bands at 238, 283, and 326 nm in  $\text{CH}_3\text{CN}$ . A new red shifted band was formed at 442 nm on addition of one equivalent of  $\text{Hg}^{2+}$  changing the color from colorless to pale yellow. A red shift from monomer (406 nm) to excimer (462 nm) was also observed in the fluorescence emission upon addition of  $\text{Hg}^{2+}$  in  $\text{CH}_3\text{CN}$ :HEPES buffer (50 mM, pH= 7.2). This observation implies that a coordination of **1.5** with  $\text{Hg}^{2+}$  ions presumably changed the structure of compound **1.5** to stacked or folded conformation resulting in the switch of the pyrene monomer emission

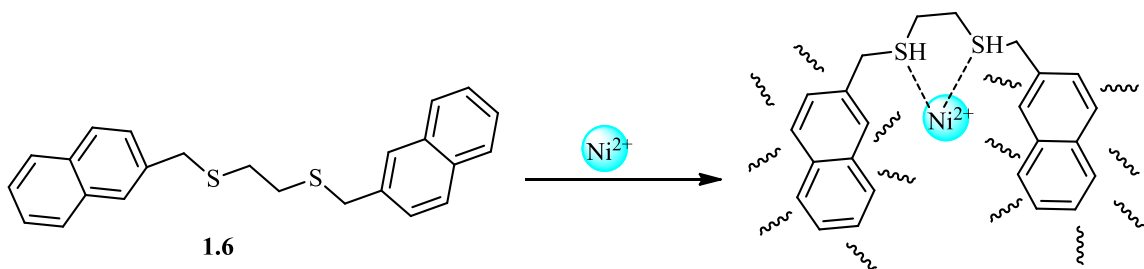
to an excimer emission. Other metal ions ( $\text{Na}^+$ ,  $\text{K}^+$ ,  $\text{Mg}^{2+}$ ,  $\text{Ca}^{2+}$ ,  $\text{Cd}^{2+}$ ,  $\text{Mn}^{2+}$ ,  $\text{Fe}^{3+}$ ,  $\text{Ni}^{2+}$ ,  $\text{Ag}^+$ ,  $\text{Pb}^{2+}$ ,  $\text{Co}^{2+}$ , and  $\text{Cr}^{3+}$ ) were also investigated but showed weak response as compared to  $\text{Hg}^{2+}$ . The association constant of **1.5** with  $\text{Hg}^{2+}$  ion was calculated to be  $4.3 \times 10^5 \text{ M}^{-1}$  with detection limit of  $2 \times 10^{-7} \text{ M}$  (40 ppb). The mode of coordination was also confirmed by  $^1\text{H}$  NMR spectroscopy whereby the imine protons were shifted by 1.22 ppm in the downfield, and ether-methylene protons shifted to up field by 0.12 ppm on coordination of  $\text{Hg}^{2+}$  ion. On the basis of the  $^1\text{H}$  NMR spectroscopy, the plausible binding mechanism of **1.5** is shown in Scheme 1.6.



*Scheme 1.6.* Proposed structure for binding  $\text{Hg}^{2+}$  ions by compound **1.5**.<sup>100</sup>

Das et al. has recently synthesized a molecular probe for  $\text{Ni}^{2+}$  ions which induced intramolecular excimer formation of a naphthalene fluorophore.<sup>101</sup> Compound **1.6** shows a monomer emission at 345 nm, characteristic of a naphthalene moiety with a low quantum yield ( $\Phi=0.011$ ) in  $\text{DMSO}:\text{H}_2\text{O}$  (1:1, v/v,  $\lambda_{\text{ex}} = 280 \text{ nm}$ ). The addition of  $\text{Ni}^{2+}$  ions quenched the monomer emission of the naphthalene moiety, but increase in the intensity of excimer emission at 430 nm with isoemissive point at 381 nm was seen. The quantum yield of excimer emission at 430 nm is ( $\Phi = 0.02$ ) after addition of  $\text{Ni}^{2+}$  ions. The naphthalene excimer formation is attributed to the *syn* conformation of two naphthalene rings of **1.6** in the presence of  $\text{Ni}^{2+}$  ions. The difference in the excitation spectra and the

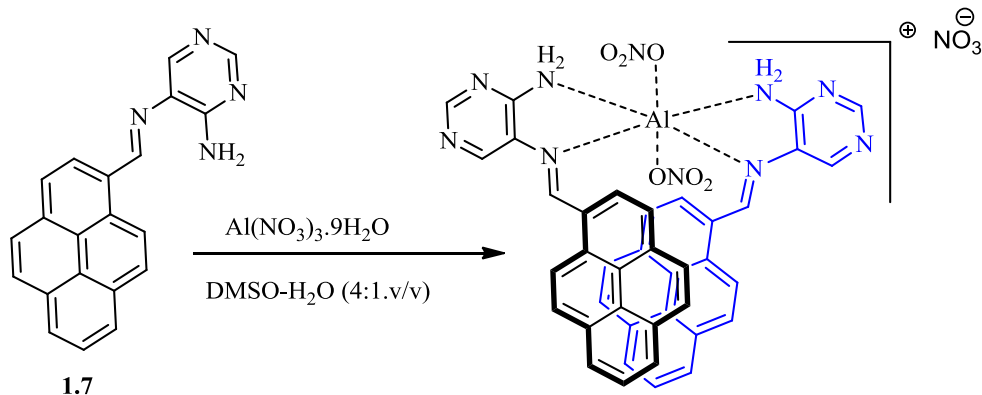
fluorescence lifetime measurement showed the emission at 430 nm is a static excimer (Figures 1.6 and 1.7) of naphthalene. The compound is selective for  $\text{Ni}^{2+}$  ion as other metal ions did not produce any emission at 430 nm. Compound **1.6** can detect  $\text{Ni}^{2+}$  ion as low as  $1 \times 10^{-6}$  M (58 ppb) with a fairly strong binding constant  $2.0 \times 10^4 \text{ M}^{-1}$ .  $^1\text{H}$  NMR titrations also supports the  $\text{Ni}^{2+}$  ion induced excimer formation of **1.6** as the up field shifts ( $\sim 0.01$  ppm) were observed for all aromatic proton of **1.6** after addition of  $\text{Ni}^{2+}$  ions. Compound **1.6** is also tested for its biological application in living cells of *Allamanda puberula* whereby fluorescence microscopy of both  $\text{Ni}^{2+}$  ion contaminated and free cell incubated with compound **1.6** showed that fluorescence is enhanced in the  $\text{Ni}^{2+}$  ion contaminated living cells. Compound **1.6** can permeate living cells without any effect as the cells remain alive even after 30 minutes of exposure to compound **1.6** at  $10 \mu\text{M}$  (Scheme 1.7).



Scheme 1.7. Proposed structure for binding  $\text{Ni}^{2+}$  by compound **1.6**.<sup>101</sup>

Recently Das also synthesized an  $\text{Al}^{3+}$  ion probe (**1.7**) by the condensation of 4,5-diaminopyrimidine with 1-pyrenecarboxaldehyde.<sup>55</sup> The structure of **1.7** was confirmed by single crystal X-ray analysis. The fluorescence spectrum of free **1.7** ( $5 \mu\text{M}$ , DMSO- $\text{H}_2\text{O}$  (4:1), 0.1 M HEPES buffer, pH 7.4,  $\lambda_{\text{ex}} = 330 \text{ nm}$ ) shows emission bands at 368 and 445 nm, attributed to the pyrene monomer and excimer emission bands, respectively. Addition of **1.7** equivalents of  $\text{Al}^{3+}$  ions to the solution of **1.7** leads to a significant

decrease of its monomer emission along with a considerable increase of the excimer emission at 445 nm with an isoemissive point at 386 nm. The values of  $I_{445}/I_{368}$  is about four folds increase with about twenty fold increase of the fluorescence quantum yield [ $\Phi$  (**1.7**) = 0.0025,  $\Phi$  [Al (**1.7**)<sub>2</sub>]<sup>3+</sup> = 0.0522]. In the UV-Vis spectrum, the addition of Al<sup>3+</sup> ions to **1.7** increased the absorption bands at 250-310 nm and decreased the absorption bands at 410 nm with a color change from yellow to colorless. Other metal ions studied such as Na<sup>+</sup>, Mg<sup>2+</sup>, Ca<sup>2+</sup>, Cd<sup>2+</sup>, Cu<sup>2+</sup>, Zn<sup>2+</sup>, Hg<sup>2+</sup>, Mn<sup>2+</sup>, Fe<sup>3+</sup>, Ni<sup>2+</sup>, Ag<sup>+</sup>, Pb<sup>2+</sup>, Co<sup>2+</sup>, and Cr<sup>3+</sup> (as their nitrate salts) did not show any significant effects. Compound **1.7** can respond to Al<sup>3+</sup> ion as low as 0.2  $\mu$ M (6 ppb) of which is far below the WHO acceptable limit of 1.8  $\mu$ M (50 ppb) in drinking water. The binding constant was calculated to be 1240 M<sup>-1/2</sup>. Binding of **1.7** with Al<sup>3+</sup> ion was further studied by <sup>1</sup>H NMR and <sup>13</sup>C NMR. Upon addition of Al(NO<sub>3</sub>)<sub>3</sub>, the protons assigned to NH<sub>2</sub> group are shifted in a downfield direction by 0.2 ppm while the protons of pyrene changes their multiplicity with a slight up field shift supporting the formation of excimer.<sup>102</sup> In <sup>13</sup>C NMR, the signals for the imine (C = NH) group shifted to up field by 1.5 ppm, and the signal for carbon attached to amine (NH<sub>2</sub>) group is shifted to downfield by 0.5 ppm on addition of Al(NO<sub>3</sub>)<sub>3</sub>. This supports the coordination of Al<sup>3+</sup> ion through the imine and amine nitrogen atoms. Furthermore, the compound **1.7** was also tested for its biological application in the living cells of *Bacillus* and *Candida albicans* and *Bauhinia acuminata*. The fluorescence is enhanced in the cells treated with Al<sup>3+</sup> ion. Further, the compound **1.7** can permeate easily into the living cells with no harm as the cells remain alive even after 0.5 h exposure to **1.7** at 10  $\mu$ M membrane (Scheme 1.8).



*Scheme 1.8.* Proposed structure for binding  $\text{Al}^{3+}$  ion by compound **1.7**.<sup>55</sup>

*Fluorescence energy transfer mechanism (FRET)*

It is a non-radiative process in which energy is transferred from the donor fluorophore in the excited state to the acceptor fluorophore in the ground state through long-range dipole-dipole interaction.<sup>103</sup> This process occurs when: 1) a donor has high quantum yield; 2) there is a substantial overlap of the donor emission spectrum with the acceptor absorption; 3) there is an appropriate alignment of the absorption and emission transition moments and their separation vectors; and 4) the donor-acceptor distances are in proximity, typically less than 10 nm through non-radiative dipole-dipole coupling (Figure 1.15).<sup>104</sup>

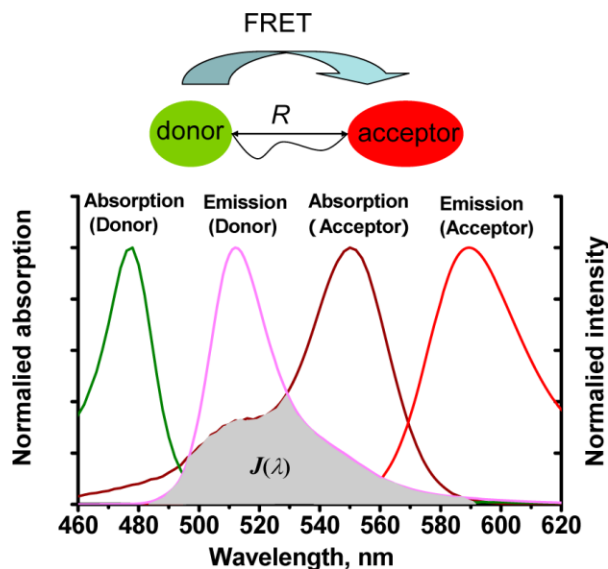


Figure 1.15. Schematic of FRET process. “Reprinted with permission from Yuan, L.; Lin, W.; Zheng, K.; Zhu, S., FRET-Based Small-Molecule Fluorescent Probes: Rational Design and Bioimaging Applications. *Acc. Chem. Res.* **2013**, *46*, 1462-1473. Copyright 2013 American Chemical Society.”

The efficiency of FRET is given by Equation 1.1.<sup>103</sup>

$$E = R_o^6 / (R_o^6 + R^6) \quad (1.1)$$

Where  $R_o$  is the Forster distance at which the transfer efficiency  $E= 50\%$ ;  $R$  is the distance between the energy donor and acceptor. The Forster distance  $R_o$  can be calculated by simplified Equation 1.2.

$$R_o = 0.211[k^2 n^{-4} \Phi_D J_{DA}]^{1/6} (\ln \hat{A}) \quad (1.2)$$

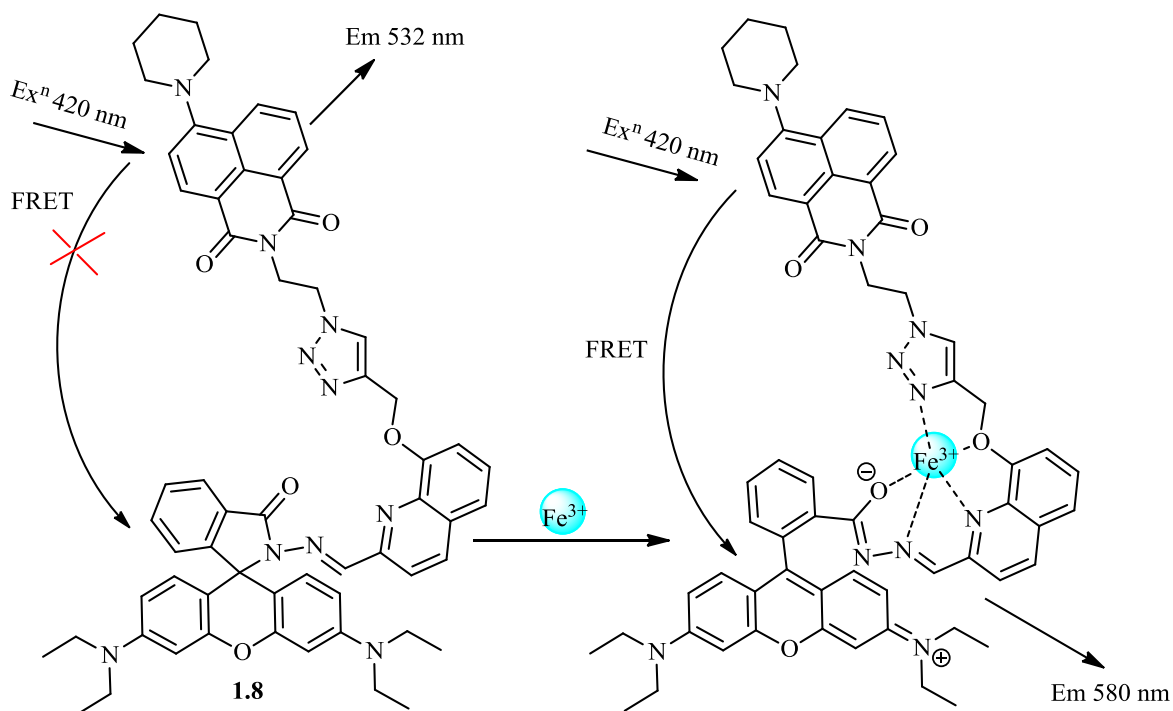
Where  $n$  is the refractive index,  $\Phi_D$  is the quantum yield of the donor,  $k$  denotes the average squared orientational part of a dipole-dipole interaction and  $J_{DA}$  express the degree of spectral overlap between the donor emission and acceptor absorption which is given by Equation 1.3.

$$J_{DA} = \int_0^\infty I_D(\lambda) \epsilon_A(\lambda) \lambda^4 d\lambda \quad (1.3)$$

Where  $I_D(\lambda)$  is the donor normalized fluorescence emission spectrum,  $\varepsilon_A(\lambda)$  is the acceptor molar absorption coefficient, and  $\lambda$  is the wavelength.

Mandal et al. synthesized a naphthalimide-rhodamine “FRET Off-On” sensor (**1.8**) for the ratiometric detection of  $\text{Fe}^{3+}$  ions.<sup>105</sup> The triazole appended quinoline-rhodamine conjugate was chosen as the FRET energy acceptor and the 8-piperzino naphthalimide moiety as the FRET energy donor. The intense fluorescence emission of the naphthalimide moiety and excellent overlap of its emission spectrum with the absorption spectrum of rhodamine B permit the intramolecular FRET in **1.8**. Compound **1.8** was pale yellow color in aqueous  $\text{CH}_3\text{CN}$  (1:1, v/v 0.01 M Tris HCl- $\text{CH}_3\text{CN}$ , pH 7.4) due to the naphthalimide donor moiety. The absorption spectrum of **1.8** showed a broad band at 415 nm which is assigned to the naphthalimide moiety. Upon the addition of  $\text{Fe}^{3+}$  ions to the solution of **1.8** enhanced the absorbance band at 560 nm with a color change from pale yellow to pink. A similar pattern was observed in the fluorescence emission profile of **1.8** on excitation at 420 nm. Upon addition of  $\text{Fe}^{3+}$  ions, emission band at 532 nm, attributed to naphthalimide moiety decreased and a new emission band at 580 nm appeared with an isoemissive point at 567 nm. This could be explained to the coordination of the  $\text{Fe}^{3+}$  ion inducing the opening of the spirocyclic ring of the rhodamine which facilitates the acceptance of fluorescence resonance energy transfer from the naphthalimide donor. Other competitive metal ions such as  $\text{Na}^+$ ,  $\text{K}^+$ ,  $\text{Mg}^{2+}$ ,  $\text{Ca}^{2+}$ ,  $\text{Cu}^{2+}$ ,  $\text{Zn}^{2+}$ ,  $\text{Hg}^{2+}$ ,  $\text{Mn}^{2+}$ ,  $\text{Fe}^{2+}$ ,  $\text{Ni}^{2+}$ ,  $\text{Pb}^{2+}$ ,  $\text{Co}^{2+}$ , and  $\text{Cr}^{3+}$  did not affect the color and fluorescence of the compound **1.8** indicating selective detection of  $\text{Fe}^{3+}$ . The dissociation constant was calculated to be  $1.04 \times 10^{-6}$  M with a detection limit of  $5.0 \times 10^{-8}$  M (Scheme 1.9).





Scheme 1.9. Proposed binding of compound **1.8** with  $\text{Fe}^{3+}$  ion.<sup>105</sup>

### Summary

In summary, the importance of  $\text{Zn}^{2+}$  and  $\text{Fe}^{3+}$  ion detection has been highlighted in terms of their role in biology and the environment. A number of methods available for the detection of these analytes were discussed such as flame photometry, inductively coupled plasma mass spectroscopy and atomic absorption spectroscopy. However, these methods are found to be cumbersome, expensive, sophisticated, and often impractical for on-site sensing. Optical spectroscopy was discussed as an important technique for the detection of these analytes in particular the use of fluorescent chemosensors as it is sensitive, selective, less expensive, and quick, and the sample is not lost in the analysis. Sensing motifs (pyrene, rhodamine, and fluorescein) and binding sites (triazole, amide and imine) are the two important parts of the chemosensors. The photo-physical properties of the pyrene and rhodamine are discussed in detail as they are used as the

sensing motifs for the design of chemosensors. The four most common mechanisms for sensing of ions: PET, PCT, excimer formation or quenching, and FRET are also discussed in detail.

This introduction describes the general background. However, the work presented in this dissertation is split into two distinct areas: the work based on the pyrene system and those on the rhodamine probes. Specific introduction material that is pertinent to each part is highlighted at the beginning of the relevant section.

### Hypothesis

A pyrene or rhodamine functional group is attached to a molecular probe as a sensing motif. These two chromo/fluorophores are chosen because of their strong UV-Vis absorbance, high quantum yield, due to their optical properties being sensitive to the local environments. The triazole and amide groups are selected as binding sites for the coordination of  $\text{Zn}^{2+}$  and  $\text{Fe}^{3+}$  ions. These groups are easily attached to organic scaffolds. Based on the general design, the following general hypothesis can be stated.

#### *General Hypothesis*

Upon the addition of metal analytes (for example  $\text{Zn}^{2+}$  or  $\text{Fe}^{3+}$  salts) to a solution of specifically designed probes, an optical response is observed, either *via* a colorimetric or fluorescence changes.

In the Part A of this dissertation, pyrene units have been used as sensing motifs in the design of molecular probes. Addition of metal ions can either produce an excimer or changes the intensity of monomer and excimer emissions. The formation of the excimer emission will be used as sensing mechanism in the molecular probes with only one

pyrene unit while monomer to excimer emission equilibrium will be used as a sensing mechanism with the molecular probes with two pyrene units.

In the Part B of the dissertation, rhodamine units have been used as sensing motifs in the design of molecular probes. Rhodamine based probes are colorless and have low fluorescence intensity due to the existence of the spiro lactam configuration, however, a strong red color and fluorescent signal is observed upon the addition of metal ions. Thus, a “turn on” in absorbance and fluorescence is used as sensing mechanism for detection of metal ions.

## CHAPTER II

PYRENE MOLECULAR TWEEZERS FOR DETECTION OF  $Zn^{2+}$  ION

## Introduction

Molecular “clefts” or “tweezers” are receptors with a pocket whereby a guest can fit within the pincer but is not completely encapsulated (Figure 2.1). They are often characterized by convergent functional groups directed towards each other but separated by a spacer. Aryl ring systems are commonly used as rigid scaffold for “preorganizing” the host into a specific shape: additionally, they are easily derivatized. Binding in molecular clefts may be mediated by a number of interactions, including dispersion forces,  $\pi$ -stacking, hydrogen bonding, and salt bridging.<sup>70</sup> The two pendent arms of the molecular cleft may either converge or diverge upon binding of an analyte which produces the changes in the spectroscopic properties of fluorophore.<sup>106</sup>

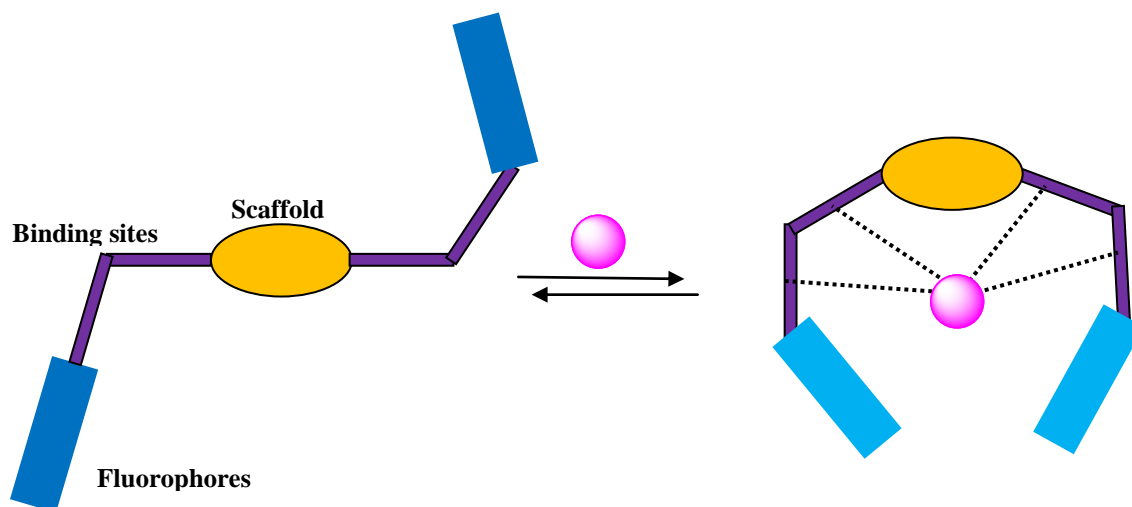


*Figure 2.1.* Cartoons showing binding of guest species by molecular cleft.

Cao and co-workers synthesized a pyrenyl-appended trazole-based sensors **2.1** and **2.2** for the recognition of  $Hg^{2+}$  ion in aqueous solution (Figure 2.2).<sup>107</sup> Compound **2.1** exhibits a monomer emission bands at 387-404 nm and an excimer emission at 495 nm

on excitation at 360 nm. This suggests that compound **2.1** is in a stacked conformation with the two pyrene units situated closely enough to yield the excimer emission. Compound **2.2** only shows monomer emission bands at 384 and 402 nm. Fluorescence emissions of both compounds **2.1** and **2.2** were decreased upon addition of  $\text{Hg}^{2+}$  ion in  $\text{CH}_3\text{CN}:\text{H}_2\text{O}$  (80:20, v/v). Quenching of fluorescence for **2.2** is less than **2.1**. Only four equivalents of  $\text{Hg}^{2+}$  ion was required to quench 80% of initial fluorescence of **2.1** while 30 equivalents of  $\text{Hg}^{2+}$  ion was needed for compound **2.2** to quench 62% of initial fluorescence. Other metal ions such as  $\text{Cu}^{2+}$ ,  $\text{Cr}^{3+}$ ,  $\text{Ag}^+$ ,  $\text{Co}^{2+}$ ,  $\text{Ni}^{2+}$ ,  $\text{Zn}^{2+}$ ,  $\text{Cd}^{2+}$ ,  $\text{Ba}^{2+}$ ,  $\text{Mg}^{2+}$ ,  $\text{Na}^+$ ,  $\text{Li}^+$ ,  $\text{Al}^{3+}$ ,  $\text{Ca}^{2+}$ , and  $\text{K}^+$  did not show any response to either compounds **2.1** and **2.2**. The quenching effect of  $\text{Hg}^{2+}$  ion may be explained to heavy metal effect (Chapter I).<sup>108</sup> The binding constant ( $K_{11}$ ) of the  $[\text{Hg}(\text{2.1})]^{2+}$  complex was calculated using Benesi-Hildebrand equation and found to be  $3.6 \times 10^4 \text{ M}^{-1}$ . The detection limit of compound **2.1** was found to be  $5.1 \times 10^{-7} \text{ M}$  (100 ppb). The binding affinity and detection limit for reference compound **2.2** was less than **2.1**. The binding mode of the compound **2.2** with  $\text{Hg}^{2+}$  ion was supported by the density functional theory (DFT) calculation. The optimized geometry indicates that nitrogen atoms of triazole and oxygen atoms of the sulfonamide group take part in the coordination of  $\text{Hg}^{2+}$  ion (Scheme 2.1). However the author did not mention anything about the binding mode of reference compound **2.2** with  $\text{Hg}^{2+}$  ion. This too was not studied by molecular modeling.

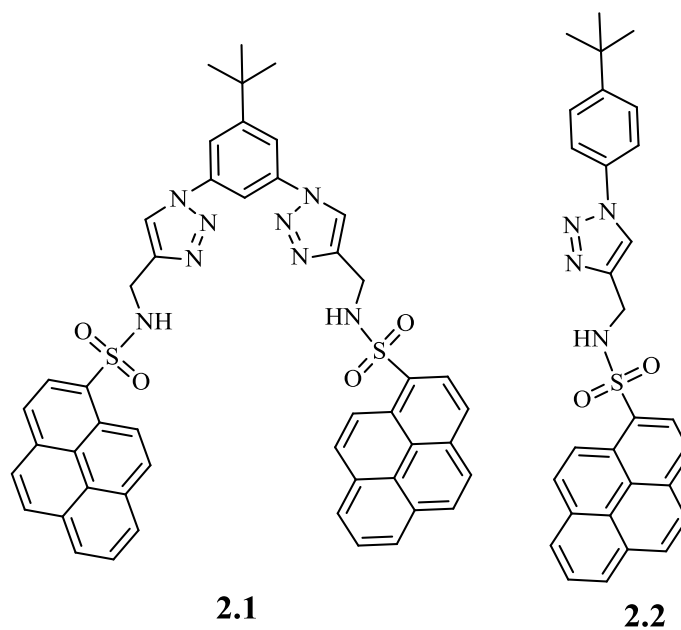
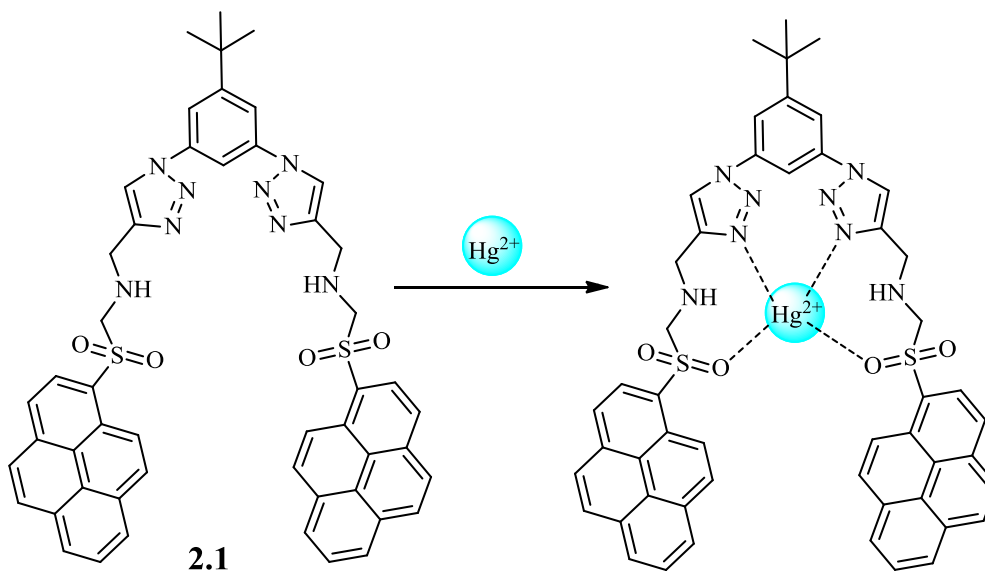


Figure 2.2. Structure for compound **2.1** and model compound **2.2**.

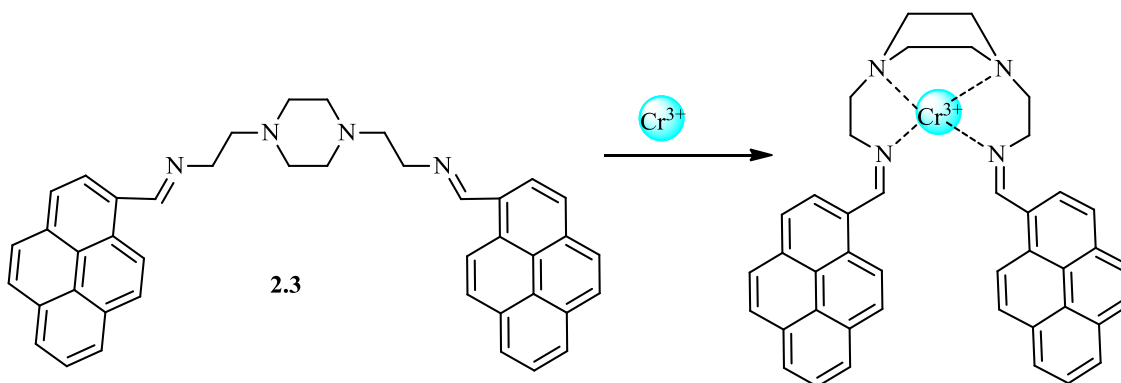


Scheme 2.1. Proposed binding mechanism of **2.1** with  $\text{Hg}^{2+}$  ion in  $\text{CH}_3\text{CN}-\text{H}_2\text{O}$  (80:20, v/v).<sup>107</sup>

Wu and co-workers synthesized a ratiometric fluorescent chemosensors for  $\text{Cr}^{3+}$  ions based on monomer-excimer conversion of a pyrene compound containing a pyrazine moiety as the scaffold.<sup>109</sup> Detection of  $\text{Cr}^{3+}$  ion is important as it is a serious

environmental pollutant and its build-up due to various industrial and agricultural activities.<sup>110</sup> Compound **2.3** shows the two fluorescent emission bands at 374 and 393 nm, typical of monomer emission, in Tris HNO<sub>3</sub> buffered solution (pH 7.0). The quantum yield ( $\Phi$ ) of **2.3** is 0.34 for the monomer emission (374 nm) and 0.0015 for the excimer emission (465 nm) using anthracene as standard ( $\Phi=0.27$ ).<sup>111</sup> A broad and new emission band with maximum at 454 nm was formed with decrease in fluorescent intensity at 374 nm upon addition of Cr<sup>3+</sup>. The quantum yield is 0.016 for the monomer emission (374 nm) and 0.29 for the excimer emission (465 nm). The fluorescence emission ratio ( $I_{454}/I_{374}$ ) exhibits nearly a 101-fold enhancement from 0.125 in the absence of Cr<sup>3+</sup> ions to 13 in the presence of Cr<sup>3+</sup> (10  $\mu$ M). In the UV-Vis spectrum the addition of Cr<sup>3+</sup> ions decreases the bands at 326 nm and 342 nm with an increase in a new red-shifted band at 400 nm. This new red shifted band at 400 nm is attributed to the interaction of Cr<sup>3+</sup> ions with the imino nitrogen atoms coordinating the metal ion, forcing the two pyrene units to come together. The compound was tested against other metal ions such as Cu<sup>2+</sup>, Ag<sup>+</sup>, Co<sup>2+</sup>, Pb<sup>2+</sup>, Zn<sup>2+</sup>, Cd<sup>2+</sup>, Ba<sup>2+</sup>, Mg<sup>2+</sup>, Na<sup>+</sup>, Li<sup>+</sup>, Al<sup>3+</sup>, Ca<sup>2+</sup>, and K<sup>+</sup> but showed no changes in fluorescent intensity ratio except by Al<sup>3+</sup> ions. Density functional theory (DFT) calculations were further used to confirm the structures of **2.3** and [Cr(**2.3**)]<sup>3+</sup> complex. The distance between the two pyrene units is 15.3 Å in the free receptor **2.3**. Therefore there is not any chance of  $\pi$ - $\pi$  stacking in the pyrene units will occur in **2.3**. However, the distance between the pyrene units changes to 4.8 Å in [Cr(**2.3**)]<sup>3+</sup> complex, which is in the range of effective  $\pi$ - $\pi$  stacking between these pyrene units and explains the gradual formation of excimer emission in the complex. It is interesting that the authors did not mention the Fe<sup>3+</sup> ion in their studies which has almost similar properties with Cr<sup>3+</sup> ions.

There was no mention of the stability of the complex as imines can be prone to hydrolysis (Scheme 2.2).

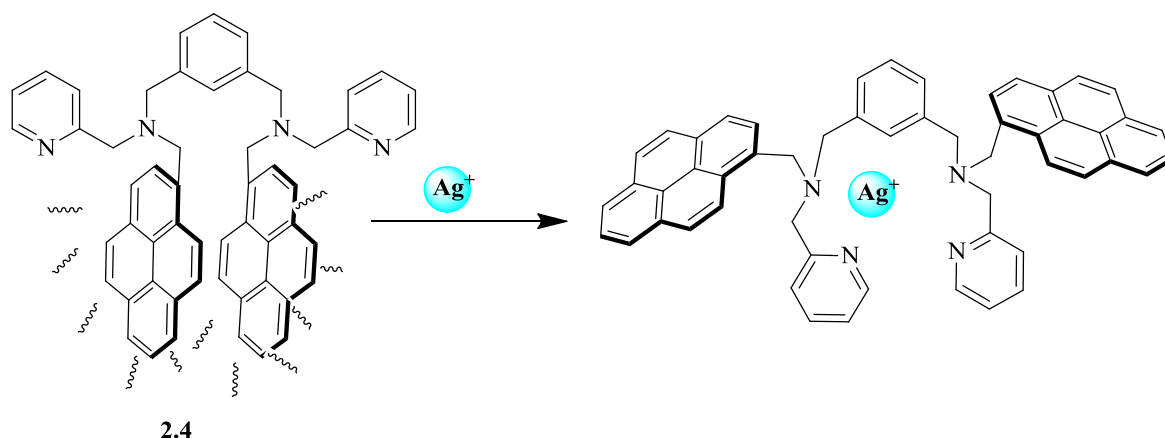


*Scheme 2.2.* Proposed binding mechanism of **2.3** with  $\text{Cr}^{3+}$  ion in Tris  $\text{HNO}_3$  buffered solution (pH 7.0). Detection limit was calculated to be  $4 \times 10^{-8}$  M (two ppb) for  $\text{Cr}^{3+}$  ions.<sup>109</sup>

Yoon and co-workers have developed a bis-pyrene derivative bearing two pyridine groups **2.4** as a selective and ratiometric fluorescent chemosensor for  $\text{Ag}^+$  ion at physiological pH 7.4.<sup>112</sup> Compound **2.4** (10  $\mu\text{M}$ ) showed a strong excimer band at 463 nm along with a monomer band at 399 nm on excitation at 344 nm in DMSO: HEPES (pH 7.4, 1:1, v/v). An excimer band was significantly quenched with the enhancement of monomer band upon addition of  $\text{Ag}^+$  ions through an isoemissive point at 410 nm. Among the other metal ions such as  $\text{Li}^+$ ,  $\text{Na}^+$ ,  $\text{K}^+$ ,  $\text{Ni}^{2+}$ ,  $\text{Mg}^{2+}$ ,  $\text{Mn}^{2+}$ ,  $\text{Ca}^{2+}$ ,  $\text{Al}^{3+}$ ,  $\text{Co}^{2+}$ ,  $\text{Sr}^{2+}$ ,  $\text{Cu}^{2+}$ ,  $\text{Zn}^{2+}$ ,  $\text{Cd}^{2+}$ ,  $\text{Hg}^{2+}$ ,  $\text{Fe}^{2+}$ ,  $\text{Fe}^{3+}$  and  $\text{Pb}^{2+}$ , only  $\text{Hg}^{2+}$  showed fluorescence quenching effects for monomer and excimer emissions. The association constants ( $K_{11}$ ) of **2.4** with  $\text{Hg}^{2+}$  and  $\text{Ag}^+$  ions were calculated to be  $1.0 \times 10^4 \text{ M}^{-1}$  and  $3.2 \times 10^5 \text{ M}^{-1}$  respectively. The  $^1\text{H}$  NMR spectrum of **2.4** and  $[\text{Ag}(\text{2.4})]^+$  were also studied to confirm the proposed structure (Scheme 2.3). The  $\text{Ag}^+$  ion causes a significant chemical shift on the protons of pyridine as a consequence of shielding effects. The large up field shifts (~



0.67 ppm) seen for the protons attached to the pyridine group is due to the close proximity of pyridine and phenyl groups upon the addition of  $\text{Ag}^+$  ions. This host-guest interaction was also confirmed by DFT calculation with the metal ion coordinated to the nitrogen atoms in a pseudo tetrahedral arrangement. Further, TDDFT calculation showed a strong interaction between the excited states of the two pyrenes in **2.4** where as in  $[\text{Ag}(\mathbf{2.4})]^+$  complex, there is no such interaction because of the intramolecular charge transfer from the pyrene to the nearby pyridine group and  $\text{Ag}^+$  ions. Therefore, the excimer emission was quenched, and only the monomer emission existed in the in  $[\text{Ag}(\mathbf{2.4})]^+$  complex (Scheme 2.3).



*Scheme 2.3.* Conformation change of receptor **2.4** on addition of  $\text{Ag}^+$  ion in a  $10\ \mu\text{M}$  concentration, DMSO: HEPES solution (pH = 7.4, 1:1, v/v).<sup>112</sup>

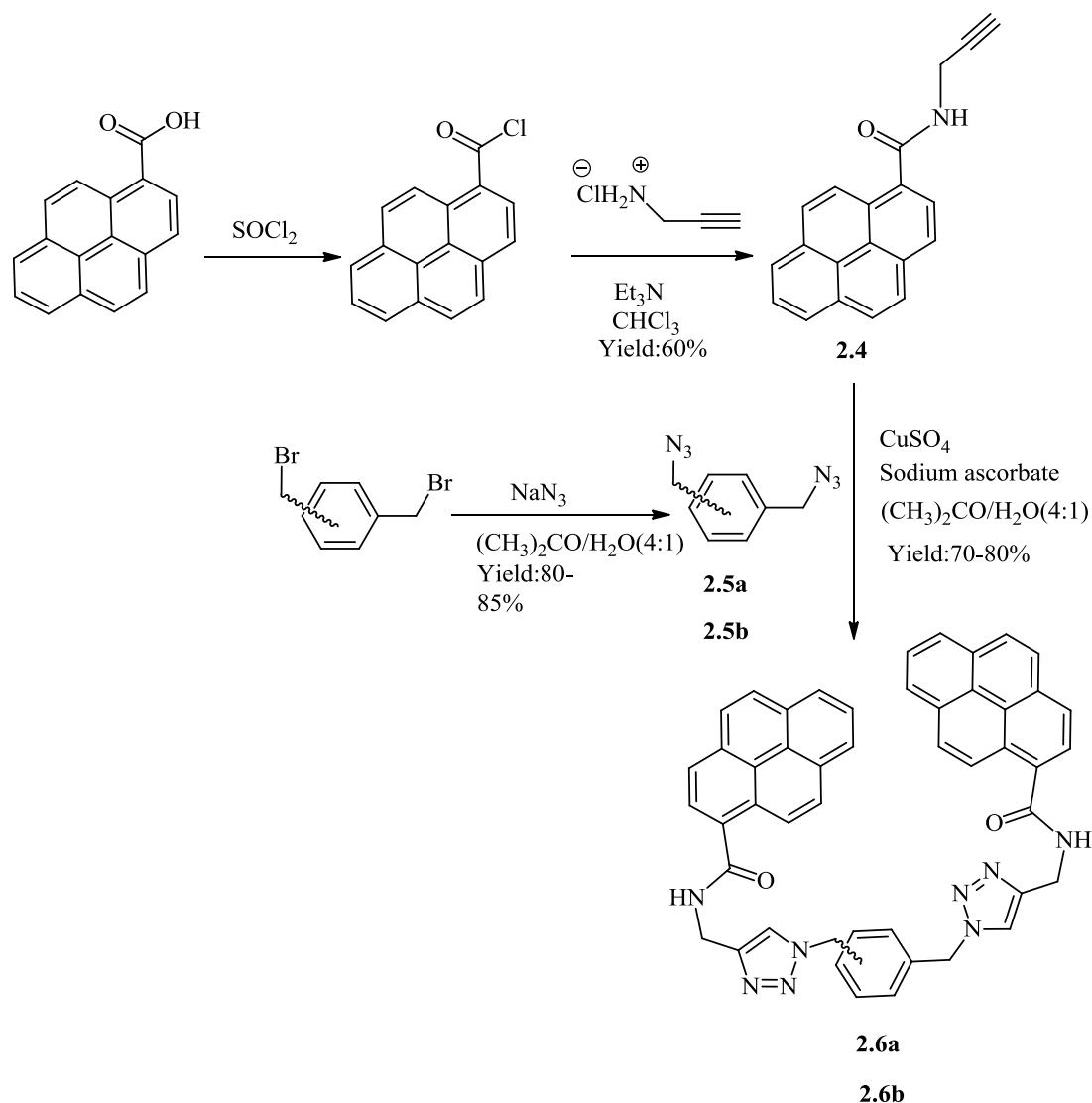
As shown the pyrene functional group has been used in molecular probes, as a consequence of the unique excimer mechanism seen (or quenched) upon the binding of metal ion. Therefore, the pyrene molecule was selected as a fluorophore for the design of molecular clefts for detection of  $\text{Zn}^{2+}$  ion. Benzene is used as scaffold, while triazole and amide groups are used as coordination sites for  $\text{Zn}^{2+}$  ion. The basicity of the nitrogen atoms of triazole and oxygen atoms of amide groups are considered complementary to the properties of  $\text{Zn}^{2+}$  ion and hence expected to bind  $\text{Zn}^{2+}$  ion selectively and in a

thermodynamically favorable manner. The molecular cleft is synthesized in two different isomers i.e., *ortho*, and *meta*, where by the “bite” angle is different between the pendent arms. It is believed that the different binding motifs will be seen for the two isomers, as free rotation can occur between two side arms through the rotation of the single bond with methylene groups attached to the benzene scaffold. Therefore, it is anticipated that a conformation change in a divergent was when binding the analyte.

### Synthesis of Molecular Probes **2.6a** and **2.6b**

The commercially available pyrene-1-carboxylic acid was used as starting material for the synthesis which is converted into the acid chloride by refluxing with thionyl chloride for an hour. The acid chloride was not isolated and reacted immediately with propargyl amine hydrochloride in the presence of triethylamine in dichloromethane (Scheme 2.4). The impure solid was purified by silica gel column chromatography [Ethyl acetate (2): Hexane (8)] to obtain N-(prop-2-ynyl) pyrene-1-carboxamide (**2.4**) as pure yellow solid in overall 60 % yield. The compound was confirmed by the signals of the amide NH proton and terminal alkyne protons at  $\delta$  6.40 and 4.42 ppm ( $\text{CDCl}_3$ ), respectively, in  $^1\text{H}$  NMR spectrum. The compound is further confirmed by IR, whereby stretching bands are seen at  $3278\text{ cm}^{-1}$  assigned to  $\text{C}\equiv\text{CH}$ ,  $2070\text{ cm}^{-1}$  for  $\text{C}\equiv\text{C}$  and 3198, 1618,  $1600\text{ cm}^{-1}$  for amide N-H, amide C=O (I) amide C=O (II) groups, respectively. The NMR data agreed with the literature value.<sup>113</sup> The *ortho* or *meta* bis(azidomethyl)benzene (**2.5a** and **2.5b**) was prepared from its corresponding isomer bis(bromomethyl)benzene by reacting with sodium azide in a 4:1 ratio ( $(\text{CH}_3)_2\text{CO} : \text{H}_2\text{O}$ ). The azide molecules (**2.5a** and **2.5b**) were confirmed by their characteristic strong stretching bands at  $2085\text{ cm}^{-1}$  in the IR spectrum, and their spectroscopic data ( $^1\text{H}$  NMR,  $^{13}\text{C}$  NMR and IR) also

agreed with the published procedure.<sup>114</sup> Compounds **2.4** and **2.5** were then “clicked” together *via* azide-alkyne Huisgen cycloaddition reaction in the presence of copper sulfate and sodium ascorbate as catalysts in 4:1 ((CH<sub>3</sub>)<sub>2</sub>CO: H<sub>2</sub>O). A solid was obtained once the reaction mixture was poured into water which was filtered, washed with water and dried to obtain the pure yellow compound (**2.6a** and **2.6b**) in an overall 70-80% yield. In <sup>1</sup>H NMR spectrum, the disappearance of the signal at δ 4.42 ppm assigned to the terminal C≡CH hydrogen atom and appearance of a new signal at δ 8.20 ppm (DMSO-*d*<sub>6</sub>) assigned to the protons of newly formed triazole skeleton confirms the formation of desired product. The compound was fully characterized by <sup>1</sup>H NMR, <sup>13</sup>C NMR, IR, ESI mass spectrum, and elemental analysis (Scheme 2.4).



*Scheme 2.4.* Synthesis of molecular receptor **2.6a** and **2.6**.

#### Job's Plot Studies of Molecular Probes **2.6a** and **2.6b**

Stoichiometry is one of the most important characteristics of the host-guest complex as it determines the overall ratio of the complex in the solution phase. For example, the binding constant of the host-guest complex, which represents its thermodynamic stability, depends on the complex stoichiometry. A key aspect in the calculation of the binding constant is the use of a correct stoichiometry model (i.e., ratio of host and guest) as the procedures used for data fitting are based on the binding models.

Therefore, it is important to know the complexes that are formed in order to apply the appropriate model. In fact, one of the main aims of host guest titration is to determine the stoichiometry of the system under study.<sup>73, 115</sup>

One simple method to determine the stoichiometry of a host-guest complex is by a Job's plot experiment. It is also known as a method of continuous variation.<sup>38</sup> In this method, both host and guest solutions are prepared with the same concentration in the same solvent. They were then combined to give overall the same total molar concentration but with a varying ratio of host and guest from 0 to 1 i.e., the mole fraction. An absorbance or fluorescence observed is proportional to the complex formation and is plotted against the mole fraction of these two components. The maximum or minimum on the plot corresponds to the stoichiometry of the host and guest.

Therefore, a Job's plot analysis was conducted to determine the stoichiometry of the binding between compounds **2.6a** and **2.6b** with  $\text{Zn}(\text{ClO}_4)_2$  (Figure 2.3). The final concentration of solution in  $\text{CH}_3\text{CN}$  after mixing host (*ortho*) and guest ( $\text{Zn}(\text{ClO}_4)_2$ ) is 100  $\mu\text{M}$  using compound **2.6a**. Whereas the final concentration for compound **2.6b** in  $\text{CH}_3\text{CN}$  solution is 50  $\mu\text{M}$ . The fluorescent intensity of the excimer band at 495 nm ( $I_{495}$  nm) is plotted against mole fraction of  $\text{Zn}^{2+}$  ion for the *ortho* isomer (Figure 2.3) while the fluorescence intensity ratio ( $I_{495/403}$ ) is plotted against mole fraction of  $\text{Zn}^{2+}$  ions in case of *meta* isomer (Figure 2.3). In both experiments, the intersection of the curve is same at 0.5 mole fraction suggesting a 1:1 binding stoichiometry between host and guest.

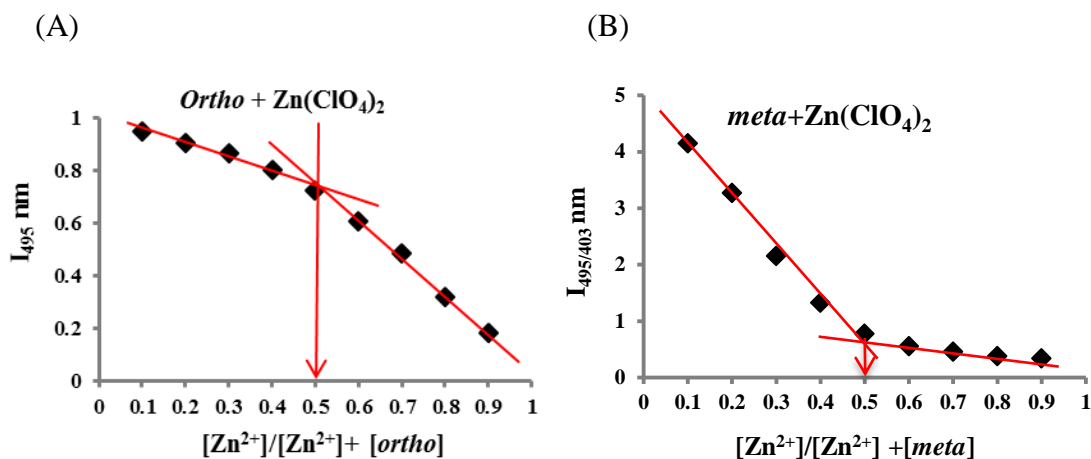


Figure 2.3. Job's plot of compound **2.6a** (A) and **2.6b** (B) with Zn(ClO<sub>4</sub>)<sub>2</sub> obtained by fluorescence measurements in CH<sub>3</sub>CN. The total concentration is 100, and 50 μM for experiment with **2.6a** and **2.6b**, respectively, where  $X \approx 0.5$  (1:1 ligand:metal ratio). The red lines are for visual interpretation only.

### Optical studies of the molecular probes **2.6a** and **2.6b**

#### Fluorescence spectroscopy

Upon the successful synthesis of the molecular probes **2.6a** and **2.6b**, their binding with metal ions was first studied by fluorescence spectroscopy. It was anticipated that the fluorescent emission of the probes should change upon binding with the target metal ions. In particular, monomer and excimer emission intensities of the pyrene should change significantly with different target metal ions because the two probes just differed in positions of connectivity with the benzene ring. The space between the two pendent arms should be smaller in the *ortho* isomer than the *meta* one and hence should have greater excimer emission. Organic solvent, CH<sub>3</sub>CN is selected to study the fluorescence of compounds **2.6a** and **2.6b** as it is medium-polar solvent and does not interact with the host molecules *via* electrostatic or hydrogen bonding interactions. Therefore it does not affect or disrupt the coordination of metal ions by the ligands.<sup>70</sup> Furthermore, the pyrene based molecular probes are more soluble in non-polar to medium-polar solvents such as

CHCl<sub>3</sub>, CH<sub>2</sub>Cl<sub>2</sub>, and CH<sub>3</sub>CN due to their hydrophobic nature. The polar solvents such as CH<sub>3</sub>OH, DMSO, and H<sub>2</sub>O normally affect the binding process by forming hydrogen bonds with the binding sites of the sensors. However, it is always good to have the sensors work in the polar and aqueous solvent from the biological and environmental aspects.

The fluorescence of both molecular probes *ortho* (**2.6a**) and *meta* (**2.6b**) show the typical monomer emission bands at 380 and 400 nm in CH<sub>3</sub>CN, which are characteristic of pyrene-derived compounds and are assigned to the  $\pi$ - $\pi^*$  electron transitions.<sup>57</sup> A very broad emission band with maximum around 495 nm is also seen and was assigned to intramolecular excimer formation, upon excitation at 325 nm. An excimer band of **2.6a** was more intense than **2.6b** showing the pyrene units are closer to each other in **2.6a** than the **2.6b** as shown in Figure 2.4. Intermolecular excimer formation was ruled out as the effect was observed in the  $\mu$ M range. Fluorescence analysis of both compounds were studied by adding ten equivalents of either chloride or perchlorate salts of different metal ions such as Na<sup>+</sup>, Ni<sup>2+</sup>, Mg<sup>2+</sup>, Ca<sup>2+</sup>, Al<sup>3+</sup>, Co<sup>2+</sup>, Cu<sup>2+</sup>, Zn<sup>2+</sup>, Cd<sup>2+</sup>, Hg<sup>2+</sup>, Fe<sup>2+</sup>, Fe<sup>3+</sup>, and Zn<sup>2+</sup> in CH<sub>3</sub>CN (Figure 2.5). The quenching of fluorescence (both monomer and excimer band) was observed for all the metal ions except for Zn<sup>2+</sup> ion (and to a lesser degree for Cd<sup>2+</sup> and Mg<sup>2+</sup> ions) in which a new band was seen to increase at 400 nm. The fluorescence intensity of new band at 400 nm was significantly more intense for **2.6b** than **2.6a** upon addition of ten equivalents of Zn<sup>2+</sup> ion (Figure 2.5-2.9). The lack of fluorescence at 400 nm for **2.6a** could be a consequence of the two pyrene units in **2.6a** complex adopting an anti-orientation which gives a greater

pyrene–pyrene separation than is available to a **2.6b** complex, in agreement with the density functional theory (DFT) calculations (Figure 2.16).

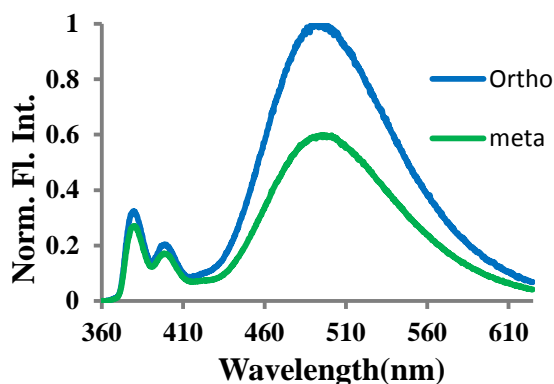


Figure 2.4. The excimer emission of compound **2.6a** and **2.6b** in CH<sub>3</sub>CN (5 μM, λ<sub>ex</sub> = 325 nm).

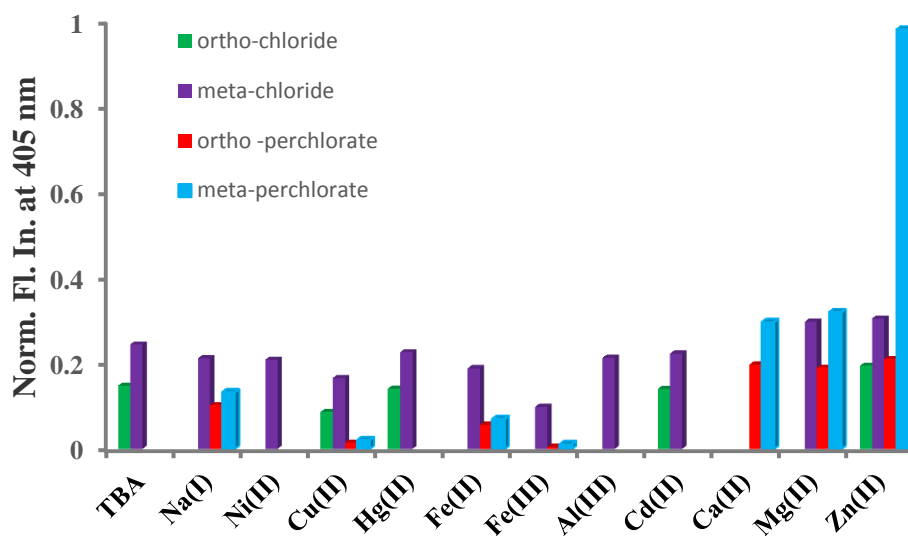


Figure 2.5. Fluorescence intensity of **2.6a** and **2.6b** (5 μM) upon addition of ten equiv. of metal chlorides and perchlorates at 405 nm (CH<sub>3</sub>CN, λ<sub>ex</sub> = 325 nm).

There are many ways in which the metals can quench the fluorescence as explained in the Chapter I. Therefore, it was not surprising that many of the metal salts studied quenched the fluorescence of the compound **2.6a** and **2.6b**. However, Zn<sup>2+</sup> ion can neither accept an electron into its *d*-orbitals as they are already filled nor is it



classified as a heavy metal. As a consequence, quenching is not observed, and signals “turn on” or fluorescence enhancement is seen.

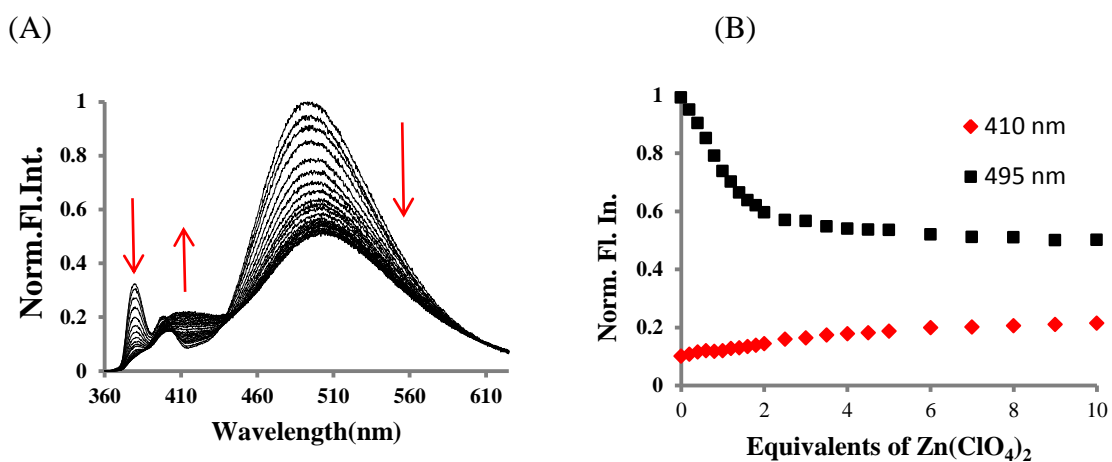


Figure 2.6. The fluorescence spectrum of compound **2.6a** (5  $\mu$ M,  $\lambda_{\text{ex}}$  = 325 nm) upon incremental additions (up to ten equiv.) of Zn(ClO<sub>4</sub>)<sub>2</sub> in CH<sub>3</sub>CN (A) and its binding isotherm (B).

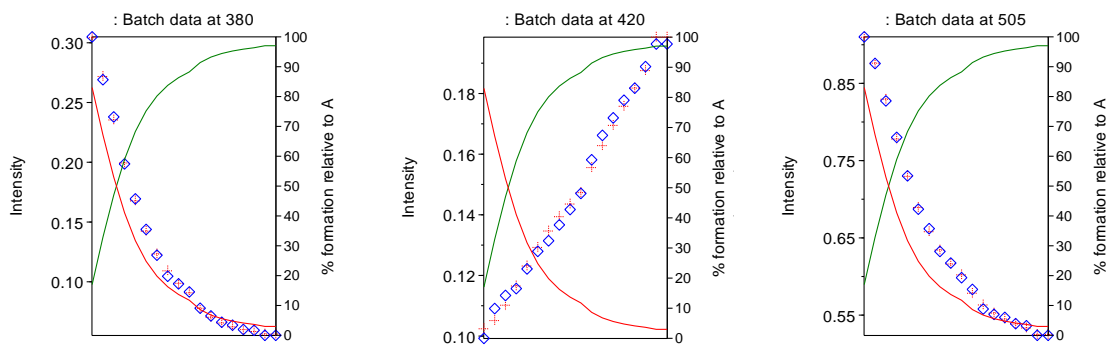


Figure 2.7. Binding isotherms for the fluorescence titration of compound **2.6a** with Zn(ClO<sub>4</sub>)<sub>2</sub> at 380, 420, and 505 nm from HypSpec program.<sup>116</sup>

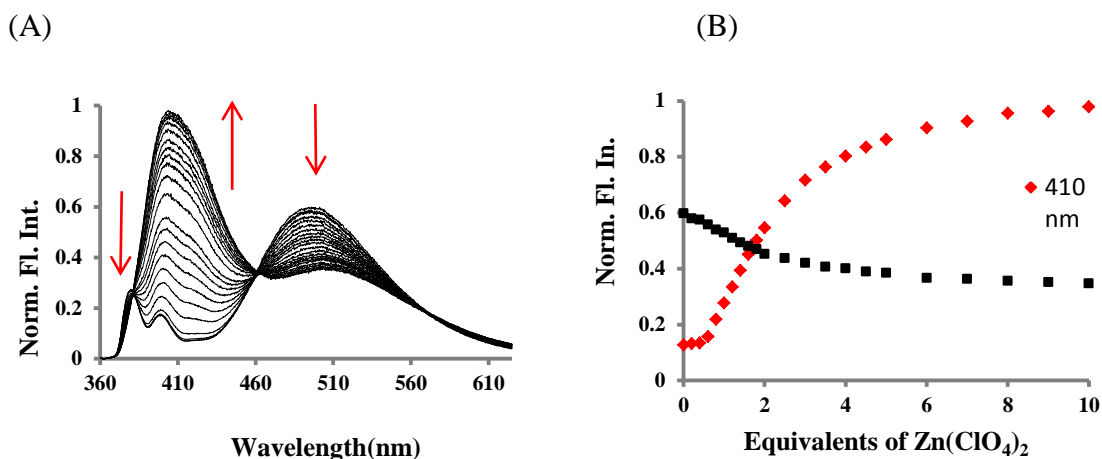


Figure 2.8. The fluorescence spectrum of compound **2.6b** (5  $\mu\text{M}$ ,  $\lambda_{\text{ex}}=325$  nm) upon incremental additions (up to ten equiv.) of  $\text{Zn}(\text{ClO}_4)_2$  in  $\text{CH}_3\text{CN}$  (A) and its binding isotherm (B).

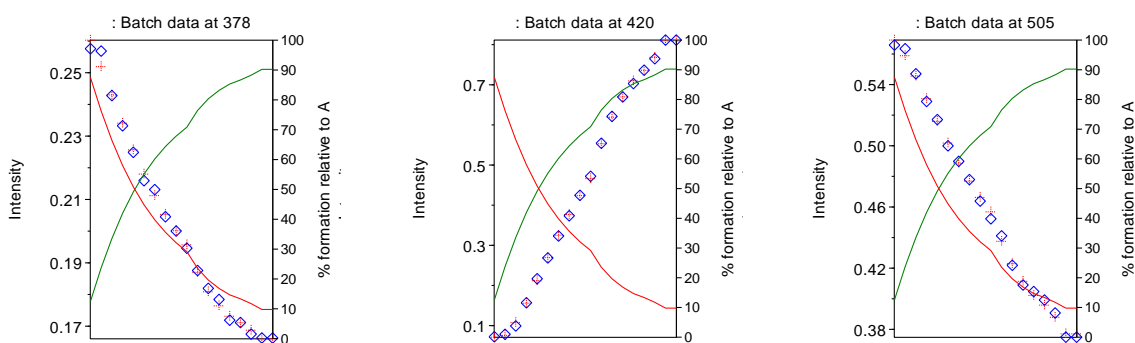


Figure 2.9. Binding isotherm for the fluorescence titration of compound **2.6b** with  $\text{Zn}(\text{ClO}_4)_2$  378 , 420, and 505 nm from HypSpec program.<sup>116</sup>

The fluorescence intensity of the compound **2.6a** and **2.6b** at 400 nm due to  $\text{ClO}_4^-$  salt was more intense than that of the  $\text{Cl}^-$  salt. Therefore, the effect of different counterions on  $\text{Zn}^{2+}$  binding of compounds **2.6a** and **2.6b** was explored as shown in Figure 2.10. The binding affinities of **2.6a** and **2.6b** towards  $\text{Zn}^{2+}$  salts ( $\text{F}^-$ ,  $\text{Cl}^-$ ,  $\text{Br}^-$ ,  $\text{I}^-$ ,  $\text{NO}_3^-$ ,  $\text{CH}_3\text{CO}_2^-$ ,  $\text{SO}_4^{2-}$ ,  $\text{BF}_4^-$ , and  $\text{ClO}_4^-$ ) in  $\text{CH}_3\text{CN}$  were investigated using fluorescence spectroscopy by excitation of a 5  $\mu\text{M}$  solution of **2.6a** and **2.6b** at 325 nm.

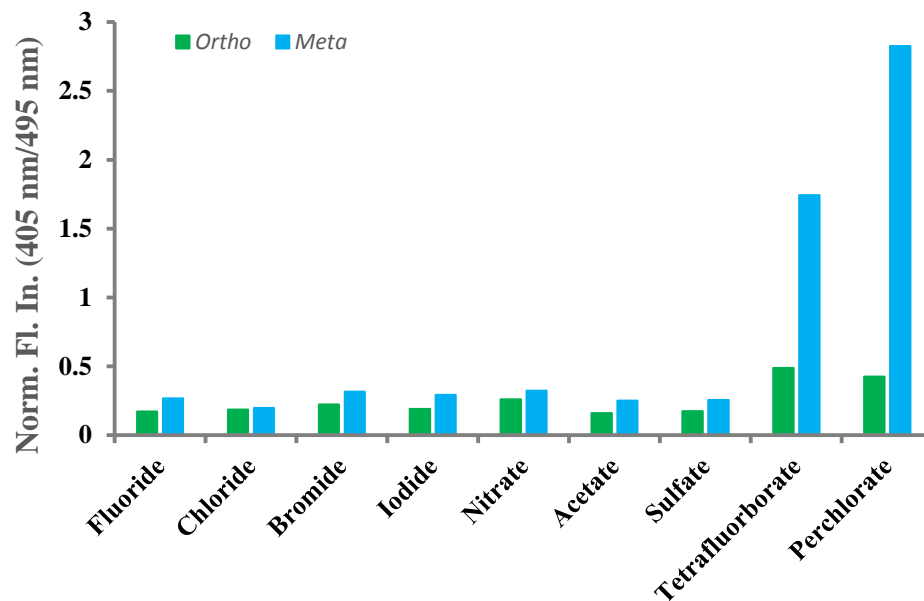


Figure 2.10. Fluorescence intensity of **2.6a** and **2.6b** (5  $\mu\text{M}$ ) upon addition of ten equivalents of various anions of  $\text{Zn}^{2+}$  salts ( $\text{CH}_3\text{CN}$ ,  $\lambda_{\text{ex}} = 325 \text{ nm}$ ).

There were significant spectroscopic changes upon the incremental addition of both  $\text{Zn}(\text{ClO}_4)_2$  and  $\text{Zn}(\text{BF}_4)_2$  (Figure 2.10). These large counter-ions seem to dissociate significantly in  $\text{CH}_3\text{CN}$  in comparison with the other anions studied. The excimer band at 495 nm shifted hypochromically with a new hyperchromic band appearing at 400 nm through an isoemissive point at 461 nm. Similar hypsochromic shifts have been observed by Nakahira et al.<sup>117</sup> and de Schryver co-workers<sup>118</sup> in pyrene-based polymeric materials and bis(pyrenyl)ether derivatives, respectively. The binding affinities of **2.6a** and **2.6b** for  $\text{Zn}(\text{ClO}_4)_2$ , calculated using HypSpec,<sup>116</sup> were  $K_{11} = 1.4 \times 10^6$  and  $3.8 \times 10^5 \text{ M}^{-1}$ , respectively. The binding constants for all of the other zinc salts are shown in Table 2.1. Interestingly, the binding affinity for  $\text{Zn}(\text{ClO}_4)_2$  was a magnitude greater for **2.6a** than for **2.6b**, even though the fluorescent change at 400 nm was not observed to be as dramatic (Figure 2.6 and 2.8). In fact, this trend is seen for all the other analytes studied, presumably due to the more favourable chelating motif. However, the lack of a

spectroscopic signal can be justified due to the pyrene moieties adopting a *trans* orientation (Figure 2.16), in which they are further apart, thus, reducing the magnitude of the electronic transition seen at 400 nm for receptor **2.6a**. These effects can be explained by the binding cleft of **2.6a** being more conducive to metal coordination than **2.6b** but its pyrene groups are further apart, reducing its fluorescence signal compared to **2.6b**.

Table 2.1

*Association constant ( $K_{11}$ ) between receptors **2.6a** and **2.6b** and  $ZnX_2$  in  $CH_3CN$*

X	<i>Ortho</i> ( $K_{11}(M^{-1})$ )	<i>Meta</i> ( $K_{11}(M^{-1})$ )
F <sup>-</sup>	$1.3 \times 10^3$	$3.5 \times 10^3$
Cl <sup>-</sup>	$1.6 \times 10^3$	$2.7 \times 10^3$
Br <sup>-</sup>	$1.1 \times 10^4$	$1.2 \times 10^4$
I <sup>-</sup>	$9.6 \times 10^3$	$5.4 \times 10^4$
NO <sub>3</sub> <sup>-</sup>	$5.0 \times 10^3$	$5.6 \times 10^3$
CH <sub>3</sub> CO <sub>2</sub> <sup>-</sup>	$1.8 \times 10^3$	$9.9 \times 10^2$
SO <sub>4</sub> <sup>-</sup>	$3.1 \times 10^4$	$5.7 \times 10^3$
BF <sub>4</sub> <sup>-</sup>	$3.6 \times 10^5$	$8.9 \times 10^4$
ClO <sub>4</sub> <sup>-</sup>	$1.4 \times 10^6$	$3.8 \times 10^5$

The binding ability of compound **2.6b** is also studied in a mixed organic–water system, but only 1% water could be added to the system before precipitation occurred. Nevertheless, a similar ratiometric response is seen, with an excimer band decrease at 495 nm and increase at 400 nm, upon the addition of  $Zn(ClO_4)_2$  (Figure 2.11).

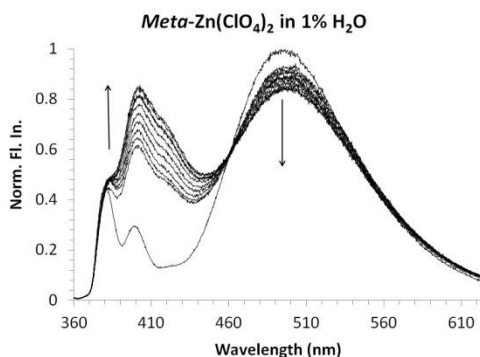


Figure 2.11. Fluorescence titrations ( $\text{CH}_3\text{CN}$ ,  $\lambda_{\text{ex}} = 325 \text{ nm}$ ) between **2.6b** and  $\text{Zn}(\text{ClO}_4)_2$  in 1%  $\text{H}_2\text{O}$ .

### 1D and 2D NMR Studies of Molecular Probe **2.6b**

Fluorescence studies of the compounds **2.6b** showed that it is selective for binding  $\text{Zn}^{2+}$  ion over other metal ions. The spectroscopic change is greatest for the fluorescence of compound **2.6b** than **2.6a**. However, fluorescence studies of compounds does not provide any qualitative information about the binding of metal ion i.e., where and how a metal ion is binding to the host. The  $^1\text{H}$  NMR titration can provide the qualitative information about the specific nuclei that are affected by the specific guest and hence some information about the regioselectivity of guest binding i.e., where is the guest bound with respect to the host. The protons attached to or near to the binding sites change its chemical shift upon binding with the metal ion. But the chemical shift observed for particular host-guest equilibria is a weighted average between the chemical shifts of the free and bound species as most host-guest equilibria are fast in the NMR spectroscopic time scale. Quantitative information can also be obtained by plotting the change in chemical shifts against added guest concentration which allows a binding constant to be calculated by least-squares curve fitting with programs such as Hyp-NMR or EQNMR.<sup>119, 120</sup>

Thus,  $^1\text{H}$  NMR titration of compound **2.6b** is carried out with  $\text{Zn}^{2+}$  ion to get the further insight into the nature of binding. Unfortunately, compound **2.6a** is insoluble in a mixture of  $\text{CDCl}_3$  and  $\text{CD}_3\text{CN}$  at the concentration required for NMR and hence not studied. Further, the  $\text{Zn}^{2+}$  ion is diamagnetic in nature and hence NMR inactive. Both compound **2.6b** and its  $\text{Zn}^{2+}$  ion complex are studied in detail by the 2D NMR such as COSY, HMQC, HMBC, TOCSY, and ROESY for their structural assignment and confirmation. The  $^1\text{H}$  NMR spectrum of compound **2.6b** shows a significant overlap of the pyrene signals in the aromatic region which is due to the presence of two pyrene functional groups in the same molecule. The protons of the compound **2.6b** have been accurately assigned on the basis of 2D NMR and molecular modelling. The aromatic pyrene protons are shifted to chemically different environments upon the addition of five equivalents of  $\text{Zn}^{2+}$  ions, presumably due to the conformational change once Zinc has coordinated to the molecular cleft (Figure 2.12). The amide and triazole protons are shifted to downfield direction by around 1.25 and 0.55 ppm, respectively. The downfield shifts could be due to increasing acidity of the NH and triazole protons upon coordination of the carbonyl oxygen and triazole nitrogen atoms to the  $\text{Zn}^{2+}$  ions.

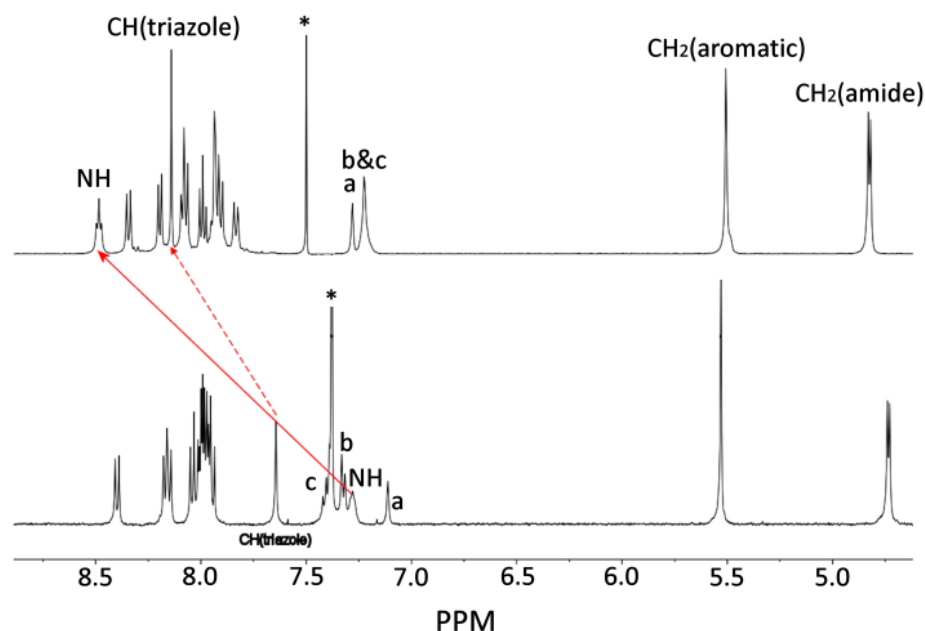


Figure 2.12. <sup>1</sup>H NMR complete spectrum of free receptor **2.6b** (bottom) and upon the addition of five equivalents of Zn<sup>2+</sup> ion in a mixture of 1:1 (CD<sub>3</sub>Cl:CD<sub>3</sub>CN).

The binding of compound **2.6b** with Zn<sup>2+</sup> ion was further studied by ROESY because it can detect through-space interactions based on the nuclear Overhauser effect (NOE). The NOE interactions can be intra and intermolecular and thus provide an important information about the spatial structure of the molecules and their relative positions.<sup>121</sup> In particular, ROESY is very helpful in the structural elucidation of the complex. The rOe spectrum of compound **2.6b** showed one very weak and nine strong rOe signals (a-i) in a mixture of CD<sub>3</sub>CN and CDCl<sub>3</sub> (1:1, v/v) (Figure 2.13). Addition of Zn(ClO<sub>4</sub>)<sub>2</sub> produced two distinct signals in the rOe spectrum of the complex (Figure 2.13 and 2.14). The first rOe signal was between CH on the pyrene (C (2) pyrene) and CH<sub>2</sub> adjacent to the NH functional group (labelled as (j) in Figure 2.13). The rOe signal between these same hydrogen atoms was absent in the free receptor ligand. Presumably, upon addition of Zn<sup>2+</sup> ions, the two oxygen atoms on the carbonyl coordinate to the metal

centre causing a rotation of the amide group such that both the oxygen atoms participate in the coordination of  $\text{Zn}^{2+}$  ions within the cleft. This contrasts with the free receptor where the carbonyl functional groups point in opposite directions. This change in geometry is in agreement with the molecular modelling calculations (Figure 2.16). The second rOe signals of interest are between the triazole proton and *ortho*-proton of the benzyl group (labelled as (h) in Figure 2.13). There is only one rOe signal in the free receptor, whereas in the complex spectrum the triazole proton has two distinct rOe signals consistent with rotation of the benzyl functional group. Inspection of the molecular model (Figure 2.16) shows that the benzyl group is rotated by  $\sim 70^\circ$ .



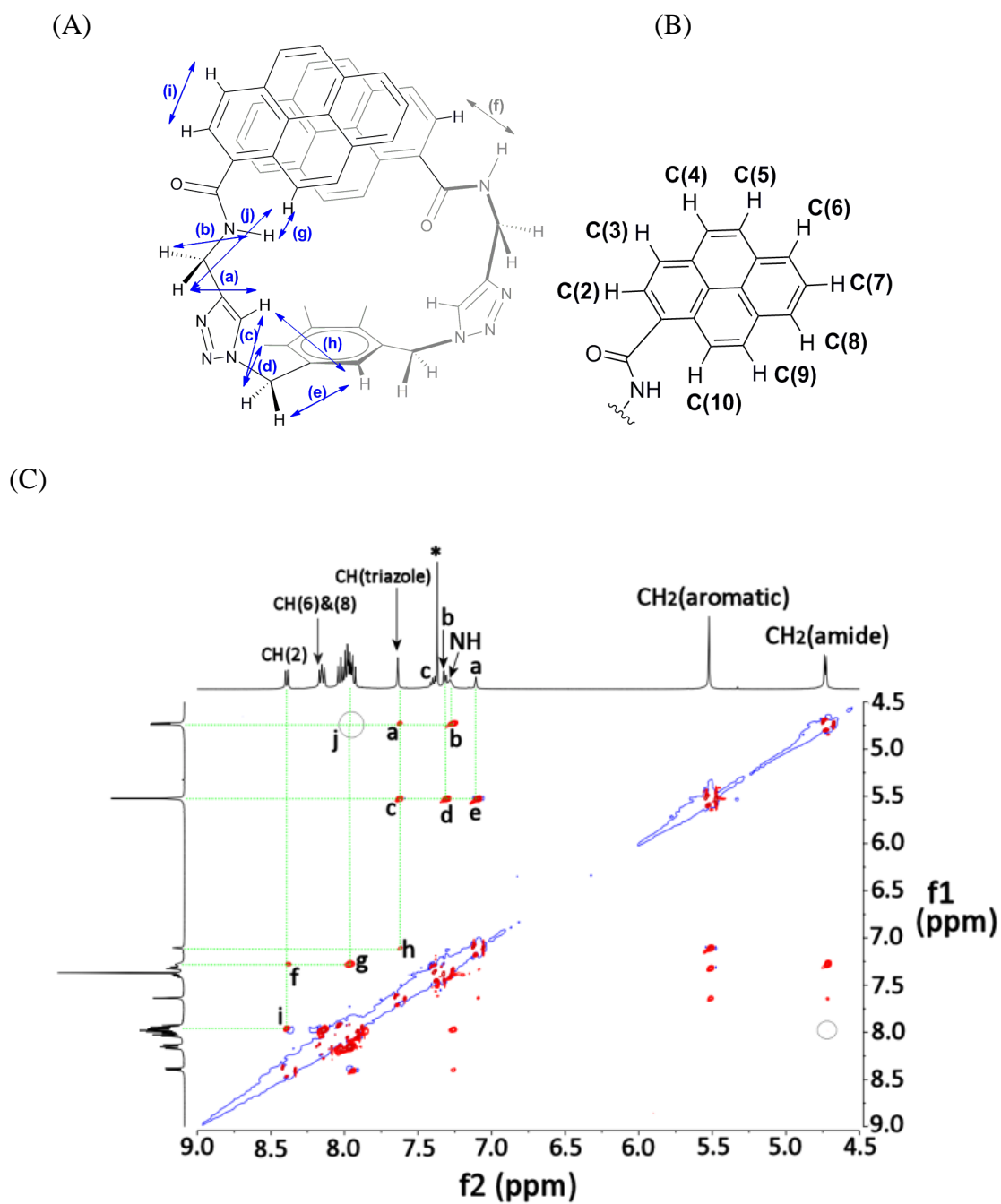
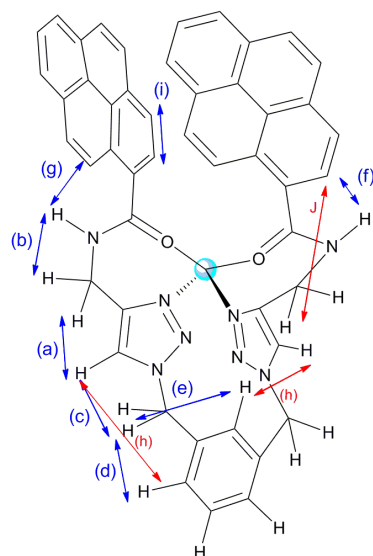


Figure 2.13. (A) rOe signals (B) numbering system, and (C) 2D ROESY of **2.6b** in a mixture of  $\text{CDCl}_3:\text{CD}_3\text{CN}$  (1:1).

(A)



(B)

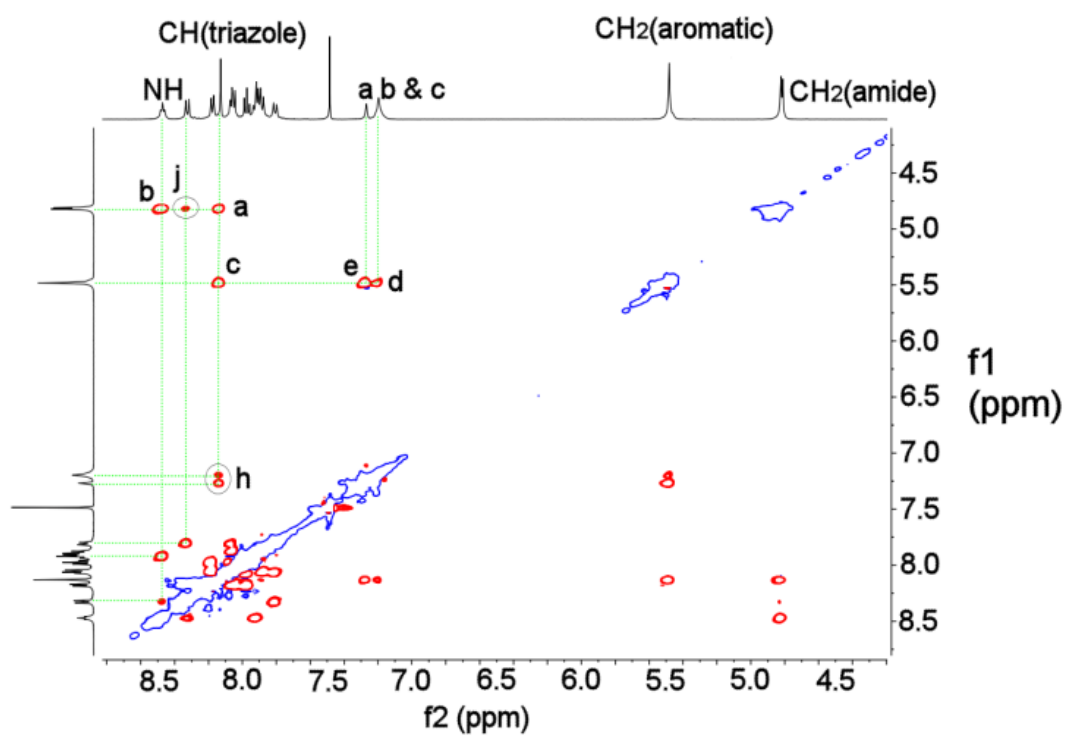


Figure 2.14. (A) Numbering system and rOe signals (B) ROESY spectrum of **2.6b** after addition of five equivalents of  $\text{Zn}^{2+}$  ions in a mixture of  $\text{CDCl}_3:\text{CD}_3\text{CN}$  (1:1).

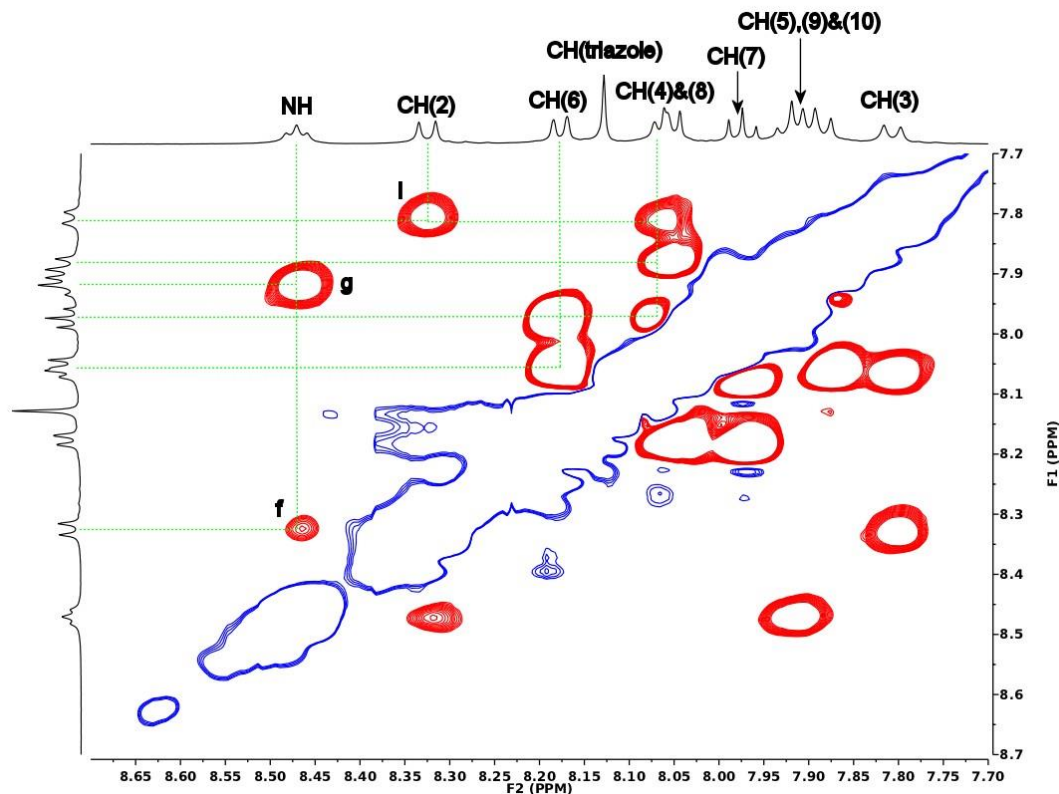


Figure 2.15. ROESY expanded spectrum (aromatic region) of **2.6b** after addition of five equivalents of  $\text{Zn}^{2+}$  ions in a mixture of  $\text{CDCl}_3:\text{CD}_3\text{CN}$  (1:1).

#### Molecular Modelling Studies of Molecular Probes **2.6a** and **2.6b**

One dimensional ( $^1\text{H}$  NMR) and 2D NMR (ROESY) studies of compound **2.6b** with the  $\text{Zn}(\text{ClO}_4)_2$  suggested that the nitrogen atoms of triazole and oxygen atoms of amide groups of two pendent arms of compound **2.6b** coordinate  $\text{Zn}^{2+}$  ion within the cleft. There is a change in the geometry of the probes upon coordination with  $\text{Zn}^{2+}$  ion. However, NMR studies did not provide the clear picture of geometry of complex i.e., whether it is binding in tetrahedral or in octahedral fashion. One way to get the information of geometry of the complex is from the crystal structure of the complex. But numerous attempts to grow the crystals of the host guest complex had been unsuccessful. Therefore, an extensive computational approach was adopted to gain insight into possible ligand and complex geometries. Molecular mechanics calculations for **2.6a** and **2.6b** and

their corresponding  $\text{Zn}(\text{ClO}_4)_2$  complexes were carried out (Figure 2.16). Both the free receptors show interesting, but very different,  $\pi$ -stacked interactions. The *ortho* isomer (**2.6a**) shows that the aromatic scaffold of the molecular probes participates in  $\pi$ -stacking, and one of the pyrene arms seems to intercalate and form an intramolecular sandwich interaction (Figure 2.16 (A)). This intercalation is not observed in the *meta*-isomer, **2.6b** which shows 4.77 Å  $\pi$ - $\pi$  distance between the two pyrene units. The distance was measured between the pyrene centroids and the C-H hydrogens on the triazole rings orientated towards the centre of the molecular probes. This is in excellent agreement with the interactions expected to generate the excimer band seen in the fluorescence spectrum. Both the  $\text{Zn}^{2+}$  ion complexes show drastically different optimised geometries. The  $\text{Zn}^{2+}$  ion is bound in a tetrahedral arrangement coordinated to the oxygen atom of the carbonyl functional group and a nitrogen atom in the triazole ring, forming a seven-membered chelating ring. The distance between two pyrene units in  $[\text{Zn}(\mathbf{2.6a})]^{2+}$  is 10.8 Å, whereas the distance between two pyrene units in  $[\text{Zn}(\mathbf{2.6b})]^{2+}$  is 5.5 Å, again in excellent agreement with the fluorescence data in which a broad excimer band is seen at 400 nm for the  $[\text{Zn}(\mathbf{2.6b})]^{2+}$ ; the same band is significantly less intense for the  $[\text{Zn}(\mathbf{2.6a})]^{2+}$ .

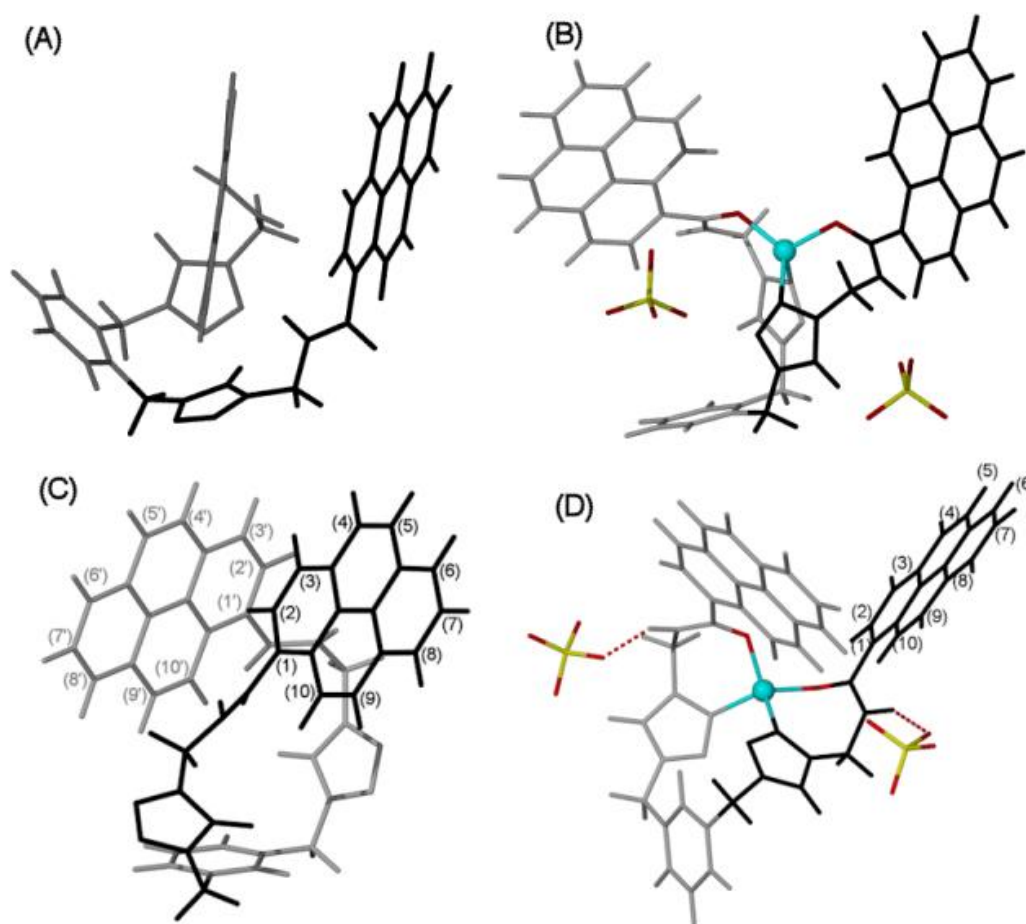


Figure 2.16. DFT fully optimized structures of (A) **2.6a**, (B)  $[\text{Zn}(\mathbf{2.6a})](\text{ClO}_4)_2$ , (C) **2.6b**, and (D)  $[\text{Zn}(\mathbf{2.6b})](\text{ClO}_4)_2$ .

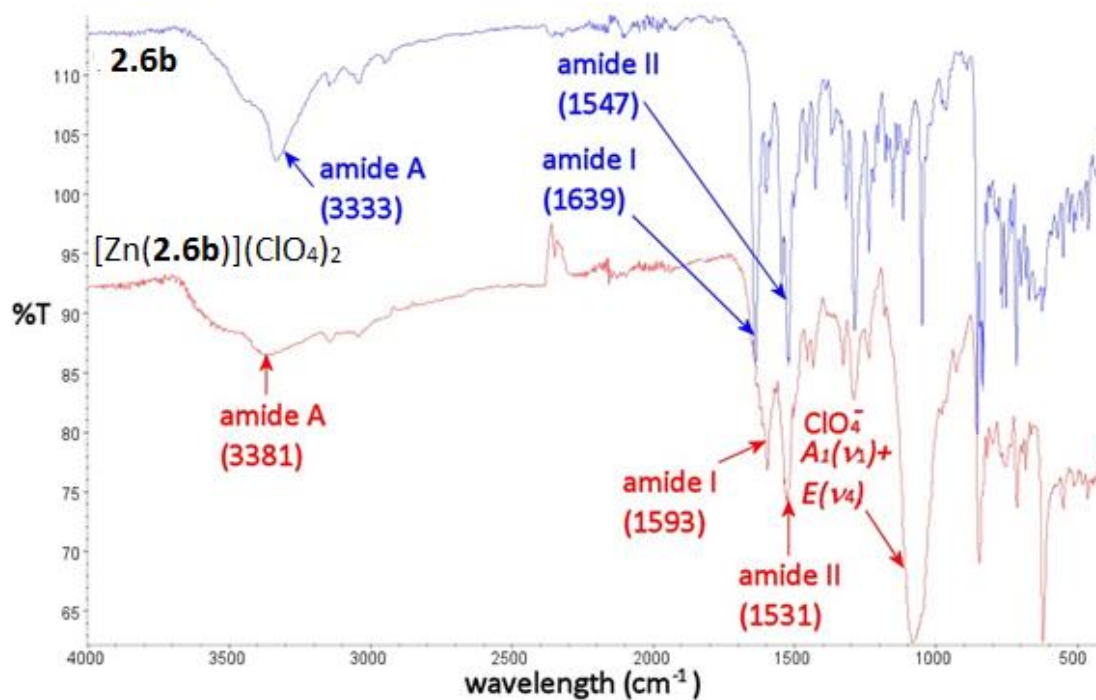
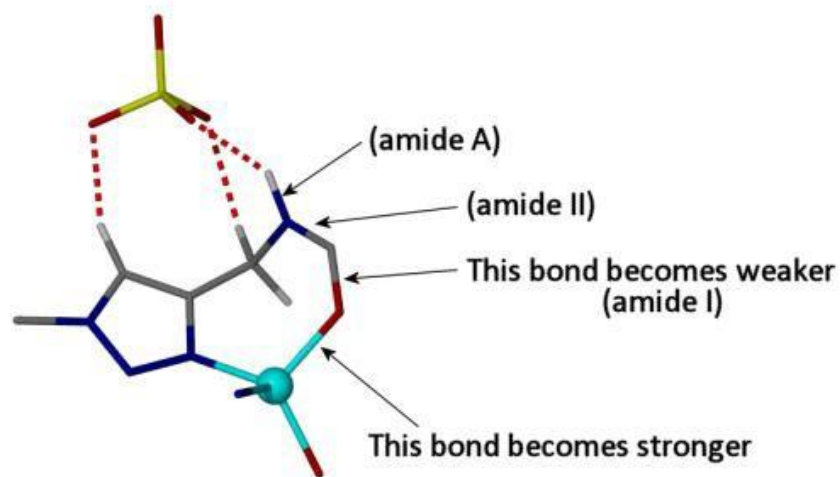
#### IR Studies of Molecular Probe **2.6b**

NMR and molecular modelling studies of the compound **2.6b** with  $\text{Zn}^{2+}$  ion showed that  $\text{Zn}^{2+}$  ion is coordinated by the carbonyl oxygen atoms of the amide group and nitrogen atoms of triazole. Though triazole functional groups do not show characteristic IR stretching bands, the amide group has characteristic IR stretching bands in the IR-spectrum. A change in either intensity or shift in the amide stretching of carbonyl oxygen atoms is expected if the amide oxygen atoms are involved in the coordination of  $\text{Zn}^{2+}$  ion. Therefore, an IR study was conducted for both free receptor

**2.6b** and its complex with  $\text{Zn}^{2+}$  ion to verify the binding mode as suggested by the NMR and molecular modelling calculations. The infrared spectrum of free receptor **2.6b** as recorded as a solid using an ATR-IR and showed the characteristic IR bands for the amide functional group. The amide A stretch appears at  $3333\text{ cm}^{-1}$  for the NH band. The amide I (C=O) stretch and the amide II (NH in plane bending) stretch are seen at  $1639$  and  $1547\text{ cm}^{-1}$  in **2.6b**, respectively (Figure 2.17). The metal complex, needed for IR study, is prepared by grinding equimolar amounts of **2.6b** and  $\text{Zn}(\text{ClO}_4)_2$  in a pestle and mortar for 30 minutes to form a green solid which was dried by keeping in oven for two hours before the ATR-IR was recorded. An IR spectrum of complex showed that the amide A band is hypsochromically shifted by  $48\text{ cm}^{-1}$  which is the consequence of the hydrogen bonding interaction between the amide proton and one of the oxygen atoms in the  $\text{ClO}_4^-$  ion (Figure 2.16 and 2.17). This is also supported by the molecular models which show that  $\text{ClO}_4^-$  participates in a number of hydrogen bonding interactions. Amide I and amide II bands are shifted by  $46$  and  $16\text{ cm}^{-1}$ , respectively, in a red direction. The shift in the IR wavelength could be explained by the increase in negative charge on the metal ion as the  $\text{Zn}\cdots\text{O}$  bond becomes stronger, and both the amide I and amide II bands become weaker.

It has been previously reported that significant infrared spectral changes occur when perchlorate coordinates to a metal ion through different modes.<sup>122</sup> Determination of changing symmetry of the  $\text{ClO}_4^-$  upon binding, from  $T_d$  (ionic) to  $C_{3v}$  (unidentate) and  $C_{2v}$  (bidentate or bridging), can help identify the binding mode of the present system. The symmetry of the  $\text{ClO}_4^-$  changed from a  $T_d$  in free  $\text{Zn}(\text{ClO}_4)_2$  to a  $C_{3v}$  in complex. As a consequence, the degeneracy of the  $T_2$  ( $\nu_3$ ) Cl-O stretching absorption at  $1059\text{ cm}^{-1}$  in the

$\text{Zn}(\text{ClO}_4)_2$  salt is split into a doublet at  $1070$  and  $1043 \text{ cm}^{-1}$  assigned to  $A_1 (\nu_1)$  plus  $E (\nu_4)$ ,<sup>123, 124</sup> which is in agreement with the binding present in the modelling calculations.



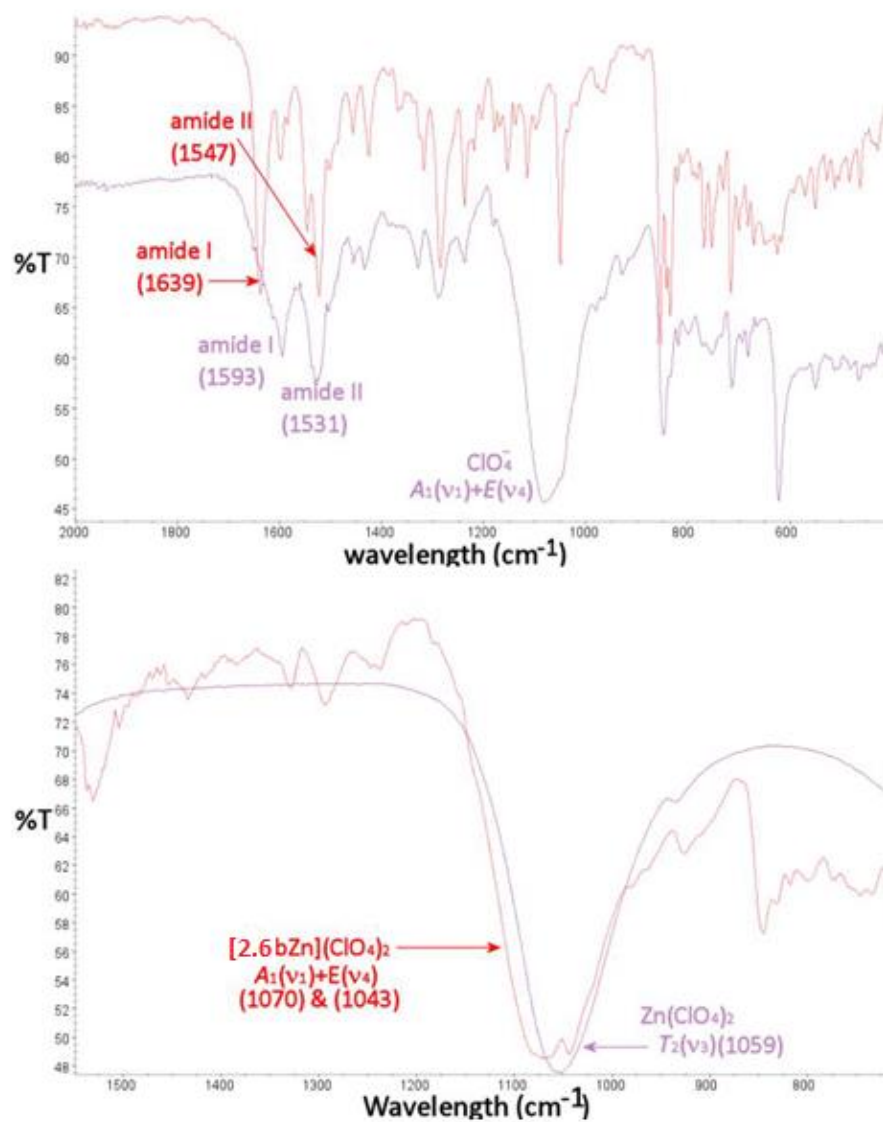


Figure 2.17. ATR-IR data of **2.6b** on the addition of Zn(ClO₄)₂.

#### Sensitivity of Molecular Probes **2.6a** and **2.6b**

The Zn<sup>2+</sup> ion is present in very trace amount (nanomolar range) in biology and environment. So molecular probes having high sensitivity for Zn<sup>2+</sup> ion is very important. Highly sensitive molecular probe can detect such a low concentration of metal ions. Limit of detection (LoD) is defined as the analyte concentration giving a signal equal to the blank signal plus three standard deviations from the blank, i.e.,  $y = y_B + 3S_B$ . The limit of



detection was calculated by titrating 0.05  $\mu\text{M}$  of compound **2.6b** with 0.5  $\mu\text{M}$   $\text{Zn}(\text{ClO}_4)_2$  in  $\text{CH}_3\text{CN}$  (Figure 2.17). The fluorescence intensity of monomer emission band at 380 nm increased (the wavelength monitored in the detection studies at such low concentrations) upon the addition of  $\text{Zn}(\text{ClO}_4)_2$ . The same experiment with **2.6a** showed no spectroscopic change at the same concentration. To determine the limit of detection (LoD), the method of least squares was used to give a line of regression. The confidence limit of the slope is defined as  $b \pm t_{sb}$ , where  $t$  is the  $t$ -value taken from the desired confidence and  $n-2$  degrees of freedom. A 95% confidence level ( $t$ -value 2.23,  $df = 10$ ) is used in this experiment (Figure 2.18). The calculated LoD values for **2.6a** and **2.6b** were 0.6  $\mu\text{M}$  (39 ppb) and 20 nM (1 ppb), respectively (Figure 2.18 and 2.19). Calcium salts often interfere with zinc in fluorescence assays; however, the  $\text{Ca}^{2+}$  complexes gave no spectroscopic responses in the same nanomolar concentration (Figure 2.18). The detection limit of the molecular probes **2.6a** and **2.6b** are well below the limits set up by both the World Health organization (WHO) and the Environmental Protection Agency (EPA) for drinking water. The recommended limits of zinc in drinking water, soil, and water supporting aquatic life are 5 mg/L (5 ppm), 7500 ppm and 0.0766 ppm, respectively, by the USEPA while the WHO has also set the 5 mg/L (5 ppm) as the maximum acceptable concentration for zinc in drinking water.<sup>125, 126</sup> In fact, the molecular probes **2.6b** is among the few molecular probes which can detect such a low concentration of  $\text{Zn}^{2+}$  ion.

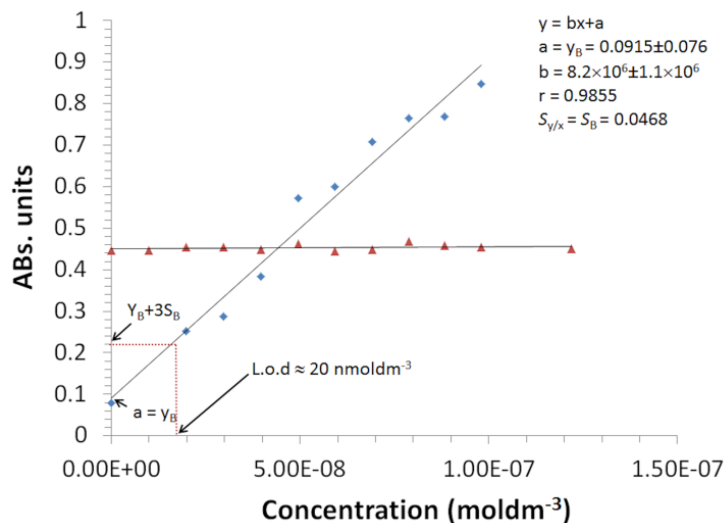


Figure 2.18. Calibration curve used to calculate the LoD for  $\text{Zn}^{2+}$  ion (blue diamond) and  $\text{Ca}^{2+}$  ion (red triangle) with **2.6b**.

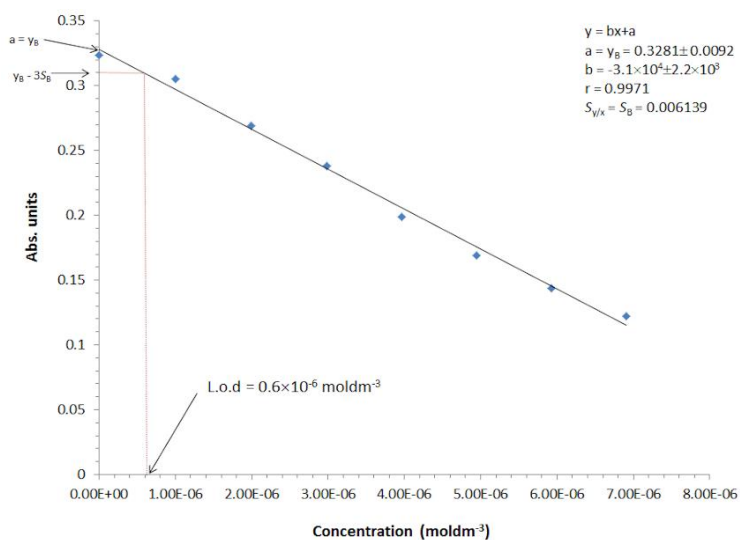
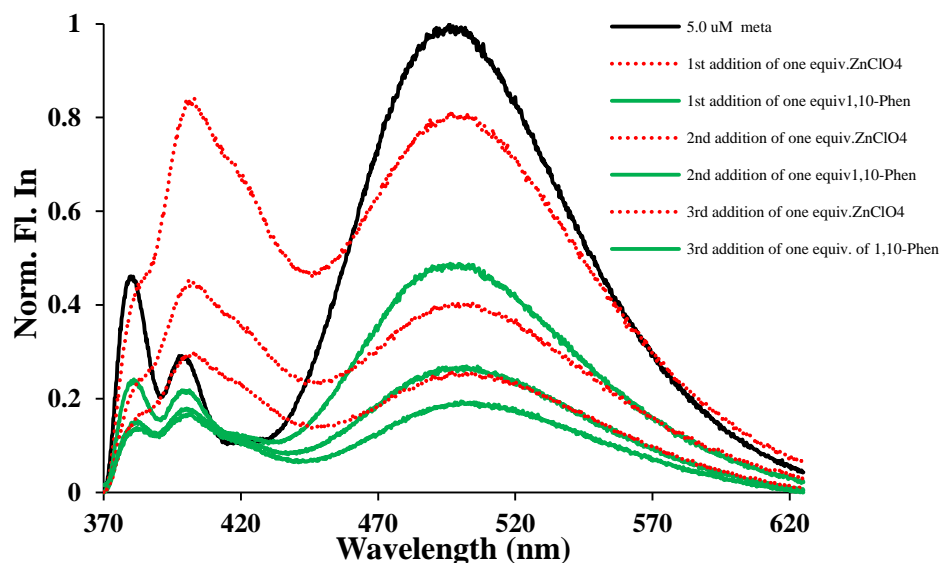


Figure 2.19. Calibration curve used to calculate the LoD for  $\text{Zn}^{2+}$  with **2.6a**.

### Reversibility of Molecular Probe **2.6b**

Reversibility in binding is a principle requirement for an ideal chemosensor. If a sensor is reversible, then it can be reused again for several times with proper treatment. If the sensor is not reversible, it becomes a reagent and can only be used in a stoichiometric manner which severely limits its application. Reversibility allows the sensor to monitor the analyte continuously and quickly in real time applications.<sup>127</sup> The Faster the

complexation and decomplexation, the faster will be the response. The 1,10-phenanthroline, a well-known  $\text{Zn}^{2+}$  ion chelator, was used to test the reversibility of **2.6b**. Addition of 1,10-phenanthroline “stripped” off the  $\text{Zn}^{2+}$  ion from the molecular cleft quenching the fluorescence completely at 400 nm. This indicates that the fluorescence spectrum returned to that of the receptor but the intensity was only ~50% of the original emission. The fluorescence at 400 nm reappeared again on the second time addition of  $\text{Zn}^{2+}$  ion to the system but less intense than the first time. This could be repeated three times (Figure 2.20), and each time 1,10-phenanthroline was removed, the intensity of the original emission was reduced by a further 50%. The quenching of fluorescence intensity can be due to the 1,10-phenanthroline electron clouds in proximity to the fluorophore of the molecular receptor, thereby preventing emission.<sup>128</sup>



*Figure 2.20.* Reversibility test: The effect of sequential addition of 1, 10-phenanthroline and  $\text{Zn}^{2+}$  ion to compound **2.6b** ( $[\text{meta}] = 5 \mu\text{M}$ ,  $[\text{Zn}^{2+}] = 500 \mu\text{M}$ ,  $[\text{1,10-phen}] = 500 \mu\text{M}$ ,  $\text{CH}_3\text{CN}$ ,  $\lambda_{\text{ex}} = 325 \text{ nm}$ ).

### Protocol to Determine Concentration of Zn<sup>2+</sup> Ion in Aqueous Sample

A simple protocol was developed to show that **2.6b** could, in principle, be used to assay Zn<sup>2+</sup> ion found in aqueous samples. In four parallel experiments, molecular receptor **2.6b** (3.8 mg, 5.0 μM) was dissolved in 20 mL CH<sub>3</sub>CN:H<sub>2</sub>O (50:50). An aliquot of Zn(ClO<sub>4</sub>)<sub>2</sub> (0.25, 0.5, 0.75, and 1.0) was added to each and the solution refluxed for 24 h. The solvents were removed in a vacuum, and the residues were redissolved in CH<sub>3</sub>CN. A 50 μM solution of each sample was prepared in 100% CH<sub>3</sub>CN, and the fluorescence spectra recorded. Fluorescence at 421 nm increased linearly with increasing Zn<sup>2+</sup> concentration, demonstrating that receptor **2.6b** could be used to determine the zinc content of aqueous samples (Table 2.2 and Figure 2.21).

Table 2.2

*Data for Zn<sup>2+</sup> ion binding calibration curve (\*\*\*) point ignored in calibration curve due to solubility)*

Concentration of Zn <sup>2+</sup> (mM)	Fluorescence intensity (421 nm)
0	0.14
0.07	0.06***
0.081	0.22
0.19	0.39
0.5	0.87

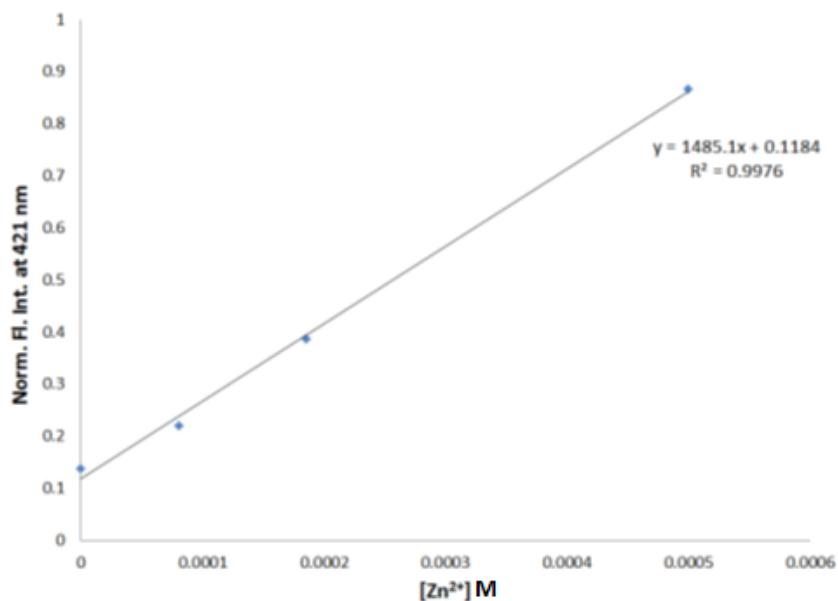


Figure 2.21. Calibration curve generated from fluorescence data of **2.6b** (5  $\mu$ M,  $\lambda_{\text{ex}}=325$  nm, CH<sub>3</sub>CN) and [Zn(**2.6b**)]<sup>2+</sup> complexes demonstrating a linear response.

#### Summary

Two pyrene-based triazole molecular probes **2.6a** and **2.6b** were synthesized in *ortho* and *meta* forms by azide-alkyne Huisgen cycloaddition reaction of N-(prop-2-ynyl) pyrene-1-carboxamide and bis(azidomethyl) benzene. Fluorescence titration studies of compound showed a significant hypsochromic shift in the excimer band from 495 to 400 nm upon addition of Zn<sup>2+</sup> salt. The fluorescence intensity at 400 nm was significantly more intense for **2.6b** than **2.6a** upon addition of Zn<sup>2+</sup> ion. The effect of different counterions on Zn<sup>2+</sup> binding of compound **2.6a** and **2.6b** was explored and showed that the fluorescence intensity at 400 nm due to ClO<sub>4</sub><sup>-</sup> salt was more intense than any other anions. Density functional theory studies suggest that Zn<sup>2+</sup> is bound in the cleft of the probes in a 1:1 host:guest ratio. <sup>1</sup>H NMR studies of compound **2.6b** with Zn(ClO<sub>4</sub>)<sub>2</sub> showed the protons of the triazole and amide groups were shifted into downfield more than any other protons suggesting the possible coordination of Zn<sup>2+</sup> ions by the amide

oxygen and triazole nitrogen atoms. The proposed structure for **2.6b** and its complex from molecular modeling is also supported by 2D NMR and IR studies. The limit of detection for  $\text{Zn}^{2+}$  is calculated in the nanomolar range, and the binding process is reversible allowing the system to be recycled several times. A protocol is proposed that would allow detection of  $\text{Zn}^{2+}$  in aqueous samples.

## Experimental

### *General technique*

All  $^1\text{H}$ ,  $^{13}\text{C}$  NMR, and 2 D NMR spectra were recorded either on a Bruker Ultashield plus 400 MHz spectrometer or 600 MHz spectrometer in the desired deuterated solvents. Chemical shifts are reported in parts per million (ppm) downfield from tetramethylsilane (0 ppm) as the internal standard, and coupling constants ( $J$ ) are recorded in hertz (Hz). The multiplicities in the  $^1\text{H}$  NMR spectra are reported as (br) broad, (s) singlet, (d) doublet, (dd) doublet of doublets, (ddd) doublet of doublet of doublets, (t) triplet, (sp) septet, and (m) multiplet. All spectra are recorded at ambient temperatures. UV-Vis experiments were performed on a Beckman DU-70 UV-Vis spectrometer. IR spectra were recorded on Nicolet Nexus 470 FT-IR paired with a Smart Orbit ATR attachment. The characteristic functional groups reported in wavenumbers ( $\text{cm}^{-1}$ ), and described as weak (w), medium (m), strong (s), and very strong (vs). Fluorescence experiments were carried out on a QuantaMaster<sup>TM</sup> 40 Intensity Based spectrofluorometer from PTI technologies; steady-state (slitwidths 0.50 mm);  $\lambda_{\text{Ex}} = 355$  nm  $\lambda_{\text{Em}} = 360$  nm to 600 nm. Elemental analysis was carried out at Atlantic Microlab Inc.

*General procedure for fluorescence experiments*

A stock solution of compound **2.6** was prepared in CH<sub>3</sub>CN. The solution was excited at  $\lambda = 325$  nm and scanned from  $\lambda$  360-625 nm with the slit widths set to 0.5 mm. A 100 times more concentrated solution of the Zn<sup>2+</sup> salt was prepared in CH<sub>3</sub>CN and 10  $\mu$ L (10  $\mu$ L = 0.1 equivalent of metal salt) aliquots was added to compound **2.6**, and the fluorescence spectra was recorded after each addition. Dilution factors were taken into consideration upon binding study determination. The binding studies were pursued by fluorescence titrations using HypSpec 2006.<sup>116</sup>

*General procedure for UV-Vis experiment*

The general procedure for the molar absorptivity of compounds **2.6a** and **2.6b** was carried out as follows. A stock solution ( $1.32 \times 10^{-5}$  M) of compound **2.6a** was prepared by dissolving 0.5 mg in 50 mL of CH<sub>3</sub>CN. Compound **2.6b** was prepared by dissolving 0.8 mg in 50 mL CH<sub>3</sub>CN then 1 mL was transferred to the UV-Vis cell. From the stock solution eight successive dilutions were carried out, and measured the absorbance to calculate the molar absorptivity. The molar absorption coefficients for compound *ortho-2.6a* and *meta-2.6b* were calculated at various wavelengths (Table 2.3)

Table 2.3

*Molar absorptivity for compounds ortho-2.6a and meta-2.6b in CH<sub>3</sub>CN ( $M^{-1}cm^{-1}$ )*

	240 nm	274 nm	326 nm	340 nm
<i>ortho-2.6a</i>	$8.9 \times 10^4$	$5.3 \times 10^4$	$4.4 \times 10^4$	$3.4 \times 10^4$
<i>meta-2.6b</i>	$5.3 \times 10^4$	$3.4 \times 10^4$	$2.0 \times 10^4$	$2.6 \times 10^4$

### *Computational methods*

Equilibrium geometries for the ligands ( $L_{\text{ortho}}$  and  $L_{\text{meta}}$ ) and their zinc complexes ( $L_{\text{meta}}\text{ZnCl}_2$ ,  $L_{\text{meta}}\text{Zn}(\text{ClO}_4)_2$  and  $L_{\text{ortho}}\text{Zn}(\text{ClO}_4)_2$ ) were determined by full conformational searches of the 676 possible structures (identified through the number of rotatable bonds) followed by molecular mechanics energy minimization methods (using the MMFF forcefield). No formal bonds between zinc and ligands or anions were introduced. Initial refinement was followed by geometry optimization at semiempirical PM3d level with the resulting structures used as input coordinates for density functional calculations (B3LYP/6-31G\*). Calculations were made using Spartan '10 installed on a desktop computer equipped with Intel Xenon Dual Quad Core CPUs running at 2.33 GHz (Table 2.4).



Table 2.4

Key interactions in angstroms (Å) and degrees (°)

	Free ligand (L <sub>ortho</sub> )	Free ligand (L <sub>meta</sub> )	L <sub>ortho</sub> Zn(ClO <sub>4</sub> ) <sub>2</sub>	L <sub>meta</sub> ZnCl <sub>2</sub>	L <sub>meta</sub> Zn(ClO <sub>4</sub> ) <sub>2</sub>
N-H	1.011	1.013	1.030	1.012	1.029
N-H'	1.012	1.012	1.023	1.011	1.027
triazoleH	1.079	1.078	1.077	1.081	1.078
triazoleH'	1.080	1.079	1.082	1.081	1.088
amide C=O	1.230	1.228	1.283	1.250	1.279
amide C=O'	1.232	1.233	1.282	1.252	1.286
triazole Zn···N	N/A	N/A	2.040	N/A	2.018
triazole Zn···N'	N/A	N/A	2.019	N/A	2.020
C=O···Zn	N/A	N/A	1.955	2.013	1.942
C=O'···Zn	N/A	N/A	1.924	2.013	1.949
anion···Zn	N/A	N/A	N/A	2.261	N/A
anion'···Zn	N/A	N/A	N/A	2.218	N/A
pyrene –pyrene distance	5.523	4.771	10.798	5.547	7.382
triazole N'···Zn···N	N/A	N/A	96.45	N/A	101.72
C=O'···Zn···O=C	N/A	N/A	115.43	104.25	110.64
anion'···Zn···anion	N/A	N/A	N/A	126.17	N/A
anion···Zn···O=C	N/A	N/A	N/A	106.12	N/A
triazole C=O···Zn···N	N/A	N/A	110.95	N/A	111.07
pyrene –pyrene angle	18.48	3.91	43.56	28.02	77.49

## General Procedure for the Synthesis

*Preparation of bis(azidomethyl)benzene(2.5a and 2.5b)*<sup>114</sup>

The desired (*ortho* or *meta*) bis(bromomethyl)benzene (1.32 g, 5.0 mmol) and sodium azide (0.97 g, 15 mmol) were dissolved in a 3:1 mixture of acetone and water (30 mL) and stirred at room temperature for 24 hours. A mixture of dichloromethane (25 mL) and water (25 mL) was then added to the reaction mixture and stirred for 10 mins. The organic layer was separated and washed three times with water (50 mL), dried over magnesium sulfate, filtered, and the solvent removed to produce a colored oil.

Characterization of compound *ortho*-2.5a: Yield 752 mg, 4.0 mmol, 80%:

<sup>1</sup>H NMR (300 K, DMSO, 400 MHz):  $\delta$  7.38 (*m*, 4H, CH<sub>Ar</sub>), 4.45 (*s*, 4H, CH<sub>2</sub>).

<sup>13</sup>C NMR (300 K, DMSO, 400MHz):  $\delta$  133.9, 130.0, 128.7, 51.0;

IR (ATR solid); 2887  $\nu_{\text{C-H}}$  (w), 2085  $\nu_{\text{N=N}}$  (vs)  $\text{cm}^{-1}$ .

Characterization of *meta*-2.5b: Yield 790 mg, 4.2 mmol, 84%:

<sup>1</sup>H NMR (300 K, DMSO, 400 MHz):  $\delta$  7.38 (*t*, 1H, *J* = 7Hz, CH<sub>Ar</sub>), 7.28-7.30 (*m*, 3H, CH<sub>Ar</sub>), 4.37(*s*, 4H, CH<sub>2</sub>).

<sup>13</sup>C NMR (300 K, DMSO, 400 MHz):  $\delta$  136.1, 129.2, 128.0, 53.4

IR (ATR solid); 2929  $\nu_{\text{C-H}}$  (w), 2086  $\nu_{\text{N=N}}$  (vs)  $\text{cm}^{-1}$ .

*Preparation of N-(prop-2-ynyl) pyrene-1-carboxamide (compound 2.4)*<sup>113</sup>

1-Pyrenecarboxylic acid (138 mg, 0.56 mmol) was dissolved in thionyl chloride (8 mL) and refluxed under argon for two hours. The excess thionyl chloride was removed under reduced pressure to form a yellow solid that was redissolved in chloroform (50 mL) to which, triethylamine (82  $\mu\text{L}$ , 0.59 mmol) and propargylamine (71  $\mu\text{L}$ , 1.28 mmol) were added drop wise at 0°C and stirred one hour. The reaction was allowed to warm to

room temperature and was stirred for a further 18 hours. A saturated solution of brine (50 mL) was then added to the reaction mixture which was subsequently extracted with chloroform (3 × 15 mL). The organic layers were combined and washed with brine (2 × 25 mL) and water (2 × 25 mL). The organic layer was dried over magnesium sulfate, filtered, and the solvent was removed under reduced pressure. Column chromatography was carried out using silica (40-63 $\mu$ m, 60 Å) and ethyl acetate in hexane as the eluent (15:75). The compound was obtained as a pure yellow solid, (95 mg, 0.33 mmol, 60%).

$^1\text{H}$  NMR ( $\text{CDCl}_3$ , 400 MHz):  $\delta$  8.53 (*d*, 1H,  $J = 10$  Hz,  $\text{CH}_{\text{py}}$ ), 8.19 (*s*, 1H,  $\text{CH}_{\text{py}}$ ), 8.10 (*s*, 1H,  $\text{CH}_{\text{py}}$ ), 8.00-8.10 (*m*, 6H,  $\text{CH}_{\text{py}}$ ), 6.40 (*s*, 1H, NH), 4.42 (*m*, 2H,  $\text{CH}_2$ ), 2.32 (*m*, 1H, CH)

$^{13}\text{C}$  NMR ( $\text{CDCl}_3$ , 400 MHz):  $\delta$  169.5, 132.7, 131.1, 130.6, 129.8, 128.8, 128.7, 127.0, 126.4, 125.9, 125.8, 124.6, 124.3, 124.2, 124.2, 79.5, 72.0, 30.0.

IR (ATR solid): 3278  $\nu_{\text{C=H}}$  (vs), 3198  $\nu_{\text{N-H}}$  (m), 2921, 2855,  $\nu_{\text{C-H}}$  (m), 2070  $\nu_{\text{C}\equiv\text{C}}$  (w), 1618  $\nu_{\text{C=O}}$  amide I (s) 1600  $\nu_{\text{C=O}}$  amide II (m)  $\text{cm}^{-1}$ .

#### *Preparation of compounds 2.6a and 2.6b*<sup>114</sup>

N-(prop-2-ynyl) pyrene-1-carboxamide<sup>113</sup> (75 mg, 0.26mmol) and the desired *ortho-* or *meta-* bis(azidomethyl)benzene (25 mg, 0.13 mmol), copper(II)sulfate (3.25 mg, 0.013 mmol) and sodium ascorbate (5.15 mg, 0.026 mmol) were dissolved in a mixture of acetone and water (15 mL, 4:1) and stirred at room temperature for 48 hours. The reaction mixture was then poured into ice cold water (20 mL) to obtain a solid which was filtered, washed with water (200 mL), and dried to give the desired isomer.

Characterization of compound (*ortho*-2.6a): Yield 75 mg, 0.1 mmol, 77 %; m.p. 244 °C

$^1\text{H}$  NMR (300 K, DMSO- $d_6$ , 400MHz):  $\delta$  9.24 (*t*, 2H,  $J = 5$  Hz, NH), 8.47 (*d*, 2H,  $J = 10$  Hz,  $\text{CH}_{\text{py}}$ ), 8.35 (*s*, 1H,  $\text{CH}_{\text{py}}$ ), 8.34 (*s*, 2H,  $\text{CH}_{\text{py}}$ ), 8.32 (*d*, 2H,  $J = 5$ Hz,  $\text{CH}_{\text{py}}$ ), 8.29 (*s*, 1H,  $\text{CH}_{\text{py}}$ ), 8.24 (*d*, 2H,  $J = 10$  Hz,  $\text{CH}_{\text{py}}$ ), 8.18-8.21 (*m*, 6H,  $\text{CH}_{\text{py}}$  and  $\text{CH}_{\text{triazole}}$ ), 8.09-8.15 (*m*, 4H,  $\text{CH}_{\text{py}}$ ), 7.37-7.39 (*dd*, 2H,  $J = 3.5, 5.6$  Hz,  $\text{CH}_{\text{Ar}}$ ), 7.20-7.22 (*dd*, 2H,  $J = 3.5, 5.6$  Hz,  $\text{CH}_{\text{Ar}}$ ), 5.89 (*s*, 4H,  $\text{CH}_{2\text{triazole}}$ ), 4.69 (*d*, 4H,  $J = 5$  Hz,  $\text{CH}_2\text{N}_{\text{amide}}$ ).

$^{13}\text{C}$  NMR (300 K,  $\text{CDCl}_3$ , 400MHz):  $\delta$  169.3, 134.8, 132.1, 131.9, 131.1, 130.6, 129.6, 129.3, 128.8, 128.7, 128.3, 127.6, 127.0, 126.3, 126.1, 125.7, 125.0, 124.8, 124.2, 124.1, 123.9, 50.4, 35.5.

ESI-MS  $m/z$   $[\text{M} + \text{H}]^+ = 755.4$  and  $[\text{M} + \text{Na}]^+ = 777.5$ ;

IR (ATR solid); 3339  $\nu_{\text{N-H}}$  (m), 3115  $\nu_{\text{C-H}}$  (w), 3037  $\nu_{\text{C-H}}$  (w), 1633  $\nu_{\text{C=O}}$  amide I(s), 1600  $\nu_{\text{C=O}}$  amide II (m),  $\text{cm}^{-1}$ .

Anal. Calcd for  $\text{C}_{48}\text{H}_{34}\text{N}_8\text{O}_2$ : H 4.54 %; N 14.84 %; C; 76.38 %

Anal. Recalcd for  $\text{C}_{48}\text{H}_{34}\text{N}_8\text{O}_2 \cdot 9\text{H}_2\text{O} \cdot 10(\text{CH}_3)_2\text{CO}$ : H 4.43 %; N 14.32 %; C; 74.50 %

Found for  $\text{C}_{48}\text{H}_{34}\text{N}_8\text{O}_2 \cdot 9\text{H}_2\text{O} \cdot 10(\text{CH}_3)_2\text{CO}$ : H 4.72 %; N 14.26 %; C; 74.47 %

Characterization of compound (*meta*-2.6b): Yield 68 mg, 0.1 mmol, 69 %; m.p. 195°C:

$^1\text{H}$  NMR (300 K, DMSO, 400 MHz):  $\delta$  9.22 (*t*, 2H,  $J = 5$  Hz, NH), 8.49 (*d*, 2H,  $J = 10$  Hz,  $\text{CH}_{\text{py}}$ ), 8.32-8.36 (*m*, 5H,  $\text{CH}_{\text{py}}$ ), 8.30 (*s*, 1H,  $\text{CH}_{\text{py}}$ ), 8.26 (*s*, 1H,  $\text{CH}_{\text{py}}$ ), 8.20-8.24 (*m*, 7H,  $\text{CH}_{\text{py}}$  and  $\text{CH}_{\text{triazole}}$ ), 8.09-8.13 (*m*, 4H,  $\text{CH}_{\text{pyrene}}$ ), 7.40-7.43 (*m*, 2H,  $\text{CH}_{\text{Ar}}$ ), 7.30-7.32 (*d*, 2H,  $J = 8$ Hz,  $\text{CH}_{\text{Ar}}$ ), 5.64 (*s*, 4H,  $\text{CH}_{2\text{triazole}}$ ), 4.67 (*d*, 4H,  $J = 5$ Hz,  $\text{CH}_2\text{N}_{\text{amide}}$ ).

$^{13}\text{C}$  NMR (300 K,  $\text{CDCl}_3$ , 400MHz):  $\delta$  169.3, 137.2, 132.1, 131.9, 131.2, 130.6, 129.7, 128.8, 128.6, 128.3, 128.2, 128.1, 127.6, 127.0, 126.3, 126.1, 125.7, 125.1, 124.8, 124.2, 124.1, 123.7, 53.0, 35.5.

ESI-MS  $m/z$   $[\text{M} + \text{H}]^+ = 755.1$  and  $[\text{M} + \text{Na}]^+ = 777.5$ ;

IR (ATR solid); 3332  $\nu_{\text{N-H}}$  (m), 3120  $\nu_{\text{C-H}}$  (w), 3036  $\nu_{\text{C-H}}$  (w), 1638  $\nu_{\text{C=O}}$  amide I(s), 1596  $\nu_{\text{C=O}}$  amide II(m),  $\text{cm}^{-1}$

Anal. Calcd for  $\text{C}_{48}\text{H}_{34}\text{N}_8\text{O}_2$ : H 4.54 %; N 14.84 %; C; 76.38 %

Anal. Recalcd for  $\text{C}_{48}\text{H}_{34}\text{N}_8\text{O}_2 \cdot 10\text{H}_2\text{O} \cdot 35(\text{CH}_3)_2\text{CO}$ : H 4.28 %; N 14.01 %; C; 72.08 %

Found for  $\text{C}_{48}\text{H}_{34}\text{N}_8\text{O}_2 \cdot 10\text{H}_2\text{O} \cdot 35(\text{CH}_3)_2\text{CO}$ : H 4.91 %; N 13.95 %; C; 71.87 %.

## CHAPTER III

## SIMULTANEOUS CATION AND ANION INDUCED SELF-ASSEMBLY

## Introduction

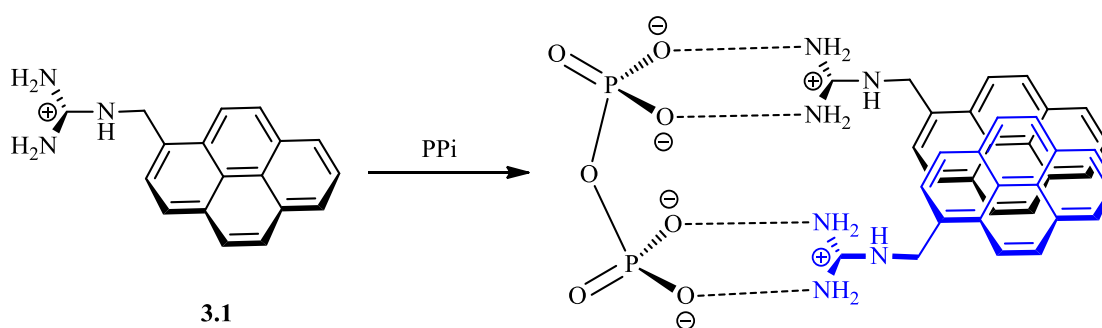
Many sensors to date have been developed for detection of a particular cation or anion, thereby ignoring the effect of the counter-ion. The counter-ion is large and does not interact in any appreciable degree with the system under study. For example, if a molecular probe has been designed to target a cation, then large bulky anions such as perchlorate ( $\text{ClO}_4^-$ ), tetrafluoroborate ( $\text{BF}_4^-$ ), and hexafluorophosphate ( $\text{PF}_6^-$ ) are used. The reverse is true if one wants to target anions. These non-competitive counter-ions are deliberately used so that they do not affect the binding process for the particular target species. However, metal ion and anions always occur as ion pairs either as solvent-separated ion pairs, contact ion pairs, or aggregated contact ion pairs. Salts rarely, if ever, exist as separate ions unless the medium is highly solvating. Hence, smaller size counter ions could not be ignored. Moreover, non-competitive counter ions are not generally encountered in real-world applications, and hence inter-ion competition can be significant. Therefore, the most effective strategy is to design a receptor which can simultaneously detect both metal ion and anion within the same molecular host.<sup>70</sup>

In Chapter II, the interactions of probes **2.6a** and **2.6b** with  $\text{Zn}^{2+}$  ions were fully investigated. However, a model compound i.e., the compound that only contains a single pendent arm was not reported. It transpires that the model system also bound  $\text{Zn}^{2+}$  ions. However, the binding mechanism is a consequence of both the cation and anion simultaneously “triggering” the molecular probe response. In particular, it is the simultaneous cation and anion induced self-assemble process.

The self-assembly process is defined as the spontaneous and reversible association of two or more components to form large, non-covalently bound aggregate. Hydrogen bonding,  $\pi$ -stacking interactions, and metal-ligand interactions are some of the most commonly used interactions in synthetic self-assembly. In metal template self-assembly, metals with specific geometrical preferences assist the formation of organized structures by self-assembly of target ligands.<sup>52</sup> The variety of oxidation states, coordination numbers, geometries, and stabilities of transition metal complexes allows for a precise control over the structure and dynamics of the resulting assemblies.<sup>129</sup> Pyrene has been used as fluorophore in most of these receptors as it forms an excimer band upon, binding of analyte in *syn* orientation. This property of pyrene has been used in numerous examples for detection of metal ions<sup>59, 130</sup> and anions<sup>56, 131</sup> through a process of self-assembly. Some recent examples have been highlighted in previous chapters.

One example that utilizes the induced self-assembly for sensing of anions is **3.1**, a guanidinium receptor which contains pyrene group.<sup>52</sup> Compound **3.1** showed a structured emission band at 370-450 nm in CH<sub>3</sub>OH which was assigned to a pyrene monomer emission. In the presence of pyrophosphate (P<sub>2</sub>O<sub>7</sub><sup>4-</sup>), a structureless band with an emission maximum at 476 nm appeared with quenching of monomer emission. The fluorescence titration of compound **3.1** with PPI in CH<sub>3</sub>OH showed that the intensity of emission at 476 nm increased up to 0.5 equivalents but reversed upon further addition of PPI. This suggested the formation of both 2:1 and 1:1 host:guest complexes whose association constants ( $K_{21}$  and  $K_{11}$ ) were calculated as  $1.2 \times 10^8 \text{ M}^{-2}$  and  $1.0 \times 10^4 \text{ M}^{-1}$ , respectively. A much less effective response was found upon addition of other anions such as HPO<sub>4</sub><sup>2-</sup>, H<sub>2</sub>PO<sub>4</sub><sup>-</sup>, CH<sub>3</sub>COO<sup>-</sup>, SCN<sup>-</sup>, Cl<sup>-</sup>, and Br<sup>-</sup>. The binding of **3.1** with PPI was

also studied by  $^1\text{H}$  NMR in  $\text{CH}_3\text{OH}-d_4$  and support the results of fluorescence that both 2:1 and 1:1 complexes are formed. The up field shifts for the methylene and pyrene protons of **3.1** were observed until a 0.5 equivalent of PPI was added after which these protons showed downfield shifts. The observed shielding effects could be due to ring current effects,<sup>132</sup> suggesting a complexation-induced aggregation of host molecules. In addition, the shape of the titration curve versus the PPI/**3.1** ratio, coinciding with that obtained by fluorescent titration studies suggested that 2:1 and 1:1 host:guest complexes are formed. The association constants are calculated as be  $9.8 \times 10^7 \text{ M}^{-2}$  and  $1.3 \times 10^4 \text{ M}^{-1}$ , respectively, for the 2:1 and 1:1 complexes (Scheme 3.1).

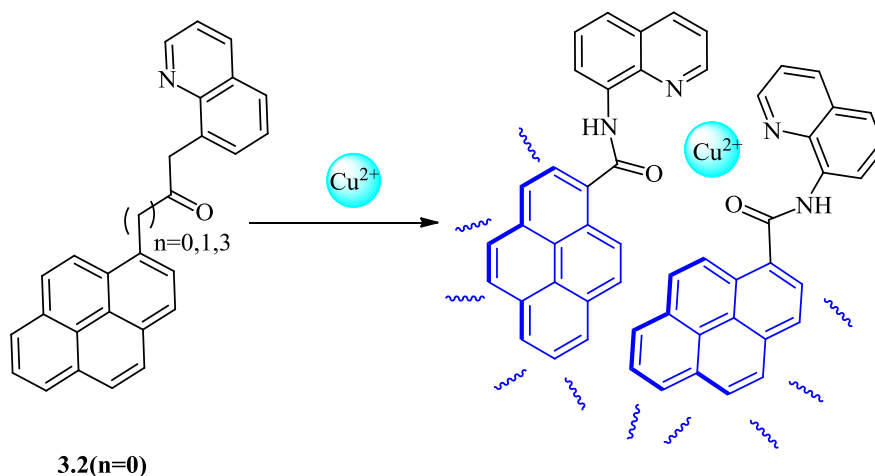


*Scheme 3.1.* The proposed binding mode of compound **3.1** with the  $\text{P}_4\text{O}_7^{4-}$ .

A simple pyrene molecular probe (**3.2**) was developed by Kim et al. They showed that the self-assembly occurs upon the coordination of  $\text{Cu}^{2+}$  ion.<sup>133</sup> Addition of  $\text{Cu}^{2+}$  ion to the compound **3.2** ( $6.0 \mu\text{M}$  in  $\text{CH}_3\text{CN}$ ) produced a strong static excimer band at 460 nm with increasing intensity in addition to weak monomer emission at 388 nm on excitation at 360 nm. The excimer emission intensity induced by the  $\text{Cu}^{2+}$  ion decreased as the space length increased ( $n = 1-3$ ) between the pyrene and amide group. This confirms that the lack of methyl functional group stabilizes the chelation ring between the nitrogen atom in the quinoline group and the oxygen atom on the amide group. Other



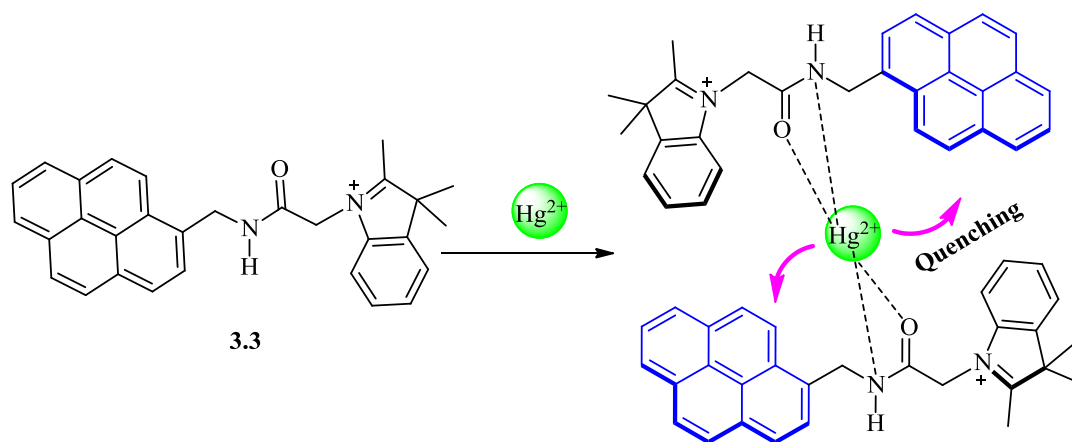
metal ions such as  $\text{Li}^+$ ,  $\text{Na}^+$ ,  $\text{K}^+$ ,  $\text{Rb}^+$ ,  $\text{Cs}^+$ ,  $\text{Mg}^{2+}$ ,  $\text{Ba}^{2+}$ ,  $\text{Ca}^{2+}$ ,  $\text{Sr}^{2+}$ ,  $\text{Ag}^+$ ,  $\text{Zn}^{2+}$ ,  $\text{Cd}^{2+}$ ,  $\text{Hg}^{2+}$ , and  $\text{Pb}^{2+}$  did not show any significant fluorescence changes. UV-Vis titration showed the band broadening and red shift (color change from colorless to red) in the spectra of **3.2** upon the addition of  $\text{Cu}^{2+}$  ion which is attributed to the favorable intermolecular  $\pi$ - $\pi$  stacked dimerization of the two pyrene groups in the ground state. The association constant ( $K_{12}$ ) was calculated to be  $5.4 \times 10^5 \text{ M}^{-2}$  in aqueous solution. The molecular probe **3.2** has a detection limit of  $1.0 \mu\text{M}$  (63 ppb) for  $\text{Cu}^{2+}$  ion within the limit of detection outlined by the EPA (Environmental Protection Act) which states the detection limit of  $\sim 20 \mu\text{M}$  (1260 ppb) of  $\text{Cu}^{2+}$  ion in water.<sup>134</sup> The experimental results are also supported by DFT calculations which indicate that the efficient excimer formation is due to the fact that LUMO and the HOMO of the complex are located on either of the two pyrenyl groups, respectively (Scheme 3.2).



*Scheme 3.2.* Proposed binding mode of compound **3.2** with  $\text{Cu}^{2+}$  ion.<sup>133</sup>

Cao and co-workers synthesized a pyrene based fluorescent sensor (**3.3**) for  $\text{Hg}^{2+}$  ion from 2,3,3-trimethylindolenine with high solubility in aqueous solution at physiological pH.<sup>135</sup> An indolium was attached to pyrene to enhance the solubility of the

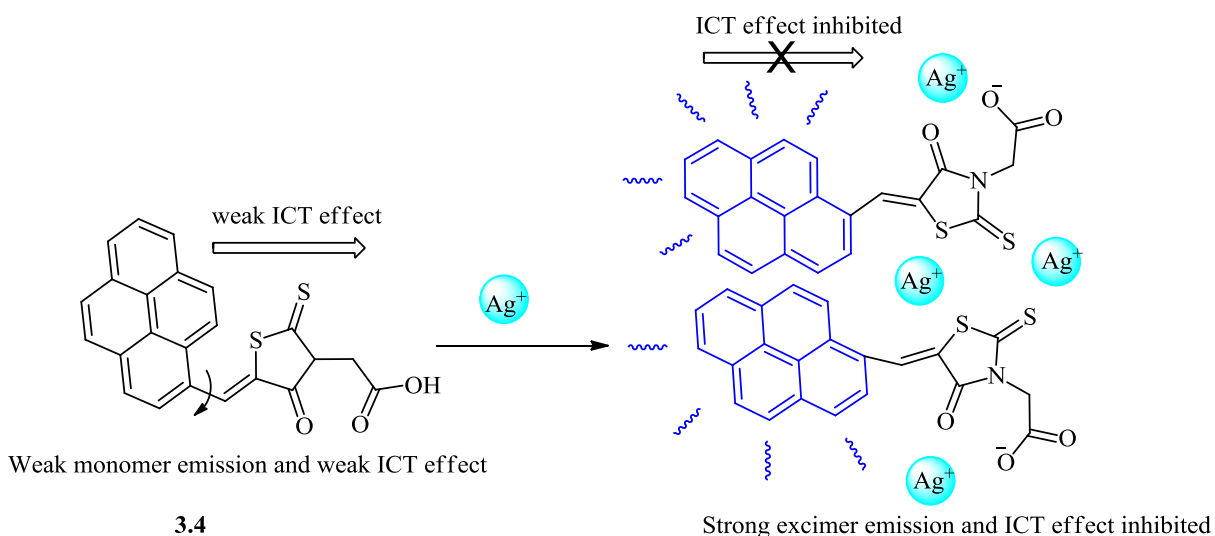
compound in aqueous solution. The fluorescence spectrum of the compound **3.3** showed the monomer emission bands at 381 and 400 nm on excitation at 340 nm in pH 7.4 HEPES buffer (10 mM) solution. Addition of  $\text{Hg}^{2+}$  (0-20  $\mu\text{M}$ ) ions, as the perchlorate salt, led to significant fluorescence quenching without any wavelength shift. The maximum quenching was calculated to be an 87% reduction in fluorescence intensity compared to the free ligand when the concentration of  $\text{Hg}^{2+}$  ion was 4  $\mu\text{M}$ . The other metal ions such as  $\text{Na}^+$ ,  $\text{K}^+$ ,  $\text{Ca}^{2+}$ ,  $\text{Mg}^{2+}$ ,  $\text{Pb}^{2+}$ , and  $\text{Cu}^{2+}$  did not show any appreciable quenching. Thus, the fluorescence quenching induced by  $\text{Hg}^{2+}$  ion was attributed to a heavy atom and CHEQ (chelation enhanced quenching) effects (Chapter I).<sup>90</sup> The association constant ( $K_{12}$ ) was calculated to be  $5.1 \times 10^7 \text{ M}^{-2}$ . The formation of  $[\text{Hg}(\mathbf{3.3})_2]^{2+}$  complex is also confirmed by  $^1\text{H}$  NMR spectroscopy. The amide proton of free ligand **3.3** showed a downfield shift in presence of  $\text{Hg}^{2+}$  ion which indicates that the nitrogen atom is involved in coordination of  $\text{Hg}^{2+}$  ion through its lone pair of electron (Scheme 3.3). The proton of amide would still shift to down field even when the  $\text{Hg}^{2+}$  ion was coordinated by the amide oxygen atoms due to an inductive effect. The author proposes that the oxygen atoms also play a role by coordinating with the  $\text{Hg}^{2+}$  ion. This is certainly a reasonable assumption; however, no IR studies and molecular modeling were carried to confirm the oxygen and metal binding interaction (Scheme 3.3).



*Scheme 3.3.* A chelation-enhanced quenching sensor complex formation of  $[\text{Hg}(\mathbf{3.3})_2]^{2+}$  in pH 7.4 HEPES buffer solution.<sup>135</sup>

Sheng and co-workers developed a highly selective ratiometric fluorescent sensor (**3.4**) for  $\text{Ag}^+$  ion based on a rhodanineacetic acid-pyrene derivative (RAAP) which was synthesized by the condensation of rhodanine-3-acetic acid with 1-formylpyrene. Rhodanine-3-acetic acid acts as an electron acceptor while pyrene acts as an electron donor. These two units are linked together by a carbon-carbon double bond which offers a bridge for intramolecular charge transfer (ICT) to form an ICT state. Rhodanine-3-acetic acid is a good ligand to coordinate  $\text{Ag}^+$  ion due to the soft sulfur atoms that have a strong interaction with the soft  $\text{Ag}^+$  ions. The fluorescence spectrum of the compound **3.4** ( $\lambda_{\text{ex}}=381$  nm) exhibits weak emission bands at 432 nm and 538 nm in  $\text{CH}_3\text{OH}$ , which is assigned to the pyrene monomer emission and ICT effects, respectively. Upon addition of two equivalents of  $\text{Ag}^+$  ion to the compound **3.4** (5  $\mu\text{M}$ ), a new pyrenyl excimer band is observed at 448 nm with an approximate 15-fold enhancement of fluorescent intensity in comparison to free ligand. Presumably, conformational change brings the two molecules of **3.4** together to switch “on” the excimer signal. On the addition of NaCl (200  $\mu\text{l}$  of 10 mM) to  $[\text{Ag}(\mathbf{3.4})_2]^+$ , the original fluorescence signal of the compound **3.4** is restored

demonstrating the reversibility of the chemosensor. Fluorescent screening against other metal ions such as  $\text{Na}^+$ ,  $\text{K}^+$ ,  $\text{Mg}^{2+}$ ,  $\text{Ca}^{2+}$ ,  $\text{Ni}^{2+}$ ,  $\text{Zn}^{2+}$ ,  $\text{Cd}^{2+}$ ,  $\text{Hg}^{2+}$ ,  $\text{Pb}^{2+}$ ,  $\text{Mn}^{2+}$ ,  $\text{Fe}^{2+}$ ,  $\text{Cu}^{2+}$ , and  $\text{Co}^{2+}$  did not induce any enhancement or red-shift of fluorescent emission at 448 nm. The detection limit of this compound **3.4** for  $\text{Ag}^+$  ion was found to be  $1.0 \times 10^{-7}$  M (10 ppb), which complies with the standard of the EPA and the World Health Organization (WHO) for drinking water ( $5.0 \times 10^{-7}$  M (54 ppb)).<sup>126</sup> The compound is also a colorimetric sensor; by adding aliquots of  $\text{Ag}^+$  ion (up to three equivalents), a hypochromic shift is seen at 446 nm and a hyperchromic shift at 382 nm *via* a pseudo-isobestic point at 410 nm which is an indicative of equilibrium other than a 1:1 complex, i.e., a 2:1 complex. The  $^1\text{H}$  NMR spectra of **3.4** in  $\text{DMSO}-d_6$  showed that the signals at 8.81 and 4.81 ppm assigned to protons linked to C=C double bond and methylene protons were gradually shifted to downfield direction on increasing the amounts of  $\text{Ag}^+$  ion. This supports carboxylate group is involved in binding with  $\text{Ag}^+$  ion. The author proposed a binding mode shown in scheme 3.4; however, no molecular modeling calculations were reported to support their proposed dimer. Further,  $\text{Ag}^+$  ion was shown to bind either by two sulfur atoms or by two oxygen atoms. It is unlikely that  $\text{Ag}^+$  ion will be bound by the oxygen atoms based on hard soft acid base principle (Scheme 3.4).



*Scheme 3.4.* The proposed binding mode of **3.4** with  $\text{Ag}^+$  ion.<sup>130</sup>

In summary, the self-assembly of all the sensors so far developed are induced either by the metal ion or by the anion as discussed above. An effect of the counter ions on the self-assembly process was not mentioned at all. Further, an excimer emission has been used as a key signal for the self-assembly process in most of the sensors containing only one pyrene unit as sensing motif.

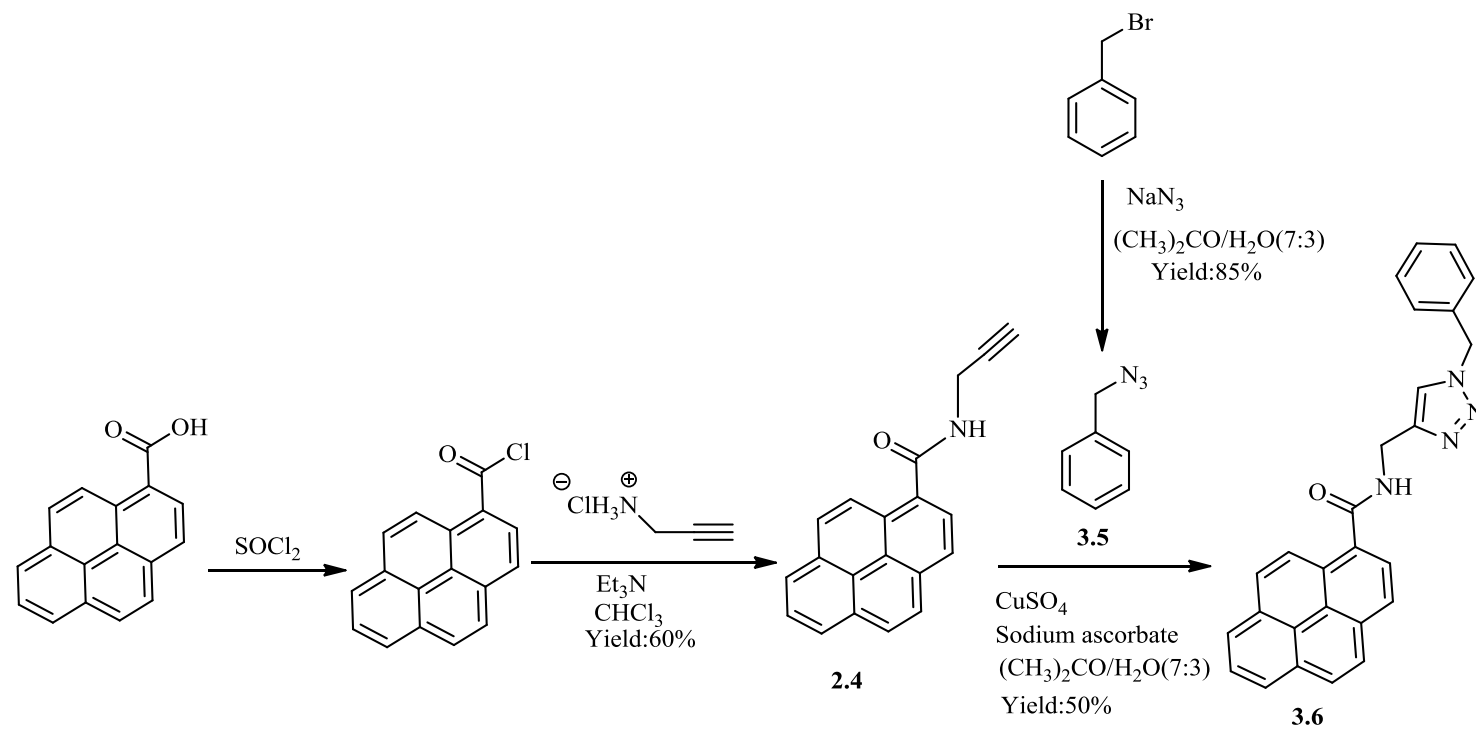
As previously mentioned, the model compound for probes **2.6a** and **2.6b** was synthesized and showed some unexpected binding behavior. It is this behavior that will be discussed in this chapter. In fact, this system was one of the first examples to show that both the anion and cation are required for the sensing mechanism to work.

#### Synthesis of Molecular Probe **3.6**

The commercially available pyrene-1-carboxylic acid is used as the starting material for the synthesis of compound **3.6**. N-(prop-2-ynyl) pyrene-1-carboxamide (**2.4**) was prepared from pyrene-1-carboxylic acid by the same procedure as described in Chapter II.<sup>113</sup> Benzyl azide (**3.5**) was prepared by reacting benzyl bromide with sodium azide in 3:1  $[(\text{CH}_3)_2\text{CO} : \text{H}_2\text{O}]$ . The benzyl azide (**3.4**) was confirmed by its characteristic

strong stretching band at  $2089\text{ cm}^{-1}$  assigned to azide group in IR spectrum and its NMR data agreed with the published procedure.<sup>136</sup> Compounds **2.4** and **3.5** were “click” together *via* the azide-alkyne Huisgen cycloaddition reaction in the presence of copper sulfate and sodium ascorbate as catalysts in a 3:1 [(CH<sub>3</sub>)<sub>2</sub>CO: H<sub>2</sub>O] solution (Scheme 3.5).<sup>113</sup> A solid was obtained once the reaction mixture was poured into water which was filtered, washed with water and recrystallized from CH<sub>3</sub>CN to get the pure yellow compound (**3.6**) in an overall 50% yield. The disappearance of the signal at  $\delta$  4.42 ppm assigned to the terminal C $\equiv$ CH hydrogen atom and appearance of a new signal at  $\delta$  7.68 ppm (CDCl<sub>3</sub>), assigned to the proton of newly formed triazole skeleton confirms the formation of desired product. The compound was fully characterized by <sup>1</sup>H NMR, <sup>13</sup>C NMR, IR, ESI mass spectrum, elemental analysis, and by X-ray crystallography.

This compound is synthesized as the model compound for the molecular cleft project in Chapter II. Therefore, it has only one pyrene as a fluorophore with triazole and amide functional groups.



Scheme 3.5. Synthesis of molecular receptor **3.6**.

### Job's Plot Study of Molecular Probe **3.6**

In order to gain the information regarding speciation, a Job's plot analysis was carried out. Here, both compound **3.6** (host) and  $\text{ZnCl}_2$  (guest) solutions are made in  $\text{CH}_3\text{CN}$  and of  $6.5 \times 10^{-4}$  M. These two solutions are combined in varying ratio of host and guest from 0 to 1 with overall the same total molar concentrations. Fluorescence is measured at each mole fraction and fluorescence intensity ratio ( $I_{382/410}$ ) is plotted against mole fraction of  $\text{ZnCl}_2$ . Since the minimum of the curve lies at 0.33, it corresponds to a 2:1 (ligand:metal) stoichiometry (Figure 3.1).

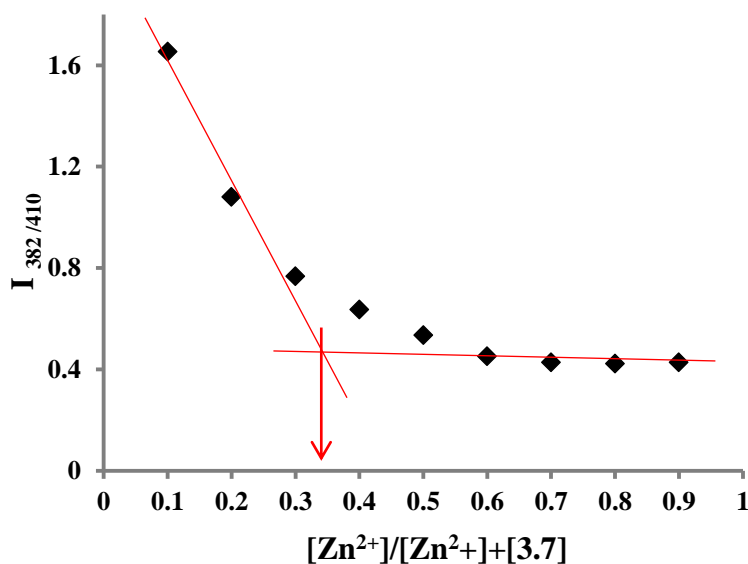


*Figure 3.1.* Job's plot of compound **3.6** with  $\text{ZnCl}_2$  obtained by fluorescence measurements in  $\text{CH}_3\text{CN}$ . The total concentration of compound **3.6** and  $\text{ZnCl}_2$  is  $6.48 \times 10^{-4}$  M where  $X \approx 0.33$  (2:1 ligand:metal ratio). The red lines are for visual interpretation only.

### X-ray Crystallographic Study of Molecular Probe **3.6**

The crystal of compound **3.6** was grown by slow evaporation in  $\text{CH}_3\text{CN}$  at room temperature. The crystal structure shows that the pyrene units are in *transoid* orientation. The crystal packing of **3.6** exhibits acceptor bifurcated hydrogen bonding between amide oxygen atom of one molecule with the hydrogens of triazole and methylene group



(connected to benzene) of another molecule. The C-H (triazole)⋯CO (carbonyl) distance is 2.457 Å, and CH<sub>2</sub> (benzene)⋯CO(carbonyl) distance is 2.394 Å. There is also hydrogen bonding between amide hydrogen of one molecule with the triazole nitrogen atom of another molecule. The N-H (amide)⋯N (triazole) distance is 2.082 Å (Figure 3.2B). The fluorescence spectrum of the compound **3.6** shows monomer emission (Figure 3.2 A) which complements the *transoid* conformation of compound **3.6** in crystal packing.

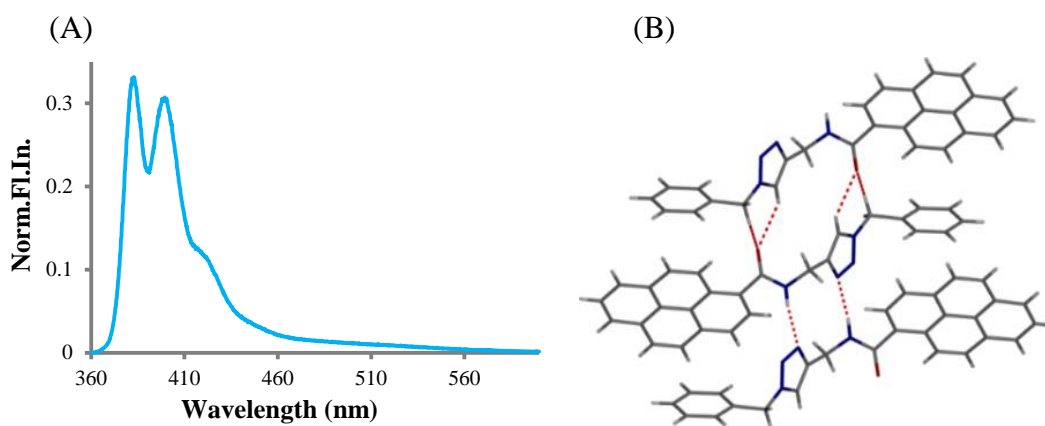


Figure 3.2. (A) Monomer emission of compound **3.6** in CH<sub>3</sub>CN ( $\lambda_{\text{ex}}=340$  nm), and (B) crystal packing in **3.6** showing hydrogen bonding. C-H (triazole)⋯CO (carbonyl)=2.457 Å, CH<sub>2</sub> (benzene)⋯CO (carbonyl)=2.394 Å, N-H (amide)⋯N (triazole) = 2.082 Å.

### Optical Studies of the Molecular Probe **3.6**

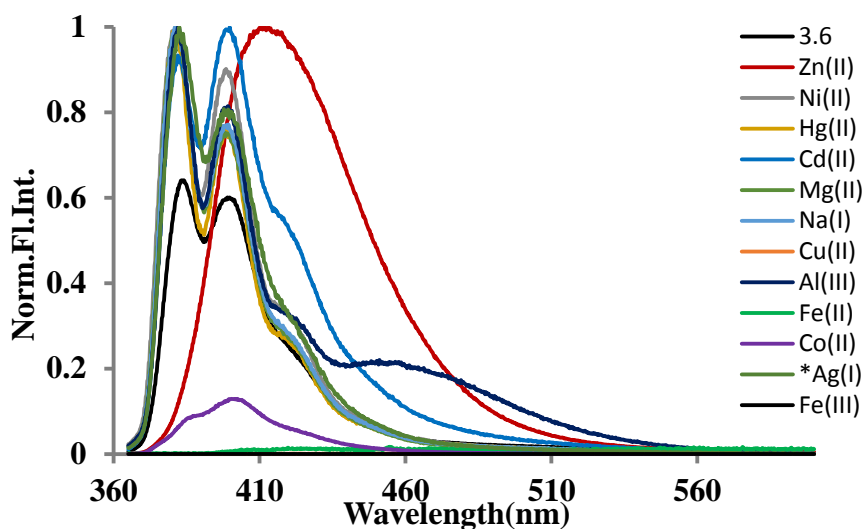
The binding of compound **3.6** with metal ions is first studied by fluorescence spectroscopy. Compound **3.6** is synthesized as the model compound for the molecular cleft project in Chapter II. Therefore, compound **3.6** has only one pyrene functional group and hence is expected to produce only monomer emission. The fluorescence emission of **3.6** should remain unchanged with metal ions as it does not have a suitable binding pocket for the binding of metal ions as in the molecular cleft (Scheme 2.4 in Chapter II). However, the formation of excimer emission upon the addition of any metal ions

normally suggests the **3.6** is binding the metal ion by the self-assembly process as reported in the introduction. Organic solvent CH<sub>3</sub>CN is selected to study the fluorescence of compounds **3.6** as explained in the Chapter II.

The fluorescence spectrum of compound **3.6** ( $6.5 \times 10^{-4}$  M) shows two distinct emission bands at 380 and 400 nm with a broad shoulder at 420 nm on excitation at 355 nm in CH<sub>3</sub>CN (Figure 3.2 and 3.3). These emissions are typical of pyrene derived monomers, assigned to the  $\pi$ - $\pi^*$  electron transitions. The fluorescence of compound **3.6** was first studied by adding ten equivalents of various metal ions such as Na<sup>+</sup>, Ag<sup>+</sup>, Mg<sup>2+</sup>, Cd<sup>2+</sup>, Zn<sup>2+</sup>, Co<sup>2+</sup>, Fe<sup>2+</sup>, Hg<sup>2+</sup>, Cu<sup>2+</sup>, Al<sup>3+</sup>, Fe<sup>3+</sup>, and Ni<sup>2+</sup> (all are chloride salt except Co(NO<sub>3</sub>)<sub>2</sub> and AgNO<sub>3</sub>) to **3.6** in CH<sub>3</sub>CN (Figure 3.3). An intense excimer band was observed with maximum around 420 nm with Zn<sup>2+</sup> ion but not with other metal ions except very little by Cd<sup>2+</sup> ion (Figure 3.3). The fluorescence was quenched by the metal ions such as Fe<sup>2+</sup>, Fe<sup>3+</sup>, and Cu<sup>2+</sup> ions which can be ascribed to a heavy atom effect or paramagnetic effect (Chapter I).<sup>137, 138</sup> Alkali and alkaline earth metal ions such as Na<sup>+</sup> and Mg<sup>2+</sup> ions were found to increase the fluorescence. Compound **3.6** was also titrated with different anions of tetrabutylammonium (TBA) salts such as TBACl, TBABr, TBAI, and TBANO<sub>3</sub> but no excimer emission was observed as shown for the titration chart for TBACl in Figure 3.7. This clearly indicates that Zn<sup>2+</sup> ion is responsible for the formation of excimer emission. The formation of excimer emission upon addition of Zn<sup>2+</sup> ion indicates that it brings two pyrene units close together within the distance of  $\pi$ - $\pi$  (0-5 Å) interaction in *syn* fashion. In order to better understand the binding process, fluorescence titration of compound **3.6** was carried out with ZnCl<sub>2</sub> in CH<sub>3</sub>CN (Figure 3.5). Fluorescence intensity of monomer bands at 380 and 400 nm was decreased with

formation of excimer emission at 420 nm upon addition of increasing concentration of ZnCl<sub>2</sub>. In the later stages of titration (> three equivalents), there is a loss of defined spectroscopic transitions giving a broad and featureless band. This is consistent with a second Zn<sup>2+</sup> ion coordination event of a much weaker affinity such as the formation of complexes with higher metal to ligand ratios. Fitting of fluorescence data to HypSpec progame<sup>116</sup> showed that compound **3.6** was found to bind ZnCl<sub>2</sub> in an exclusively 2:1 ratio with a binding constant calculated to be  $K_{2l}=1.8 \times 10^6 \text{ M}^{-2}$ .

(A)



(B)

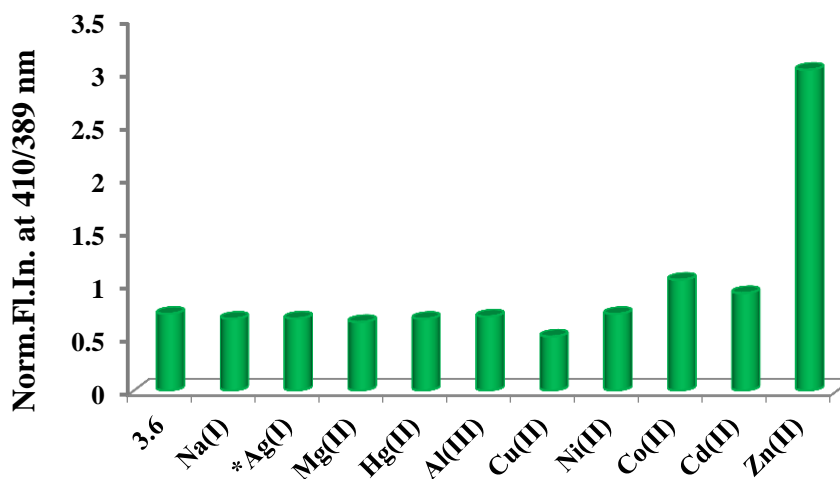


Figure 3.3. (A) Fluorescence selectivity chart, and (B) bart chart of compound **3.6** ( $6.5 \times 10^{-4}$  M and  $\lambda_{\text{ex}} = 355$  nm) in  $\text{CH}_3\text{CN}$  upon the addition of ten equivalents of different metal ions as their  $\text{Cl}^-$  salts (\* $\text{NO}_3^-$  salt).

In the second part, the effect of different counter-ions of  $\text{Zn}^{2+}$  ion on the intensity of excimer emission of compound **3.6** was explored. Ten equivalents of different anions of  $\text{Zn}^{2+}$  (anion =  $\text{F}^-$ ,  $\text{Cl}^-$ ,  $\text{Br}^-$ ,  $\text{I}^-$ ,  $\text{BF}_4^-$ ,  $\text{SO}_4^{2-}$ ,  $\text{H}_2\text{PO}_4^-$ ,  $\text{ClO}_4^-$  and  $\text{NO}_3^-$ ) were added to

compound **3.6** in CH<sub>3</sub>CN. A distinct excimer emission at 420 nm was observed for only Cl<sup>-</sup>, Br<sup>-</sup>, NO<sub>3</sub><sup>-</sup>, BF<sub>4</sub><sup>-</sup>, and ClO<sub>4</sub><sup>-</sup> of Zn<sup>2+</sup> (Figure 3.4 B), whereas no excimer emission was observed for other anions (Figure 3.4 A). An increase in the fluorescence intensity of the monomer at 380 and 400 nm was seen for the remaining anions such as F<sup>-</sup>, I<sup>-</sup>, CN<sup>-</sup>, SO<sub>4</sub><sup>2-</sup>, PO<sub>4</sub><sup>3-</sup>, and CH<sub>3</sub>COO<sup>-</sup>. Furthermore, the intensity of the excimer emission is found more intense for ZnCl<sub>2</sub> than any other zinc salts indicating that ZnCl<sub>2</sub> brings two pyrene units closer than other zinc salt (Figure 3.4 B).

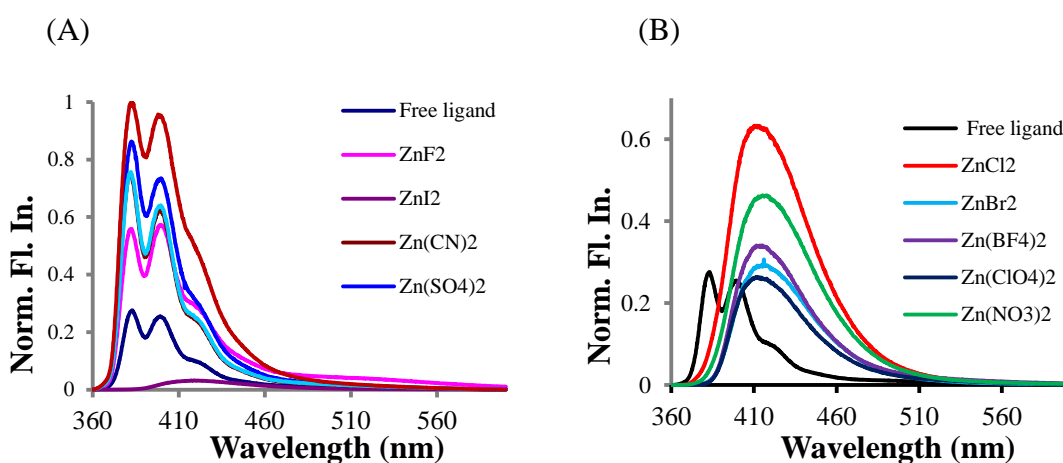


Figure 3.4. (A) Fluorescence spectra of compound **3.6** ( $6.5 \times 10^{-4}$  M and  $\lambda_{\text{ex}} = 355$  nm) upon addition of ten equivalents of F<sup>-</sup>, I<sup>-</sup>, CN<sup>-</sup>, SO<sub>4</sub><sup>2-</sup>, PO<sub>4</sub><sup>3-</sup>, and CH<sub>3</sub>COO<sup>-</sup> (B) Cl<sup>-</sup>, Br<sup>-</sup>, BF<sub>4</sub><sup>-</sup>, ClO<sub>4</sub><sup>-</sup>, and NO<sub>3</sub><sup>-</sup> of zinc in CH<sub>3</sub>CN.

The absence of an excimer emission with ZnF<sub>2</sub>, ZnI<sub>2</sub>, Zn(CN)<sub>2</sub>, and Zn(OAc)<sub>2</sub> clearly suggests that zinc salt as a whole is templating the pyrene units to form the excimer emission. Full titration of the compound **3.6** was carried out for ZnCl<sub>2</sub>, ZnBr<sub>2</sub>, ZnI<sub>2</sub>, Zn(NO<sub>3</sub>)<sub>2</sub>, Zn(ClO<sub>4</sub>)<sub>2</sub>, ZnI<sub>2</sub>, and Zn(BF<sub>4</sub>)<sub>2</sub> (Figure 3.5 and 3.6). The binding constant was calculated for all of these zinc salts using data from fluorescence titrations by HypSpec program (Table 3.1). Only ZnCl<sub>2</sub> was found to bind the compound **3.6** exclusively in a 1:2 ratio while other zinc salts bind in different ratios. The binding constant of compound **3.6** was also higher for ZnCl<sub>2</sub> than other zinc salts. This could

mean  $\text{ZnCl}_2$  has the perfect shape and size to bind **3.6** in an exclusively 1:2 ratio to give the intense excimer emission whereas other zinc salts such as  $\text{ZnBr}_2$ ,  $\text{ZnI}_2$ , and  $\text{Zn}(\text{NO}_3)_2$  due to bigger in size and shape, bind **3.6** with more than one ratio such as 1:1 and 2:1 ratios, and hence less intense excimer emission was observed (Figure 3.6). This is further supported by the absence of excimer emission with bigger size zinc salts such as  $\text{Zn}(\text{CN})_2$  and  $\text{Zn}(\text{CH}_3\text{COO})_2$ .

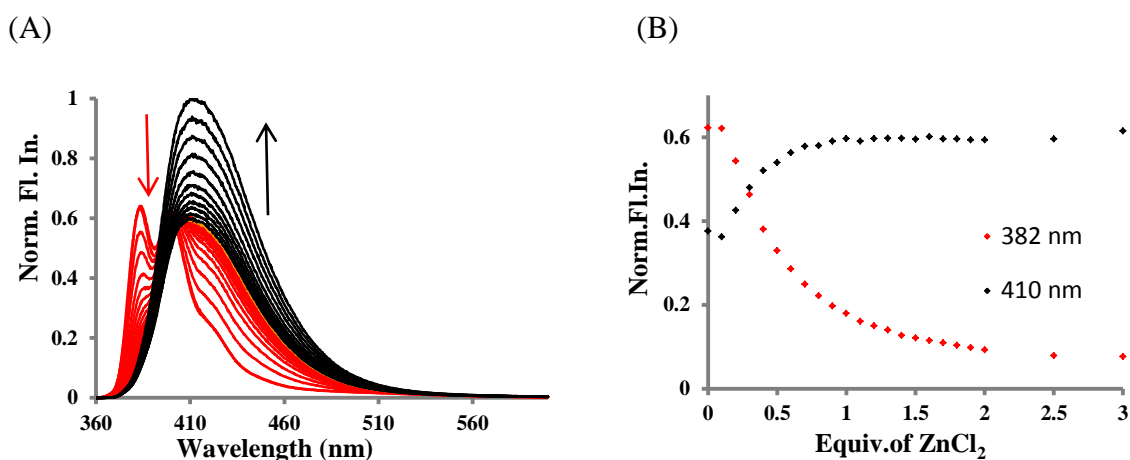


Figure 3.5. Fluorescence titration of compound **3.6** ( $6.5 \times 10^{-4}$  M and  $\lambda_{\text{ex}} = 355$  nm) with  $\text{ZnCl}_2$  in  $\text{CH}_3\text{CN}$ . (A) fluorescence spectra and (B) binding isotherm.

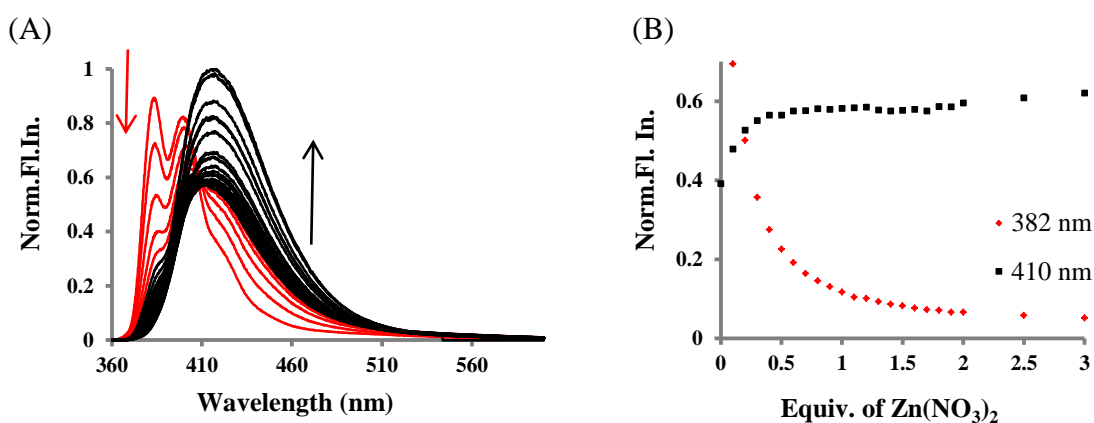


Figure 3.6. Fluorescence titration of compound **3.6** ( $6.5 \times 10^{-4}$  M and  $\lambda_{\text{ex}} = 355$  nm) with  $\text{Zn}(\text{NO}_3)_2$  in  $\text{CH}_3\text{CN}$ . (A) fluorescence spectra and (B) binding isotherm.

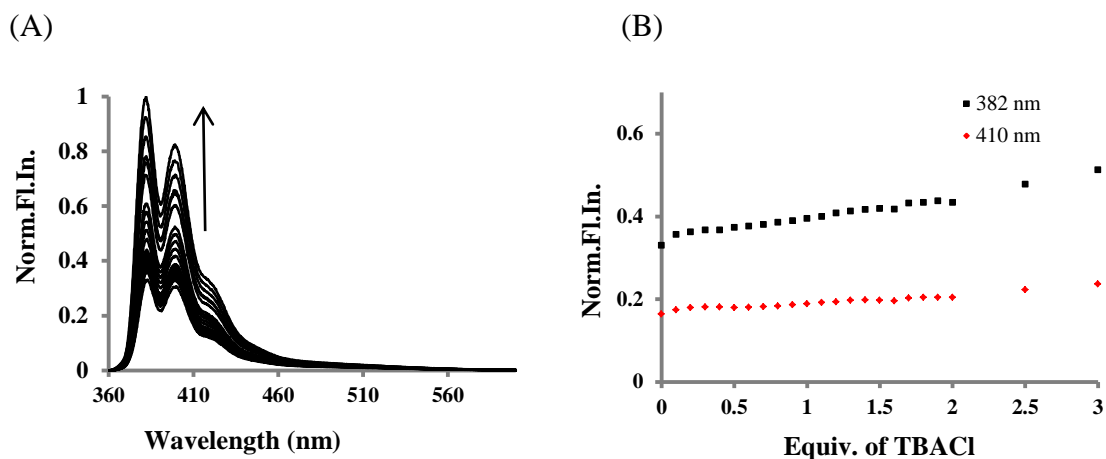


Figure 3.7. Fluorescence titration of compound **3.6** ( $6.5 \times 10^{-4}$  M and  $\lambda_{\text{ex}} = 355$  nm) with TBACl in  $\text{CH}_3\text{CN}$ . (A) Fluorescence spectra and (B) Binding isotherm

Table 3.1

Binding constants ( $K_{21}$  &  $K_{11}$ ) determined by fluorescence titrations for the interactions between compound **3.6** and  $\text{Zn}^{2+}$  salts. The binding constant for TBAX ( $X = \text{Cl}^-$ ,  $\text{Br}^-$ ,  $\text{I}^-$ ,  $\text{NO}_3^-$ ) were also determined, but their values were magnitudes smaller than the  $\text{Zn}^{2+}$  salts

Zinc salts	$K$ ( $\text{M}^{-1}$ & $\text{M}^{-2}$ )	Fluorescence
$\text{ZnCl}_2$	$K_{11}$	$\approx 0$
	$K_{21}$	$1.8 \times 10^6$
$\text{ZnBr}_2$	$K_{11}$	$1.3 \times 10^4$
	$K_{21}$	$1.2 \times 10^2$
$\text{ZnI}_2$	$K_{11}$	$2.5 \times 10^3$
	$K_{21}$	$7.4 \times 10^5$
$\text{Zn}(\text{NO}_3)_2$	$K_{11}$	$1.6 \times 10^3$
	$K_{21}$	$5.2 \times 10^4$

The  $\text{Zn}^{2+}$  ion is versatile with respect to the number of ligands it can adopt in its coordination sphere.  $\text{Zn}^{2+}$  ion is known to be tetrahedrally coordinated with halides in the inner coordination sphere, whereas octahedral  $\text{Zn}^{2+}$  is most common in aqueous solutions.<sup>139</sup> However, there are many tetrahedral biological  $\text{Zn}^{2+}$  ion complexes, and

some of these systems are supported by extensive DFT studies to show the preference for the tetrahedral  $\text{Zn}^{2+}$  ion.<sup>140</sup> Therefore, it is assumed that compound **3.6** is self-assembled around the  $\text{ZnCl}_2$  in a tetrahedral fashion. Nitrate, on the other hand, can coordinate to the metal centre *via* two oxygen atoms and form an octahedral geometry. Therefore, we turned our attention to investigating the geometry by trying to elucidate the structure.

### <sup>1</sup>H NMR Studies of Molecular Probe **3.6**

Fluorescence studies of compound **3.6** with different metal ions showed that an excimer band is produced upon the addition of  $\text{Zn}^{2+}$  ion. Further, the intensity of the excimer band depends upon counter ions of  $\text{Zn}^{2+}$  and is found to be more intense for  $\text{ZnCl}_2$ . However, as explained in Chapter II, fluorescence studies do not give any specific information about the nature of binding with the metal ion and its geometry. In order to gain further insight into the nature of binding and support the fluorescence results, the <sup>1</sup>H NMR titration of compound **3.6** was carried with different anions of  $\text{Zn}^{2+}$  ( $\text{ZnF}_2$ ,  $\text{ZnCl}_2$ ,  $\text{ZnBr}_2$ ,  $\text{ZnI}_2$ , and  $\text{Zn}(\text{NO}_3)_2$ ) in  $\text{CD}_3\text{CN}$ . A 10 and 100 mM concentration of compound **3.6** and  $\text{Zn}^{2+}$  ions were used for the titration. The signals followed in the NMR experiment are highlighted in Figure 3.8 with their chemical shifts values in the free ligand in  $\text{CD}_3\text{CN}$ .



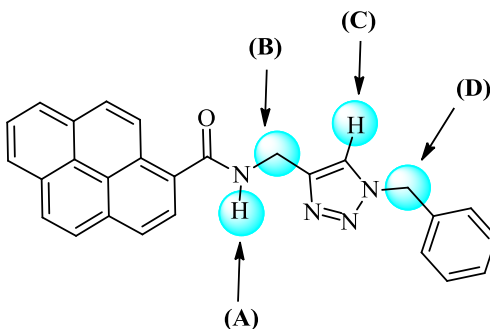


*Figure 3.8.* <sup>1</sup>H NMR assignments that are followed in the NMR titration experiments in CD<sub>3</sub>CN. The chemical shifts values of A, B, C, and D in the free ligand **3.6** are δ 7.46, 4.74, 7.85, and 5.56 ppm, respectively).

There were significant downfield chemical shifts for the amide proton (A), triazole proton (C), and to a lesser extent, a modest chemical shifts for the singlet of CH<sub>2</sub> protons attached to amide (B) and benzene group (D), respectively, upon addition of Zn<sup>2+</sup> salts (Figure 3.9). The largest spectral shifts were seen upon addition of ZnCl<sub>2</sub>. The changes in chemical shifts for the NH (A), CH<sub>2</sub> (B), CH (C), and CH<sub>2</sub> (D) were 0.90, 0.16, 0.25, and 0.10 ppm, respectively after addition of two equivalents of ZnCl<sub>2</sub>. (Figure 3.9-3.11). The NMR shifts can be rationalized through close contacts between the triazole hydrogen and chloride atom on the Zn<sup>2+</sup> ion centre. The chemical shift seen for the amide proton can be rationalized by the inductive effect. The coordination of amide oxygen atom to Zn<sup>2+</sup> ion makes the carbonyl carbon more positive which in turn withdraws more electrons from nitrogen making amide hydrogen more acidic in nature and is shifted to downfield. On closer inspection of the NMR spectra, specifically the aromatic region around 7.0 ppm, compound **3.6** shows two sets of multiplets assigned to the benzene protons. Upon the addition of ZnCl<sub>2</sub>, only one set of equivalent signals is observed as shown in Figure 3.9. This can be explained by the lack of free rotation of the benzyl group upon coordination of Zn<sup>2+</sup> ion and the resultant symmetry of the ZnCl<sub>2</sub> complex.

Further, it could be indication of the formation of only one complex species as it is not observed in the titration of compound **3.6** with  $\text{Zn}(\text{NO}_3)_2$ . The multiplets assigned to the protons of benzene remained almost unchanged, and protons of pyrene are slightly shifted up field in comparison to  $\text{ZnCl}_2$ . This suggests that the binding of compound **3.6** with  $\text{Zn}(\text{NO}_3)_2$  might be different in comparison to  $\text{ZnCl}_2$ . The binding affinity of compound **3.6** with different anions of  $\text{Zn}^{2+}$  ion was calculated by using the HypNMR program<sup>141</sup> and is shown in Table 3.2. The binding affinity of **3.6** with  $\text{ZnCl}_2$  was found greatest among the zinc salts and calculated to be greater than  $K_{21} = 1.0 \times 10^5 \text{ M}^{-2}$ . Besides, the binding of compound **3.6** with  $\text{ZnCl}_2$  forms a  $[\text{ZnCl}_2(\text{3.6})_2]$  complex that exists exclusively in the 2: 1 ratio, whereas non-linear curve fitting analysis can only be successfully refined for the other  $\text{Zn}^{2+}$  salts if other ligand-to metal stoichiometry are taken into consideration (Figure 3.14-3.15 and Table 3.2). This result is in good agreement with fluorescence studies and further supports that  $\text{ZnCl}_2$  binds the compound **3.6** in completely 2:1 ratio in tetrahedral geometry to give the intense excimer emission. The  $^1\text{H}$  NMR titration of compound **3.6** was also carried out with different anions of tetrabutyl ammonium salts. The changes in the chemical shifts are insignificant as shown in Figure 3.13 for  $\text{TBANO}_3$  (Figure 3.16 for binding isotherm) and binding constant also magnitudes lower than zinc salts.

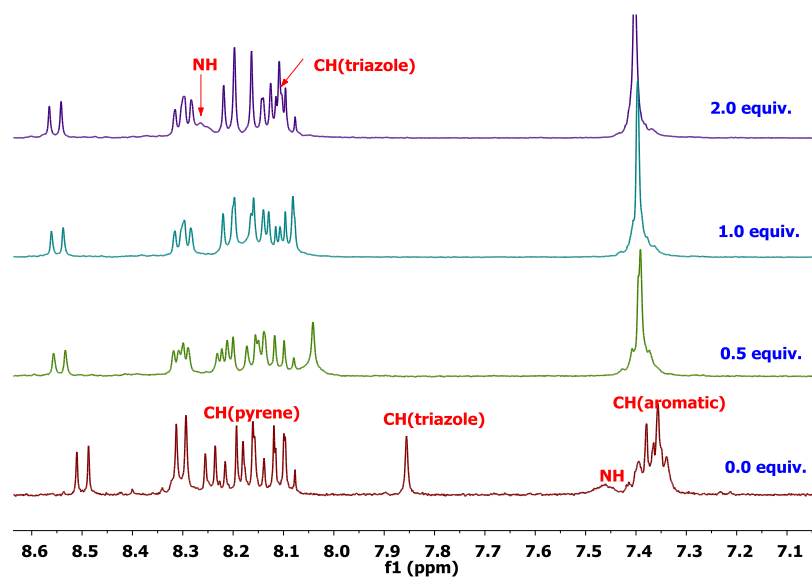


Figure 3.9. Partial  $^1\text{H}$  NMR Stack plot: Addition of  $\text{ZnCl}_2$  with compound **3.6** (10 mM) in  $\text{CD}_3\text{CN}$  (aromatic region only).

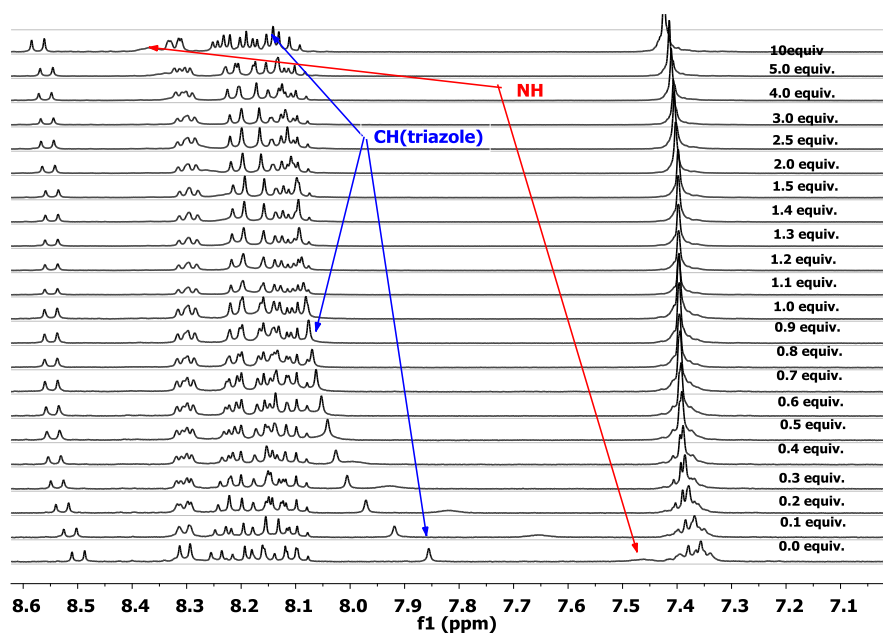


Figure 3.10.  $^1\text{H}$  NMR Stack plot: Addition of  $\text{ZnCl}_2$  with compound **3.6** (10 mM) in  $\text{CD}_3\text{CN}$  for aromatic protons.

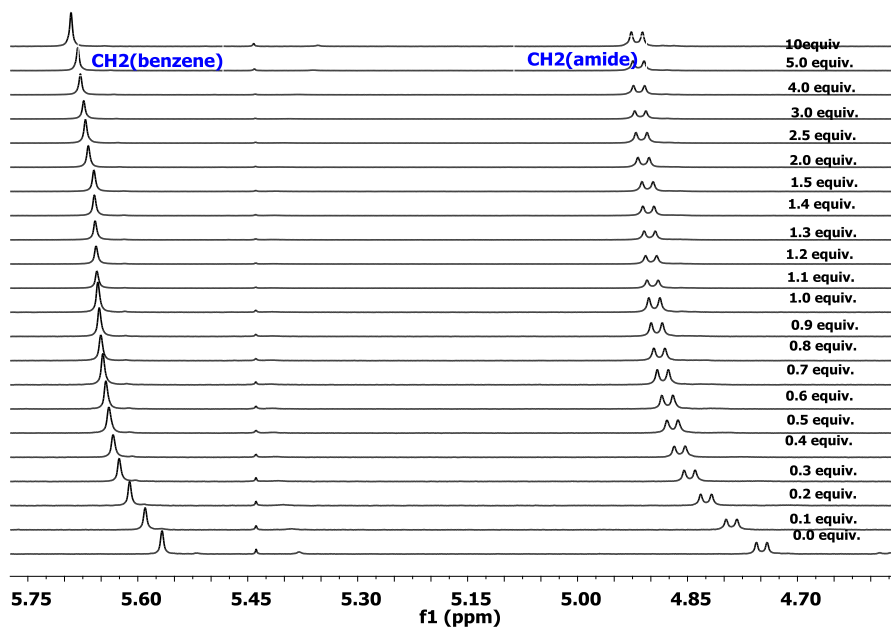


Figure 3.11.  $^1\text{H}$  NMR Stack plot: Addition of  $\text{ZnCl}_2$  with compound **3.6** (10 mM) in  $\text{CD}_3\text{CN}$  for  $\text{CH}_2$  protons attached to amide group ( $\delta$  4.74 ppm) and for  $\text{CH}_2$  protons attached to benzene group ( $\delta$  5.56 ppm).

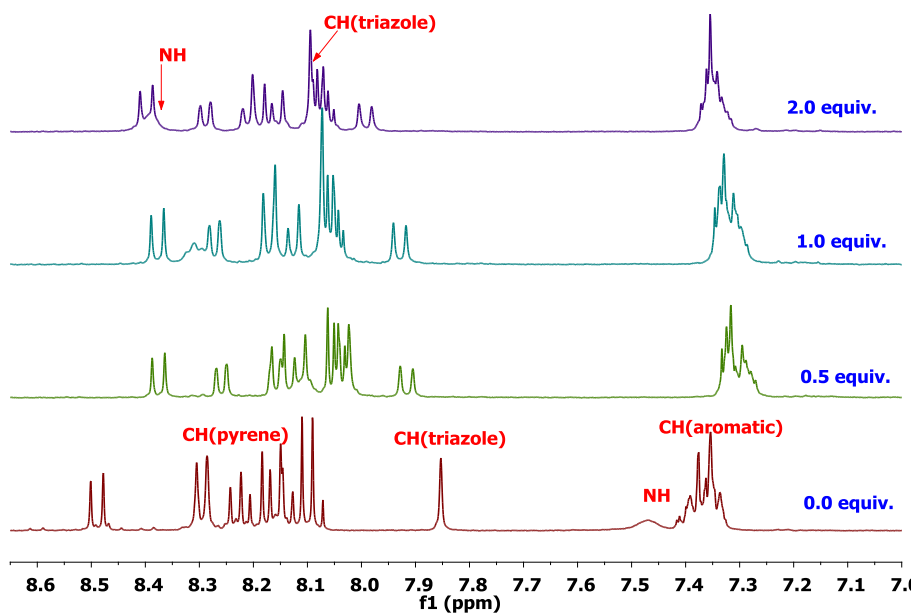


Figure 3.12. Partial  $^1\text{H}$  NMR Stack plot: Addition of  $\text{Zn}(\text{NO}_3)_2$  with compound **3.6** (10 mM) in  $\text{CD}_3\text{CN}$  (aromatic region only).

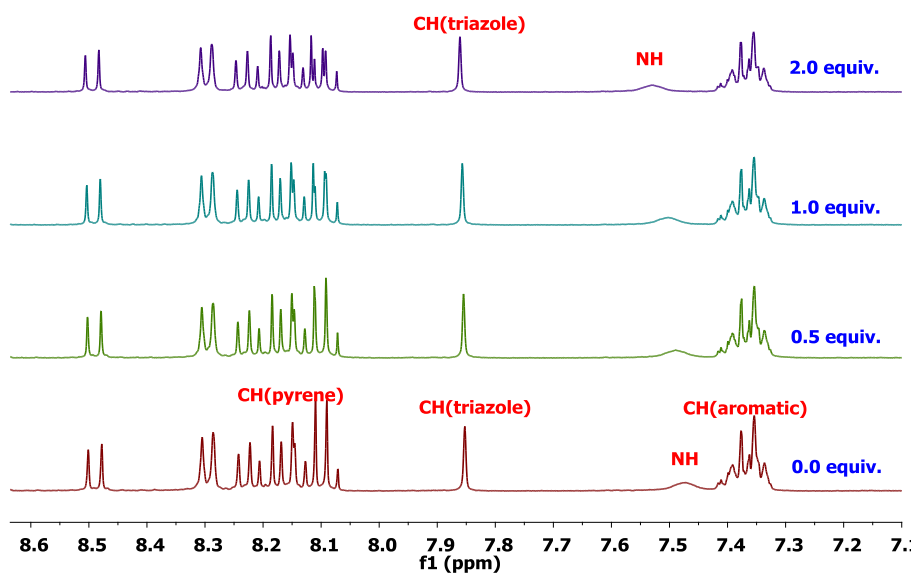


Figure 3.13. Partial  $^1\text{H}$  NMR Stack plot: Addition of  $\text{TBANO}_3$  with compound **3.6** (10 mM) in  $\text{CD}_3\text{CN}$  (aromatic region only).

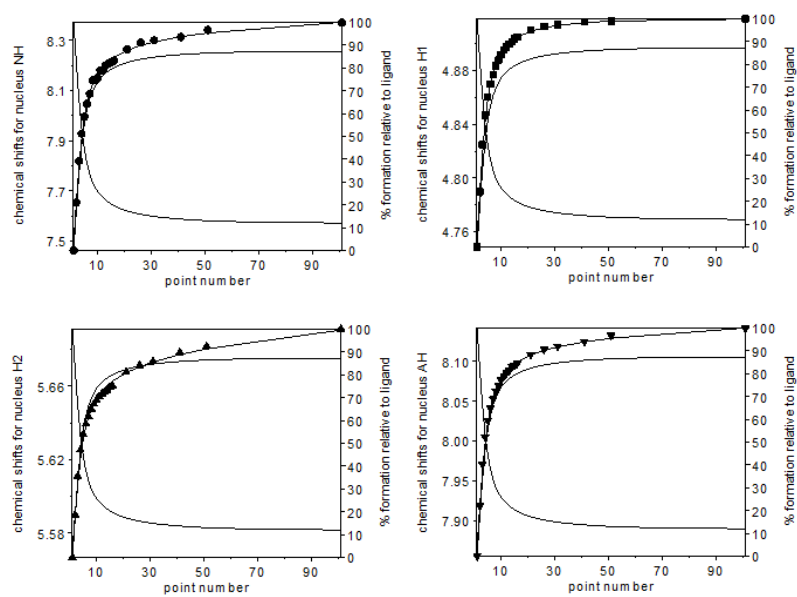


Figure 3.14.  $^1\text{H}$  NMR binding isotherms of compound **3.6** (10 mM) plus the addition of  $\text{ZnCl}_2$ .

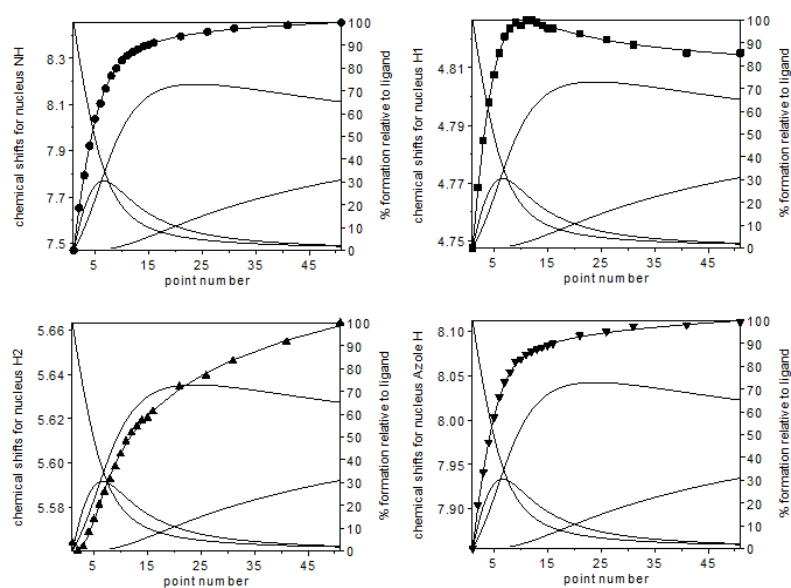


Figure 3.15.  $^1\text{H}$  NMR binding isotherms of compound **3.6** (10 mM) plus the addition of  $\text{Zn}(\text{NO}_3)_2$ .

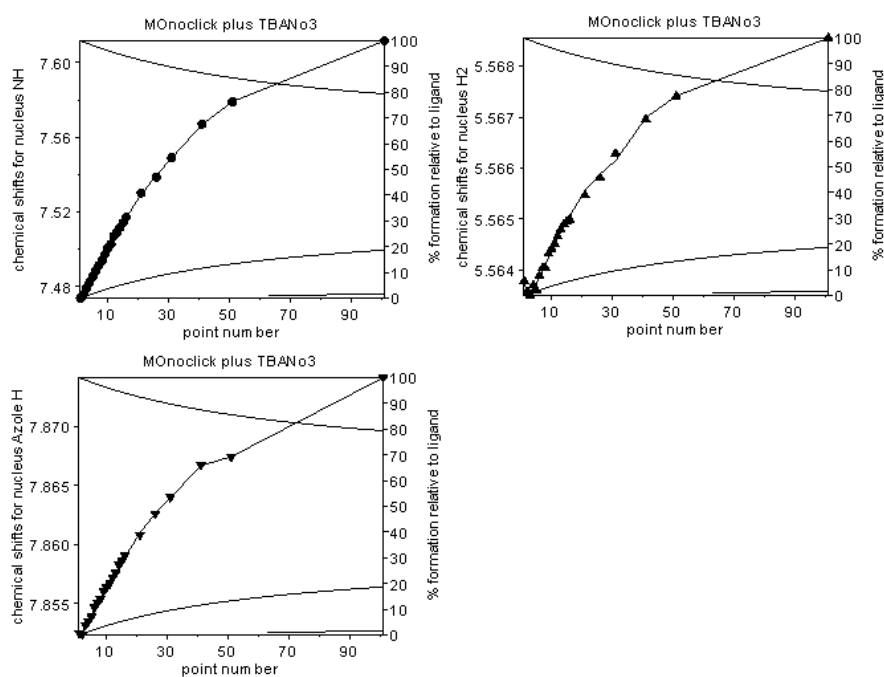


Figure 3.16.  $^1\text{H}$  NMR binding isotherms of compound **3.6** (10 mM) plus the addition of  $\text{TBANO}_3$ .

Table 3.2

*Binding constants ( $K_{21}$  &  $K_{11}$ ) determined by  $^1\text{H}$  NMR titrations for the interactions between compound **3.6** and  $\text{Zn}^{2+}$  salts. The binding constant for TBAX ( $X=\text{Cl}^-$ ,  $\text{Br}^-$ ,  $\text{I}^-$ ,  $\text{NO}_3^-$ ) were also determined, but their values were magnitudes smaller than the  $\text{Zn}^{2+}$  salts*

Zinc salts	$K$ ( $\text{M}^{-1}$ & $\text{M}^{-2}$ )	NMR
$\text{ZnCl}_2$	$K_{11}$	$\approx 0$
	$K_{21}$	$1.3 \times 10^5$
$\text{ZnBr}_2$	$K_{11}$	$1.7 \times 10^3$
	$K_{21}$	$5.2 \times 10^5$
$\text{ZnI}_2$	$K_{11}$	$3.3 \times 10^3$
	$K_{21}$	$3.6 \times 10^5$
$\text{Zn}(\text{NO}_3)_2$	$K_{11}$	$1.5 \times 10^3$
	$K_{21}$	$1.1 \times 10^5$

### 2D NMR Studies of Molecular Probe **3.6**

Binding of compound **3.6** with  $\text{ZnCl}_2$  was studied in greater detail by 2D NMR spectroscopy such as COSY, HMQC, HMBC, TOCSY, and ROESY to support the proposed coordination environment of  $[\text{ZnCl}_2(\mathbf{3.6})_2]$  that gives rise to the excimer band seen in the fluorescence. The structure of both compound and its  $\text{ZnCl}_2$  complex are confirmed by 2D NMR, and protons and carbons atoms are assigned accurately. As explained in Chapter II, ROESY, in particular gives a correlation of protons in space between same or different molecules. Hence, it plays an integral role in the structure elucidation of complex  $[\text{ZnCl}_2(\mathbf{3.6})_2]$ . Therefore, both free compound **3.6** and its  $\text{ZnCl}_2$  complex are studied in detail by ROESY.

A rOe spectrum of compound **3.6** showed five strong rOe signals labelled as (a), (b), (c), (d), and (e) in Figures 3.17 and 3.18. One of the most distinctive and important

rOe signal is between the NH proton and the hydrogen atom attached to C(10) on the pyrene moiety which is labelled as (a) in Figure 3.18. This rOe signal disappeared upon addition of  $\text{ZnCl}_2$ , and a new rOe signal is observed between the NH and C(2) proton (Figures 3.19 and 3.20). This clearly indicates that rotation about the C(1) has occurred upon binding of compound **3.6** with  $\text{ZnCl}_2$ . This is also supported by the molecular modelling (Figures 3.22-3.23). The calculated distance between the NH group and C(2) H is greater than 4 Å for compound **3.6**, so there is no rOe signal in the compound **3.6** spectrum. But the calculated bond distance between the NH and C(2) H is 2.386 Å for the complex, a reasonable distance for an rOe signal. The proposed geometry is also supported by an additional weak rOe signal between the triazole proton and the *ortho* proton of the benzyl group which is labelled as (f) in Figure 3.20. But this rOe signal was not present in the free ligand. This suggests that  $\text{ZnCl}_2$  acts as a template for two equivalents of compound **3.6** to give the tetrahedral geometry.

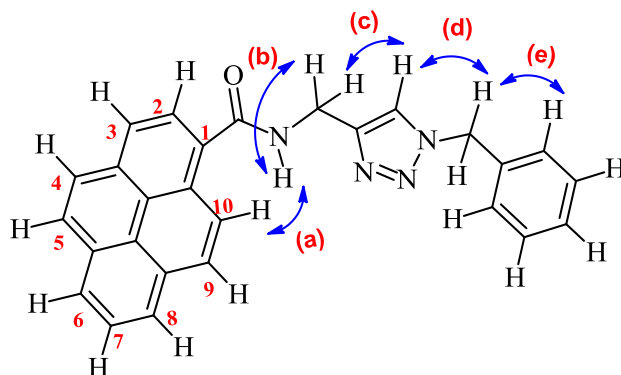


Figure 3.17. Correlation of protons labelled as (a), (b), (c), (d), and (e) seen in the 2D ROESY of free ligand (**3.6**) in  $\text{CD}_3\text{CN}$ .



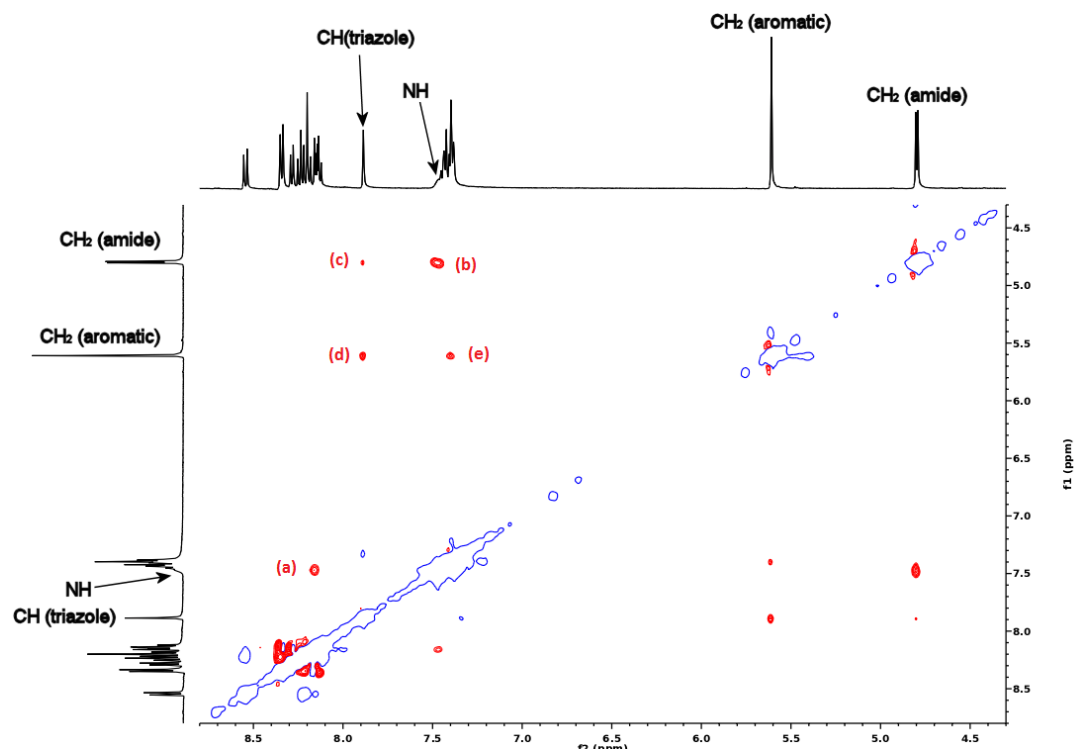


Figure 3.18. gROSEY of compound **3.6** (10 mM) in  $\text{CD}_3\text{CN}$ . Calculated distances (a) 2.585 Å, (b) 2.592 Å, (c) 2.861 Å, (d) 2.805 Å, and (e) 2.404 Å. from molecular modelling structures (Figure 3.23).

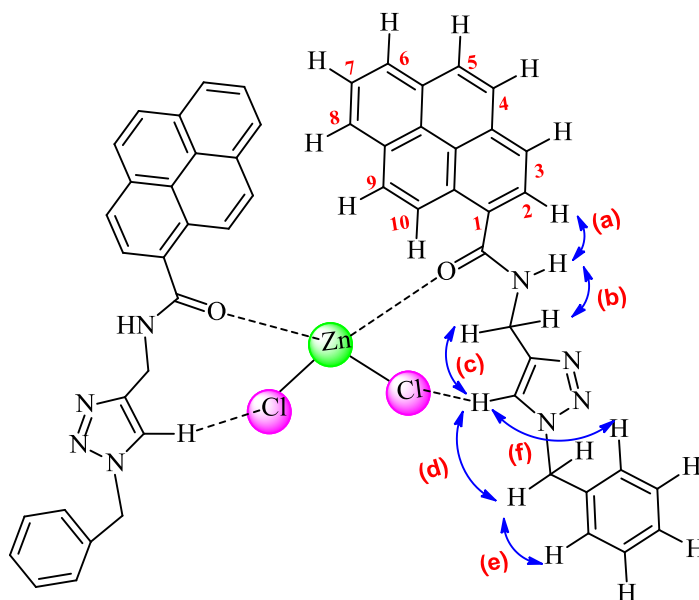


Figure 3.19. Correlation of protons labelled as (a), (b), (c), (d), (e), and (f) seen in the 2D ROESY of complex  $[\text{ZnCl}_2(\mathbf{3.6})_2]$  in  $\text{CD}_3\text{CN}$ .

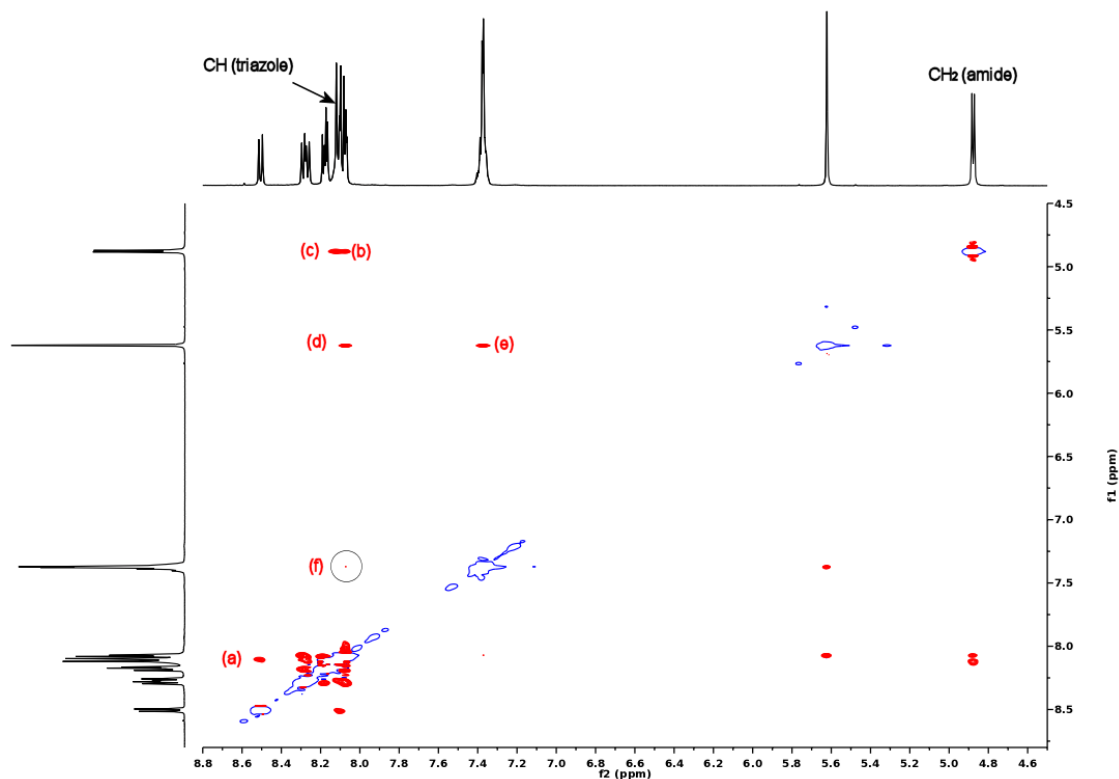


Figure 3.20. gROSEY of complex  $[\text{ZnCl}_2(\mathbf{3.6})_2]$  in  $\text{CD}_3\text{CN}$ : Calculated distances (a) 2.386 Å, (b) 2.336 Å, (c) 2.983 Å, (d) 2.738 Å, (e) 2.471 Å, and (f) 2.96 Å from molecular modelling structures (Figure 3.22).

### Molecular Modeling's Studies of Molecular Probe **3.6**

The  $^1\text{H}$  NMR titration studies of the compound **3.6** with different anions of  $\text{Zn}^{2+}$  salts is in agreement with the results of the fluorescence. In particular, 1D and 2D NMR studies with  $\text{ZnCl}_2$  support the tetrahedral geometry of  $[\text{ZnCl}_2(\mathbf{3.6})_2]$  complex which is proposed based on the results of fluorescence. Further, it suggests that oxygen atoms of the amide group and hydrogen atoms of triazole groups are involved in the binding of zinc and chloride atoms of  $\text{ZnCl}_2$ , respectively. However, as explained in Chapter II, the geometry of complex cannot be confirmed solely on the basis of NMR studies. Attempts to grow the crystal of the host guest complex were unsuccessful. So molecular modeling

was carried out between molecular probe **3.6** and  $\text{Zn}^{2+}$  ions to explain the optical properties and geometry of the complex.

All possible isomers for the  $[\text{ZnCl}_2(\mathbf{3.6})_2]$  ( $\text{X} = \text{F}^-$ ,  $\text{Cl}^-$  and  $\text{NO}_3^-$ ) complexes were modelled as shown in Figure 3.21: two tetrahedral enantiomers with non-coordinated anions (i and ii); two octahedral enantiomers with anions bound in *cis* positions and ligand nitrogens *trans* to each other (iii and iv); two octahedral enantiomers with anions bound in *cis* positions and ligand nitrogens *cis* to each other (v and vi); one octahedral isomer with anions bound in *trans* positions and ligand nitrogens *trans* to each other (vii); and one octahedral isomer with anions bound in *trans* positions and ligand nitrogens *cis* to each other (viii)

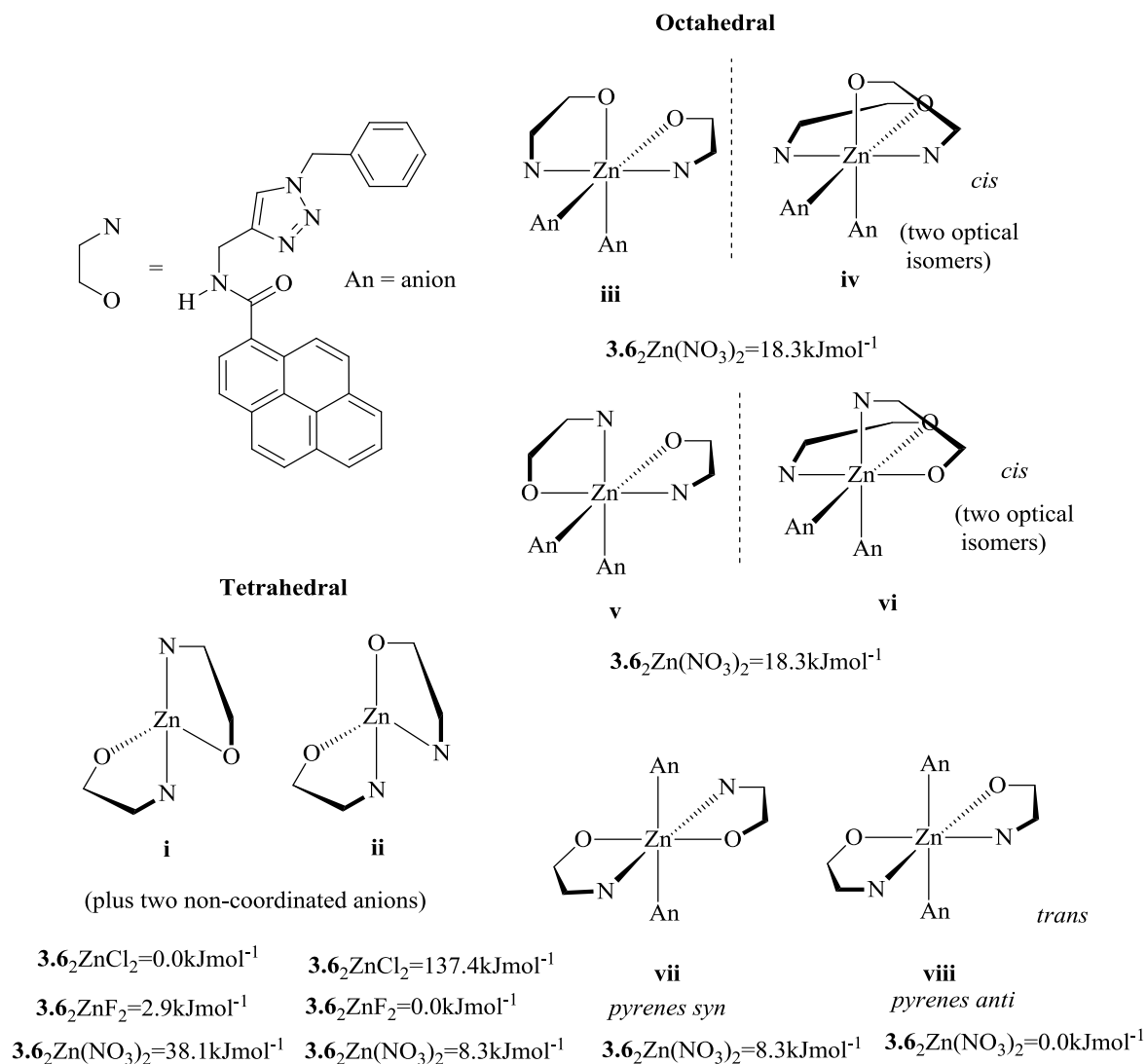


Figure 3.21. Relative energies of the geometric and optical isomers, for  $[ZnX_2(3.6)_2]$  ( $X = F, Cl^-$  and  $NO_3^-$ ).

The equilibrium conformers for structures i through viii, as the dinitrate complexes, was determined using full conformational searching and molecular mechanics energy minimization methods (MMFF). Formal bonds between zinc and the ligands and anions were then removed, and the geometries reoptimized. The relative energies of the unconstrained complexes are given in Figure 3.25. The unconstrained five structures collapsed into either structure vii or viii. Structure viii has the potential for excimer activity, as observed experimentally, whereas vii does not. Structures vii and viii were

used as starting points for equilibrium geometry calculations. Initial refinement was at the semiempirical PM3d level, and the resulting structures used as input coordinates for density functional calculations (B3LYP/6-31G\*). Calculations were undertaken in the gas phase as the titrations were carried out in mixed solvents for which adequate solvation models have yet to be developed. In the gas phase the binding energy of the *syn*-[ZnCl<sub>2</sub>(**3.6**)<sub>2</sub>] was -230 kJmol<sup>-1</sup>; the *anti*-conformer was less stable at -184.83 kJmol<sup>-1</sup>. The large values reflect complexation in the gas phase, and the experimental binding energies would be expected to be considerably lower due to the competitive nature of the solvents.

Binding energies were determined as:

$$\Delta E_{\text{(binding)}} = E_{\text{(complex)}} - (E_{\text{(Zn}^{2+})} + 2 E_{\text{(Cl}^-)} + 2 E_{\text{(ligand)}})$$

Energies used are those of the geometry optimised complex and free ligand.

The pyrene-pyrene interactions suggested that the more stable *syn*-[Zn(NO<sub>3</sub>)<sub>2</sub>(**3.6**)<sub>2</sub>], was an excimer with the two pyrene groups separated by 6.8 Å at an angle of 36° (Figure 3.25 and Table 3.3). The pyrene groups in the [ZnF<sub>2</sub>(**3.6**)<sub>2</sub>] structures were a similar distance apart: however, the angle between the pyrene moieties was now 76°, explaining the lack of excimer signal in the fluorescence study (Figure 3.21 and Table 3.3). In the analogous [ZnCl<sub>2</sub>(**3.6**)<sub>2</sub>] complex, the interplane distance was calculated to be 4.4 Å at an angle of 4.9° (Figure 3.22 and Table 3.3). This explains why the excimer signal observed in the fluorescence studies is more intense for the chloride than the other Zn<sup>2+</sup> salts studied. The result can also be attributed to the ionic size of F<sup>-</sup> (1.33 Å), Cl<sup>-</sup> (1.81 Å), and NO<sub>3</sub><sup>-</sup> (1.96 Å). The larger size of the chloride forces the pyrene units closer together. Another factor is the electronegativity of the fluorine and oxygen atoms, which

spreads the pyrene units further apart. The observation is supported by the calculated bond distances between the anion and CH (triazole), CH (methyl amide), and CH (benzyl) protons. The distance is shorter for anions that are more electronegative than chloride (Table 3.3). This is in agreement with the less intense excimer behavior observed in the  $\text{NO}_3^-$  and  $\text{F}^-$  fluorescence studies.

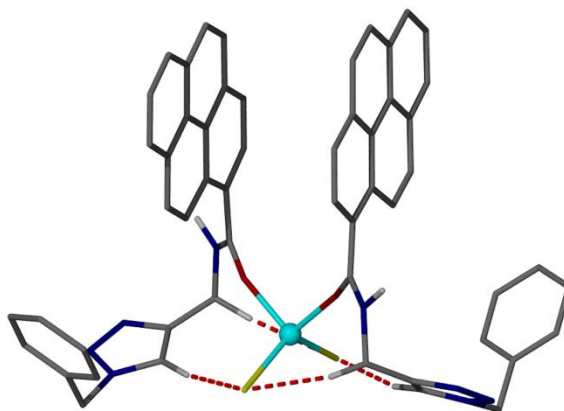


*Figure 3.22.* DFT fully optimised structure of  $[\text{ZnCl}_2(\mathbf{3.6})_2]$ . Calculated pyrene distance 4.4 Å and angle 4.91°.

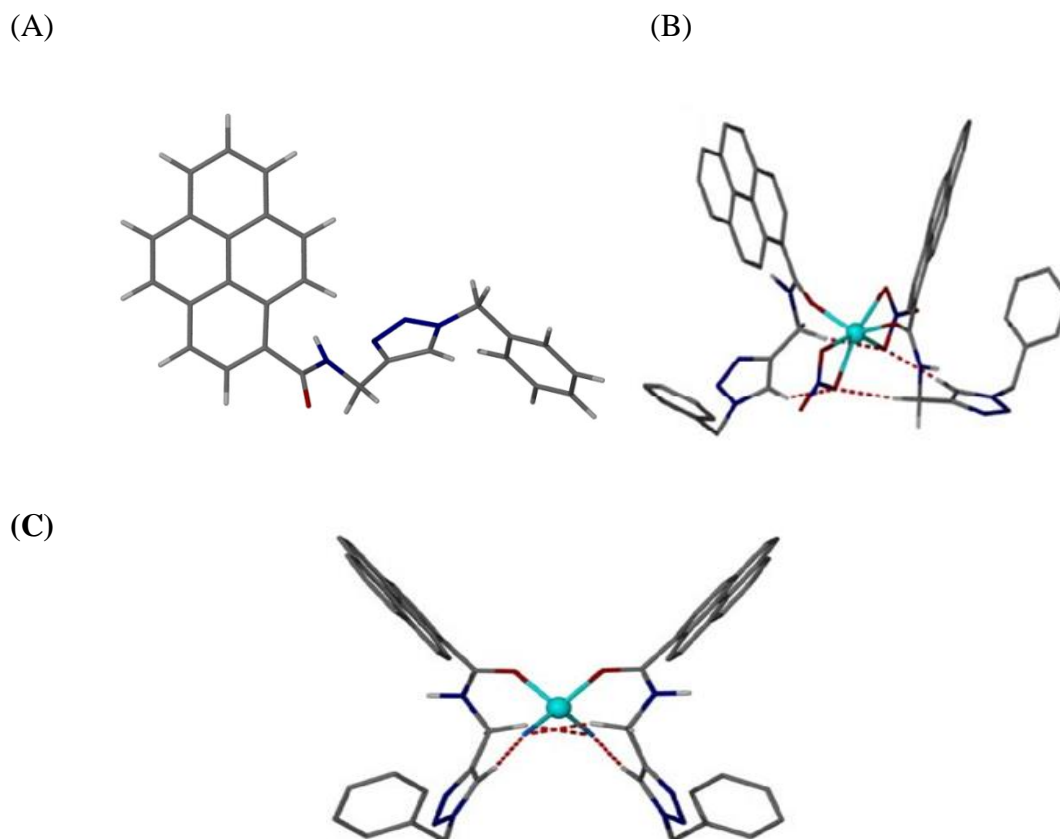


Figure 3.23. (A) Molecular models of compound **3.6** (B) *syn* [Zn(NO<sub>3</sub>)<sub>2</sub>(**3.6**)<sub>2</sub>], and (C) *syn* [ZnF<sub>2</sub>(**3.6**)<sub>2</sub>].

Table 3.3

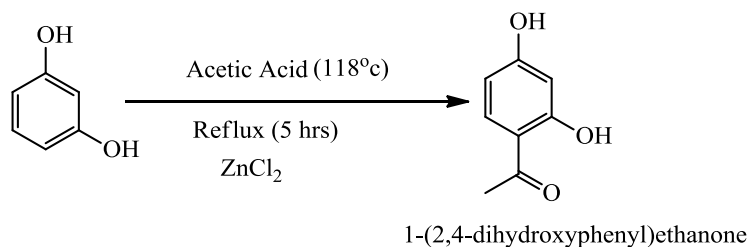
*X-H and X-H<sup>⋯</sup>halide distances in angstroms (Å)*

	Free ligand(A)	<i>Syn</i> - L <sub>2</sub> Zn(NO <sub>3</sub> ) <sub>2</sub> (B)*	L <sub>2</sub> ZnF <sub>2</sub> (C)	L <sub>2</sub> ZnCl <sub>2</sub>
N-H	1.009	1.111	1.013	1.1012
Triazole H	1.079	1.082	1.085	1.081
Triazole H....anion	N/A	2.303	1.930	2.683
CH <sub>2</sub> (amide)....anion	N/A	2.457	2.376	2.783
BzH..anion	N/A	2.456	1.93	3.008
Pyerne excimer angle(°)	N/A	36.38	76.06	4.9

## Friedal Craft Acylation Protocol

Metal salts often play a key role in chemical transformations, prevalent in drug synthesis. These metal salts are normally used as Lewis acids to catalyze the reaction. For example,  $\text{ZnCl}_2$  is commonly used as a Lewis acid in a Friedal Crafts alkylation,<sup>142</sup> Friedal Craft acylation<sup>143</sup>, and Fischer indole synthesis.<sup>144</sup> However, if proper purification is not carried out, then impurities can be found in the drug. The government has put high restrictions on the levels of heavy metal residues in the end product. Therefore, it is the subject of interest for the detection and removal of metal ions in the drug development. The contamination level of heavy metal remaining in the organic phase after an experimental work up generally ranges from five to 100 ppm.<sup>145</sup>

In order to check whether a compound **3.6** can detect the residual  $\text{ZnCl}_2$  after the chemical reaction work up, a simple Friedal Craft acylation protocol was established by preparing 1-(2,4-dihydroxyphenyl)-ethanone from resorcinol using  $\text{ZnCl}_2$  as a Lewis acid (Scheme 3.6).<sup>143</sup> The initial result showed that we do observe an excimer formation. But the amount of water in the system competes with the self-assembly process and prevents the qualitative detection limit. Detailed procedure for this test is described as follows:



*Scheme 3.6.* Preparation of 1-(2,4 dihydroxyphenyl) ethanone *via* a Friedel-Crafts acylation.<sup>143</sup>



*Protocol*

In order to test our probe, a protocol was developed. To the solution of resorcinol (550 mg, 5 mM) in 2 mL of acetic acid was added 700 mg (5 mM) of ZnCl<sub>2</sub>. The mixture was heated under reflux on the oil bath for five hours. After cooling, the product was poured into 40 mL of ice water. The precipitate was sucked and crystallized from water to give desired product as dark red needles (92% yield).

Observations of fluorescence changes, as preliminary tests for Zn<sup>2+</sup> salts, were made after each test described below:

*Protocol one*

After the reaction was cooled, 40 mL of ice water was added to the solution. A red solid was precipitated out from the solution. The red solid was collected by filtration, and the filtrate was tested for residual ZnCl<sub>2</sub>. For this,  $6.48 \times 10^{-4}$  M concentration of compound **3.6** was prepared in CH<sub>3</sub>CN, and 2 mL of it was taken in the fluorescence cell. Aliquots of the filtrate were added to the fluorescence cell and run the fluorescence. Figure 3.24 shows the fluorescence spectrum of compound **3.6** alone and the addition of filtrate (50  $\mu$ L). The two spectra are different, and we can see clearly an excimer peak at 415 nm at this concentration. This initial test suggests that we can monitor the residual ZnCl<sub>2</sub>.

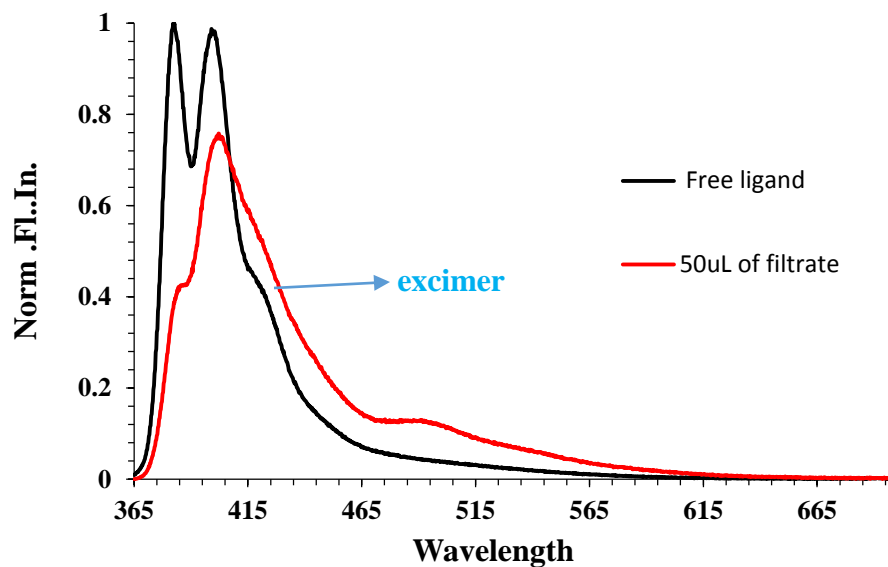


Figure 3.24. Fluorescence chart for protocol one.

To observe whether or not any metal salt is remaining in the red solid, two additional tests were carried out as described below:

*Protocol two (First crystallization)*

The red solid which was collected in protocol 1 above was recrystallized using hot water. Red needles of the desired 1-(2,4- dihydroxyphenyl) ethanone product were collected upon cooling. The filtrate was then tested for residual  $\text{ZnCl}_2$  and tested using the same procedure as described above. Figure 3.25 shows the fluorescence spectrum of compound 3.6 alone and the addition of filtrate (50  $\mu\text{L}$ ). No significant spectral changes were observed: this suggests no  $\text{Zn}^{2+}$  salt was detected after this process.

*Protocol three (pure compound i.e., red needles)*

The pure compound obtained in protocol 2 was tested further for residual  $\text{ZnCl}_2$  by preparing a solution of 1-(2,4- dihydroxyphenyl) ethanone ( $1.31 \times 10^{-2}$  M) in 100% water: small aliquots was again added to a 2 mL solution of 3.6 as described above. No spectral changes are seen.

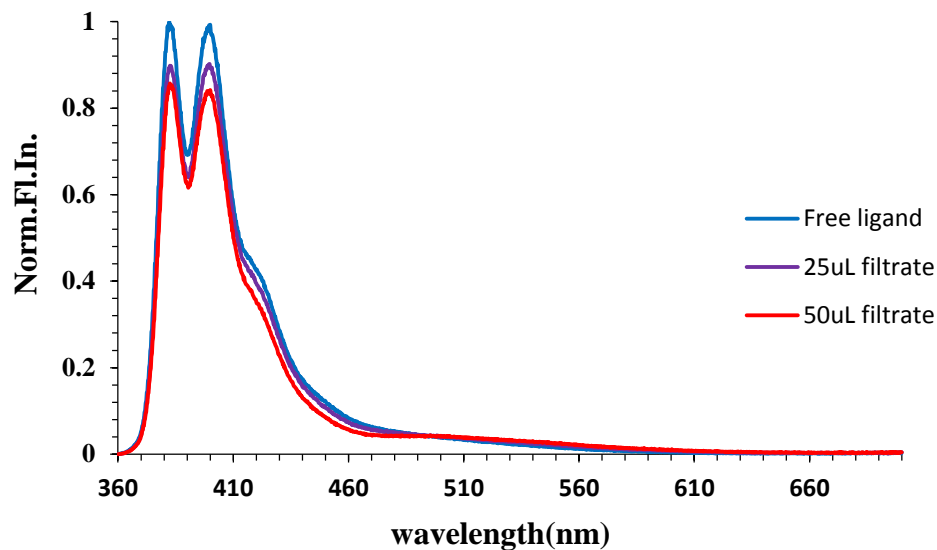


Figure 3.25. Fluorescence chart for protocol two.

In summary, this protocol showed that an excimer emission was observed from the solution of the first filtrate (protocol one). However, the excimer emission was not observed in the filtrate used for the recrystallization of the product (protocol two) as well as in the solid product (protocol three). It could be possible that  $\text{ZnCl}_2$  is present in very small amount at this stage (protocol two and three). The amount of water present in the system is also found to compete with the self-assembly process. Final confirmation of the presence of  $\text{ZnCl}_2$  can be carried out by other techniques such as atomic absorption spectroscopy and inductively coupled plasma mass spectrometry.

#### Summary

A pyrene-based triazole receptor was synthesized in good yield by azide-alkyne Huisgen cycloaddition reaction between N-(prop-2-ynyl) pyrene-1-carboxamide and benzyl azide. The structure of compound was also confirmed by X-ray crystal structure which shows that pyrene units are in *transoid* orientation. Fluorescence titration studies of compound (**3.6**) showed that an excimer emission is produced upon addition of  $\text{Zn}^{2+}$

ion. Only  $\text{ZnCl}_2$ ,  $\text{ZnBr}_2$ ,  $\text{Zn}(\text{BH}_4)_2$ ,  $\text{Zn}(\text{ClO}_4)_2$ , and  $\text{Zn}(\text{NO}_3)_2$  were found to produce an excimer emission with compound **3.6** showing the importance of size and shape of anions. Among zinc salts,  $\text{ZnCl}_2$  produced the most intense excimer signal suggesting  $\text{ZnCl}_2$  has the correct shape (tetrahedral geometry) and size to bind compound **3.6**. Fluorescence titrations are found in good agreement with the  $^1\text{H}$  NMR titration studies and showed the compound **3.7** coordinate  $\text{ZnCl}_2$  exclusively in 2:1 ratio. The calculated binding constants from both  $^1\text{H}$  NMR and fluorescence showed that compound **3.7** has the higher affinity for the  $\text{ZnCl}_2$ . 2D NMR, and DFT calculations also support the tetrahedral geometry of  $[\text{ZnCl}_2(\mathbf{3.6})_2]$ . This was the first time that the self-assembled simultaneous cation and anion induced excimer formation was shown.

## Experimental

### *General procedure for fluorescence experiments*

A stock solution ( $6.48 \times 10^{-4}$  M) of compound **3.6** was prepared in  $\text{CH}_3\text{CN}$ . The solution was excited at  $\lambda = 355$  nm and scanned from  $\lambda$  360-600 nm with the slit widths set to 0.5 mm. A 10 times more concentrated solution of the  $\text{Zn}^{2+}$  salt was prepared in  $\text{CH}_3\text{CN}$ , and 10  $\mu\text{L}$  (10  $\mu\text{L} = 0.1$  equivalent of metal salt) aliquots were added to compound **3.6**. The fluorescence spectra was recorded after each addition. Dilution factors were taken into consideration upon binding study determination. The binding studies were pursued by fluorescence titrations using HypSpec 2006.<sup>116</sup>

### *General procedure for $^1\text{H}$ NMR experiment*

A 10 mM solution of compound **3.6** was prepared by dissolving 2 mg in 0.5 mL in  $\text{CD}_3\text{CN}$ . A 10 times more concentrated solution of the  $\text{Zn}^{2+}$ /tetrabutylammonium salts were prepared in  $\text{CD}_3\text{CN}$ . Aliquot of 5  $\mu\text{L}$  (5  $\mu\text{L} = 0.1$  equivalent of metal salt) was

added to the host, and the  $^1\text{H}$  NMR spectrum recorded after each addition. The binding studies were pursued by  $^1\text{H}$  NMR titrations using HypNMR 2006.<sup>141</sup>

#### *General procedure for UV-Vis experiment*

A stock solution ( $6.5 \times 10^{-4}$  M) of compound **3.6** was prepared by dissolving 2.7 mg in 10 mL of  $\text{CH}_3\text{CN}$ , and then 1 mL was transferred to the UV-Vis cell. From the stock solution eight dilute solutions ranging from  $1.5 \times 10^{-5}$  to  $8.0 \times 10^{-5}$  M were prepared and the UV-Vis spectra were recorded for each sample. Molar absorptivity of compound **3.6** was calculated at various wavelengths: 338 nm ( $\epsilon = 6087 \text{ M}^{-1} \text{ cm}^{-1}$ ), 323 nm ( $\epsilon = 6087 \text{ M}^{-1} \text{ cm}^{-1}$ ), 273 nm ( $\epsilon = 6487 \text{ M}^{-1} \text{ cm}^{-1}$ ), and 239 nm ( $\epsilon = 10851 \text{ M}^{-1} \text{ cm}^{-1}$ ).

#### General Procedure for the Synthesis

##### *Preparation of azidomethylbenzene (compound 3.5)<sup>146</sup>*

Bromomethylbenzene (1.44g, 8.40 mmol) and sodium azide (1.04 g, 16.00 mmol) were dissolved in a 3:1 mixture of acetone and water (30 mL), respectively and stirred at room temperature for two hours. A mixture of dichloromethane (25 mL) and water (25 mL) was then added to the reaction and stirred for 10 minutes. The organic layer was separated and washed three times with water (50 mL), dried over magnesium sulfate, filtered, and the solvent pumped down to produce yellowish oil. The oil was then subjected to column chromatography on silica (40-63 $\mu\text{m}$ , 60 Å) using hexane and ethyl acetate as eluent (80:20), respectively, to produce the desired azidomethylbenzene as an oil; Yield (1.00 g, 7.5 mmol, 89%);

$^1\text{H}$  NMR ( $\text{CDCl}_3$ , 400 MHz);  $\delta$  7.26-7.40 (m, 5H,  $\text{CH}_{\text{Ar}}$ ), 4.30 (s, 2H,  $\text{CH}_2$ )

IR (ATR solid); 3000,  $\nu_{\text{C-H}}$  (w), 2089  $\nu_{\text{N=N}}$  (vs),  $\text{cm}^{-1}$ .

*Preparation of compound (3.6)*<sup>113</sup>

Compound **2.4** (100 mg, 0.34 mmol), azidomethylbenzene **3.5** (46 mg, 0.34 mmol), copper(II)sulfate (20 mg, 0.08 mmol), and sodium ascorbate (67 mg, 0.34 mmol) were dissolved in a 75% acetone water solution (20 mL) and stirred at room temperature for 48 hours. The reaction mixture was then poured into ice cold water (20 mL), where a precipitate formed. The solid was filtered, washed with water (25mL), and recrystallized with CH<sub>3</sub>CN, filtered and dried (70 mg, 0.168 mmol, 50%).

<sup>1</sup>H NMR (CDCl<sub>3</sub>, 400 MHz): δ 8.52 (*d*, 1H, *J* = 9 Hz, CH<sub>py</sub>), 8.22 (*d*, 1H, *J* = 3 Hz, CH<sub>py</sub>), 8.20 (*d*, 1H, *J* = 4 Hz, CH<sub>py</sub>), 8.00-8.12 (*m*, 6H, CH<sub>py</sub>), 7.68 (*s*, 1H, CH<sub>triazole</sub>), 7.38-7.40 (*m*, 3H, CH<sub>Ar</sub>), 7.28-7.32 (*m*, 2H, CH<sub>Ar</sub>), 6.99 (*s*, 1H, NH), 5.55 (*s*, 2H, CH<sub>2</sub>C<sub>Ar</sub>), 4.86 (*d*, 2H, *J* = 5 Hz, CH<sub>2</sub>N<sub>amide</sub>)

<sup>13</sup>C NMR (CDCl<sub>3</sub>, 400 MHz): δ 170.0, 134.5, 132.7, 131.1, 130.6, 130.2, 129.2, 128.8, 128.7, 128.1, 127.1, 126.3, 125.8, 125.7, 124.7, 124.3, 124.3, 122.4, 54.3, 35.7.

IR (ATR solid): 3243 ν<sub>N-H</sub> (*m*), 3034, 3962, ν<sub>C-H</sub> (*m*), 1640 ν<sub>C=O</sub> amide I (*s*) 1596 ν<sub>C=O</sub> amide II (*m*) cm<sup>-1</sup>.

Anal. Calcd for C<sub>27</sub>H<sub>20</sub>N<sub>4</sub>O: H 4.84 %; N 13.45 %; C 77.87 %

Anal Recalcd for C<sub>27</sub>H<sub>20</sub>N<sub>4</sub>O.0.5 CH<sub>3</sub>CO<sub>2</sub>CH<sub>2</sub>CH<sub>3</sub>: H 5.25 %; N 12.15 %; C 75.63%;

Found for C<sub>27</sub>H<sub>20</sub>N<sub>4</sub>O.0.5 CH<sub>3</sub>CO<sub>2</sub>CH<sub>2</sub>CH<sub>3</sub>; H 4.77 %; N 12.70 %; C 75.43 %.

## CHAPTER IV

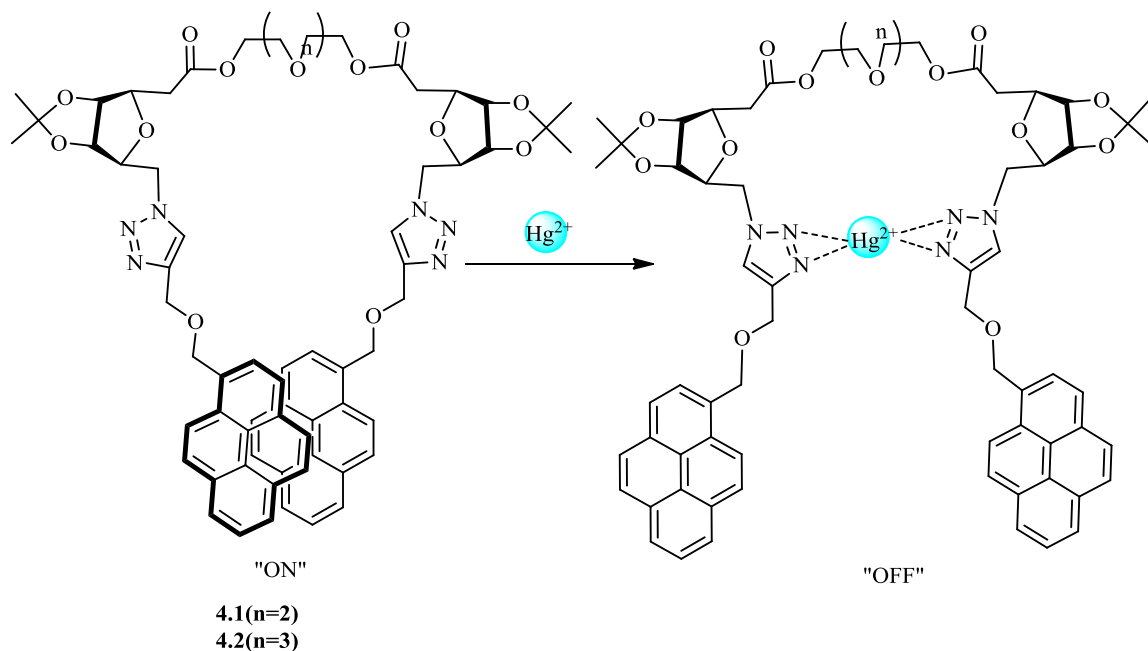
SUGAR FUNCTIONALIZED MOLECULAR PROBE FOR Fe<sup>3+</sup> ION

## Introduction

A significant disadvantage of the molecular probes discussed in Chapters II and III is their poor solubility in most of the polar solvents such as CH<sub>3</sub>CH<sub>2</sub>OH, CH<sub>3</sub>OH, and H<sub>2</sub>O due to pyrene's hydrophobic nature. The solubility issue is more pronounced when the sensors contain more than one pyrene unit. In fact, this is the major issue for many pyrene based molecular receptors. This limits the practical application of pyrene based sensors, particularly in the detection of ions in biological and environmental situations. Development of chemosensors incorporating the sugar group either as a scaffold or as binding sites is one effective strategy to overcome the water solubility issue.<sup>147, 148</sup> The hydroxyl groups and oxygen atoms of the sugar units can also act as the suitable coordination sites for cations.<sup>149</sup> The uses of sugar groups impart the high water solubility features for the sensors. Moreover, the sugar units are naturally abundant, biocompatible, and low toxic raw materials with rich configurational and structural diversities.<sup>150</sup> Hence, sugars can act as useful platform for making water soluble molecular receptors.

The Wu group has carried out significant work on sugar based chemosensors for the detection of metal ions.<sup>151, 152</sup> One example which uses D-ribose sugar and pyrene as a fluorophore is fluorescent chemosensors **4.1** and **4.2** for detection of Hg<sup>2+</sup> ion.<sup>153</sup> Both compounds **4.1** and **4.2** showed selective quenching of monomer and excimer emissions on the addition of Hg<sup>2+</sup> ion in CH<sub>2</sub>Cl<sub>2</sub>:CH<sub>3</sub>OH (80:20, v/v, λ<sub>ex</sub>=344 nm) solution. This is attributed to the quenching induced by the electron transfers. The chain lengths of the ethylene ether groups did not affect their selectivity for the Hg<sup>2+</sup> ion. The association

constant for  $[\text{Hg}(\mathbf{4.1})]^{2+}$  and  $[\text{Hg}(\mathbf{4.2})]^{2+}$  were calculated to be  $1.73 \times 10^5 \text{ M}^{-1}$  and  $4.43 \times 10^5 \text{ M}^{-1}$  by a Stern-Volmer plot. The detection limits for the  $\text{Hg}^{2+}$  ion were determined to be 10 and 15  $\mu\text{M}$  for **4.1** and **4.2**, respectively. Molecular modeling showed that the  $\text{Hg}^{2+}$  ion is coordinated by the triazole nitrogen atoms (i.e., average calculated bond length of Hg-N (2) and Hg-N (3) was estimated at 4.09 and 4.17 Å, respectively) (Scheme 4.1).



*Scheme 4.1.* Proposed binding mechanism of **4.1** and **4.2** with  $\text{Hg}^{2+}$  ion based on computation calculation.<sup>153</sup>

Rao et al. has also carried out significant work based on the sugar system.<sup>154, 155</sup>

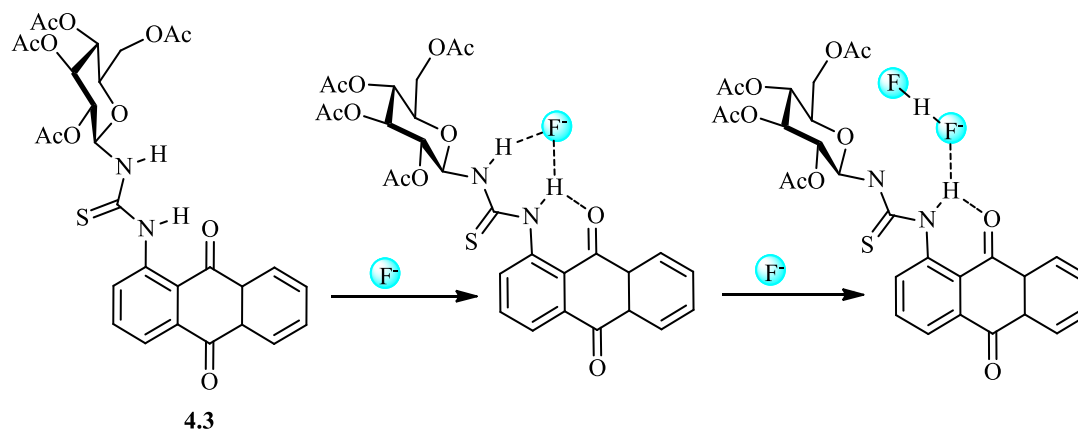
One recent example of their work utilizing sugar and a thiourea is acetylated glucopyranosyl-antraquinone (**4.3**) which acts as both a colorimetric and fluorescent "On-Off" chemosensor selective for  $\text{F}^-$  ion in  $\text{CH}_3\text{CN}$ .<sup>156</sup> The fluorescent intensity of compound **4.3** (5  $\mu\text{M}$ ,  $\lambda_{\text{ex}}=430 \text{ nm}$ ) at 540nm enhanced gradually only in the case of  $\text{F}^-$  ion but not with other anions such as  $\text{Cl}^-$ ,  $\text{Br}^-$ ,  $\text{CH}_3\text{COO}^-$ ,  $\text{N}_3^-$ ,  $\text{CO}_3^-$ ,  $\text{NO}_2^-$ ,  $\text{NO}_3^-$ ,  $\text{SCN}^-$ ,  $\text{SO}_4^{2-}$ ,  $\text{ClO}_4^-$ ,  $\text{HSO}_4^-$ ,  $\text{HCO}_3^-$ ,  $\text{H}_2\text{PO}_4^-$ ,  $\text{P}_2\text{O}_7^{4-}$ , as well as disodium salts of adenosine mono, di or tri phosphates. The fluorescent emission intensity of **4.3** was enhanced by a



~ 13-folds upon binding with F<sup>-</sup> ion, which is attributed to the inhibition of ESIPT.<sup>157</sup>

The binding constant of **4.3** with F<sup>-</sup> ion was calculated to be 5903 M<sup>-1</sup> by using a Benesi-Hildebrand equation. The minimum concentration of F<sup>-</sup> ion that can be detected by **4.3** is  $1.03 \times 10^{-6}$  M. The reversibility of compound **4.3** was demonstrated by the titration with F<sup>-</sup> ion followed by Ca<sup>2+</sup> ion for several cycles. Furthermore, the compound **4.3** shows a bathochromic shift of 75 nm in its absorption maximum upon interaction with F<sup>-</sup> ion. This could be the result of the involvement of the F<sup>-</sup> ion in H-bonding which in turn leads to the deprotonation of thioamide-NH to form HF<sub>2</sub><sup>-</sup> ion. Formation of HF<sub>2</sub><sup>-</sup> ion was also shown by <sup>1</sup>H NMR and <sup>19</sup>F NMR studies. The <sup>1</sup>H NMR spectrum shows the signals at 11.5 and 9.9 ppm for thioamide protons next to anthraquinone and sugar, respectively. Thioamide proton attached to anthraquinone shifted to downfield and broadened after one equivalent F<sup>-</sup> ion indicating the hydrogen-bonding interaction between F<sup>-</sup> and N-H protons. After the addition of two equivalents, a new triplet signal appears at 16.1 ppm ( $J = 126$  Hz) of which the intensity increases upon further addition of F<sup>-</sup> ion. This signal is indeed suggestive of the formation of bifluoride (HF<sub>2</sub><sup>-</sup>) ion thus supporting the deprotonation of the thioamide NH proton. <sup>19</sup>F NMR spectrum of TBAF (tetrabutyl ammonium fluoride) in DMSO-*d*<sub>6</sub> shows a singlet at -102.1 ppm corresponding to the F<sup>-</sup> ion. Upon the addition of F<sup>-</sup> ion to **4.3**, an up field shift by -103.3 is seen for the F<sup>-</sup> ion signal. The formation of HF<sub>2</sub><sup>-</sup> ion has been shown through the doublet observed at -142 ppm ( $J = 128$  Hz). The structural features of the F<sup>-</sup> ion bound **4.3** and the formation of HF<sub>2</sub><sup>-</sup> ion complexes were established by DFT modelling (Scheme 4.2). The fluorescence responses of compound **4.3** is utilized as output to build an INHIBIT logic gate by using F<sup>-</sup> and Ca<sup>2+</sup> ions as inputs (Table 4.1 and Figure 4.1). The output is zero when (a) both F<sup>-</sup>

and  $\text{Ca}^{2+}$  ions are absent, (b)  $\text{Ca}^{2+}$  ion alone is present, or (C) both  $\text{F}^-$  and  $\text{Ca}^{2+}$  ions are present, and this corresponds to the gate being closed and hence termed as “OFF”. When  $\text{F}^-$  ion alone is present, the output is one, and this corresponds to the gate being open and hence termed as “ON”. Thus, **4.3** can act as INHIBIT (INH) logic gate as shown in Table 4.1 and Figure 4.1.



*Scheme 4.2.* Proposed binding mechanism of **4.3** with  $\text{F}^-$  ion based upon DFT calculations.<sup>156</sup>

Table 4.1

*Molecular logic gate table*

Inputs		Output	
$\text{F}^-$	$\text{Ca}^{2+}$	INHIBIT logic gate (Intensity), $\lambda_{\text{ex}} = 540 \text{ nm}$	
0	0	Low fluorescence	0
1	0	High fluorescence	1
0	1	Low fluorescence	0
1	1	Low fluorescence	0

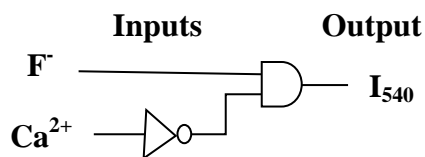
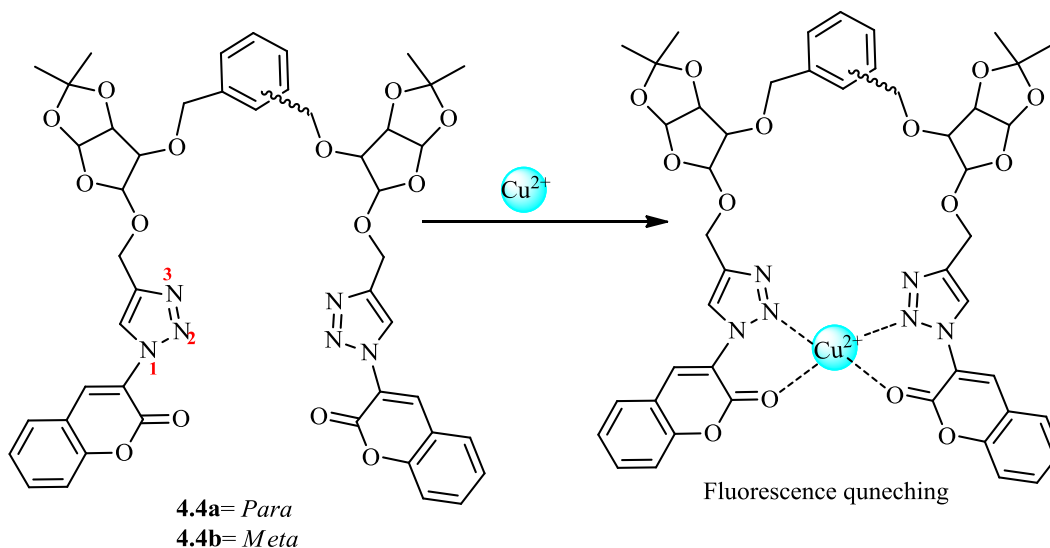


Figure 4.1. The symbolic representation of the INHIBIT logic gate function.

Tiwari and co-workers developed two sugar based fluorescent chemosensors **4.4a**(*para*) and **4.4b** (*meta*) for the selective recognition of  $\text{Cu}^{2+}$  ion.<sup>158</sup> The fluorescence of **4.4a** and **4.4b** showed a broad and strong emission band at 355 nm ( $\lambda_{\text{ex}}= 320$  nm) in  $\text{CH}_3\text{CN}$ . This is a typical emission band for a coumarin group. The fluorescence of both compounds **4.4a** and **4.4b** is quenched in the presence of  $\text{Cu}^{2+}$  ion but not with the other metal ions ( $\text{Li}^+$ ,  $\text{K}^+$ ,  $\text{Na}^+$ ,  $\text{Cd}^{2+}$ ,  $\text{Zn}^{2+}$ ,  $\text{Mn}^{2+}$ ,  $\text{Hg}^{2+}$ ,  $\text{Co}^{2+}$ ,  $\text{Ni}^{2+}$  and  $\text{Fe}^{2+}$ ). The fluorescent quenching efficiency of about 71% and 68% was observed upon addition of ten equivalents of  $\text{Cu}^{2+}$  ion for **4.4a** and **4.4b**, respectively. The  $\text{Cu}^{2+}$  ion induced fluorescence quenching might be ascribed to the photo induced electron transfer (PET) from coumarin fluorophore to bound  $\text{Cu}^{2+}$  ion (Figure 1.12). The detection limit of probes **4.4a** and **4.4b** with  $\text{Cu}^{2+}$  ion were both calculated to be around  $7\mu\text{M}$  (445 ppb), respectively. The binding constants for  $[\text{Cu}(\mathbf{4.4a})]^{2+}$  and  $[\text{Cu}(\mathbf{4.4b})]^{2+}$  complexes were calculated to be  $3.3 \times 10^3$  and  $5.9 \times 10^3 \text{M}^{-1}$ , respectively. DFT calculations were carried out to examine the precise co-ordination mode of **4.4a** or **4.4b** with  $\text{Cu}^{2+}$  ion. Theoretical calculations showed that optimized structures of **4.4a** adopted *trans*, and **4.4b** adopted *cis* arrangement of triazolocoumarin arms with respect to central phenyl ring. DFT study also showed that  $\text{Cu}^{2+}$  ion was coordinated to the triazole nitrogen (N (2) of triazole) atom and oxygen atoms of coumarin carbonyl groups. The optimized structures of  $[\text{Cu}(\mathbf{4.4a})]^{2+}$  and  $[\text{Cu}(\mathbf{4.4b})]^{2+}$  adopted a square planner and distorted square planner geometry (Scheme 4.3). However, it was interesting to note that the author did not mention the effect of

other trivalent metal ions such as  $\text{Fe}^{3+}$ ,  $\text{Cr}^{3+}$ , and  $\text{Al}^{3+}$  ions on the fluorescence of compound **4.4a** and **4.4b**. In fact,  $\text{Fe}^{3+}$  ion is well known for quenching fluorescence due to its paramagnetic properties, and it is suspected that this may also have a similar response.



*Scheme 4.3.* Proposed binding mechanism of **4.4a** and **4.4b** with  $\text{Cu}^{2+}$  ion.<sup>158</sup>

In summary, the use of sugar groups as a scaffold or as potential coordinating sites in the development of chemesensors has improved significantly the solubility in most of the polar solvents. However, there are still very few sensors that utilize sugar groups, presumably due to the challenges associated with carbohydrate chemistry.

In the previous chapter (II), it was shown that pyrene functionalized with amide and triazole groups can form a simultaneous anion-cation binding. The signal is generated by the self-assembled induced excimer that forms upon the addition of zinc salts. In this chapter, an analogous compound **4.7** is designed by replacing the benzene ring for a sugar group (methyl-2, 3, 4-tri-O-acetyl- $\alpha$ -D-Glucopyranoside). It is expected that the compound **4.7** should be highly soluble in the polar solvent and undergo self-assembly process upon addition of  $\text{Zn}^{2+}$  ions as discussed in the Chapter II. It could be

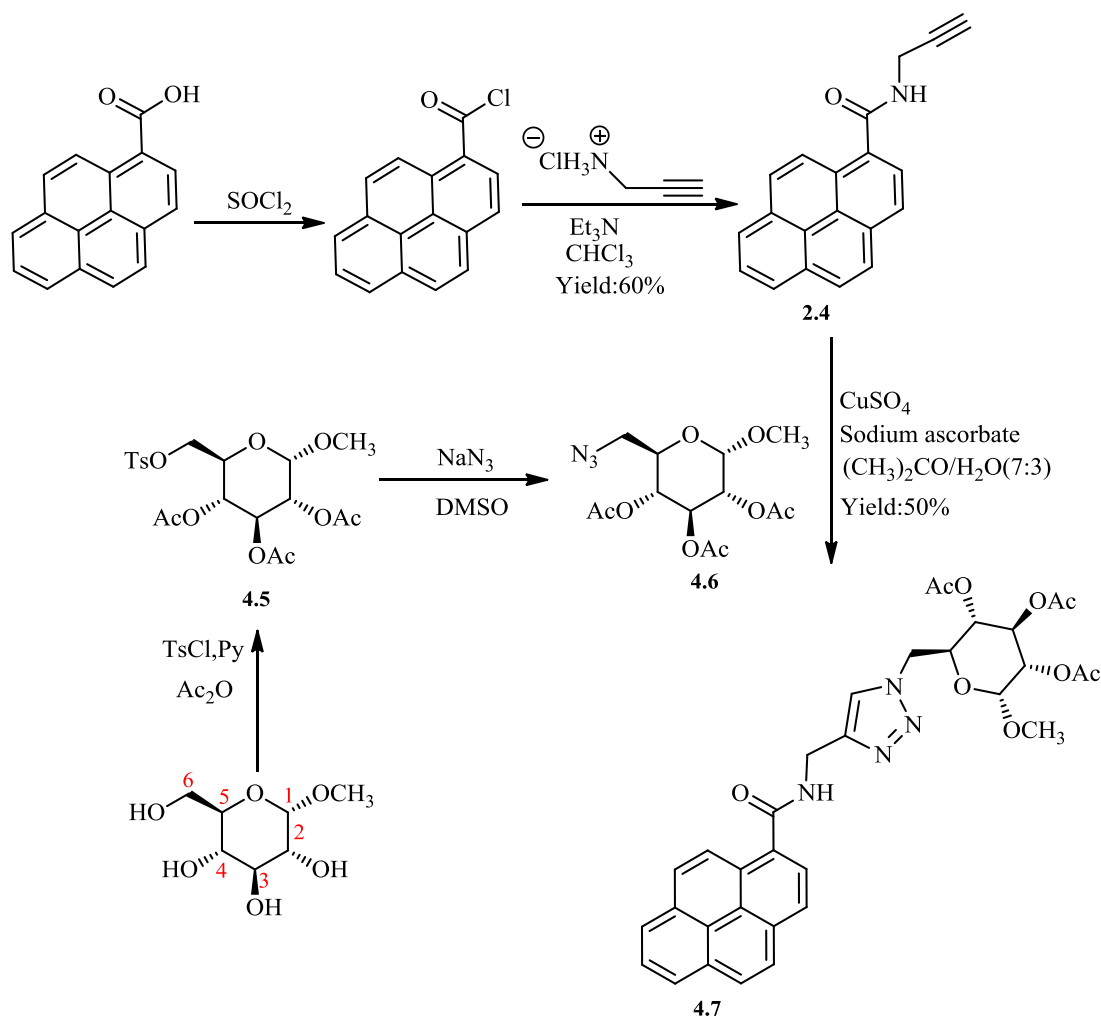
possible that the sugar group might involve in the binding of metal ions and undergo self-assembly process with different metal ion. It is expected that the sugar group might help the self-assembly to occur in the polar solvents.

#### Synthesis of Molecular Probe **4.7**

N-(prop-2-ynyl) pyrene-1-carboxamide (**2.4**) was prepared from pyrene-1-carboxylic by the same procedure as described before in the previous Chapter.<sup>113</sup>  $\alpha$ -D-methyl glucopyranoside was used as the starting material for the preparation of methyl 2,3,4-tri-*O*-acetyl-6-azido-6-deoxy- $\alpha$ -D-glucopyranoside.  $\alpha$ -D-methyl glucopyranoside was first tosylated selectively at the primary OH group (attached to CH<sub>2</sub> (C<sub>6</sub>)) by reacting with tosyl chloride in dry pyridine at 0° C for six-eight hours (Scheme 4.4). The remaining secondary hydroxyl groups at 2, 3, and 4 positions were then acylated by reacting with acetic anhydride at room temperature for 12 hours. The impure viscous liquid obtained after evaporation of CHCl<sub>3</sub> was extracted, and the mixture was then purified by silica gel column chromatography [ethyl acetate (2):hexane(8)] to obtain methyl 2,3,4-tri-*O*-acetyl-6-*O*-*p*-toulenesulfonyl- $\alpha$ -D-glucopyranoside (**4.5**) as a pure clear viscous liquid in overall 75% yield. The compound **4.5** was confirmed by the signals of three acetyl groups ( $\delta$  1.87-1.895 ppm) and tosyl groups (at  $\delta$  2.37 for CH<sub>3</sub> group attached to benzene and double doublet signals for benzene at  $\delta$  7.69 and 7.29 ppm in CDCl<sub>3</sub>), respectively in <sup>1</sup>H NMR spectrum. The <sup>13</sup>C NMR also clearly showed the signals for carbonyl groups at 169 ppm. Compound **4.5** is further confirmed by the stretching band of C=O group of acetyl at 1748 cm<sup>-1</sup> in the IR spectrum. Its spectroscopic data (<sup>1</sup>H NMR, <sup>13</sup>C NMR and IR) is in agreement with the literature value.<sup>159-161</sup> Methyl 2, 3, 4-tri-*O*-acetyl-6-*O*-*p*-toulenesulfonyl- $\alpha$ -D-glucopyranoside (**4.5**) was then converted

into methyl 2, 3, 4-tri-*O*-acetyl-6-azido-6-deoxy- $\alpha$ -D-glucopyranoside by reacting with sodium azide in DMSO at 100 °C for four hours followed by stirring at room temperature for 16 hours. The compound (**4.6**) was obtained a pure white solid after column chromatography [ethyl acetate (1): hexane (9)] of the viscous liquid obtained after evaporation of CH<sub>2</sub>Cl<sub>2</sub>. The azide (**4.6**) was confirmed by its characteristic strong stretching band at 2092 cm<sup>-1</sup> for azide functional group in IR spectrum and the disappearance of aromatic signals of benzene protons in the <sup>1</sup>H NMR spectrum. Its spectroscopic data, (<sup>1</sup>H NMR, <sup>13</sup> C NMR and IR) was in agreement with the published procedure.<sup>159</sup> The final step was to carry out the “click” reaction by refluxing **2.4** and **4.6** in the presence of copper sulfate and sodium ascorbate as catalysts in 1:1 ((CH<sub>3</sub>)<sub>2</sub>CO: H<sub>2</sub>O) solvent for overnight.<sup>114</sup> The evaporation of ethyl acetate extract of the reaction mixture gives the compound as a pure light yellow solid (**4.7**). No further purification was needed. The disappearance of the signal at  $\delta$  4.42 ppm for the terminal C $\equiv$ CH hydrogen and the appearance of new signals at  $\delta$  7.89 and 7.54 ppm (CD<sub>3</sub>CN) in the <sup>1</sup>H NMR indicates the formation of the desired product. The IR spectrum also showed the stretching bands of amide group at 3285, 1633, and 1601 cm<sup>-1</sup> for  $\nu_{\text{N-H}}$  (m),  $\nu_{\text{C=O}}$  (s) amide I, and  $\nu_{\text{C=O}}$  (w) amide II, respectively. The compound **4.7** was characterized by <sup>1</sup>H NMR, <sup>13</sup> C NMR, IR, ESI mass spectrum, and elemental analysis (Scheme 4.4).

This compound is synthesized as analogous to compound **3.6** in Chapter III hoping that the compound will be highly soluble in water and helps the self-assembly process to occur in polar solvents.



Scheme 4.4. Synthesis of molecular probe **4.7**.

#### Job's Plot Study of Molecular Probe **4.7**

As explained in previous chapters, stoichiometry of the complex is very important to calculate the binding constant from any optical titration experiment. Therefore, the stoichiometry of binding of compound **4.7** with the  $\text{Fe}(\text{ClO}_4)_3$  is determined by a Job's plot analysis. Each host and guest solution is prepared in  $\text{CH}_3\text{CN}$  and of  $1 \times 10^{-4}$  M. Both solutions are then mixed to give overall the same total molar concentration i.e.,  $1 \times 10^{-4}$  M but varying ratio of host and guest from 0 to 1. Fluorescence is measured for each mole fraction, and the fluorescence intensity of monomer emission at 376 nm was plotted

against the mole fraction of  $\text{Fe}(\text{ClO}_4)_3$ . The minimum of the curve lies at 0.33 which corresponds to 2:1 (Ligand: metal) stoichiometry (Figure 4.2).

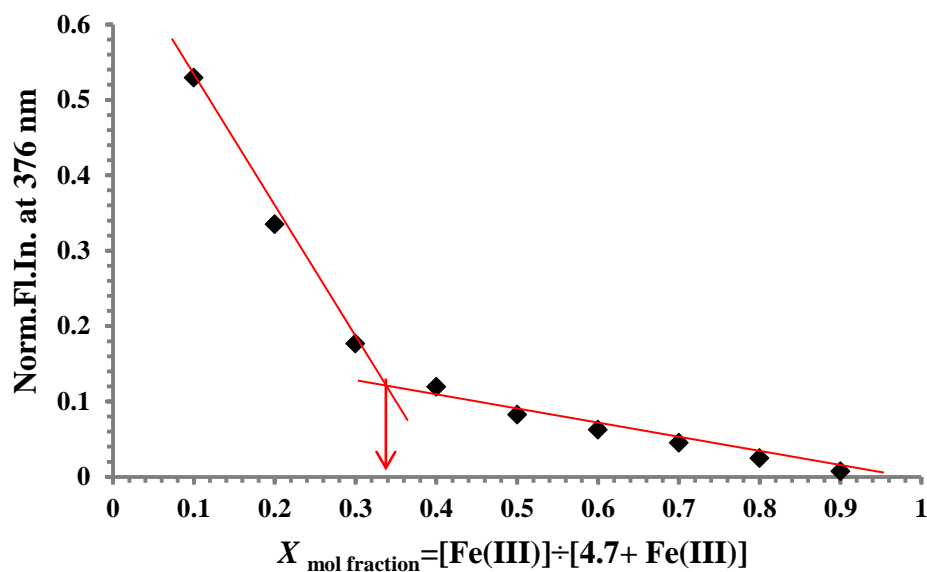


Figure 4.2. Job's plot of compound **4.7** with  $\text{Fe}(\text{ClO}_4)_3$  obtained by fluorescence measurement. The total concentration of compound **4.7** and  $\text{Fe}(\text{ClO}_4)_3$  is  $1 \times 10^{-4}$  M in  $\text{CH}_3\text{CN}$ .

### Optical Studies of the Molecular Probe **4.7**

#### Fluorescence spectroscopy

The binding behavior of compound **4.7** was first studied towards various metal ions by fluorescence spectroscopy. As discussed in Chapter II, compound **4.7** is expected to produce only monomer emission as it has only one pyrene unit as a sensing motif. However, compound **4.7** should undergo self-assembly process by the formation of excimer emission upon the addition of target metal ion ( $\text{Zn}^{2+}$  ion). Organic solvent  $\text{CH}_3\text{CN}$  is selected to study the fluorescence of compounds **4.7** as explained in the Chapter II.

The fluorescence spectrum of compound **4.7** ( $10 \mu\text{M}$ ) shows typical pyrene monomer emission bands at 378 and 398 nm on excitation at 340 nm as we saw for the



other pyrene compounds in Chapter I and II. The fluorescence of compound **4.7** was studied by adding one and a half equivalent of various metal ions such as  $\text{Na}^+$ ,  $\text{K}^+$ ,  $\text{Ag}^+$ ,  $\text{Ca}^{2+}$ ,  $\text{Mg}^{2+}$ ,  $\text{Cd}^{2+}$ ,  $\text{Zn}^{2+}$ ,  $\text{Co}^{2+}$ ,  $\text{Fe}^{2+}$ ,  $\text{Hg}^{2+}$ ,  $\text{Cu}^{2+}$ ,  $\text{Al}^{3+}$ ,  $\text{Cr}^{3+}$ , and  $\text{Fe}^{3+}$  (all are perchlorate salts except  $\text{CrCl}_3$  and  $\text{HgCl}_2$ ) to compound **4.7**. An excimer emission was observed with a maximum around 465 nm with  $\text{Fe}^{3+}$  ion instead of  $\text{Zn}^{2+}$  ion. It could be possible that sugar functional groups might change the selectivity of metal ion from  $\text{Zn}^{2+}$  to  $\text{Fe}^{3+}$  ions. Further, an excimer emission was produced at 465 nm instead of 420 nm. The red shift in excimer emission indicates that this could be the dynamic excimer. (Figure 1.7, Chapter I). None of the other metal ions forms the excimer band around 465 nm except very little by  $\text{Al}^{3+}$  and  $\text{Fe}^{2+}$  ions (Figure 4.3). In fact, almost all other metal ions quench the fluorescence of compound **4.7**. In case of transition metal ions, quenching may be ascribed to the cation- $\pi$  interactions between heavy atom and electron rich pyrene (Chapter I).<sup>90</sup> The excimer emission was also not observed upon the titration of compound **4.7** with tetrabutylammonium salts such as TBACl in Figure 4.7 which clearly suggests that  $\text{Fe}^{3+}$  ion is responsible for the formation of the excimer band and is templating the two pyrene units.

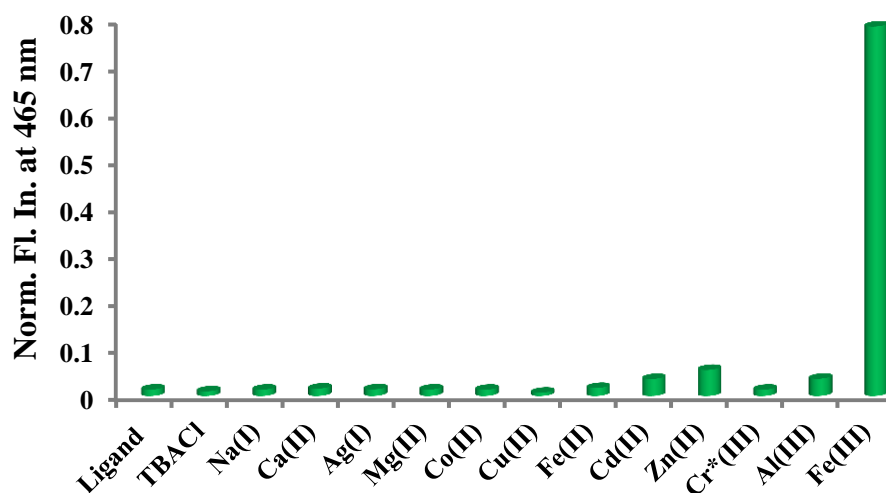


Figure 4.3. Bar chart of compound **4.7** ( $10 \mu\text{M}$  and  $\lambda_{\text{ex}} = 340 \text{ nm}$ ) in  $\text{CH}_3\text{CN}$  upon the addition of 1.5 equivalents of different metal ions as their  $\text{ClO}_4^-$  salts (\*Cl- salt).

Fluorescence titration of compound **4.7** was carried out with  $\text{Fe}(\text{ClO}_4)_3$  to better understand the binding mechanism. Addition of  $\text{Fe}^{3+}$  ion to the solution of compound **4.7** decreased the pyrene monomer emission bands at 380 and 400 nm with a concomitant formation of a new red shifted; structureless broad band centered on 465 nm, a typical of pyrene excimer fluorescence, with a clear isoemissive point at 425 nm (Figure 4.4). The isoemissive point was observed only up to 1.2 equivalents indicating the formation of only one complex species. The intensity of excimer band increased with the increase in the concentration of  $\text{Fe}^{3+}$  ion but plateaued out after one equivalent. A higher concentration of  $\text{Fe}^{3+}$  ion results in a decrease of both monomer and excimer band intensities due to the quenching ability of the  $\text{Fe}^{3+}$  ions. Fitting of fluorescence data to the HypSpec programme<sup>116</sup> (Figure 4.5) showed that compound **4.7** was found to bind  $\text{Fe}^{3+}$  ion in an exclusively 2:1 ratio with a binding constant calculated to be  $K_{21} = 1 \times 10^{10} \text{ M}^{-2}$ .

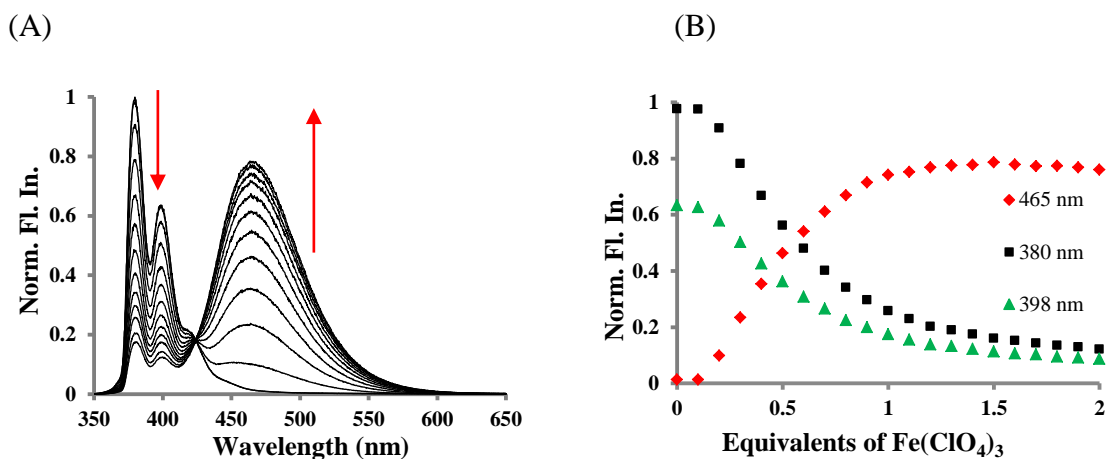


Figure 4.4. Fluorescence titration of compound **4.7** (10  $\mu\text{M}$ ) with  $\text{Fe}(\text{ClO}_4)_3$  (100  $\mu\text{M}$ ) in  $\text{CH}_3\text{CN}$ . Fluorescence spectrum (A), and (B) its binding isotherm.  $\lambda_{\text{ex}} = 340 \text{ nm}$ .

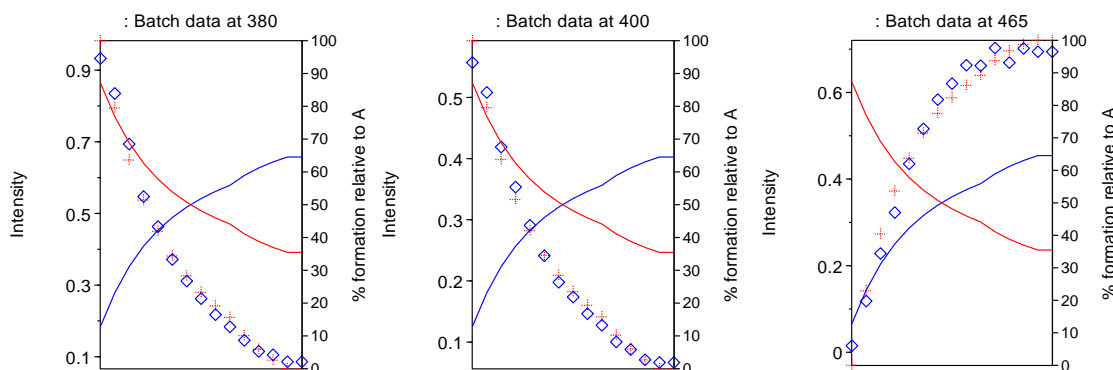


Figure 4.5. Binding isotherm of fluorescence titration of compound **4.7** with  $\text{Fe}(\text{ClO}_4)_3$  from HypSpec program.<sup>116</sup>

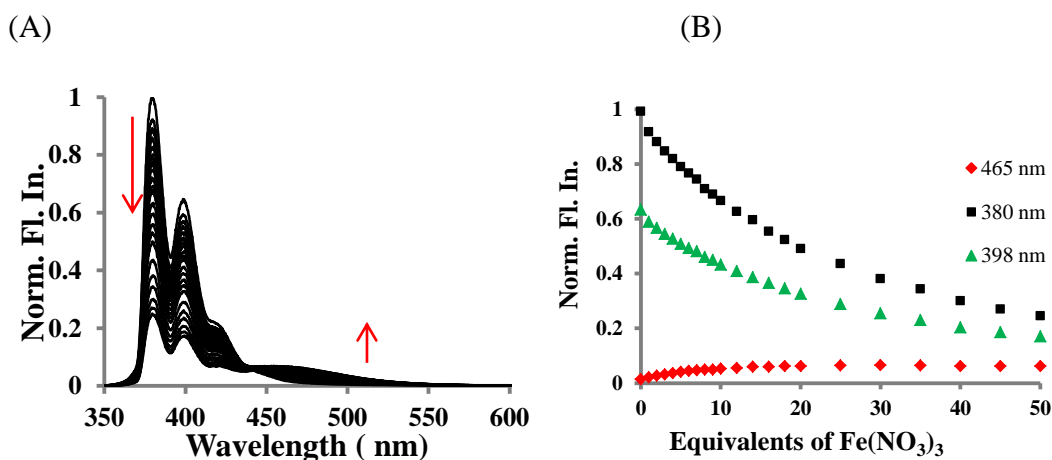


Figure 4.6. Fluorescence titration of compound **4.7** (10  $\mu\text{M}$ ) with  $\text{Fe}(\text{ClO}_4)_3$  (100  $\mu\text{M}$ ) in  $\text{CH}_3\text{CN}$ . Fluorescence spectrum (A), and (B) its binding isotherm.  $\lambda_{\text{ex}} = 340 \text{ nm}$ .

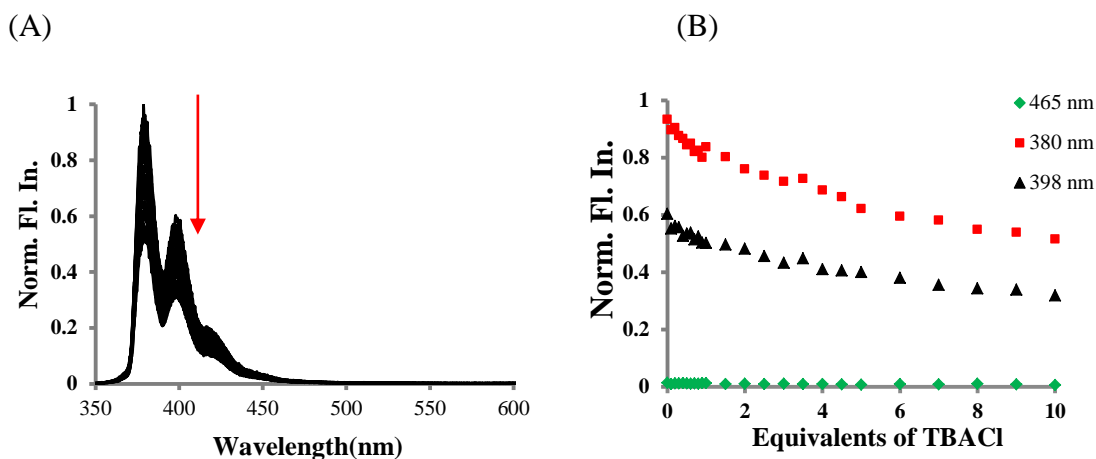


Figure 4.7. Fluorescence titration of compound **4.7** (10  $\mu\text{M}$ ) with TBACl (100  $\mu\text{M}$ ) in  $\text{CH}_3\text{CN}$ . Fluorescence spectrum (A), and (B) its binding isotherm.  $\lambda_{\text{ex}} = 340 \text{ nm}$ .

Compound **4.7** was also titrated with various anions of  $\text{Fe}^{3+}$  ion such as  $\text{Fe}(\text{ClO}_4)_3$ ,  $\text{FeCl}_3$ ,  $\text{FeBr}_3$ , and  $\text{Fe}(\text{NO}_3)_3$  (Figures 4.6 and 4.8). A very little excimer band was formed with decrease in monomer emission even at higher concentration (1 mM) for  $\text{FeBr}_3$  and  $\text{Fe}(\text{NO}_3)_3$  (Figure 4.8). This shows that the size of anions also plays a key role in the formation of excimer emission. More importantly, the iron salts such as  $\text{FeBr}_3$  and  $\text{Fe}(\text{NO}_3)_3$  do not dissociate as freely than the  $\text{Fe}(\text{ClO}_4)_3$  in  $\text{CH}_3\text{CN}$ . This makes the two pyrene units far enough to feel the excimer band though  $\text{Fe}^{3+}$  ion is still coordinated to the compound **4.7**.<sup>162</sup> The geometry around the  $\text{Fe}^{3+}$  ion is proposed to be octahedral, and pyrene units adopt a *syn* configuration (Scheme 4.5).

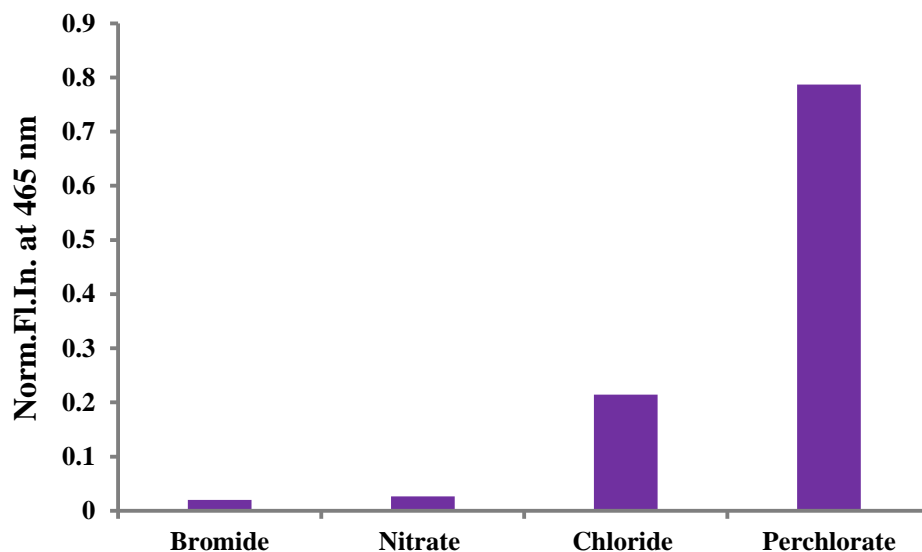
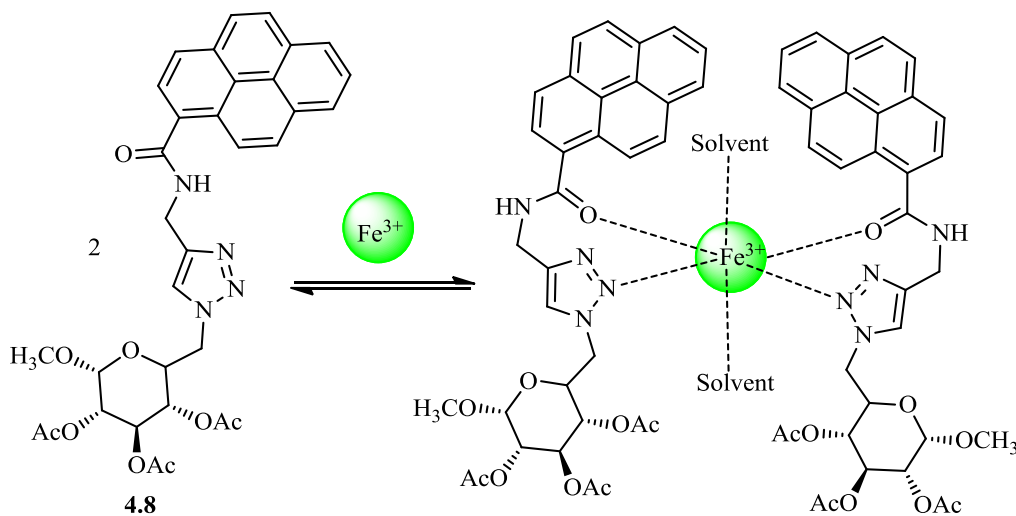


Figure 4.8. Bar chart of compound **4.7** (10  $\mu$ M and  $\lambda_{\text{ex}} = 340$  nm) in  $\text{CH}_3\text{CN}$  upon the addition of 1.5 equivalents of different anions of iron.



Scheme 4.5. Proposed binding mechanism of compound **4.7** with  $\text{Fe}^{3+}$  ion.

### $^1\text{H}$ NMR Studies of Molecular Probe **4.7**

Fluorescence studies of compound **4.7** with different metal ions showed that an excimer emission is produced around 465 nm upon addition of  $\text{Fe}^{3+}$  ion. However, as explained in Chapters II and III, fluorescence studies do not give information about the particular functional groups that is involved in the binding of metal ion. Particularly in

this project, it is very important to know whether a sugar group (acetyl, ring oxygen, and  $-\text{OCH}_3$  groups of glucose) is involved in the coordination of  $\text{Fe}^{3+}$  ion or not. In order to get this binding information and support the fluorescence results,  $^1\text{H}$  NMR titration of compound **4.7** was carried out with  $\text{Al}(\text{ClO}_4)_3$  in  $\text{CD}_3\text{CN}$ .  $\text{Al}(\text{ClO}_4)_3$  is selected instead of  $\text{Fe}(\text{ClO}_4)_3$  for the  $^1\text{H}$  NMR titration as the signals of protons became excessively broad and quenched upon addition of  $\text{Fe}(\text{ClO}_4)_3$  in the  $^1\text{H}$  NMR spectrum. However,  $\text{Al}^{3+}$  salts can be used as the geometry mimic of  $\text{Fe}^{3+}$  ions due to the same size and charge. Both aluminium and iron are paramagnetic species. Aluminium has a spin quantum number of nucleus greater than one ( $I=5/2$  for  $\text{Al}^{3+}$ ). Thus, they have a non-spherical charge distribution and affect the relaxation time, which consequently affect the line width of the signal and coupling with neighboring nuclei.<sup>163</sup>

A 10 mM solution for compound **4.7** and a 100 mM for  $\text{Al}(\text{ClO}_4)_3$  were used in  $^1\text{H}$  NMR titration. The signals followed in the  $^1\text{H}$  NMR experiment are highlighted in Figure 4.9 with their chemical shifts values in the free ligand in  $\text{CD}_3\text{CN}$ .

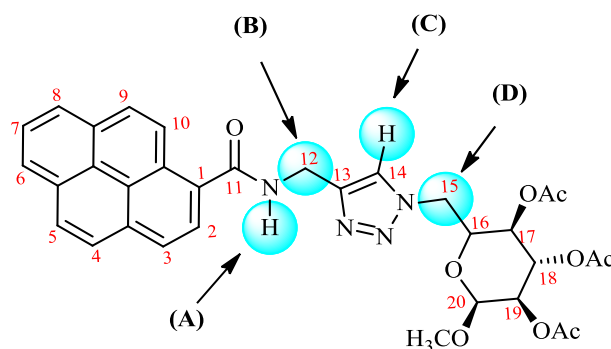


*Figure 4.9.*  $^1\text{H}$  NMR assignments that are followed in the NMR titration experiments in  $\text{CD}_3\text{CN}$ . The chemical shifts values of A, B, C and D in the free ligand **4.7** are  $\delta$  7.54, 4.76 7.92, and 3.12 ppm, respectively.

The protons of compound **4.7** are assigned on the basis of 2D NMR (COSY, HMQC, HMBC, and ROESY). A significant change in the chemical shifts was observed

for amide proton (A) and triazole proton (C) while the other protons such as CH<sub>2</sub> groups attached to amide (B) and sugar (D) changed to a lesser extent (Table 4.2 and Figure 4.10). For example, the changes in the chemical shift for NH (A), CH<sub>2</sub> (B), and CH(C) groups after the addition of one equivalent of Al(ClO<sub>4</sub>)<sub>3</sub> were 0.35, 0.09, and 0.57 ppm, respectively (Figures 4.9-4.11). The downfield shifts of triazole and amide protons can be rationalized through the inductive effect after coordination with the metal ion. For example, the amide oxygen atom on coordination with metal ion makes the carbonyl carbon more positive which, in turn, pulls out electron from amide nitrogen becoming more acidic. The hydrogen atom attached to carbon number two of pyrene also shifted into downfield by 0.08 ppm (from 8.55 to 8.63 ppm) after the addition of Al(ClO<sub>4</sub>)<sub>3</sub>. This further supports that the coordination of Al<sup>3+</sup> ions by the carbonyl oxygen atoms of compound **4.7** is reasonable. Surprisingly, the changes in the chemical shifts of the protons of sugar (acetyl, ring oxygen, and -OCH<sub>3</sub> groups of glucose) are negligible which indicates that the sugar group might not be involved in the coordination of Al<sup>3+</sup> ion. The binding affinity ( $K_{21}$ ) of **4.7** for Al<sup>3+</sup> ions was calculated to be greater than  $1 \times 10^6 \text{ M}^{-1}$  (Figure 4.12). Most importantly, there was almost no change in the chemical shifts of the protons after addition of half equivalent of Al(ClO<sub>4</sub>)<sub>3</sub> (Figures 4.10-4.11). This confirmed that **4.7** is binding Al<sup>3+</sup> ion in 2:1 stoichiometry ratio.

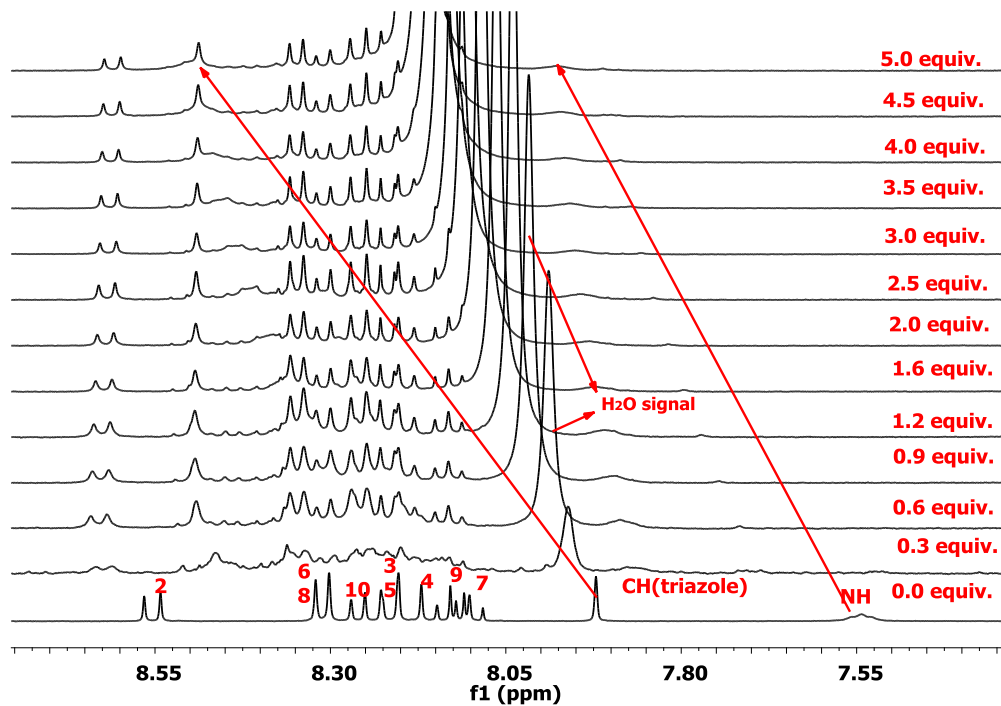


Figure 4.10. Partial  $^1\text{H}$  NMR stack plot: Addition of  $\text{Al}(\text{ClO}_4)_3$  to compound **4.7** in  $\text{CD}_3\text{CN}$  (aromatic regions only).

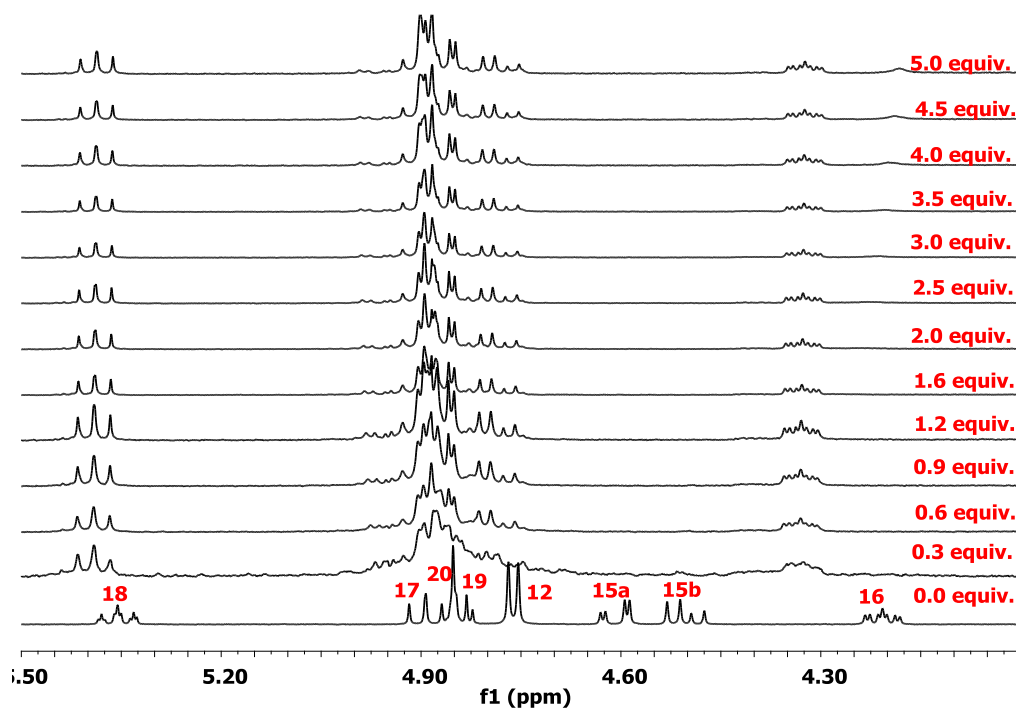


Figure 4.11. Partial  $^1\text{H}$  NMR stack plot: Addition of  $\text{Al}(\text{ClO}_4)_3$  to compound **4.7** in  $\text{CD}_3\text{CN}$  (sugar group only).



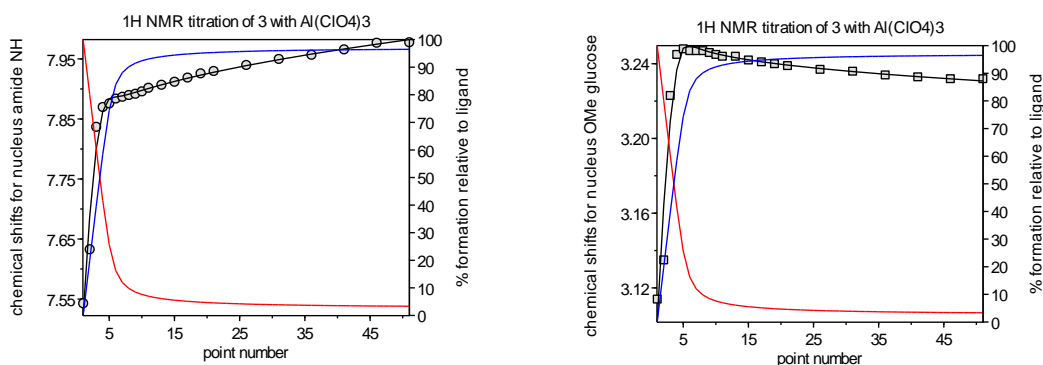


Figure 4.12.  $^1\text{H}$  NMR binding isotherm of amide proton (A) and  $-\text{OCH}_3$  (attached to carbon number 20) group of sugar of compound **4.7** upon addition of  $\text{Al}(\text{ClO}_4)_3$ .

Table 4.2

Change in chemical shift of compound **4.7** after addition of one equivalent of  $\text{Al}(\text{ClO}_4)_3$  in  $\text{CD}_3\text{CN}$

Signals	Chemical shift at 0.0 equivalent	Chemical shift after 1.0 equivalent	Difference
2-CH	8.55	8.62	0.07
NH	7.54	7.90	0.36
12- $\text{CH}_2$	4.76	4.85	0.09
14-CH	7.92	8.49	0.57
15- $\text{CH}_2$	4.49 and 4.60	4.78	0.28-0.18
16-CH	4.20	4.33	0.13
17-CH	4.89	4.90	0.008
18-CH	5.33	5.38	0.06
19-CH	4.82	4.87	0.05
20-CH	4.84	4.88	0.04
20- $\text{OCH}_3$	3.11	3.24	0.13

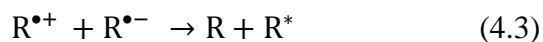
### Electrogenerated Chemiluminescence (ECL) Studies of Molecular Probe **4.7**

Poly aromatic hydrocarbons (PAHs) such as rubrene, fluorine, diphenyl anthracene (DPA), liminol, and acridinium esters are known to produce electrogenerated chemiluminescence because of their high fluorescence quantum yields and stable radical cations and anions in aprotic media.<sup>164, 165</sup> Electrogenerated chemiluminescence of pyrene

and its derivatives have also been reported.<sup>166-168</sup> <sup>169</sup> Since compound **4.7** is a chemosensor containing pyrene group, it is expected to produce ECL. The fluorescence result of compound **4.7** showed that excimer emission is produced on addition of  $\text{Fe}^{3+}$  ions suggesting self-assembly process. Therefore, we expect that ECL intensity of compound **4.7** should be changed upon addition of  $\text{Fe}^{3+}$  ions as the ECL is produced by the complex rather than free ligand. Since the self-assembled system (i.e., complex) has two pyrene units coordinated with  $\text{Fe}^{3+}$  ions, it may enhance the intensity of electrogenerated chemiluminescence. Therefore, ECL study is carried out for compound **4.7** in order to support the self-assembly process.

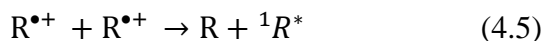
Electrogenerated chemiluminescence (abbreviated as ECL) is defined as the process where light is produced at the electrode surface by the excited state of the species formed during the electron transfer reaction.<sup>170</sup> ECL does not require the use of external light source as chemiluminescence. As analytical techniques, ECL possesses a number of advantages over chemiluminescence. For example, electrochemical reaction in ECL allows the time and position of the light emitting reaction to be controlled. It is more selective than chemiluminescence as the generation of excited state can be selectively controlled by varying the electrode potential. ECL is also a non-destructive technique as ECL emitters can be regenerated after ECL emission.<sup>165, 171</sup> ECL can be produced by two pathways namely the ion annihilation and coreactant pathways.

In ion annihilation pathway, oxidized and reduced species are produced on the electrode surface by a potential step or sweep. These species then interact to produce a ground state and electronically excited state which then relaxes by emission of light (pathways 4.1-4.4).



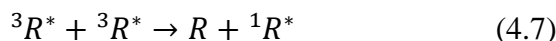
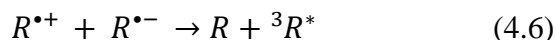
Depending on the energy available in an ion annihilation, the produced  $R^*$  could be either the lowest excited state species ( $^1R^*$ ) or the triplet species ( $^3R^*$ ). If the reaction produces singlet excited species, it is called an energy-sufficient system, and the reaction is said to follow the *S-route* (pathway 4.5). A typical example is the  $DPA^{\bullet+}/DPA^{\bullet-}$  (DPA=9,10-diphenylanthracene).<sup>172</sup>

*S-route*



In a system with insufficient energy, the triplet state energy  $^3R^*$  will first be produced, then  $^1R^*$  will be generated by the subsequent annihilation of  $^3R^*$  (triplet-triplet annihilation). This system is said to follow a *T-route* (Equation 4.6-4.7).  $TMPD^{\bullet+}/DPA^{\bullet-}$  and  $TMPD^{\bullet+}/AN^{\bullet-}$  (TMDP=*N, N, N, N'*-tetramethyl-*p*-phenylenediamine and AN = anthracene) are two examples of *T-route* systems (pathways 4.6 and 4.7).<sup>173</sup>

*T-route*



In the coreactant pathway, ECL is generated by one directional potential scanning on the electrode in a solution containing luminophore and in the presence of a deliberately added reagent called coreactant. ECL coreactant is a species that upon electrochemical oxidation or reduction, immediately forms a strong reducing or oxidizing

intermediate which then reacts with an oxidized or reduced ECL luminophore to generate excited states capable of emitting light.<sup>174, 175</sup> Use of coreactant make ECL possible even when ion annihilation ECL is not applicable due to oxygen quenching effect, instability of radical cation or anion, and potential window of solvent is small. Some common coreactants used in ECL are oxalate ( $C_2O_4^-$ ), tri-n-propyl amine (TPrA), hydrazine ( $N_2H_4$ ), persulfate ( $S_2O_8^{2-}$ ), and bezoyl peroxide. An ECL system that contains  $Ru(bpy)_3^{2+}$  and tri-n-propylamine (TPrA) as a coreactant has shown the highest ECL efficiency so far and forms the basis of commercial system for flow cell bead based and multi spot plate based immunoassay and DNA analysis.<sup>165, 171</sup> The ECL mechanism of  $Ru(bpy)_3^{2+}/TPrA$  system is very complicated.<sup>165</sup>

ECL behaviour of the compound **4.7** was studied using tri-n-propylamine (TPrA) as a co-reactant and tetrabutylammonium perchlorate (TBAP) as a supporting electrolyte. The ECL intensity of compound **4.7** was enhanced upon the addition of  $Fe(ClO_4)_3$ . Figure 4.13 shows the ECL spectrum of the compound **4.7** and its complex (after the addition of one equivalent) with 0.02 M TPrA and 0.1 M TBAP at a platinum electrode with the scan rate of 100 mV/s. The compound **4.7** (50 $\mu$ M) produced an ECL intensity of around 5 nA current at 1.6 V which is enhanced up to 28 nA upon addition of one equivalent of  $Fe(ClO_4)_3$  (500  $\mu$ M) (Figure 4.13). The increase in ECL intensity could possibly be due to a self-assembly process and its exact mechanism for enhancement in ECL is under study. Furthermore, ECL is carried out for different mole ratio in order to find the binding stoichiometry between ligand **4.7** and  $Fe(ClO_4)_3$  (Figure 4.14). ECL intensity is found maximum at a 2:1 [**4.7**: $Fe(ClO_4)_3$ ] ratio further confirming the compound **4.7** is binding  $Fe(ClO_4)_3$  in 2:1 stoichiometry. The ECL intensity of compound **4.8** was also

studied with the addition of one equivalent of other different metal ions such as  $\text{Zn}^{2+}$ ,  $\text{Cu}^{2+}$  and  $\text{Ca}^{2+}$  but do not show any enhancement (Figure 4.15). The proposed mechanism for the ECL produced by the compound **4.7** is shown in Figure 4.16.

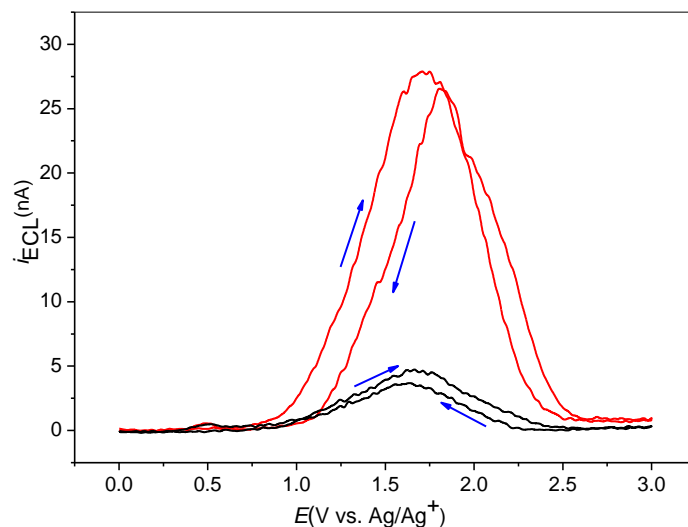


Figure 4.13. ECL response of 50  $\mu\text{M}$  **4.7** (black) and after addition of one equivalent of 500  $\mu\text{M}$   $\text{Fe}(\text{ClO}_4)_3$  (red) with a 0.02M TPrA and 0.1M TBAP in  $\text{CH}_3\text{CN}$  at a 2mm Pt electrode with a scan rate of 100 mV/S.

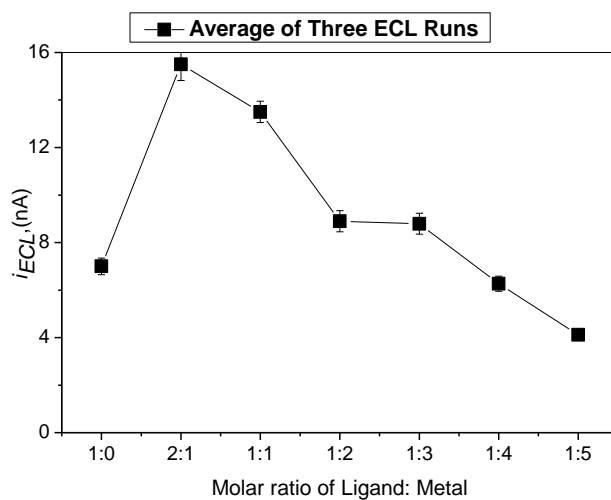


Figure 4.14. ECL plot vs different mole ratio of ligand **4.7** to  $\text{Fe}(\text{ClO}_4)_3$ .

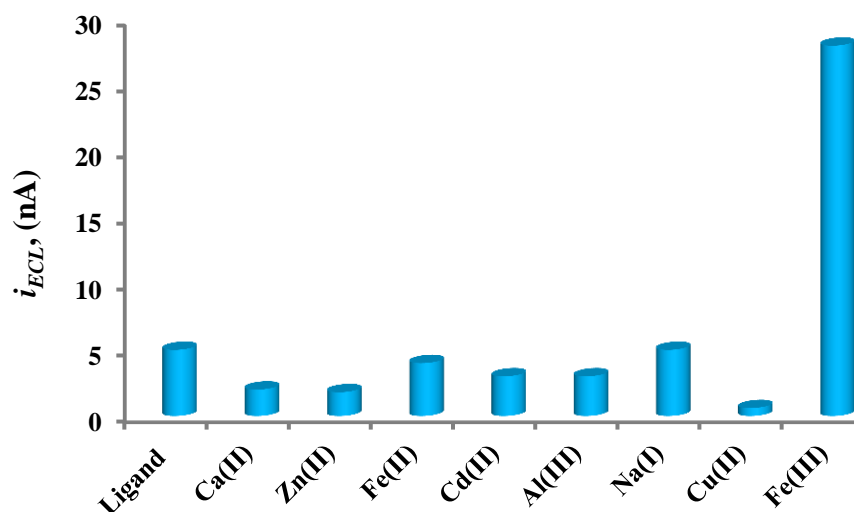


Figure 4.15. Bar chart of electrogenerated chemiluminescence of **4.7** with one equivalent of different metal ions in CH<sub>3</sub>CN (**4.7**= 50 μM, TBAP= 0.1 M, TPrA= 20 mM).

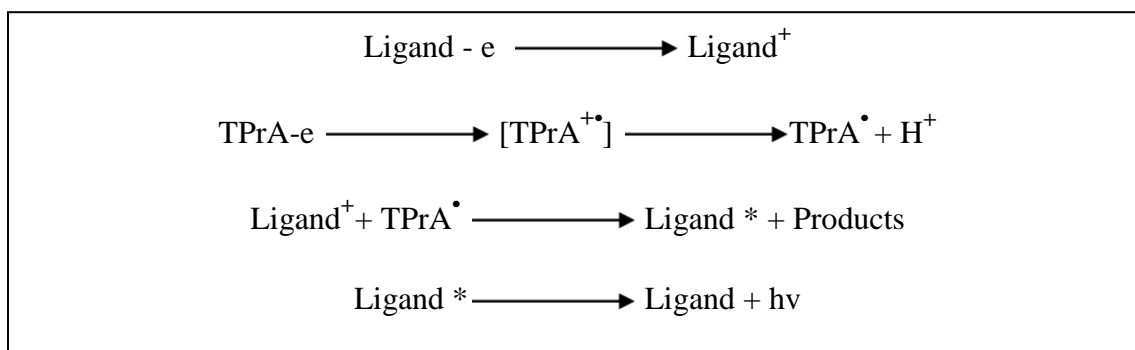


Figure 4.16. Proposed ECL mechanism for the compound **4.7**.

#### Summary

In conclusion, a sugar functionalized pyrene based triazole receptor was synthesized in good yield by an azide-alkyne Huisgen cycloaddition reaction between N-(prop-2-ynyl) pyrene-1-carboxamide and methyl 2, 3, 4-tri-*O*-acetyl-6-azido-6-deoxy- $\alpha$ -D-glucopyranoside. The fluorescence titration studies of compound **4.7** with different metal ions showed that an excimer emission was produced only upon the addition of the Fe<sup>3+</sup> ion. Further, an effect of the different anions of iron on fluorescence of compound **4.7** was studied and found that Fe(ClO<sub>4</sub>)<sub>3</sub> produced the most intense excimer emission.

The formation of excimer emission suggested that the compound **4.7** is self-assembled in the presence of  $\text{Fe}^{3+}$  ion in a 2:1 stoichiometric ratio, which is also confirmed by Job's plot.

The binding of compound **4.7** is also studied by  $^1\text{H}$  NMR titration with  $\text{Al}(\text{ClO}_4)_3$  and shows that  $\text{Al}^{3+}$  ion is possibly coordinated by oxygen atoms of amide and nitrogen atoms of triazole groups. The change in the chemical shift is almost constant after a half equivalent of  $\text{Al}(\text{ClO}_4)_3$  indicating the binding stoichiometry is 2:1 (ligand:metal).

The binding of compound **4.7** with  $\text{Fe}^{3+}$  ion is further studied by electrogenerated chemiluminescence which shows that the ECL intensity is enhanced upon binding with the  $\text{Fe}^{3+}$  ion. Other metal ions did not show any increase in the ECL intensity. The ECL intensity is maximum when the mole ratio is 2:1 [**4.7**:  $\text{Fe}(\text{ClO}_4)_3$ ] supporting the binding stoichiometry.

## Experimental

### *General techniques for ECL instruments*

Cyclic voltammetry (CV) was performed with a model 660A electrochemical workstation (CH Instruments, Austin, TX). A conventional three-electrode cell was used, with a Pt wire as the counter electrode and an  $\text{Ag}/\text{Ag}^+$  (10 mM  $\text{AgNO}_3$  in 0.10 M TBAP  $\text{CH}_3\text{CN}$ ) as the reference electrode. A Platinum electrode with 2mm in diameter was used for CV and ECL measurement. The electrode was polished with 0.3-0.05  $\mu\text{m}$  alumina slurry, thoroughly rinsed with water, and dried with the Kim wipes facial tissue before each experiment. The electrolyte solution was purged with high purity nitrogen (Nordan Smith, Hattiesburg, MS) for 10 min and kept under nitrogen atmosphere during the measurement of CV. The ECL signals along with the CV responses were measured

simultaneously with a homemade ECL instrument as described previously.<sup>23-24</sup> This instrument combined the 660A electrochemical workstation with a photomultiplier tube (PMT, Hamamatsu R928, Japan) based at a voltage of -700 V *via* a high voltage power supply (Model 472A Brandenburg PMT power supply, England), and the photocurrent detected with a high sensitive Keithley 6514 electrometer (Keithley, Cleveland, OH) was converted to a voltage before it was sent to the electrochemical workstation computer. ECL spectra were obtained by collecting the peak ECL intensity of the forward scan (1.6 V vs Ag/Ag<sup>+</sup> in CH<sub>3</sub>CN) during the cyclic potential cycling at a scan rate of 100 mV/s with 24 pieces of interference filters (Intro, Inc. Socorro, NM) over a spectral range of 360 to 820 nm. These filters had an average half-peak width of 10 nm and a transmittance value of 50% at the specified wavelength.

#### *General procedure for fluorescence experiments*

A stock solution (10 μM) of compound **4.7** was prepared in CH<sub>3</sub>CN. The solution was excited at λ= 340 nm and scanned from λ=350-660 nm with a slit width set to 0.5mm. A 10 times more concentrated solution of the metal salt was prepared in CH<sub>3</sub>CN and 20 μL (20μL = 0.1 equivalent of metal salt) aliquots were added to compound **4.7**. Fluorescence spectra were recorded after each addition. Dilution factors were taken into consideration upon binding study determination. The binding constants were determined from fluorescence titrations using HypSpec 2006.<sup>116</sup>

#### *General procedure for <sup>1</sup>H NMR experiment*

A 10 mM solution of compound **4.7** was prepared by dissolving 3.2 mg in 0.5 mL in CD<sub>3</sub>CN. A 10 times more concentrated solution of the Al(ClO<sub>4</sub>)<sub>3</sub> was prepared in CD<sub>3</sub>CN, and 5 μL (5 μL = 0.1 equivalent of metal salt) aliquots was added to compound



**4.7.**The  $^1\text{H}$  NMR spectrum recorded after each addition. The binding studies were pursued by  $^1\text{H}$  NMR titrations using HypNMR 2008.<sup>141</sup>

*General procedure for UV-Vis experiment*

A stock solution ( $4.8 \times 10^{-5}$  M) of compound **4.7** was prepared by dissolving 0.6 mg in 20 mL of  $\text{CH}_3\text{CN}$ , and then 2 mL was transferred to the UV-Vis cell. From the stock solution, twelve dilute solutions ranging from  $1.2 \times 10^{-5}$  to  $4.2 \times 10^{-5}$  M were prepared, and the UV-Vis spectra were recorded for each sample. The molar absorptivity of compound **4.7** at various wavelengths were calculated as: 240 nm ( $\epsilon=20043 \text{ M}^{-1}\text{cm}^{-1}$ ), 274 nm ( $\epsilon=11864 \text{ M}^{-1}\text{cm}^{-1}$ ), 326 nm ( $\epsilon=7283 \text{ M}^{-1}\text{cm}^{-1}$ ) and 340 nm ( $\epsilon=10186 \text{ M}^{-1}\text{cm}^{-1}$ ).

General Procedure for ECL Experiment to Determine Binding Stoichiometry

Ligand (**4.7**) = 0.00005 M (50  $\mu\text{M}$ ) + 0.1 M TBAP + 20 mM TPrA ( $\text{CH}_3\text{CN}$ )

$\text{Fe}(\text{ClO}_4)_3$  = 0.0005 M (500  $\mu\text{M}$ ) in 0.1 M TBAP

$\text{CH}_3\text{CN}$  = contains 0.1 M TBAP (tetrabutyl ammonium perchlorate)

Table 4.3

*Volume and concentration used for ECL experiment for calculating binding stoichiometry*

	Vial 1	Vial 2	Vial 3	Vial 4	Vial 5	Vial 6	Vial 7
50 $\mu\text{M}$ Ligand Solution with 0.1 M TBAP and 20 mM TPrA in $\text{CH}_3\text{CN}$	2 mL	2 mL	2 mL	2 mL	2 mL	2 mL	2 mL
$\text{CH}_3\text{CN}$ with 0.1 M TBAP	1 mL	0.9 mL	0.8 mL	0.6 mL	0.4 mL	0.2 mL	0.2 mL

Table 4.3 (continued).

	Vial 1	Vial 2	Vial 3	Vial 4	Vial 5	Vial 6	Vial 7
500 $\mu$ M Fe(ClO <sub>4</sub> ) <sub>3</sub> with 0.1 M TBAP	0 mL	0.1 mL	0.2 mL	0.4 mL	0.6 mL	0.8 mL	1 mL
Total Volume	3 mL	3 mL	3 mL	3 mL	3 mL	3 mL	3 mL
Ligand:Metal	1:0	1:0.5	1:1	1:2	1:3	1:4	1:5

#### General Procedure for the Synthesis

##### *Methyl 2,3,4-tri-O-acetyl-6-O-p-toulenesulfonyl- $\alpha$ -D-glucopyranoside (4.5)*<sup>159-161</sup>

The  $\alpha$ -Methyl-glucopyranoside (1.5 g, 7.8 mmol) was dissolved in 20 ml of dry pyridine and cooled to 0° C. Tosyl chloride (2.0 g, 10.3 mmol) was slowly added and stirred at 0° C for eight-ten hours. Acetic anhydride (20 mL, 180 mmol) was added and stirred at room temperature for 12-14 hours. The solution was poured onto crushed ice, and the mixture was extracted with CHCl<sub>3</sub> (3 $\times$  30 mL). The combined extracts were washed with saturated aqueous NaHCO<sub>3</sub> solution, saturated aqueous NaCl solution, and distilled water, consecutively, and dried over MgSO<sub>4</sub>, filtered, and concentrated under reduced pressure. The crude product was purified by chromatography (EtOAc /Hexane =2/8) to give the compound **4.5** (2.775 g, 5.85 mmol, 75%).

<sup>1</sup>H NMR (300 K, CDCl<sub>3</sub>, 400MHz):  $\delta$ 7.69 (d, 2H,  $J$ =8.1Hz, CH<sub>Ar</sub>), 7.29 (d, 2H,  $J$ =8.1Hz, CH<sub>Ar</sub>), 5.32 (t, 1H,  $J$ =9.8 Hz, CH<sub>Glu</sub>), 4.77(d, 1H,  $J$ =3.5 Hz, CH<sub>Glu</sub>), 4.71(dd,1H,  $J$ =3.5 Hz, 10.2 Hz, CH<sub>Glu</sub>), 3.98-4.09 (m, 2H, CH<sub>Glu</sub>), 3.89-4.92 (m, 1H, CH<sub>Glu</sub>), 3.26 (s, 3H, CH<sub>3</sub>), 2.37 (s, 3H, CH<sub>3</sub>), 1.95 (s, 3H, CH<sub>3</sub>), 1.89 (s, 3H, CH<sub>3</sub>), 1.87 (s, 3H, CH<sub>3</sub>);

<sup>13</sup>C NMR (300 K, CDCl<sub>3</sub>, 400MHz):  $\delta$ 169.72, 169.16, 144.98, 132.50, 129.76, 127.85, 96.44, 70.30, 69.74, 68.36, 67.67, 66.88, 66.80, 55.26, 21.33, 20.32, 20.19

IR (ATR solid); 2943  $\nu_{\text{C-H}}$  (w), 1748  $\nu_{\text{C=O}}$  (vs)  $\text{cm}^{-1}$ .

*Methyl 2, 3, 4-tri-O-acetyl-6-azido-6-deoxy- $\alpha$ -D-glucopyranoside (4.6)*<sup>159</sup>

A solution of compound **4.6** (7.00 g, 20.09 mmol) and  $\text{NaN}_3$  (10.0 g, 0.154 mol) in dry DMSO (100 mL) was stirred at 50°C for four hours followed by stirring at room temperature for 16 hours. The resulting slurry was poured onto crushed ice, and the mixture was extracted with dichloromethane (4  $\times$  50 mL). The combined extracts were washed two times with water, dried over  $\text{MgSO}_4$ , and filtered. Concentration of the filtrate in vacuum and column chromatography of the residue (10-13% ethyl acetate/ n-hexane) give white solid **4.7** ( 5.618 g, 16.27mmol, 81%).  $^1\text{H}$  NMR (300 K,  $\text{CDCl}_3$ , 400MHz):  $\delta$ 5.46 (t, 1H,  $J=9.7$  Hz,  $\text{CH}_{\text{Glu}}$ ), 4.97(m, 2H,  $\text{CH}_{\text{Glu}}$ ), 4.88(dd,1H,  $J=3.6$  Hz, 11 Hz,  $\text{CH}_{\text{Glu}}$  ), 3.45 (s, 3H,  $\text{CH}_3$ ), 3.31 (m, 2H,  $\text{CH}_{\text{Glu}}$ ), ), 2.06 (s, 3H,  $\text{CH}_3$ ), 2.03 (s, 3H,  $\text{CH}_3$ ), ), 2.01 (s, 3H,  $\text{CH}_3$ );

$^{13}\text{C}$  NMR (300 K,  $\text{CDCl}_3$ , 400MHz):  $\delta$ 169.08, 169.02, 168.64, 95.65, 69.78, 68.87, 68.78, 67.57, 54.57, 50.07, 19.67, 19.63, 19.60

IR (ATR solid); 2960  $\nu_{\text{C-H}}$  (w), 2930  $\nu_{\text{C-H}}$  (w), 2837  $\nu_{\text{C-H}}$  (w), 2092  $\nu_{\text{N=N}}$  (vs), 1738  $\nu_{\text{C=O}}$ (vs)  $\text{cm}^{-1}$ .

*Preparation of Compound (4.7)*<sup>114</sup>

Compound **2.4**<sup>113</sup> (173 mg, 0.5 mmol), compound **4.6** (142 mg, 0.5 mmol), copper(II)sulfate (7 mg, 0.025 mmol), and sodium ascorbate (10 mg, 0.05 mmol) were dissolved in a mixture of acetone and water solution (1:1, 20 mL) and refluxed for overnight. The reaction mixture was then poured into ice cold water, and the mixture was extracted with ethyl acetate (3x30 mL).The combined ethyl acetate is dried over

magnesium sulphate, filtered, and evaporated to get the solid which is washed in methanol to get the pure compound **4.7**. (220 mg, 0.35mmol, 70%).

$^1\text{H}$  NMR (300 K,  $\text{CD}_3\text{CN}$ , 400MHz):  $\delta$  8.51 (d, 1H,  $J=9.3$  Hz,  $\text{CH}_{\text{py}}$ ), 8.27 (d, 2H,  $J=7.6$  Hz,  $\text{CH}_{\text{py}}$ ), 8.12-8.22 (m, 3H,  $\text{CH}_{\text{py}}$ ), 8.06-8.10 (m, 3H,  $\text{CH}_{\text{py}}$ ), 7.89 (s, 1H,  $\text{CH}_{\text{triazole}}$ ), 7.54 (s, 1H, NH), 5.31-5.35 (m, 1H,  $\text{CH}_{\text{Glu}}$ ), 4.87 (t, 1H,  $J=9.78$  Hz,  $\text{CH}_{\text{Glu}}$ ), 4.83-4.84 (m, 2H,  $\text{CH}_{\text{Glu}}$ ), 4.73 (d, 2H,  $J=5.87$  Hz,  $\text{CH}_2$ ), 4.57-4.60 (dd, 1H,  $J=2.85$  Hz, 14.68 Hz,  $\text{CH}_{\text{Glu}}$ ), 4.45-4.50 (dd, 1H,  $J=7.83$  Hz, 14.48 Hz,  $\text{CH}_{\text{Glu}}$ ), 4.16-4.21 (m, 1H,  $\text{CH}_{\text{Glu}}$ ), 3.09 (s, 3H,  $\text{CH}_3$ ), 2.02 (s, 3H,  $\text{CH}_3$ ), 1.94 (s, 3H,  $\text{CH}_3$ ), 1.92 (s, 3H,  $\text{CH}_3$ ).

$^{13}\text{C}$  NMR (300 K,  $\text{CD}_3\text{CN}$ , 400MHz):  $\delta$  169.99, 169.86, 169.69, 169.36, 145.39, 132.34, 131.41, 131.17, 130.70, 128.48, 128.36, 128.34, 127.17, 126.58, 125.85, 125.70, 124.98, 124.57, 124.42, 124.35, 124.01, 123.69, 96.64, 70.29, 69.61, 69.56, 67.86, 54.82, 50.25, 35.31, 20.01, 19.87, 19.79.

IR (ATR solid); 3285  $\nu_{\text{N-H}}$  (m), 2934  $\nu_{\text{C-H}}$  (w), 1744  $\nu_{\text{C=O}}$  (vs), 1633  $\nu_{\text{C=O}}$  (s) amide I, 1601  $\nu_{\text{C=O}}$  (w) amide II  $\text{cm}^{-1}$ .

## CHAPTER V

RHODAMINE BASED MOLECULAR PROBES FOR  $\text{Fe}^{3+}$  AND  $\text{Al}^{3+}$  IONS

## Introduction

In Part A (Chapters II, III, and IV), the pyrene motif was incorporated into the chemosensors for detection of  $\text{Zn}^{2+}$  and  $\text{Fe}^{3+}$  ions in  $\text{CH}_3\text{CN}$ . It was also shown that an ion induced self-assembly can occur in the presence of  $\text{Zn}^{2+}$  and chlorine atoms, the first self-assembled approach to simultaneous use of metal and anions. As mentioned, the pyrene based sensors have poor solubility in polar solvent such as  $\text{CH}_3\text{OH}$ ,  $\text{CH}_3\text{CH}_2\text{OH}$  and  $\text{H}_2\text{O}$  due to its hydrophobicity. In Chapter IV, a sugar group is introduced as a scaffold to overcome this solubility issues. Even though it improves the solubility ( $\text{EtOH}:\text{H}_2\text{O}$ ), it is found that a sensor still does not work in the polar solvents ( $\text{CH}_3\text{OH}$ ,  $\text{H}_2\text{O}$ ). All of the sensors performed best in organic medium only in particular  $\text{CH}_3\text{CN}$ . It is important to have the sensors work in the aqueous system for their biological and environmental applications. Another disadvantage of the pyrene based sensor is that its absorption and emission bands are in the UV-region with the excitation wavelength around 350 nm. This is not conducive for biological applications: the molecular probes should have high excitation wavelength in the region of visible to near infrared (> 500 nm) because of minimum photo-damage to biological samples, deep tissue penetration, and minimum interference from the background auto fluorescence of biomolecules in the living system.<sup>176</sup> Furthermore, pyrene based sensors are colorless and cannot be used as “naked eye” sensors (colorimetric sensors) for metal ions.

Among the various fluorophores, the rhodamine dyes have excellent photophysical properties as explained in Chapter I. Therefore, rhodamine was used as a

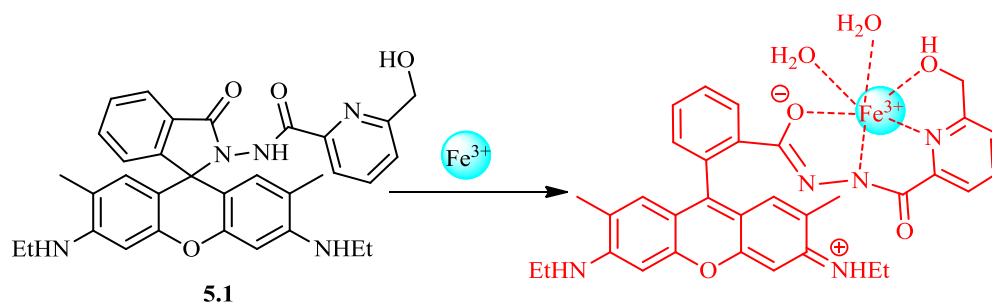
sensing motif for the second part of this dissertation. Rhodamine is less expensive and more soluble in the polar solvents than pyrene. Rhodamine based sensors are colorless and have low fluorescence. But they give red color and high fluorescence upon coordination of metal ions (Chapter I). Rhodamine based sensors act as an “On-Off” mechanism and can be used as naked eye detection (colorimetric sensors) for metal ions. This property is, in particular, important for metal ions that are known to quench the fluorescence intensity such as  $\text{Fe}^{3+}$ ,  $\text{Hg}^{2+}$ , and  $\text{Cu}^{2+}$  ions due to heavy metal effect and electron or energy transfer mechanism (See Chapter I).<sup>138, 177</sup> In fact, the chemosensors showing fluorescence “turn on” is more preferred than those showing “turn off” response on binding with the analytes.

Based on this spirolactam (colorless, non-fluorescent) to ring-open amide (pink, fluorescent) equilibrium of rhodamine, a number of rhodamine derivatives have been synthesized and utilized for the detection of biological relevant ions and bio-molecules.<sup>67, 69, 178</sup> However, there are still very few triazole based rhodamine system in the literature for the detection of metal ions.<sup>179-181</sup>

The importance of  $\text{Zn}^{2+}$  and  $\text{Fe}^{3+}$  ions is discussed in the introduction (Chapter I) and therefore will not be discussed further. However,  $\text{Al}^{3+}$  ion needs to be addressed at this point as this metal ion competes with the  $\text{Fe}^{3+}$  ion in the current system. The  $\text{Al}^{3+}$  ion plays a crucial role in various environment and biological processes.<sup>182, 183</sup> Aluminium is the third most abundant metal (approximately 8% by weight) in the earth’s crust after oxygen and silicon.<sup>182</sup> It is extensively used in modern life in the form of food additives, water treatment, and medicines (antiperspirants, deodorants, and antacids) which is often the source for human exposure to  $\text{Al}^{3+}$  ions.<sup>182</sup> However, excessive exposure to  $\text{Al}^{3+}$  ions

can damage certain human tissues and cells resulting in serious health problems including diseases such as Alzheimer's diseases,<sup>184</sup> Parkinson's diseases,<sup>185</sup> and osteoporosis.<sup>184, 186, 187</sup> Furthermore, acid rain increases the concentration of free  $\text{Al}^{3+}$  ions in the environment and surface water due to the high solubility of aluminium minerals at lower pH which is deadly to plant growth.<sup>180</sup> Therefore, the detection of  $\text{Al}^{3+}$  ion is also important in terms of both environmental and biological aspects.

Goswami and co-workers synthesized a CHEF (Chapter I) induced selective and sensitive "turn-on" sensor (**5.1**) for  $\text{Fe}^{3+}$  ion in an aqueous solution.<sup>188</sup> The compound itself does not show any color in a  $\text{CH}_3\text{CN-H}_2\text{O}$  (1:1, v/v, pH 7.2) indicating that the structure predominantly exists in spirolactam framework. The absorbance at 530 nm is enhanced upon addition of  $\text{Fe}^{3+}$  ion. The absorbance is increased by almost 116 times upon the addition of two equivalents of  $\text{Fe}^{3+}$  ions. The detection limit and association constant ( $K_{11}$ ) was calculated to be  $5.6 \times 10^{-7}$  M (31 ppb) and  $1.0 \times 10^4 \text{ M}^{-1}$ , respectively, for  $\text{Fe}^{3+}$  ion by UV-Vis method. The fluorescence of compound **5.1** exhibits a weak emission at 550 nm but showed a remarkable enhancement upon addition of  $\text{Fe}^{3+}$  ion. The fluorescence is increased by greater than 20 folds upon the addition of 0-1.0 equivalents of  $\text{Fe}^{3+}$  ion. The detection limit and association constant were calculated to be  $3.4 \times 10^{-8}$  M (2 ppb) and  $5.9 \times 10^5 \text{ M}^{-1}$ , respectively, for  $\text{Fe}^{3+}$  ion by fluorescence experiment. The effect of other metal ions such as  $\text{Cd}^{2+}$ ,  $\text{Co}^{2+}$ ,  $\text{Cu}^{2+}$ ,  $\text{Na}^+$ ,  $\text{K}^+$ ,  $\text{Fe}^{2+}$ ,  $\text{Mg}^{2+}$ ,  $\text{Ni}^{2+}$ ,  $\text{Mn}^{2+}$ ,  $\text{Zn}^{2+}$ ,  $\text{Hg}^{2+}$ ,  $\text{Pb}^{2+}$ ,  $\text{In}^{3+}$ ,  $\text{Cr}^{3+}$ , and  $\text{Al}^{3+}$  are also studied but did not show any significant enhancement in fluorescence and absorption. The coordination of compound **5.1** with  $\text{Fe}^{3+}$  ion centre was also studied by DFT calculations supporting the octahedral environment often found in  $\text{Fe}^{3+}$  ion coordination complexes (Scheme 5.1).



*Scheme 5.1.* Proposed binding mode of **5.1** with  $\text{Fe}^{3+}$  ion.<sup>188</sup>

The first part of the dissertation (Chapter II, III, and IV) has shown that the triazole group has been used to coordinate metal ions. However, the incorporation of this motif in rhodamine system is rare. One example is the compound **5.2** synthesized by Mandal et al. for the detection of  $\text{Fe}^{3+}$  ion.<sup>179</sup> Compound **5.3** is also prepared without triazole group as a “model” system (Figure 5.1). The model compound **5.3** formed a colored complex with both  $\text{Fe}^{3+}$  and  $\text{Cu}^{2+}$  ions in an aqueous buffer ( $\text{CH}_3\text{CN}$ : Tris HCl, 10 mM, 1:1, v/v, pH 7.4), while compound **5.2** showed a red color with only  $\text{Fe}^{3+}$  ion. Other metal ions such as  $\text{Li}^+$ ,  $\text{Na}^+$ ,  $\text{K}^+$ ,  $\text{Fe}^{2+}$ ,  $\text{Mg}^{2+}$ ,  $\text{Ca}^{2+}$ ,  $\text{Sr}^{2+}$ ,  $\text{Mn}^{2+}$ ,  $\text{Co}^{2+}$ ,  $\text{Hg}^{2+}$ ,  $\text{Pb}^{2+}$ ,  $\text{Co}^{2+}$ ,  $\text{Ni}^{2+}$ , and  $\text{Cr}^{3+}$  did not influence the absorption and emission. This shows that the incorporation of extra binding motif in the form of triazole group on **5.2** imparts the selectivity for  $\text{Fe}^{3+}$  ion over  $\text{Cu}^{2+}$  ion. The limit of detection for compound **5.2** was reported to be  $5 \times 10^{-8}$  M (3 ppb) and the association constant ( $K_{11}$ ), as calculated by Benesi-Hildebrand method is  $4.5 \times 10^4 \text{ M}^{-1}$ . The compound **5.2** was also used for imaging of live mouse fibroblast cells treated with  $\text{Fe}^{3+}$  ions. Fibroblast is the most common cells of connective tissues in animals. It synthesizes the extracellular matrix, collagen (structural protein), and structural framework for animal tissues.<sup>189</sup> Fibroblast cells treated with both **5.2** and  $\text{Fe}^{3+}$  ions displayed intense red fluorescence but without  $\text{Fe}^{3+}$  ions; compound **5.2** did not show any fluorescence. The compound is also found to be



non-cytotoxic up to 6  $\mu\text{M}$  as assessed by MTT assay. However, it should be noted that any studies towards  $\text{Al}^{3+}$  ions is missing, which is often the case in these systems, more often than not  $\text{Al}^{3+}$  ions responds in a similar way. Furthermore, molecular modeling is absent: therefore, exact coordination is questionable (Scheme 5.2).

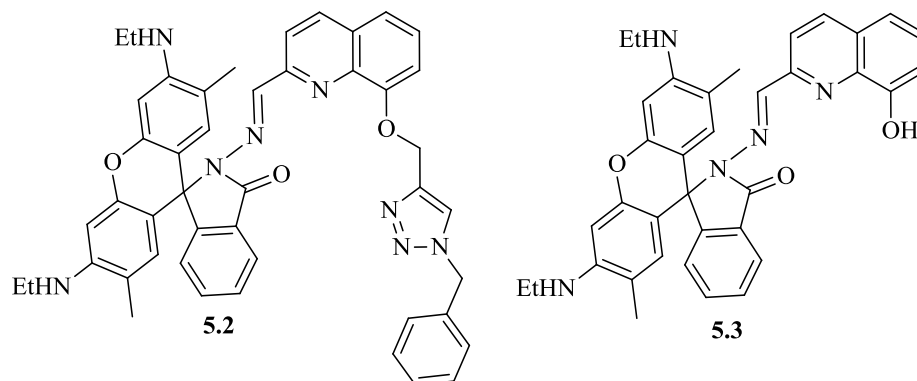
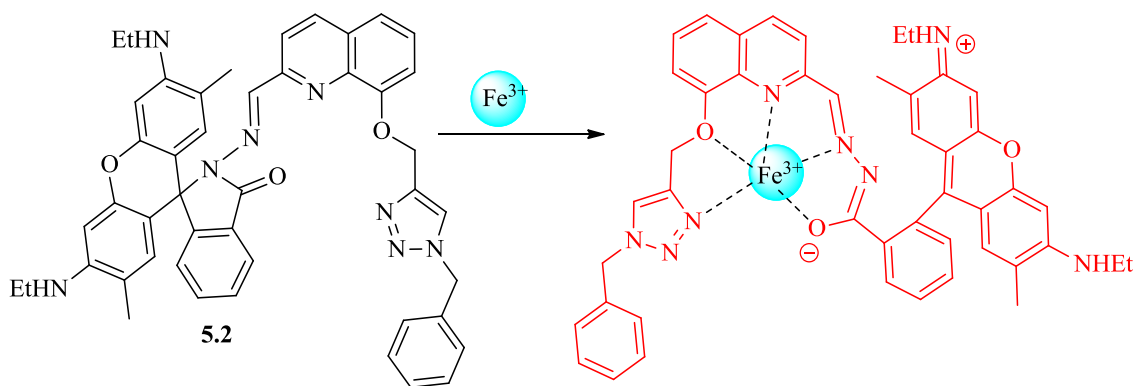


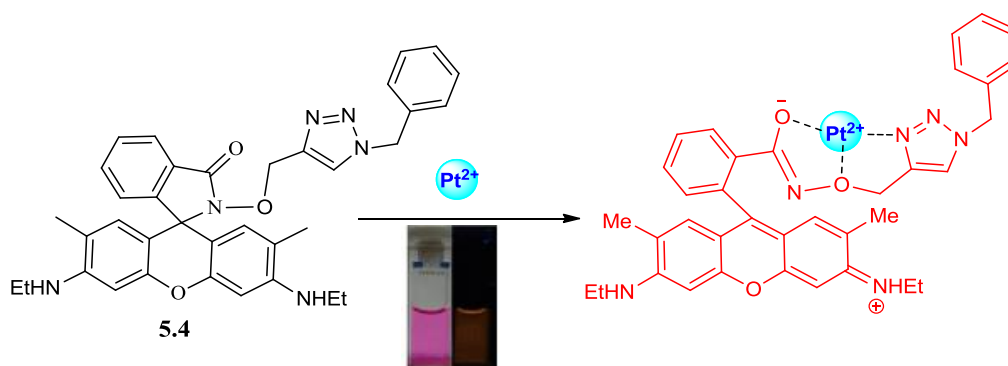
Figure 5.1. Structures for compounds **5.2** and **5.3** synthesized using rhodamine 6G.



Scheme 5.2. Proposed binding mode of  $\text{Fe}^{3+}$  ion by compound **5.2**.<sup>179</sup>

Another similar probe (**5.4**) was synthesized by Tae et al. for the detection of  $\text{Pt}^{2+}$  ion by a click reaction of alkyne derivative of rhodamine 6G (prepared from rhodamine hydroxamic acid) with benzyl azide.<sup>190</sup> Compound **5.4** has a dual binding unit composed of a hydroxamate and a triazole group for coordination of metal ion. Compound **5.4** is colorless and has no fluorescence in  $\text{H}_2\text{O}$  (1% DMSO, v/v). Upon addition of five

equivalents of  $\text{Pt}^{2+}$  ion, **5.4** gives a strong fluorescence with pink-red color. Compound **5.4** can monitor  $\text{Pt}^{2+}$  ion in the pH range of 5-9. Other metal ion such as  $\text{Li}^+$ ,  $\text{Na}^+$ ,  $\text{K}^+$ ,  $\text{Ag}^+$ ,  $\text{Fe}^{2+}$ ,  $\text{Mg}^{2+}$ ,  $\text{Ca}^{2+}$ ,  $\text{Ba}^{2+}$ ,  $\text{Pd}^{2+}$ ,  $\text{Cd}^{2+}$ ,  $\text{Sr}^{2+}$ ,  $\text{Mn}^{2+}$ ,  $\text{Co}^{2+}$ ,  $\text{Hg}^{2+}$ ,  $\text{Cu}^{2+}$ ,  $\text{Zn}^{2+}$ ,  $\text{Pb}^{2+}$ ,  $\text{Co}^{2+}$ ,  $\text{Fe}^{3+}$ ,  $\text{Al}^{3+}$ , and  $\text{Cr}^{3+}$  have no effect on both fluorescence and absorption. The competitive metal ion  $\text{Pd}^{2+}$  ion show very little fluorescence intensity changes but still induces color change indicating  $\text{Pd}^{2+}$  ion quenches the expressed fluorescence intensity. The binding constant ( $K_{11}$ ), calculated based on fluorescence titration, is  $1.6 \times 10^5 \text{ M}^{-1}$ . The fluorescence titration of  $\text{Pt}^{2+}$  ion with  $0.5 \mu\text{M}$  of **5.4** demonstrates the detection limit is  $125 \text{ nM}$  (24 ppb). Compound **5.4** was also tested for detecting *cis*-platin to demonstrate its potential application. It was found that a  $\mu\text{M}$  concentration of *cis*-platin in aqueous solution could be monitored (Scheme 5.3). The paper lacked detail in regard to the coordination environment of the metal ion. They did not report any  $^{195}\text{Pt}$  NMR nor report any modelling studies to support their predicted binding environment.



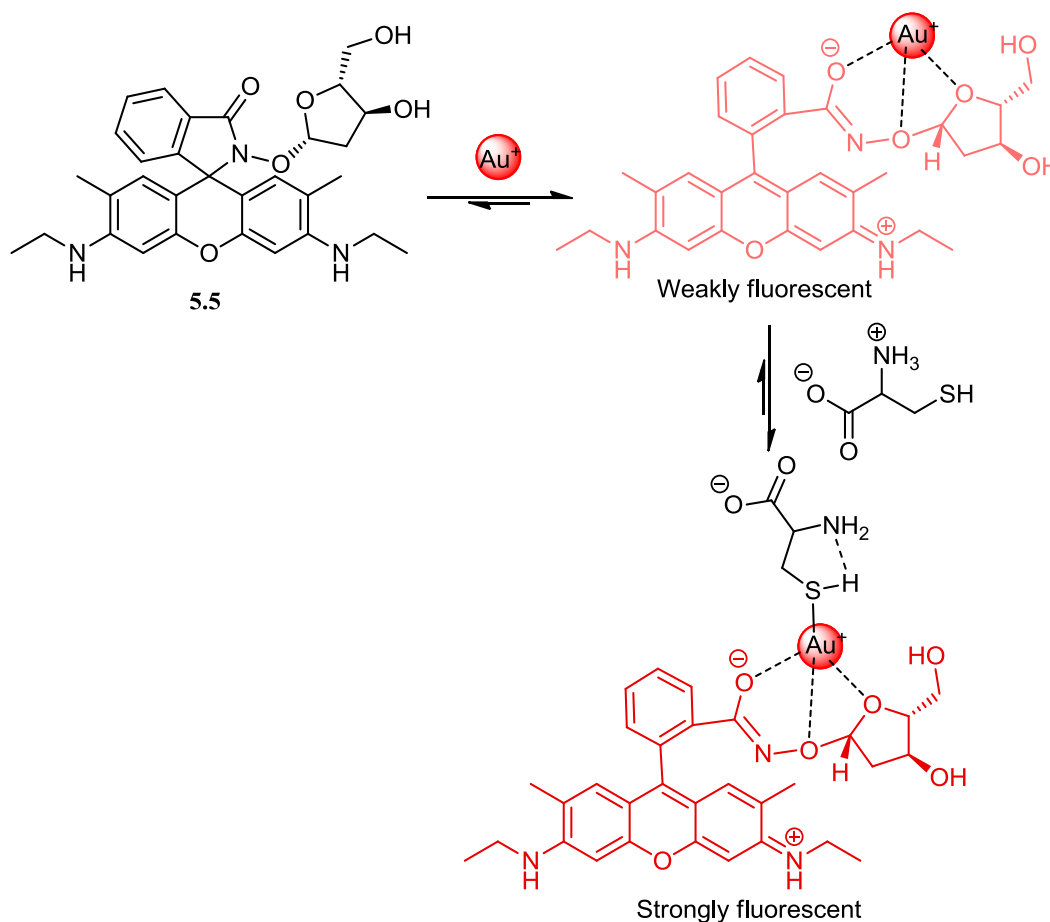
**Scheme 5.3.** Proposed structure for binding  $\text{Pt}^{2+}$  ion by rhodamine 6G based compound **5.4**.<sup>190</sup>

The synthesis of sugar-based chemosensors is increasing in recent years.<sup>154, 191, 192</sup>

The introduction of a sugar groups in chemosensors improve both water solubility and bio-compatibility as explained in Chapter IV. These features make the sugar-based probes interesting candidates for the practical detection of metal ions in both biology and

environmental applications. There are only a few examples of rhodamine sugar system: some recent examples will be highlighted.<sup>191, 193, 194</sup>

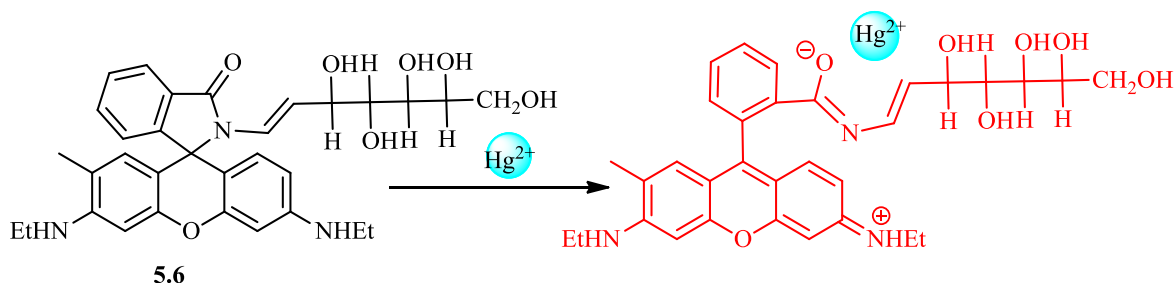
Tae et al. report a turn-on “chemosensing ensemble” for the detection of thio-containing amino acids (cysteine and homocysteine) based on a rhodamine– furanose sugar based probe.<sup>195</sup> The chemosensing ensemble is a method where an indicator molecule is combined with other components such as a receptor or metal ion through non-covalent interactions.<sup>196, 197</sup> Compound **5.5** shows neither color nor fluorescence in water (1% CH<sub>3</sub>OH) but showed enhancement in fluorescence upon addition of Au<sup>+</sup> ion. The [Au (**5.5**)]<sup>+</sup> complex is then used as a chemosensing ensemble for detection of cysteine and homocysteine. The fluorescence intensity induced by [Au (**5.5**)]<sup>+</sup> is further increased by the addition of cysteine. Among the various metal ions tested, only [Au (**5.5**)]<sup>+</sup>-cysteine showed a strong fluorescence enhancement ( $\lambda_{\text{ex}}=500$  nm,  $\lambda_{\text{em}}=560$  nm). This implies that [Au (**5.5**)]<sup>+</sup> complex acts as chemosensing ensemble for selective sensing of cysteine. Among the various amino acids, only cysteine and homocysteine showed an enhancement of fluorescence of [Au (**5.5**)]<sup>+</sup> complex. The recognition of cysteine and homocysteine is attributed to the binding of the thiol of cysteine to the Au<sup>+</sup>-bound probe. The binding constant in H<sub>2</sub>O (1% CH<sub>3</sub>OH) from the UV-Vis titration is  $K_{11}= 6.7 \times 10^3$  with a limit of detection ~100 nM cysteine in aqueous solution (Scheme 5.4).



*Scheme 5.4.* A proposed structure of the ternary complex between  $[\text{Au}(\mathbf{5.5})]^+$  and cysteine.<sup>195</sup>

Another rhodamine sugar system was developed by Duan and co-workers who synthesized a water-compatible fluorescent molecular probe (**5.6**) for selective detection of  $\text{Hg}^{2+}$  ion in natural water and cell imaging.<sup>198</sup> Detection of  $\text{Hg}^{2+}$  ion is important as it is considered one of the most toxic and widespread pollutant. Specifically, methylmercury, yielded from the microbial biomethylation of  $\text{Hg}^{2+}$  ion is known to cause brain damage and other chronic diseases.<sup>199</sup> Compound **5.6** exhibits a weak fluorescence band at about 550 nm in aqueous solution ( $\lambda_{\text{ex}}=500$  nm). The fluorescence was increased significantly upon the addition of  $\text{Hg}^{2+}$  ion. A Benesi-Hildbrand analysis establishes a 1:1 stoichiometry for the  $[\text{Hg}(\mathbf{5.6})]^{2+}$  with an association constant calculated as  $5.4 \times 10^5 \text{ M}^{-1}$

<sup>1</sup>The limit of detection of compound **5.6** for  $\text{Hg}^{2+}$  ion was calculated to be one ppb. The UV-Vis titration showed that **5.6** exhibits a weak absorbance at 525 nm but increased with a red shift to 535 nm upon titration of  $\text{Hg}^{2+}$  ion with color change from colorless to pink. In both UV-Vis and fluorescence, no significant spectral changes of **5.6** were observed in the presence of metal ions such as  $\text{Na}^+$ ,  $\text{K}^+$ ,  $\text{Ag}^+$ ,  $\text{Mg}^{2+}$ ,  $\text{Ca}^{2+}$ ,  $\text{Mn}^{2+}$ ,  $\text{Fe}^{2+}$ ,  $\text{Co}^{2+}$ ,  $\text{Ni}^{2+}$ ,  $\text{Cu}^{2+}$ ,  $\text{Zn}^{2+}$ ,  $\text{Cd}^{2+}$ , and  $\text{Pb}^{2+}$ . The coordination of compound **5.6** with  $\text{Hg}^{2+}$  ion was also studied by  $^1\text{H}$  NMR in  $\text{DMSO}-d_6$ . The signal of amine (NH) group at  $\delta$  5.73 ppm is not seen in the  $[\text{Hg}(\mathbf{5.6})]^{2+}$  coordination complex suggesting the formation of delocalized xanthenone ring upon coordination of  $\text{Hg}^{2+}$  ion. Furthermore, the OH group adjacent to the imine functionality is shifted in the downfield direction by approximate  $\delta$  0.13 ppm suggesting this the oxygen atom of OH group is coordinated to the  $\text{Hg}^{2+}$  ion. This makes hydrogen atom becomes more acidic as the coordination to the  $\text{Hg}^{2+}$  ion pulls the electron density away from the oxygen atom. The molecular probe **5.6** was also used to image  $\text{Hg}^{2+}$  ions in HeLa cells. The HeLa cells treated with compound **5.6** did not show any fluorescence in confocal microscopy. However, the cells supplemented with  $\text{Hg}(\text{NO}_3)_2$  showed a significant increase in fluorescence (Scheme 5.5). However, they do not carry out any other experiments to confirm the binding mode of  $\text{Hg}^{2+}$  ion.



Scheme 5.5. Proposed structure for binding  $\text{Hg}^{2+}$  ion by compound **5.6**.<sup>198</sup>

In summary, rhodamine based sensors have been used as “Off –On” sensors for detection of metal ions and anions as discussed above. In particular, this signaling mechanism is useful for the metal ions such as  $\text{Cu}^{2+}$ ,  $\text{Fe}^{3+}$ , and  $\text{Hg}^{2+}$  ions which are known to quench the fluorescence. Rhodamine based sensors have absorption and emission in the visible region which make them useful for “naked eye” probes and some have been used for in vivo studies.

Here, this dissertation will report the synthesis of rhodamine based sensors which contain triazole functional groups as coordination sites to the metal ion centre. These were attached to a benzene, pyridine, and sugar scaffolds, respectively. The rhodamine sensor which contains only the benzene ring is prepared as a model to investigate the potential binding motifs with pyridine and sugar groups as they also have nitrogen and oxygen.

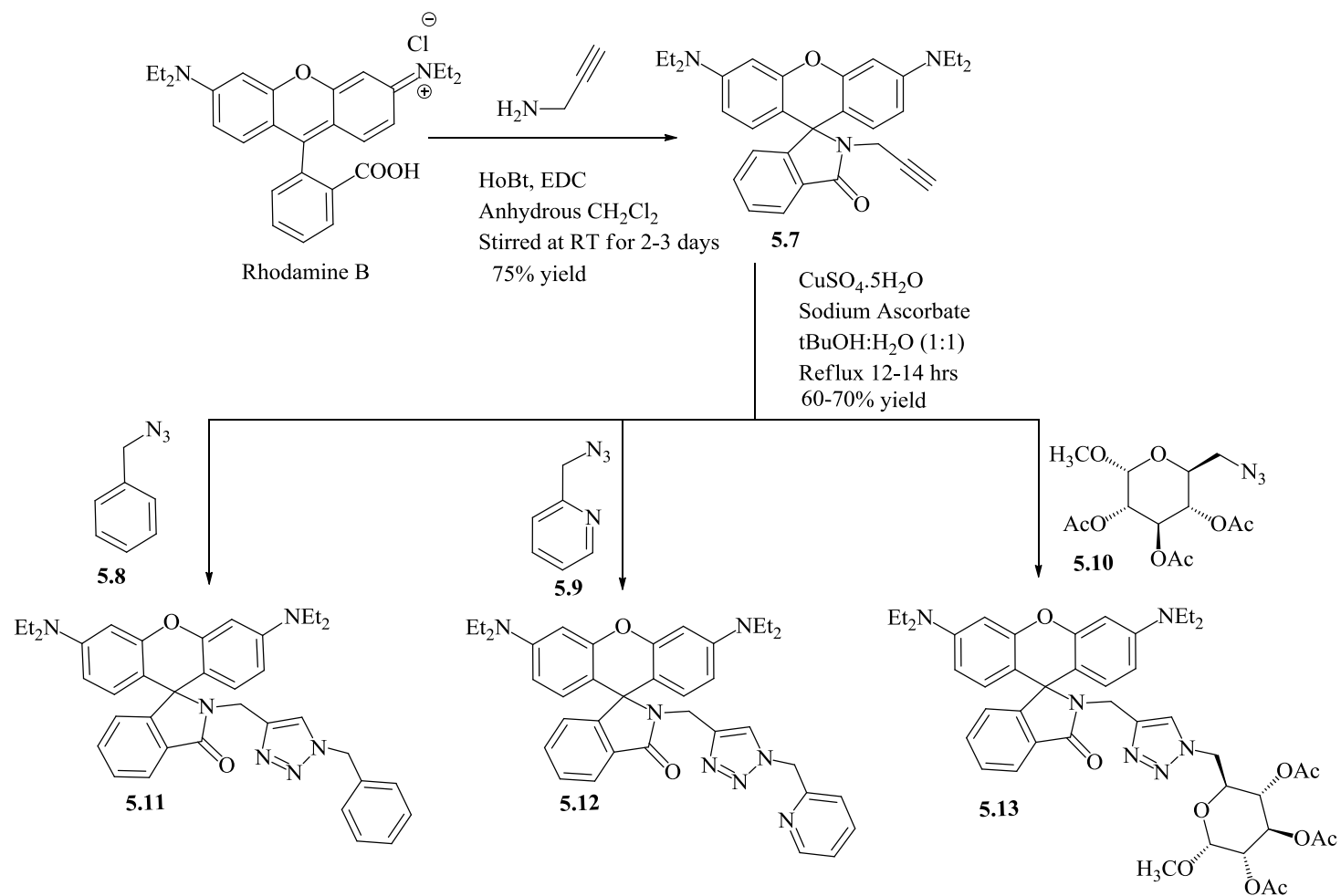
It is expected that both UV-Vis and fluorescence of the compounds are low but should be increased with color change upon binding with target metal ions as the metal ions triggered the opening of spirolactam ring. It is proposed that metal ions will be coordinated by the oxygen and nitrogen atoms of lactam and triazole groups, respectively, which act like the catechol motifs.

#### Synthesis of Molecular Probes **5.11**, **5.12**, and **5.13**.

As discussed in the Introduction, three compounds are synthesized using rhodamine as sensing motifs and triazole as coordination sites for metal ions with benzene, pyridine, and sugar groups as scaffolds.

The commercially available rhodamine B is first converted into 3',6'-bis(diethylamino)-2-(prop-2-ynyl)spiro [isoindoline-1,9'-xanthen]-3-one (**5.7**) by

coupling propargylamine using standard peptide based reagents for example HoBt (1-hydroxy benzotriazole) and EDC [1-ethyl-3-(3-diethylaminopropyl) carbodiimide] in  $\text{CH}_2\text{Cl}_2$ . A pink white solid was obtained during the reaction which was filtered and purified by silica gel column chromatography using 2:8 (ethyl acetate: hexane) to form **5.7** as pure white solid in 80% yield. The colorless solid indicates that **5.7** is in spiro lactam conformation. Compound **5.7** was confirmed by a hydrogen atom attached to the alkyne seen at  $\delta$  1.75 ppm ( $\text{CDCl}_3$ ). The compound is further confirmed by the stretching bands at  $3299\text{ cm}^{-1}$  assigned to the  $\text{C}\equiv\text{CH}$ ,  $2070\text{ cm}^{-1}$  for  $\text{C}\equiv\text{C}$  and  $1693\text{ cm}^{-1}$  for a carbonyl group of lactam ring in the IR spectrum. The compound **5.7** was fully characterized and agreed with the literature value.<sup>200</sup> Picolyl azide (**5.9**) was prepared from picolyl hydrochloride by reacting with sodium azide in the presence of 18-Crown-6 and TBAI as catalysts and DIPEA (N, N-diisopropylethylamine) as a base in DMF in 80% yield. The azide (**5.9**) was confirmed by its characteristic strong stretching signal at  $2089\text{ cm}^{-1}$  for an azide group in IR spectrum, and its spectroscopic data ( $^1\text{H}$  NMR and IR) also agreed with the published procedure.<sup>201</sup> Finally, **5.7** was then reacted with benzyl azide (**5.8**) or picolyl azide (**5.9**) or methyl 2, 3, 4-tri-*O*-acetyl-6-azido-6-deoxy- $\alpha$ -D-glucopyranoside (**5.10**) *via* the click reaction.<sup>190, 200</sup> Pure products were obtained in all three cases by column chromatography of the ethyl acetate extracts of the reaction mixture. The product was confirmed by the signal of a triazole proton at  $\delta$  7.08-7.15 ppm ( $\text{CDCl}_3$ ). The compounds were fully characterized by  $^1\text{H}$  NMR,  $^{13}\text{C}$  NMR, IR, ESI mass spectrum, elemental analysis, and by X-ray crystallography (Scheme 5.6).



Scheme 5.6. Synthesis of molecular probes **5.11**, **5.12**, and **5.13**.



X-ray Crystallographic Study of Molecular Probes **5.11** and **5.12**

The X-ray quality crystals for both compounds were grown by slow evaporation of their saturated solution in ethyl acetate. In both compounds, a xanthene ring is orthogonal to the spiro-lactam moiety. There is  $\pi$ - $\pi$  interaction between the triazole and xanthene ring of the same molecule. A weak hydrogen bond is seen between the hydrogen of a benzene ring attached to spiro-lactame moiety with the pyridine ring of another molecule (Figure 5.2).

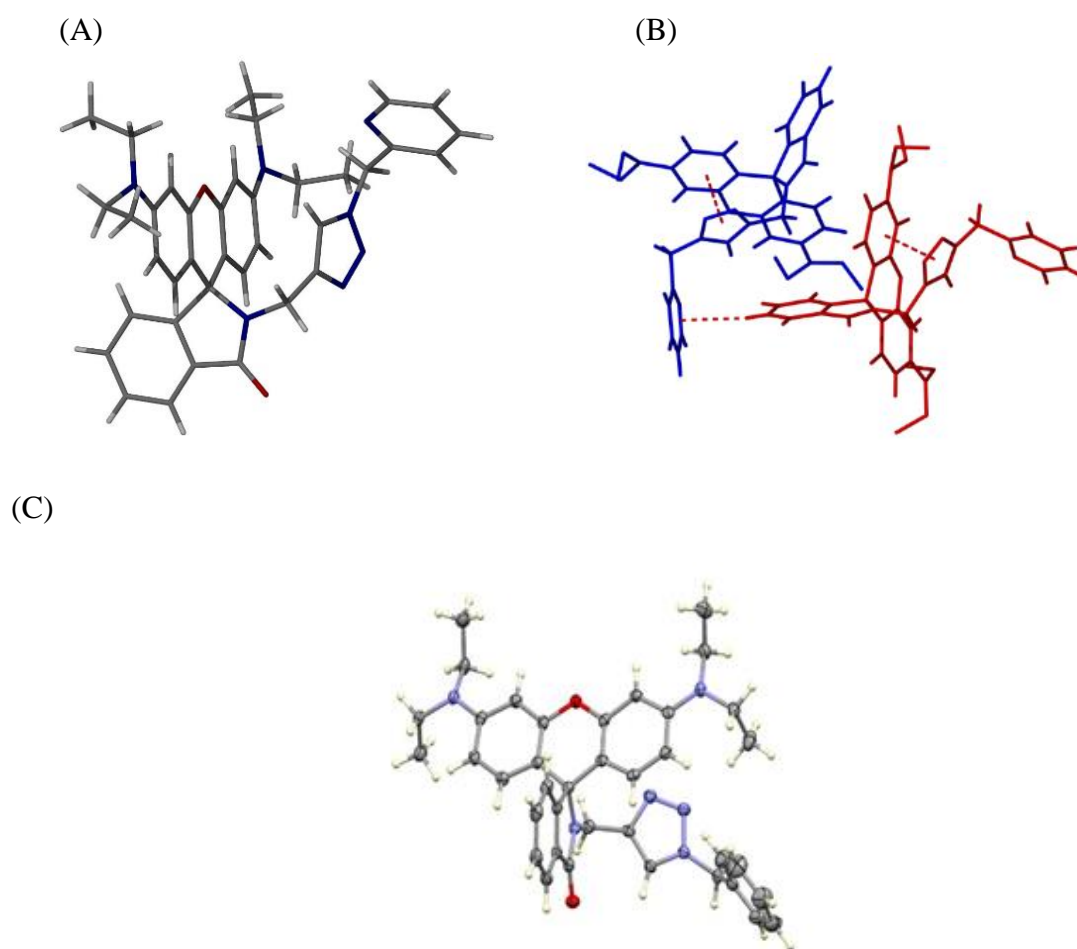


*Figure 5.2.* X-ray crystal structures of (A) compounds **5.12** (B) its crystal packing and (C) crystal structure of compound **5.11**.

### Job's Plot Studies of Molecular Probes **5.12** and **5.13**

The stoichiometry of a binding of compound **5.12** and **5.13** with  $\text{Fe}(\text{ClO}_4)_3$  or  $\text{Al}(\text{ClO}_4)_3$  is confirmed by a Job's plot analysis. Each of host (**5.12** or **5.13**) and guest ( $\text{Fe}(\text{ClO}_4)_3$  or  $\text{Al}(\text{ClO}_4)_3$ ) solution is prepared of  $1 \times 10^{-4}$  M in EtOH:H<sub>2</sub>O (1:1). Both solutions are then mixed in different ratios to get the solutions having mole fractions from zero to one, each of which have same volume and same total molar concentration i.e.,  $1 \times 10^{-4}$  M. The fluorescence is measured for each mole fraction, and the fluorescence intensity at 577 nm was plotted against the mole fraction of  $\text{Fe}(\text{ClO}_4)_3$  or  $\text{Al}(\text{ClO}_4)_3$ . The apex of the curve lies at 0.5 mole fraction in both cases which corresponds to a 1:1 (Ligand: metal) stoichiometry. Figure 5.3 and 5.4 show the Job's plot of compound **5.12** with  $\text{Fe}(\text{ClO}_4)_3$  and  $\text{Al}(\text{ClO}_4)_3$ , respectively.

One important point during Job's plot studies is that lower mole fractions (from 0 to 0.3) normally give less fluorescence or absorbance than expected as seen in Figure 5.4. It could be due to the fact that the low amount of metal ions present in these mole fractions cannot drive the equilibrium towards the complex side or the system is kinetically slow.

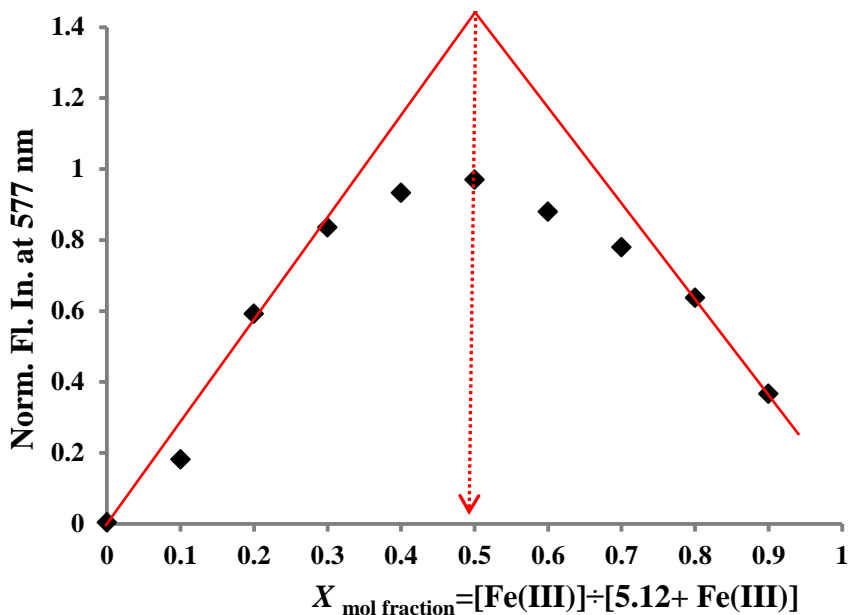


Figure 5.3. Job's plot of compound **5.12** with  $\text{Fe}(\text{ClO}_4)_3$  obtained by fluorescence measurements in 1:1 (EtOH :H<sub>2</sub>O). The total concentration of compound **5.12** and  $\text{Fe}(\text{ClO}_4)_3$  is 100  $\mu\text{M}$  where  $X \approx 0.55$  (1:1 ligand:metal ratio). The red lines are for visual interpretation only.

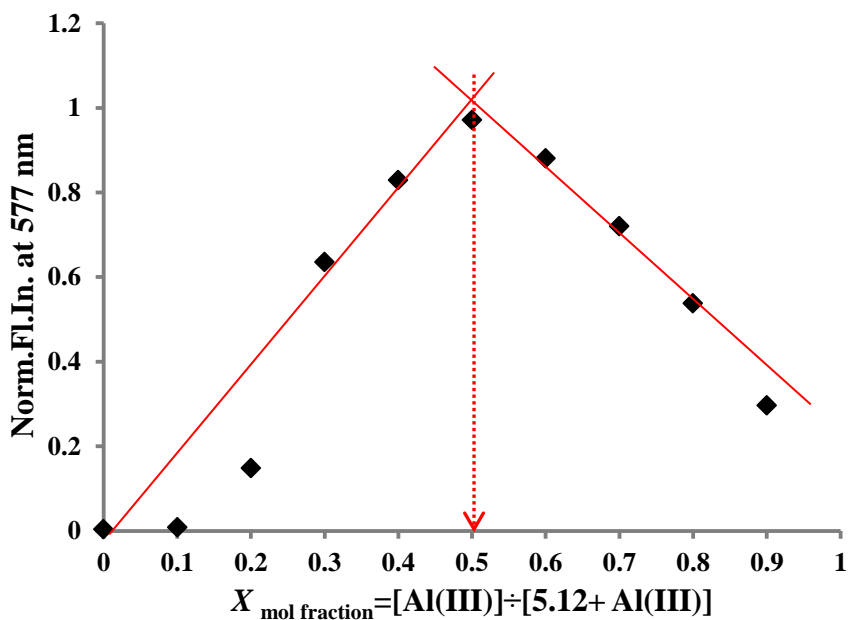


Figure 5.4. Job's plot of compound **5.12** with  $\text{Al}(\text{ClO}_4)_3$  obtained by fluorescence measurements in 1:1 (EtOH :H<sub>2</sub>O). The total concentration of compound **5.12** and  $\text{Al}(\text{ClO}_4)_3$  is 100  $\mu\text{M}$  where  $X \approx 0.55$  (1:1 ligand:metal ratio). The red lines are for visual interpretation only.

### pH Studies on the Molecular Probes **5.12** and **5.13**

The effect of pH on a rhodamine system is important: this was briefly mentioned in chapter I (Figures 1.9 and 1.10). Most of the sensors based on rhodamine B have a spirolactam ring conformation which can be opened with the addition of acid producing a red color and are highly fluorescent. Therefore, it is important to know the pH window whereby these molecular probes will function towards metal binding and not produce a false positive due to any acid in the system which is also known to ring open. It is important to have the sensor work in the physiologic pH range for its environmental and biological application.

Therefore, the effect of pH on the fluorescence response of the sensor **5.12** or **5.13** to  $\text{Fe}^{3+}$  and  $\text{Al}^{3+}$  ions was initially evaluated in 1:1 (EtOH:H<sub>2</sub>O). There is almost no change in a fluorescence emission of free sensors between pH 4 and 10 in the absence of metal ions. This suggests that a spirolactam ring is intact and does not open in the pH range of 4-10. However, a significant fluorescence enhancement was observed upon the addition of  $\text{Fe}^{3+}$  and  $\text{Al}^{3+}$  ions in the range of pH 4–10, which is attributed to an opening of the spirolactam ring. This data demonstrates that compounds **5.12** or **5.13** can act as a fluorescent probe for  $\text{Fe}^{3+}$  and  $\text{Al}^{3+}$  ions under physiological pH conditions. Figure 5.5 shows the effect of pH on the compound **5.12** after an addition of  $\text{Fe}(\text{ClO}_4)_3$  and  $\text{Al}(\text{ClO}_4)_3$ .

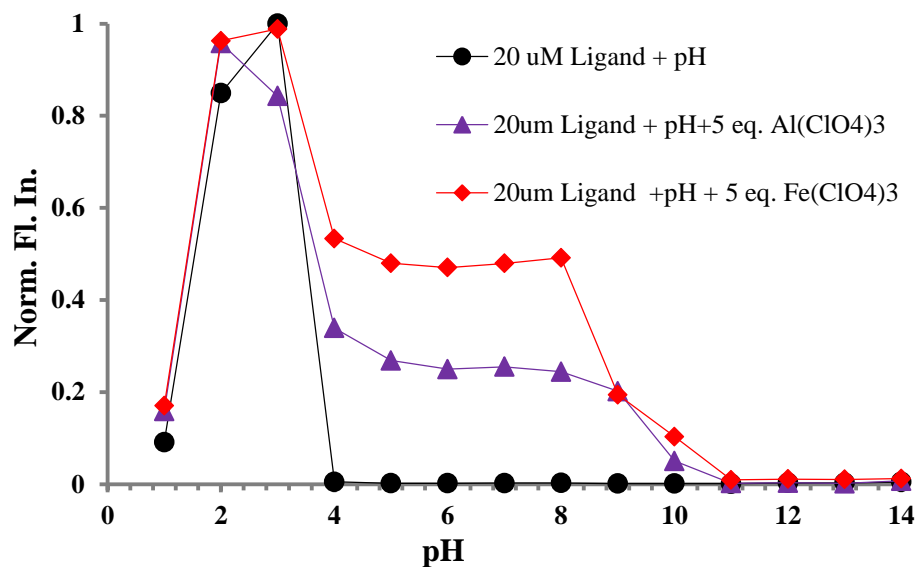


Figure 5.5. pH profile of compound **5.12** (20  $\mu\text{M}$ ) with pH from 1-14 (bottom black circle) and upon the addition of five equivalents of  $\text{Fe}^{3+}$  ions (upper red diamond) and  $\text{Al}^{3+}$  ions (middle purple triangle) in  $\text{EtOH}:\text{H}_2\text{O}$ .

#### Optical Studies of the Molecular Probes **5.11**, **5.12**, and **5.13**

##### *UV-Vis spectroscopy*

The binding behavior of compounds **5.11**, **5.12**, and **5.13** towards various metal ions was first studied by UV-Vis spectroscopy. Rhodamine based sensors are colorless compounds but gives a red/pink color upon the addition of suitable metal ions (Chapter D). Therefore it is expected that the compounds **5.11**, **5.12**, and **5.13** should have a low absorption band, but the intensity is increased upon binding with target metal ions.

Hence, an UV-Vis study is carried out to see whether a target metal ion can be detected *via* a colorimetric method.

Unfortunately, compounds **5.11**, **5.12**, and **5.13** are not 100% soluble in aqueous system. Therefore, mixture of organic solvent and water is used as solvent system for the UV-Vis studies. The 1:1 ratio of  $\text{EtOH}$  and  $\text{H}_2\text{O}$  is selected as the solvent system as the increase in the amount of water more than 1:1 ratio may precipitate the compounds. The

pH of 1:1 (EtOH:H<sub>2</sub>O) is 7.1 which is in the range of pH 4-10 that the compounds can work based on the studies of a pH effect.

The absorption spectra of all compounds **5.11**, **5.12**, and **5.13** (100  $\mu$ M) showed no characteristic absorption bands of rhodamine moiety at 550 nm in an aqueous ethanol solution of 1:1 (EtOH:H<sub>2</sub>O) at pH 7.1 suggesting that all three compounds **5.11**, **5.12**, and **5.13** are in ring closed forms. Upon addition of one equivalent of Fe<sup>3+</sup> or Al<sup>3+</sup> ions (500  $\mu$ L of 200  $\mu$ M) to 100  $\mu$ M concentration of **5.11** or **5.12** or **5.13**, a new absorption band appears at 550 nm (colorless to pink). This can be explained by the formation of the ring opened amide tautomer as a result of Fe<sup>3+</sup> or Al<sup>3+</sup> ion bindings. The intensity of an absorption band due to Fe<sup>3+</sup> ion is ~1.5 times higher than Al<sup>3+</sup> ion. However, the addition of other metal ions such as Na<sup>+</sup>, K<sup>+</sup>, Ca<sup>2+</sup>, Mg<sup>2+</sup>, Cr<sup>3+</sup>, Fe<sup>3+</sup>, Fe<sup>2+</sup>, Zn<sup>2+</sup>, Cd<sup>2+</sup>, Co<sup>2+</sup>, and Hg<sup>2+</sup> did not alter the absorption spectrum of compounds suggesting that compounds **5.11** or **5.12** or **5.13** could serve as a “naked-eye” chemosensors that can response selective to Fe<sup>3+</sup> or Al<sup>3+</sup> ions in an aqueous ethanol solution. For example, Figure 5.6 shows the selectivity of compound **5.12** with various metals. The comparison for selectivity of compounds **5.11**, **5.12**, and **5.13** to Fe<sup>3+</sup> and Al<sup>3+</sup> ions is shown in Figure 5.7. The model compound (**5.11**) showed less intense absorption bands in comparison to compound **5.12** and **5.13** for both Al<sup>3+</sup> and Fe<sup>3+</sup> ions. Compound **5.13** showed the most intense band for Fe<sup>3+</sup> ion while compound **5.12** showed for Al<sup>3+</sup> ions. This is reasonable considering the presence of sugar groups (acetyl and oxygen atom of ring) and nitrogen atoms (pyridine ring) in compounds **5.12** and **5.13**. This is further supported by the fact that the intensity of the absorption band due to the addition of Al<sup>3+</sup> ion is almost half the intensity of the Fe<sup>3+</sup> ion study for compound **5.13**.

Therefore, it could be possible that the nitrogen atom in the pyridine ring or the oxygen atom in the sugar (acetyl, ring oxygen atoms) might be involved in the coordination of metal ions or at least impart the selectivity for the metal ions.

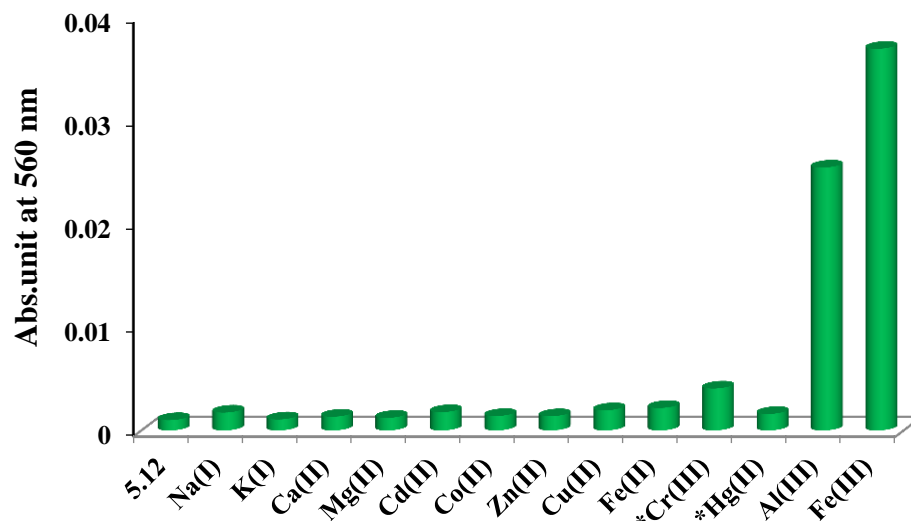


Figure 5.6. UV-Vis selectivity chart of compound **5.12** (100  $\mu\text{M}$ ) in 1:1 (EtOH:H<sub>2</sub>O), pH=7.1, upon the addition of one equivalent of metal ions as their ClO<sub>4</sub><sup>-</sup> salts (\*Cl<sup>-</sup> salt).

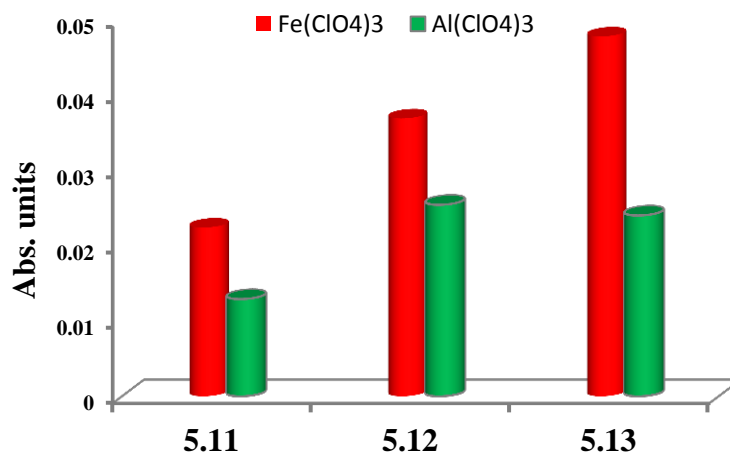


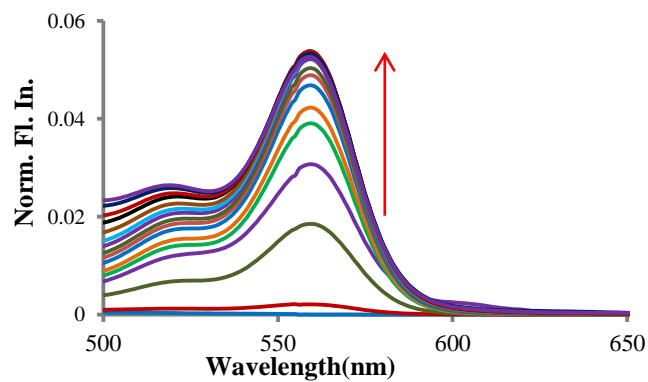
Figure 5.7. Comparison of UV-Vis selectivity chart of compound **5.11** (benzene), **5.12** (pyridine) and **5.13** (sugar) (10  $\mu\text{M}$ ) in 1:1 (EtOH:H<sub>2</sub>O), pH=7.1, upon the addition of one equivalent of Fe<sup>3+</sup> and Al<sup>3+</sup> ions as their ClO<sub>4</sub><sup>-</sup> salts.

UV-Vis titration of compounds **5.11** or **5.12** or **5.13** (50  $\mu\text{M}$ ) was carried out with Fe(ClO<sub>4</sub>)<sub>3</sub> and Al(ClO<sub>4</sub>)<sub>3</sub> to investigate the further interaction. Figures 5.8 and 5.9 shows

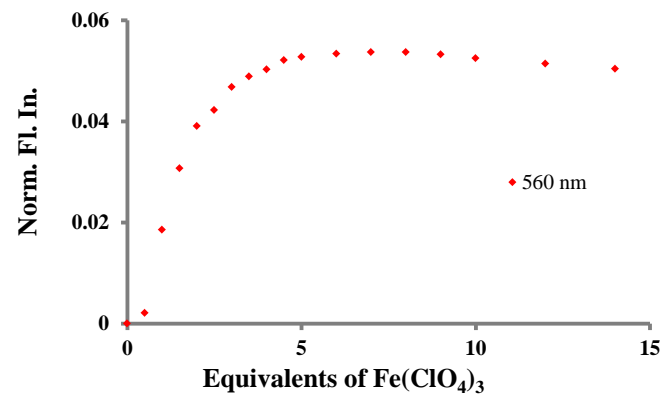
the UV-Vis titration of compounds **5.12** with  $\text{Fe}(\text{ClO}_4)_3$  and  $\text{Al}(\text{ClO}_4)_3$ , respectively. The UV-Vis absorption is increased with a maximum at 560 nm on addition of  $\text{Fe}(\text{ClO}_4)_3$  or  $\text{Al}(\text{ClO}_4)_3$ . The absorbance bands plateaued after five and 15 equivalents for  $\text{Fe}^{3+}$  and  $\text{Al}^{3+}$  ions, respectively. The quick plateaued of the absorbance band by  $\text{Fe}^{3+}$  ions could possibly be due to the quenching properties of  $\text{Fe}^{3+}$  ions. Data obtained during UV-Vis titration is analysed using the Benesi-Hildebrand double reciprocal plot and HypSpec program.<sup>116</sup> The binding constants calculated by these two methods are shown in Table 5.1 and are in good agreement. Both methods showed that compounds **5.12** and **5.13** are binding with  $\text{Fe}^{3+}$  or  $\text{Al}^{3+}$  ion in 1:1 stoichiometry (Figures 5.3 and 5.4).



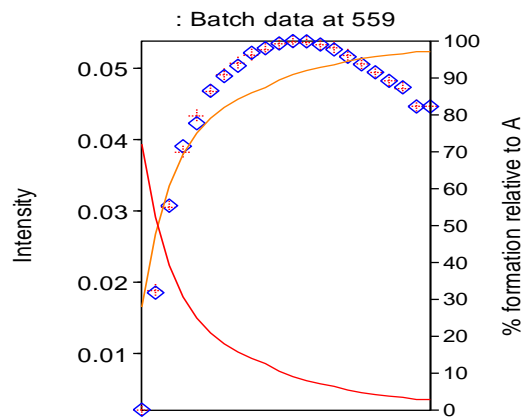
(A)



(B)



(C)



(D)

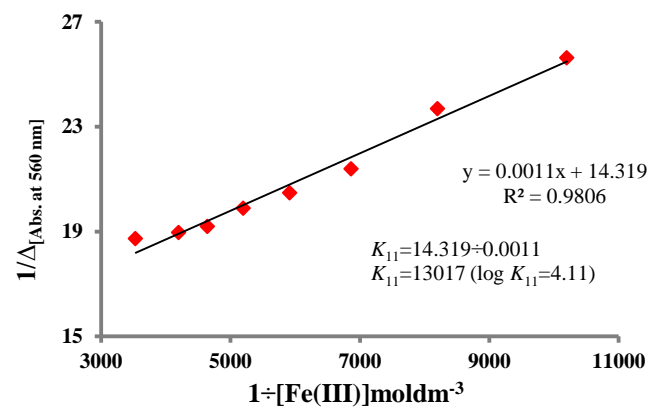


Figure 5.8. (A) UV-Vis spectrum of compound **5.12** (50  $\mu\text{M}$ ) upon addition of  $\text{Fe}(\text{ClO}_4)_3$ , (B) its binding isotherm in 1:1 (EtOH:H<sub>2</sub>O) pH=7.1, (C) Binding isotherm for HypSpec program,<sup>116</sup> and (D) Benesi-Hildbrand plot.

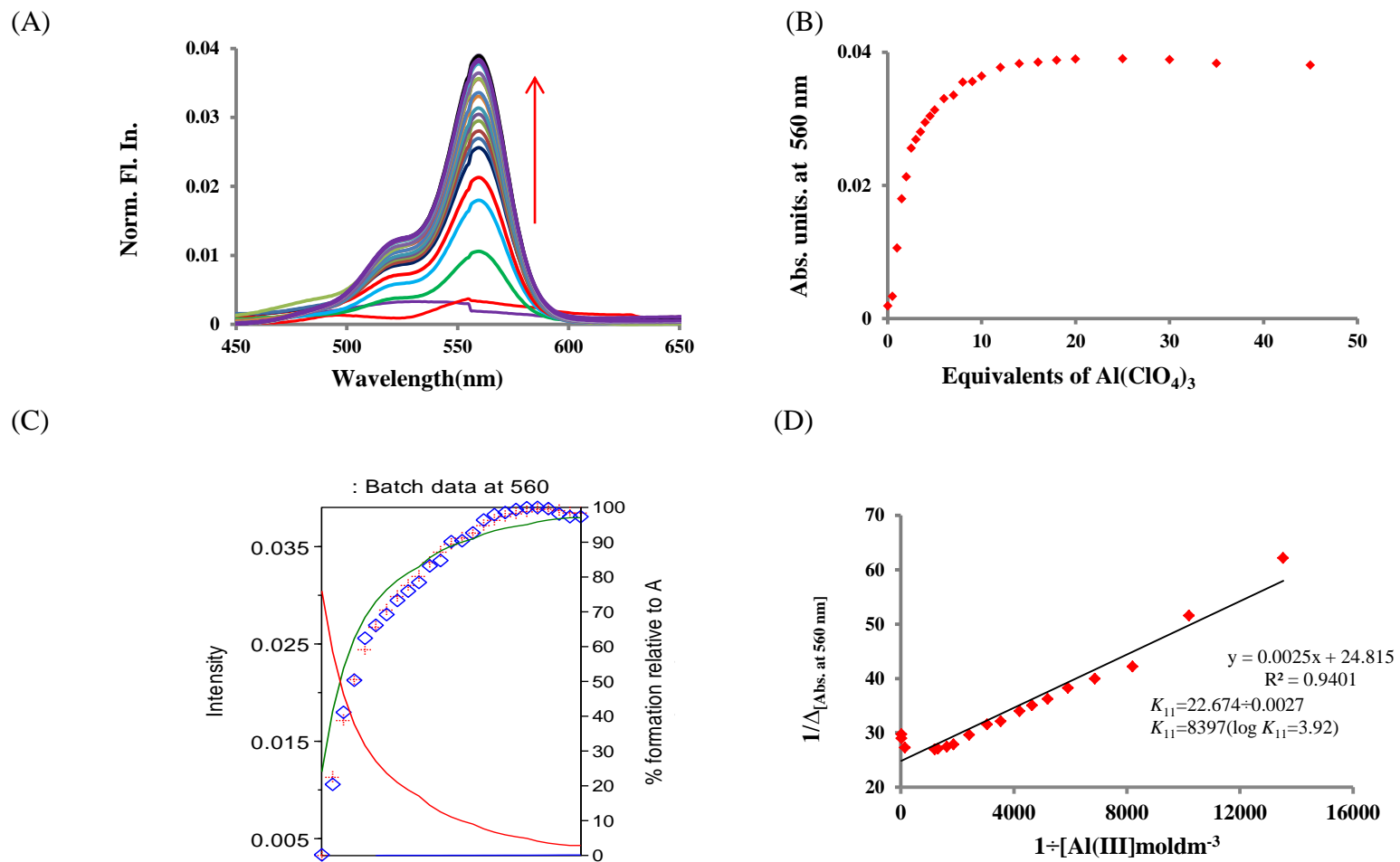


Figure 5.9. (A) UV-Vis spectrum of compound **5.12** (50  $\mu\text{M}$ ) upon addition of  $\text{Al}(\text{ClO}_4)_3$ , (B) its binding isotherm in 1:1 (EtOH:H<sub>2</sub>O) pH=7.1, (C) binding isotherm for HypSpec program,<sup>116</sup> and (D) Benesi-Hildbrand plot.

The BH method is good for reaction equilibrium which forms 1:1 complexes.<sup>202</sup> This method assumes that one of the reactants (either host or guest) should be present in an excess amount over other reactant so that the characteristic electronic absorption spectra of the other reactant will be transparent in the collective absorption of the system. In fact, this is the major drawback of this method. Whenever it breaks down, it deviates from its linear nature and exhibits scatter plot characteristics or curvature if other ratio exists in a solution. Other issues include: different values of extinction coefficient ( $\epsilon$ ) with different concentrations scales, dependency of binding constant ( $K$ ) and extinction coefficient ( $\epsilon$ ), and zero and negative intercepts.<sup>203-205</sup>

HypSpec is another program to calculate the binding constant.<sup>116</sup> It gives more accurate binding constant than the Benesi-Hildbrand method. More than one stoichiometry can be modeled simultaneously at the same time and hence gives information about the different species formed in the solution. It also gives the percentage of each species formed in the solution at each point of titration.<sup>206</sup>

It is important to mention that binding constants calculated by HypSpec program are normally a magnitude greater than the binding constant calculated by the Benesi-Hildbrand methods. Particularly, it is found in the fluorescence titrations as it is carried out in lower concentration than the UV-Vis absorption. One important criteria for the Benesi-Hildbrand method as mentioned above is that one of the reactants (either host or guest) must be in excess to another reactant. However, it is not always followed during titrations. Normally fewer data of titration is involved in the calculation of binding constant in the Benesi-Hildbrand method in comparison to the HypSpec program.

Table 5.1

*Binding constants ( $K_{11}$ ) calculated for UV-Vis titration of **5.12** and **5.13** with  $Fe(ClO_4)_3$  and  $Al(ClO_4)_3$  using Benesi-Hildbrand and HypSpec program.<sup>116</sup>*

Compounds	Salts	Bemesi-Hildbrand ( $K_{11}$ , $M^{-1}$ )	HypSpec ( $K_{11}$ , $M^{-1}$ )
<b>5.12</b>	$Fe(ClO_4)_3$	$1.3 \times 10^4$	$3.5 \times 10^4$
	$Al(ClO_4)_3$	$8.3 \times 10^3$	$2.4 \times 10^4$
<b>5.13</b>	$Fe(ClO_4)_3$	$9.2 \times 10^3$	$5.0 \times 10^4$
	$Al(ClO_4)_3$	$7.0 \times 10^3$	$6.6 \times 10^4$

### *Fluorescence spectroscopy*

Rhodamine based sensors have low fluorescence in the spirolactam form but give an intense fluorescence band upon the addition of metal ions (Chapter I). Therefore, compounds **5.11**, **5.12**, and **5.13** are expected to have low i.e., off fluorescence signal but should increase upon binding with target metal ions. The UV-Vis studies showed that compounds **5.11**, **5.12**, and **5.13** responded to both  $Fe^{3+}$  and  $Al^{3+}$  ions. However, fluorescence is different, and under this circumstances compounds **5.11**, **5.12**, and **5.13** may show selectivity as the fluorescence signal may respond differently to these metal ions. It could be possible that fluorescence is quenched even though the probe is colored.

The binding behavior of compounds **5.11**, **5.12**, and **5.13** towards different metal ions such as  $Na^+$ ,  $K^+$ ,  $Ca^{2+}$ ,  $Mg^{2+}$ ,  $Cr^{3+}$ ,  $Al^{3+}$ ,  $Fe^{3+}$ ,  $Fe^{2+}$ ,  $Zn^{2+}$ ,  $Cd^{2+}$ ,  $Co^{2+}$ , and  $Hg^{2+}$  ions was studied by fluorescence in same solvent system 1:1 (EtOH:H<sub>2</sub>O) at pH 7.1. Compounds **5.11**, **5.12**, or **5.13** (10  $\mu$ M) have a low fluorescence at 577 nm. Upon the addition of five equivalents of  $Al^{3+}$  or  $Fe^{3+}$  ions, a strong fluorescence emission at 577 nm was observed with a distinct color change from colorless to pink. But the addition of other metal ions mentioned above did not produce any significant enhancement in

fluorescence intensity. This clearly indicates that compounds **5.11**, **5.12**, or **5.13** could be used as potential fluorescent chemosensors for either  $\text{Fe}^{3+}$  or  $\text{Al}^{3+}$  ions. For example, Figure 5.10 shows a selectivity chart of compound **5.12** with all metals. The comparison chart of compounds **5.11**, **5.12**, or **5.13** for  $\text{Al}^{3+}$  and  $\text{Fe}^{3+}$  ions is shown in Figure 5.11. All compounds showed almost the same fluorescent intensity for  $\text{Fe}^{3+}$  ion. However, model compound **5.11** showed less fluorescent intensity for  $\text{Al}^{3+}$  ion in comparison to the compounds **5.12** and **5.13**. The fluorescent intensity due to  $\text{Al}^{3+}$  ion is almost half of  $\text{Fe}^{3+}$  ions. This could probably be due to the presence of the nitrogen atom of pyridine ring in **5.12** or sugar group in **5.13** which may impart some kind of selectivity to  $\text{Al}^{3+}$  ion either through direct coordination or through hydrogen bonding to a metal ion.

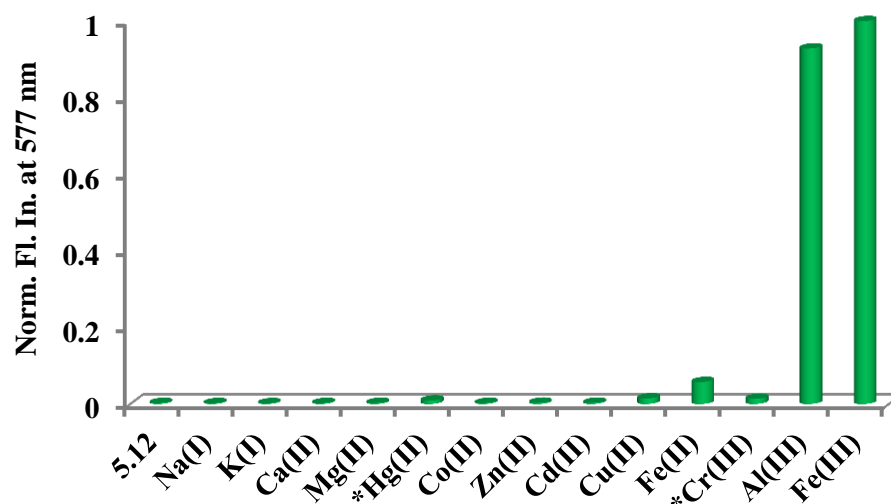
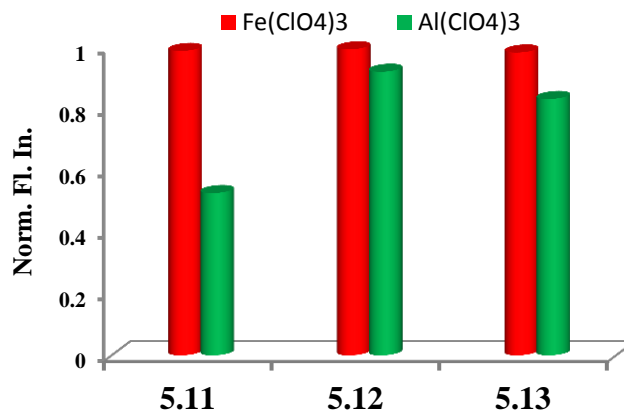


Figure 5.10. Fluorescence selectivity chart of compound **5.12** (10  $\mu\text{M}$ ) in 1:1 (EtOH:H<sub>2</sub>O), pH=7.1, upon the addition of metal ions (five equivalents) as their  $\text{ClO}_4^-$  salts (\*Cl<sup>-</sup> salt)  $\lambda_{\text{ex}}=550$  nm.



*Figure 5.11.* Comparison of fluorescence selectivity chart of compounds **5.11** (benzene), **5.12** (pyridine), and **5.13** (sugar) (10  $\mu$ M) in 1:1 (EtOH:H<sub>2</sub>O), pH=7.1, upon the addition of five equivalents of Fe<sup>3+</sup> and Al<sup>3+</sup> ions as their ClO<sub>4</sub><sup>-</sup> salts ( $\lambda_{\text{ex}}$ =550 nm).

In order to further investigate the interaction of **5.12** and **5.13** with Fe<sup>3+</sup> and Al<sup>3+</sup> ions, full fluorescence titrations were carried out in an aqueous ethanol solution of 1:1 (EtOH:H<sub>2</sub>O). For example, Figures 5.12 and 5.13 showed the fluorescence titration of compound **5.12** with Fe(ClO<sub>4</sub>)<sub>3</sub> and Al(ClO<sub>4</sub>)<sub>3</sub>. The addition of increasing concentration of Al<sup>3+</sup> or Fe<sup>3+</sup> ions to the solution of compounds **5.12** or **5.13** resulted in the gradual increase of fluorescence intensity at 577 nm, reaching saturation after the addition of five equivalents of Fe<sup>3+</sup> or Al<sup>3+</sup> ions. Binding constants were calculated by two methods: (a) Benesi-Hildebrand method and (b) HypSpec program<sup>116</sup> and are shown in Table 5.2. Both methods showed the binding stoichiometry is 1:1. As explained above, the binding constants calculated by the HypSpec program is a magnitude greater than those calculated from the Benesi-Hildebrand method.

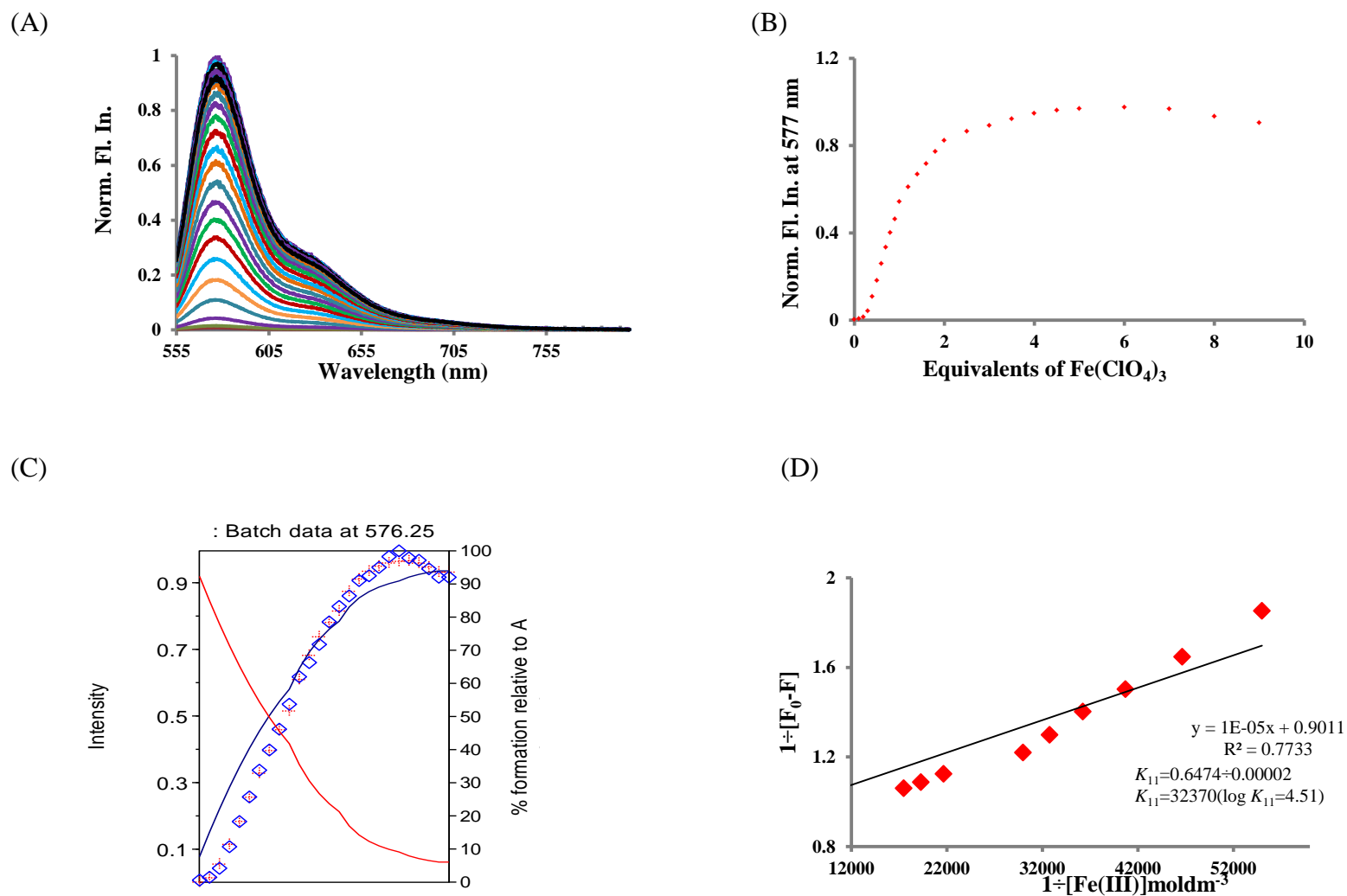


Figure 5.12. (A) Fluorescence spectrum of compound **5.12** (20  $\mu\text{M}$ ) upon addition of  $\text{Fe}(\text{ClO}_4)_3$ , (B) binding isotherm in 1:1 (EtOH:H<sub>2</sub>O), pH=7.1, (C) binding isotherm from HypSpec program,<sup>116</sup> and (D) Benesi-Hildbrand plot.

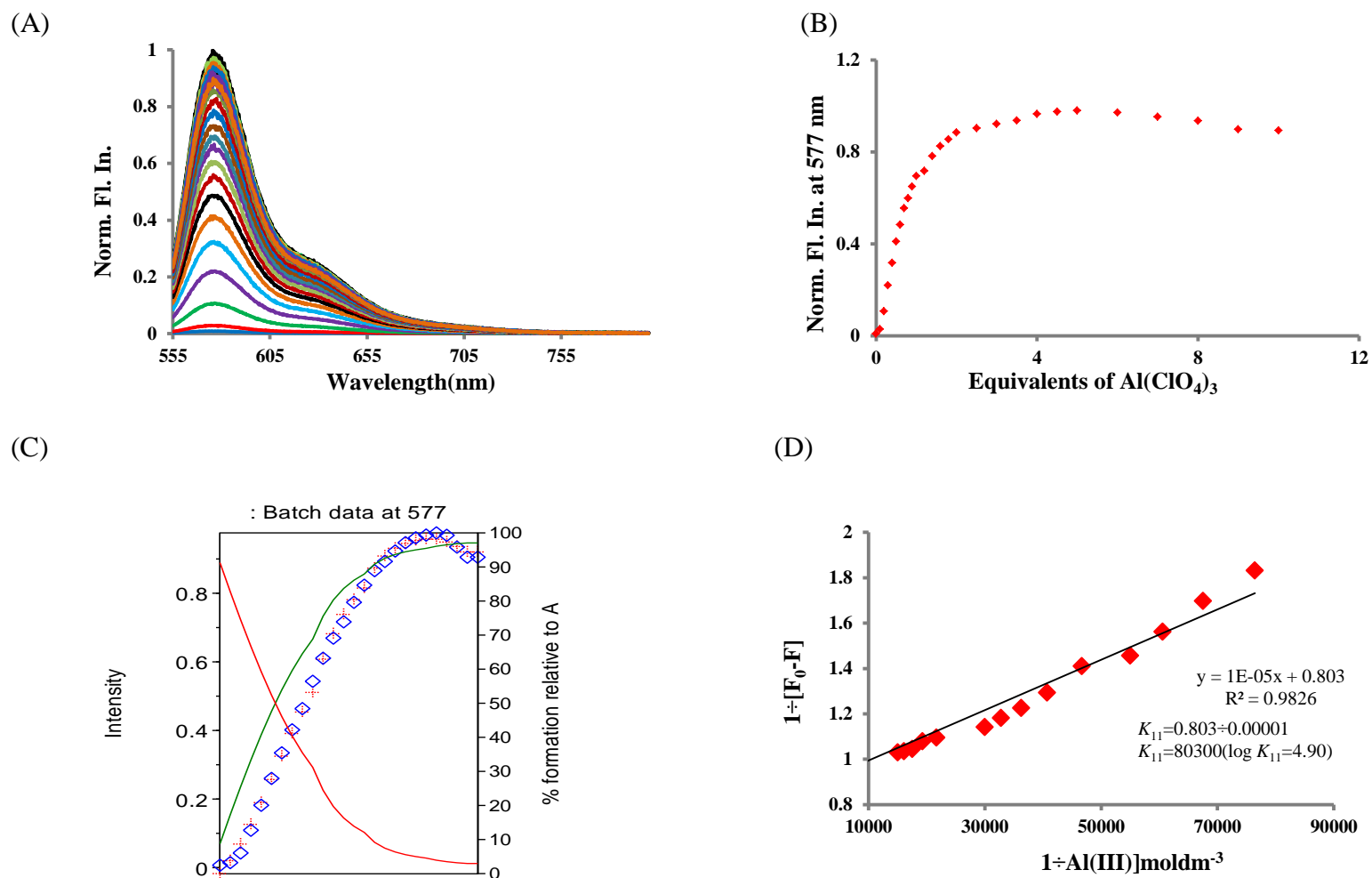


Figure 5.13. (A) Fluorescence spectrum of compound **5.12** (20  $\mu\text{M}$ ) upon addition of  $\text{Al}(\text{ClO}_4)_3$ , (B) binding isotherm in 1:1 (EtOH:H<sub>2</sub>O), pH=7.1, (C) binding isotherm from Hyp Spec program,<sup>116</sup> and (D) Benesi-Hildbrand plot.



Table 5.2

*Binding constants ( $K_{11}$ ) calculated for fluorescence titration of **5.12** and **5.13** with  $\text{Fe}(\text{ClO}_4)_3$  and  $\text{Al}(\text{ClO}_4)_3$  using Benesi-Hildbrand and HypSpec program<sup>116</sup>*

Compounds	Salts	Bemesi-Hildbrand ( $K_{11}, \text{M}^{-1}$ )	HypSpec ( $K_{11} \text{M}^{-1}$ )
<b>5.12</b>	$\text{Fe}(\text{ClO}_4)_3$	$3.23 \times 10^4$	$1.2 \times 10^5$
	$\text{Al}(\text{ClO}_4)_3$	$8.0 \times 10^4$	$3.9 \times 10^4$
<b>5.13</b>	$\text{Fe}(\text{ClO}_4)_3$	$3.3 \times 10^4$	$5.3 \times 10^5$
	$\text{Al}(\text{ClO}_4)_3$	$3.5 \times 10^4$	$1.2 \times 10^5$

Based upon the UV-Vis and fluorescence results, it is assumed that  $\text{Fe}^{3+}$  or  $\text{Al}^{3+}$  ion could be coordinated by the carbonyl oxygen atom of lactam ring and nitrogen atoms of triazole ring. It is possible that the nitrogen atom of pyridine ring in **5.12** and sugar functional groups in **5.13** could be involved in coordination of metal ions or at least can impart aid in the coordination. Therefore, detailed 1D and 2D NMR and IR studies have been carried out in order to gain further insight into the binding of metal ions.

#### <sup>1</sup>H NMR Studies of Molecular Probes **5.11**, **5.12**, and **5.13**

UV-Vis and fluorescence studies of the compounds **5.11**, **5.12**, and **5.13** showed that either  $\text{Fe}^{3+}$  or  $\text{Al}^{3+}$  ions can be detected *via* a spectroscopic signal. It is reasonable to believe that the coordination of metal ions can occur *via* the oxygen atoms of the lactam and nitrogen atoms of the triazole group. However, this is difficult to prove using UV-Vis and fluorescence spectroscopy alone as these techniques do not elucidate structure. On the other hand, NMR spectroscopy is very informative regarding the coordination geometry. Therefore, we turned to extensive NMR studies (1D and 2D) to obtain an understanding of the coordination mode. <sup>1</sup>H NMR titrations are carried out in  $\text{CD}_3\text{CN}$ , and  $\text{Al}(\text{ClO}_4)_3$  is used instead of  $\text{Fe}(\text{ClO}_4)_3$  as explained in Chapter IV. The signals were

assigned based on the 2D NMR such as COSY, HMQC, HMBC, and ROESY. As all three compounds are similar, compound **5.12** is discussed in detail.

A 10 mM solution for compound **5.12** and a 100 mM for  $\text{Al}(\text{ClO}_4)_3$  were used in  $^1\text{H}$  NMR titration. The signals followed in the  $^1\text{H}$  NMR experiment of compound **5.12** are highlighted in Figure 5.14 with their chemical shifts values in the free ligand **5.12** in  $\text{CD}_3\text{CN}$ .

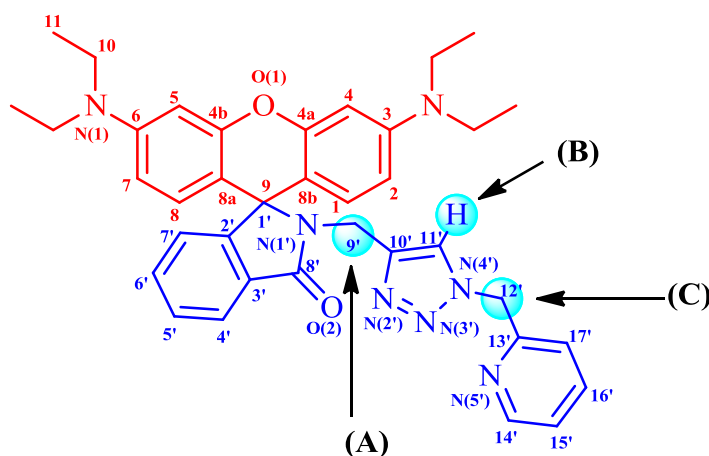


Figure 5.14.  $^1\text{H}$  NMR assignments that are followed in the NMR titration experiments in  $\text{CD}_3\text{CN}$ . The chemical shifts values of A, B, and C in the free ligand **5.12** are  $\delta$  4.32, 7.19 and 5.36 ppm, respectively.

Three important changes were found during  $^1\text{H}$  NMR titration of compound **5.12** with  $\text{Al}(\text{ClO}_4)_3$ .

- 1) Significant down field shifts of the protons (A, B, and C in Figure 5.14)
- 2) Broadness of the signals (0.1 to 0.7 equivalents)
- 3) Chemical shifts remained almost constant after one equivalent

There were significant downfield chemical shifts in  $^1\text{H}$  NMR spectrum upon the addition of  $\text{Al}^{3+}$  ions. In particular, the proton at carbon number 11' on the triazole ring (B), protons at carbon number 1, 2, 4, 5, 7, 8 on the xanthene ring, and protons at carbon number 14', 15', 16' of pyridine ring are more shifted into down field with lesser extent

for CH<sub>2</sub> group attached to lactam amide (A), and pyridine ring (C) (Figures 5.15 and 5.16). A change in chemical shift for all of the protons for both compounds **5.12** before and after addition of five equivalents Al(ClO<sub>4</sub>)<sub>3</sub> are summarized in Table 5.3. The downfield shift of the protons attached to carbon numbers 1, 2, 4, 5, 7, and 8 of xanthenes ring can be explained by the conjugation effect and electron deficient nature of the xanthene ring after a spirocyclic form of rhodamine is opened to a ring open amide form upon binding with Al<sup>3+</sup> ions. The down field shift of the other protons such as the protons assigned to triazole (B), pyridine (protons attached to carbon numbers 14', 15', 16,' and 17'), CH<sub>2</sub> group attached to lactam amide (A), and pyridine ring (C) can be explained by the inductive effect once the Al<sup>3+</sup> ion is possibly coordinated by the carbonyl oxygen atoms, the nitrogen atoms in the triazole and pyridine ring. There was almost no change in chemical shifts after addition of one equivalent of Al(ClO<sub>4</sub>)<sub>3</sub>. The binding affinity of **5.12** for Al<sup>3+</sup> ion was calculated to be  $K_{11} = 2.9 \times 10^5 \text{ M}^{-1}$  using the HypNMR program<sup>141</sup> (Figure 5.17).

All the proton signals were broadened upon addition of Al<sup>3+</sup> ions. In particular, the signals assigned to xanthene ring (protons attached to carbon numbers 1, 2, 4, 5, 7, 8) are broad, very difficult to distinguish, and difficult to follow in the early addition of titration (from 0.1 to 0.7 equivalents) suggesting that none of the free ligand or complex is predominant up to 0.7 equivalents (Figure 5.15). Broadness in the NMR signals assigned to rhodamine based sensors upon addition of metal ions are seen in many examples.<sup>207, 208</sup> This basically indicates that there is equilibrium between the free ligand **5.12** and its complex [Al (**5.12**)]<sup>3+</sup>. An average signal is obtained in NMR time scale for

all the species involved during equilibrium. The other reason could be due to the paramagnetic properties of aluminium which are explained in Chapter IV.<sup>163</sup>

A new signal appears at 8.09 ppm after addition of one equivalent of  $\text{Al}(\text{ClO}_4)_3$  whose intensity grows with shifting to downfield upon further addition of  $\text{Al}(\text{ClO}_4)_3$  (Figure 5.15). It is assigned as the signal for the protons of water molecules that are coordinated to the metal centre. On addition of excess  $\text{Al}(\text{ClO}_4)_3$ , the ligand (**5.12**) became saturated, and added  $\text{Al}(\text{ClO}_4)_3$  would not bind the ligand and remains as free in the solution. Water molecules coordinated with  $\text{Al}(\text{ClO}_4)_3$  increase during titration which explain the increase in the intensity of the signal. The downfield shift of the signal after each equivalent could be due to the change in the solvent composition of  $\text{CD}_3\text{CN}$  and water molecules which comes from water molecules associated with  $\text{Al}(\text{ClO}_4)_3$ . In fact, the signal at 8.09 ppm is found interchangeable with the signal at 2.03 ppm, which is the standard chemical shift for free water signal in  $\text{CD}_3\text{CN}$ .

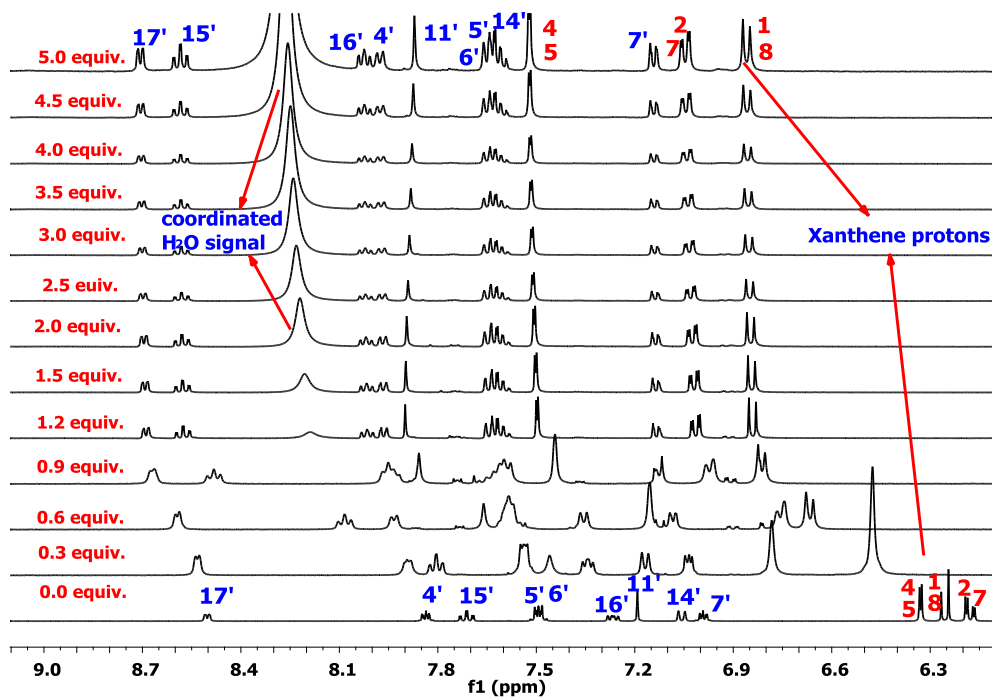


Figure 5.15. Partial <sup>1</sup>H NMR stack plot: Addition of Al(ClO<sub>4</sub>)<sub>3</sub> with compound **5.12** (10 mM) in CD<sub>3</sub>CN (aromatic region only).

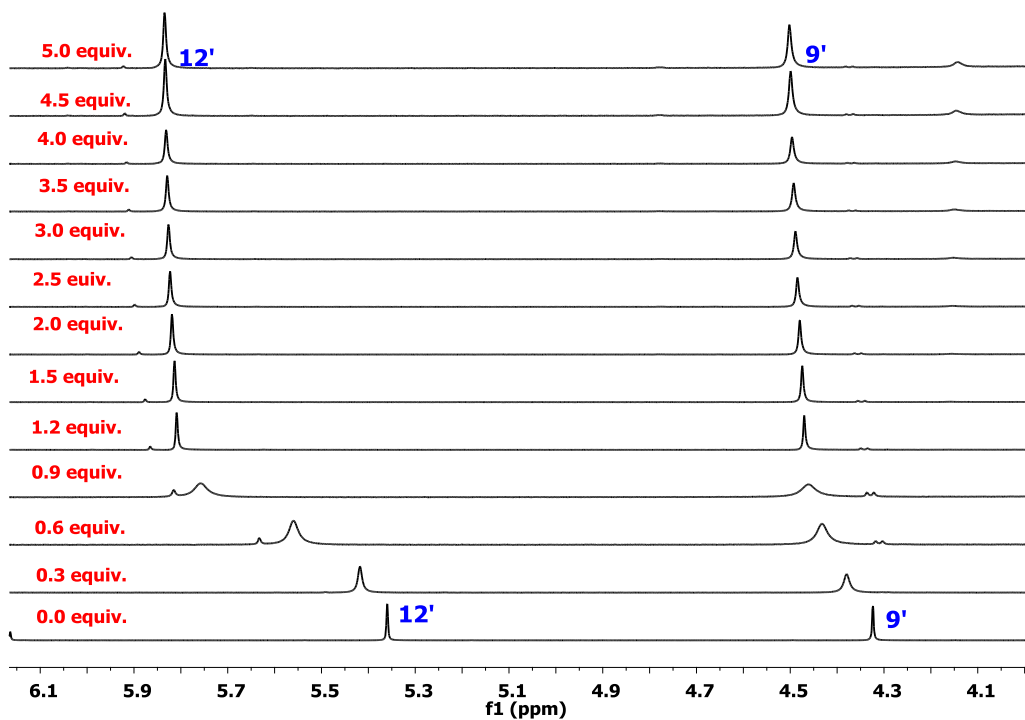


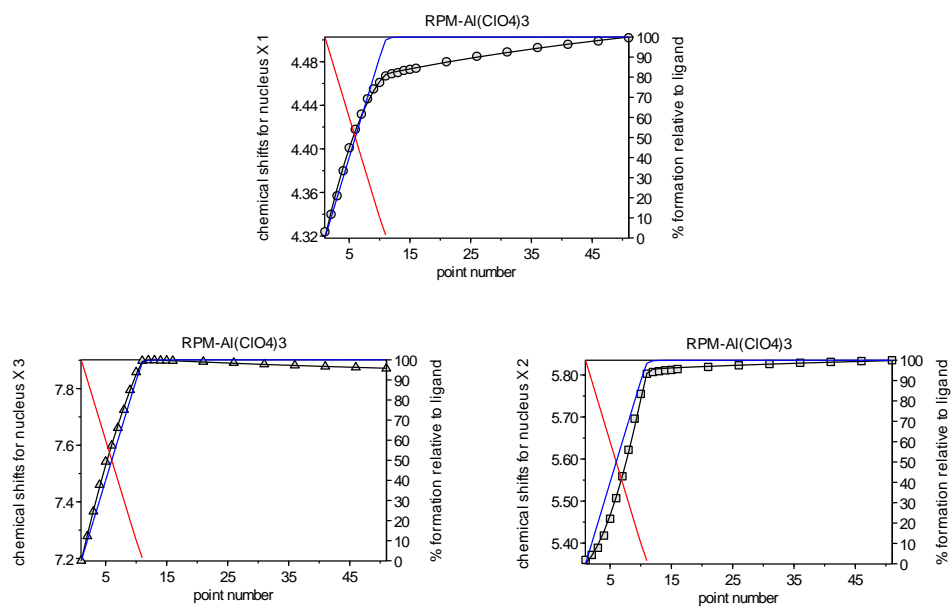
Figure 5.16. <sup>1</sup>H NMR Stack plot: Addition of Al(ClO<sub>4</sub>)<sub>3</sub> with compound **5.12** (10 mM) in CD<sub>3</sub>CN for CH<sub>2</sub> protons attached to lactam (A) at δ 4.32 ppm, and for CH<sub>2</sub> protons attached to pyridine (C) at δ 5.36 ppm.

Table 5.3

Change in  $^1\text{H}$  NMR chemical shift of compound **5.12** (10 mM) after addition of five equivalents of  $\text{Al}(\text{ClO}_4)_3$  in  $\text{CD}_3\text{CN}$ .

Protons	$^1\text{H}$ -NMR (500 MHz) $\text{CH}_3\text{CN-d}_3$ (J = Hz) <b>5.12</b>	$^1\text{H}$ -NMR (500 MHz) $\text{CH}_3\text{CN-d}_3$ (J = Hz) <b>5.12</b> + five equivalents	Difference [Complex-ligand]
<b>1</b>	6.25 (d, $J = 8.9$ )	6.89(d, $J=8.0$ Hz)	0.64
<b>2</b>	6.18 (dd, $J = 7.8, 2.6$ )	7.08(d, $J=7.0$ Hz)	0.9
<b>3</b>	N/A	N/A	N/A
<b>4</b>	6.33 (d, $J = 2.6$ )	7.56(s)	1.23
<b>4a</b>	N/A	N/A	N/A
<b>4b</b>	N/A	N/A	N/A
<b>5</b>	6.33 (d, $J = 2.6$ )	7.56(s)	1.23
<b>6</b>	N/A	N/A	N/A
<b>7</b>	6.18 (dd, $J = 7.8, 2.6$ )	7.08(d, $J=7.0$ Hz)	0.9
<b>8</b>	6.25 (d, $J = 8.9$ )	6.89(d, $J=8.0$ Hz)	0.64
<b>8a</b>	N/A	N/A	N/A
<b>8b</b>	N/A	N/A	N/A
<b>9</b>	N/A	N/A	N/A
<b>10</b>	3.32 (q, $J = 7.1$ )	3.68(s)	0.36
<b>11</b>	1.10 (t, $J = 7.0$ )	1.17(t, $J=7.1$ Hz)	0.07
<b>1'</b>	N/A	N/A	N/A
<b>2'</b>	N/A	N/A	N/A
<b>3'</b>	N/A	N/A	N/A
<b>4'</b>	7.89-7.80 (m)	8.01(d, $J=6.35$ Hz))	0.12-0.21
<b>5'</b>	7.54-7.45 (m)	7.74-7.61(m)	0.2-0.16
<b>6'</b>	7.54-7.45 (m)	7.74-7.61(m)	0.2-0.16
<b>7'</b>	7.06 (d, $J = 7.8$ )	7.17(d, $J=7.2$ Hz)	0.11
<b>8'</b>	N/A	N/A	N/A
<b>9'</b>	4.33 (s)	4.54(s)	0.23
<b>10'</b>	N/A	N/A	N/A
<b>11'</b>	7.19 (s)	7.89(s)	0.17
<b>12'</b>	5.36 (s)	5.87(s)	0.51
<b>13'</b>	N/A	N/A	N/A
<b>14'</b>	7.06(d, $J = 8.9$ )	7.74-7.61(m)	0.68-0.55
<b>15'</b>	7.71 (td, $J = 7.7, 1.8$ Hz)	8.62(t, $J=7.4$ Hz)	0.91
<b>16'</b>	7.27 (dd, $J = 6.7, 4.9$ )	8.06(t, $J=6.6$ Hz)	0.79
<b>17'</b>	8.85 (d, $J = 4.7$ Hz)	8.74(d, $J=5.4$ Hz)	-0.11

Note. Negative sign in difference of chemical shift means up field signals in complex



*Figure 5.17.*  $^1\text{H}$  NMR Binding isotherms of compound **5.12** (10 mM) for the protons (A), (B), and (C) after the addition of  $\text{Al}(\text{ClO}_4)_3$  from HypNMR program.<sup>141</sup>

The  $^1\text{H}$  NMR studies of compounds **5.11** and **5.13** with  $\text{Al}(\text{ClO}_4)_3$  are also carried out and showed the similar pattern as compound **5.12**. The only difference is the sugar and benzene groups instead of pyridine ring in compounds **5.12** and **5.13**, respectively. The changes in the chemical shifts of the protons attached to the benzene scaffold in **5.11** are negligible in comparison to the chemical shifts observed in the pyridine ring of compound **5.12**. This confirms that the nitrogen atom of pyridine ring in compound **5.12** is involved in the coordination of  $\text{Fe}^{3+}$  or  $\text{Al}^{3+}$  ion (Figure 5.18 and scheme 5.7). Surprisingly in compound **5.13**, the changes in the chemical shifts for the protons of sugar are small indicating that the sugar functional groups (acetyl, ring oxygen atoms) might not involve the coordination of  $\text{Al}^{3+}$  ions.

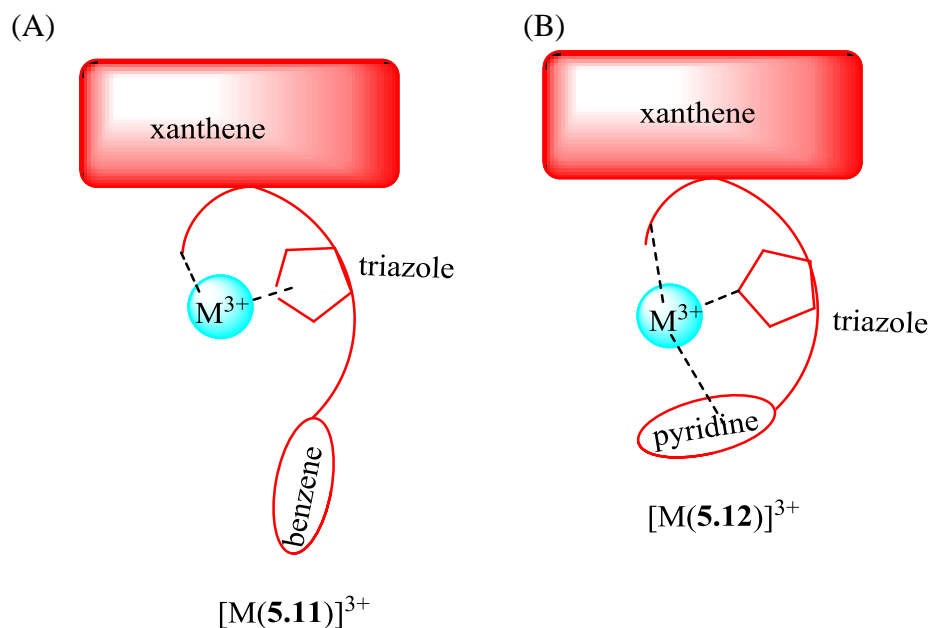
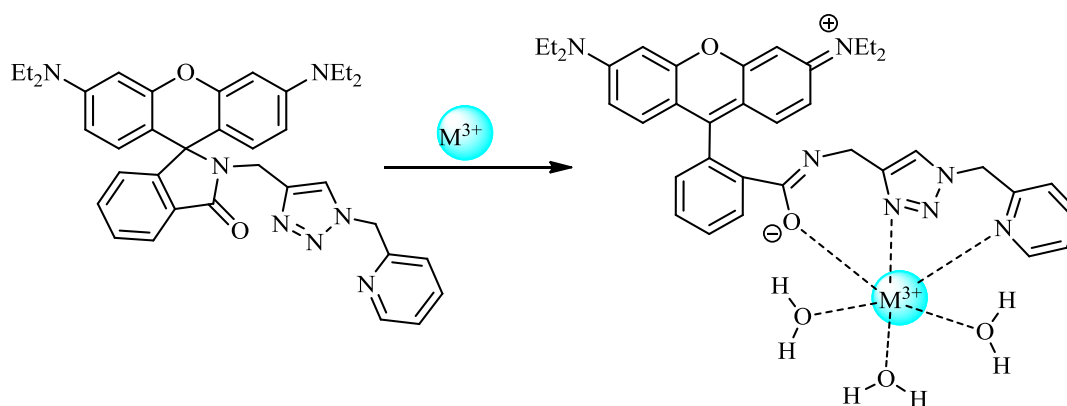


Figure 5.18. Cartoons showing the proposed binding mechanism of metal ion by compound **5.11** (A) and **5.12** (B).



Scheme 5.7. Proposed binding mode of compound **5.12** with  $Fe^{3+}/Al^{3+}$  ion.

### $^{13}C$ NMR studies of Molecular Probe **5.11** and **5.12**

The  $^1H$  NMR studies of compound **5.12** with  $Al(ClO_4)_3$  showed that the carbonyl oxygen atoms on the lactam group and the nitrogen atom of triazole and pyridine ring are involved in the coordination of metal ions. In general, it is the carbonyl oxygen atoms of the lactam ring that normally triggered the ring opening of spirolactam after the coordination of metal ion and is seen in almost all rhodamine based sensors. The



carbonyl group is in conjugation once the spirolactame ring is open and hence should have less double bond character (Chapter I). Therefore, the signal for the carbonyl group should be different either in the intensity has changed (increased or decreased), or there is a chemical shift in signal. Besides, all of the free rhodamine based sensors showed the  $^{13}\text{C}$  signal for the spirocyclic carbon atom at  $\sim 65$  ppm, which is in fact, the evidence for the compound's existence in spirolactam configuration. The intensity of  $^{13}\text{C}$  signal for the spirocyclic carbon atom should be decreased or absent in the  $^{13}\text{C}$  NMR spectrum of the complex as it does not exist in the ring open structures. Furthermore, the chemical shift change in the  $^{13}\text{C}$  NMR signals gives important information about the coordination environment of the metal ion.

The  $^{13}\text{C}$  NMR studies of compound **5.12** with  $\text{Al}^{3+}$  ion will be used as an example. The  $^{13}\text{C}$  NMR of the free ligand (**5.12**) showed the signal of the spirocyclic carbon and carbonyl groups at  $\delta$  65.84 and 168.75 ppm, respectively (Figure 5.19). The signals of these carbons are significantly reduced in intensity in the  $^{13}\text{C}$  NMR spectrum of the complex containing five equivalents of  $\text{Al}(\text{ClO}_4)_3$  (Figure 5.20). The low intensity signals for the spirocyclic carbon and carbonyl carbon indicate that the spirolactam ring open to bind the metal ion with the carbonyl group possibly coordinating the metal ion. The low intensity signals suggest that the binding is an equilibrium process with the major product being a desired complex. The carbonyl group is slightly deshielded by 0.32 ppm in the  $^{13}\text{C}$  NMR spectrum of the complex indicating the coordination of a metal ion by a carbonyl oxygen atom lowers and pulls the electron density away from a carbonyl carbon group. While the  $^{13}\text{C}$  signal for spirocyclic carbon is shifted to up field by 1.36 ppm indicating the increase in electron density by conjugation. A change in chemical

shifts for all the carbons of both compounds **5.12** before and after addition of five equivalent  $\text{Al}(\text{ClO}_4)_3$  is given in Table 5.4.

Compound **5.11** and **5.13** are also studied by  $^{13}\text{C}$  NMR with five equivalents  $\text{Al}(\text{ClO}_4)_3$  and showed the similar pattern as compound **5.12**. The signal of spirocyclic carbon and lactam carbonyl groups at  $\delta$  65.8 and 168.75 ppm respectively are significantly reduced in the  $^{13}\text{C}$  NMR spectrum of the complex suggesting the coordination of metal ions by carbonyl oxygen atoms.

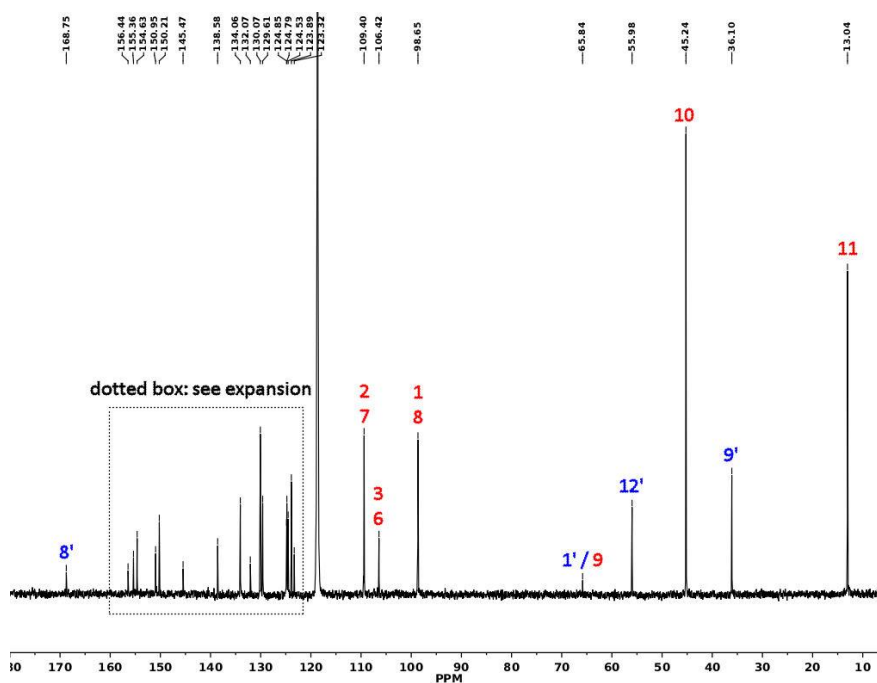


Figure 5.19.  $^{13}\text{C}$  NMR spectrum of free ligand **5.12** (10 mM) in  $\text{CD}_3\text{CN}$  (Figure 5.13).

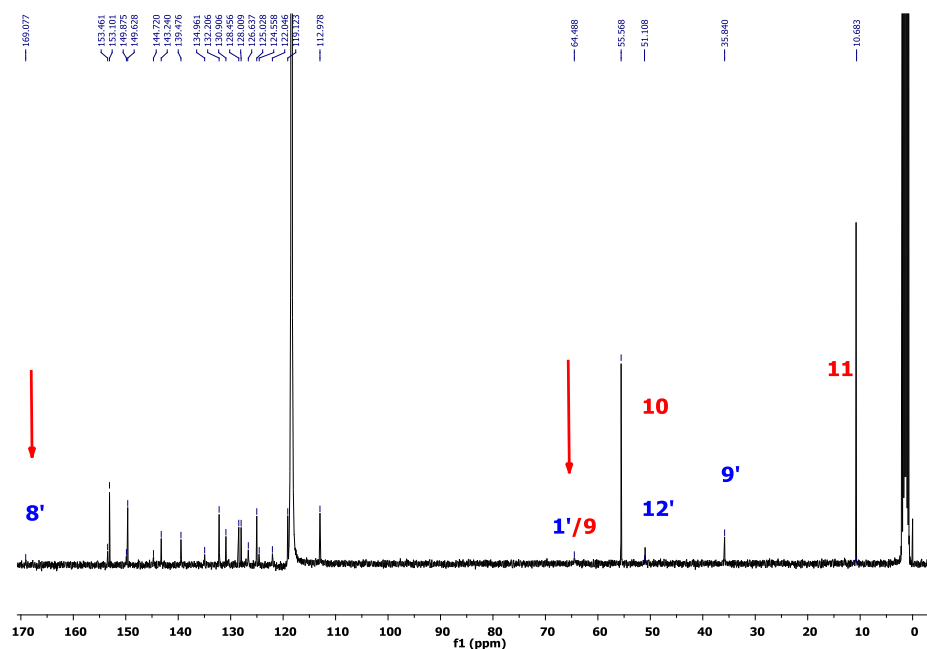


Figure 5.20.  $^{13}\text{C}$  NMR spectrum of complex of ligand **5.12** (10 mM) with five equivalents  $\text{Al}(\text{ClO}_4)_3$  in  $\text{CD}_3\text{CN}$ .

Table 5.4

Change in  $^{13}\text{C}$  NMR chemical shift of compound **5.12** (10 mM) after addition of five equivalents of  $\text{Al}(\text{ClO}_4)_3$  in  $\text{CD}_3\text{CN}$ .

Carbon	$^{13}\text{C}$ NMR (500 MHz) $\text{CH}_3\text{CN}-d_3$ <b>5.12</b>	$^{13}\text{C}$ NMR (500 MHz) $\text{CH}_3\text{CN}-d_3$ <b>5.12</b> + five equivalents $\text{Al}(\text{ClO}_4)_3$	Difference (Complex-ligand)
<b>1</b>	130.1	132.2	2.1
<b>2</b>	109.4	119.0	9.6
<b>3</b>	106.4	122.0	15.6
<b>4</b>	98.7	112.9	14.2
<b>4a</b>	150.2	153.0	2.8
<b>4b</b>	150.2	153.0	2.8
<b>5</b>	98.7	112.9	14.2
<b>6</b>	106.4	122.0	15.6
<b>7</b>	109.4	119.0	9.6
<b>8</b>	130.1	132.2	2.1
<b>8a</b>	154.6	139.4	-15.2
<b>8b</b>	154.6	139.4	-15.2
<b>9</b>	65.8	64.4	-1.4

Table 5.4 (continued).

Carbon	<sup>13</sup> C NMR (500 MHz) CH <sub>3</sub> CN- <i>d</i> <sub>3</sub> <b>5.12</b>	<sup>13</sup> C NMR (500 MHz) CH <sub>3</sub> CN- <i>d</i> <sub>3</sub> <b>5.12</b> + five equivalents Al(ClO <sub>4</sub> ) <sub>3</sub>	Difference (Complex-ligand)
10	45.2	55.5	10
11	13.0	10.7	2.3
1'	65.8	64.4	-1.4
2'	155.4	130.4	-25
3'	132.1	153.4	21.3
4'	123.9	124.5	0.6
5'	129.6	134.9	5.3
6'	134.1	130.8	-3.3
7'	124.8	125.0	0.2
8'	168.8	169.0	0.2
9'	36.1	35.8	-0.3
10'	145.5	144.7	-0.8
11'	124.8	126.5	1.7
12'	56.0	55.5	-0.5
13'	156.4	149.9	-6.9
14'	123.3	127.9	4.6
15'	138.6	149.5	10.9
16'	124.5	128.4	3.9
17'	151.0	143.2	-7.8

Note. Negative sign in difference of chemical shift means up field signals in complex

### 2D NMR Studies of Molecular Probe **5.11** and **5.12**

<sup>1</sup>H NMR and <sup>13</sup>C NMR indicate that compounds **5.12** coordinates the Al<sup>3+</sup> ions *via* the carbonyl oxygen atoms of lactam and nitrogen atoms of triazole and pyridine rings. However, it does not provide the information about the geometry or three dimensional structure of the coordination environment. The conformation of rhodamine based sensors should be completely changed in the complex as the spirolactam configuration is opened upon coordination with the metal ions. Therefore the coordination of compound **5.12** with Al(ClO<sub>4</sub>)<sub>3</sub> was studied in detail by 2D NMR

(COSY, HMQC, HMBC, and ROESY). In particular, the ROESY was important and gives the correlation of protons in space and helps in the structure elucidation of both free ligand (**5.12**) and its complex  $[\text{Al}(\mathbf{5.12})]^{3+}$ . The protons and carbons of both compound **5.12** and its complex are assigned accurately on the basis of 2D NMR.

The rOe spectrum of compound **5.12** showed seventeen rOe signals in  $\text{CD}_3\text{CN}$ . The three important rOe signals are labelled as (A) (B) and (C) in Figure 5.22. An rOe signal (A) showed that the protons attached to carbon number 12' are near to the protons attached to carbon number 10 on the xanthene ring. The rOe signals (B) and (C) showed the proton attached to carbon number 2 of xanthene ring is closer to the proton of triazole ring (attached to 11' carbon) and  $\text{CH}_2$  group attached to lactam ring (Figure 5.25). These rOe signals are reasonable as the calculated bond distances are within 5 Å calculated from the crystal structure of compound **5.12**(Figure 5.23). These rOe signals labelled as (A) (B) and (C) are absent in the rOe spectrum of the complex with the  $\text{Al}(\text{ClO}_4)_3$ (Figure 5.24 and 5.25). The disappearance of these signals in the coordination complex indicates that the pendant arm of the compound **5.12** is far away from the main xanthene ring after binding with the  $\text{Al}^{3+}$  ion as shown in Figure 5.21.

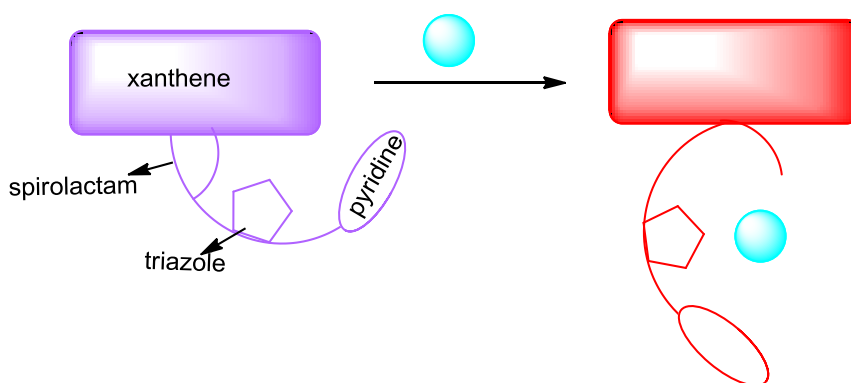


*Figure 5.21.* Cartoon showing the pendent arm becomes far from the xanthene ring after coordination of metal ion.

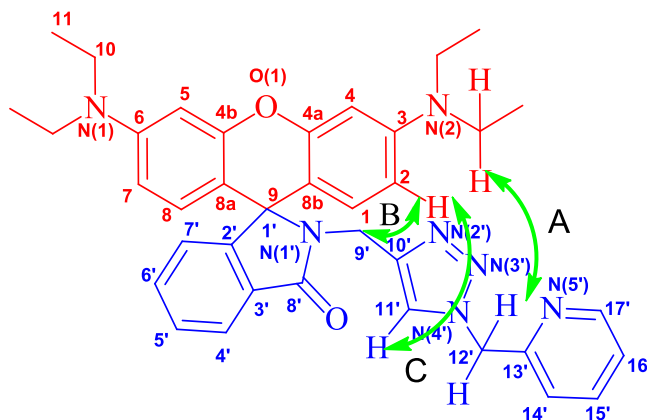


Figure 5.22. Correlation of protons labelled as A, B, and C seen in the 2D ROESY of free ligand (**5.12**) in  $\text{CD}_3\text{CN}$ .

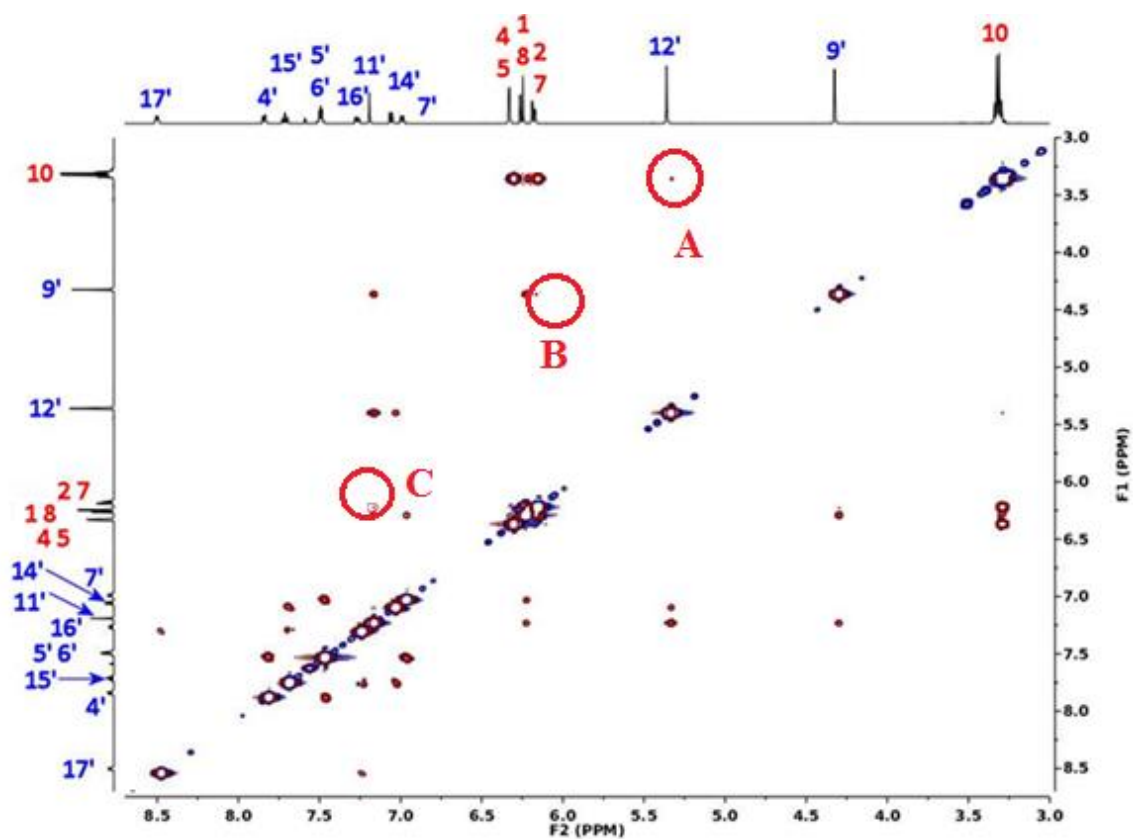


Figure 5.23. ROSEY of compound **5.12** (10 mM) in  $\text{CD}_3\text{CN}$ . Calculated distances (A) 3.25 Å (B) 3.07 Å, and (C) 4.82 Å.

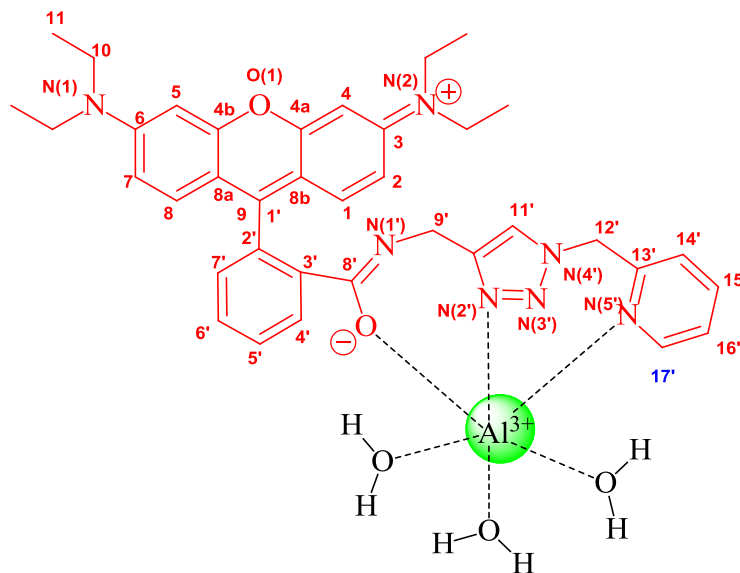


Figure 5.24. Proposed structures of complex  $[Al(5.12)]^{3+}$ .

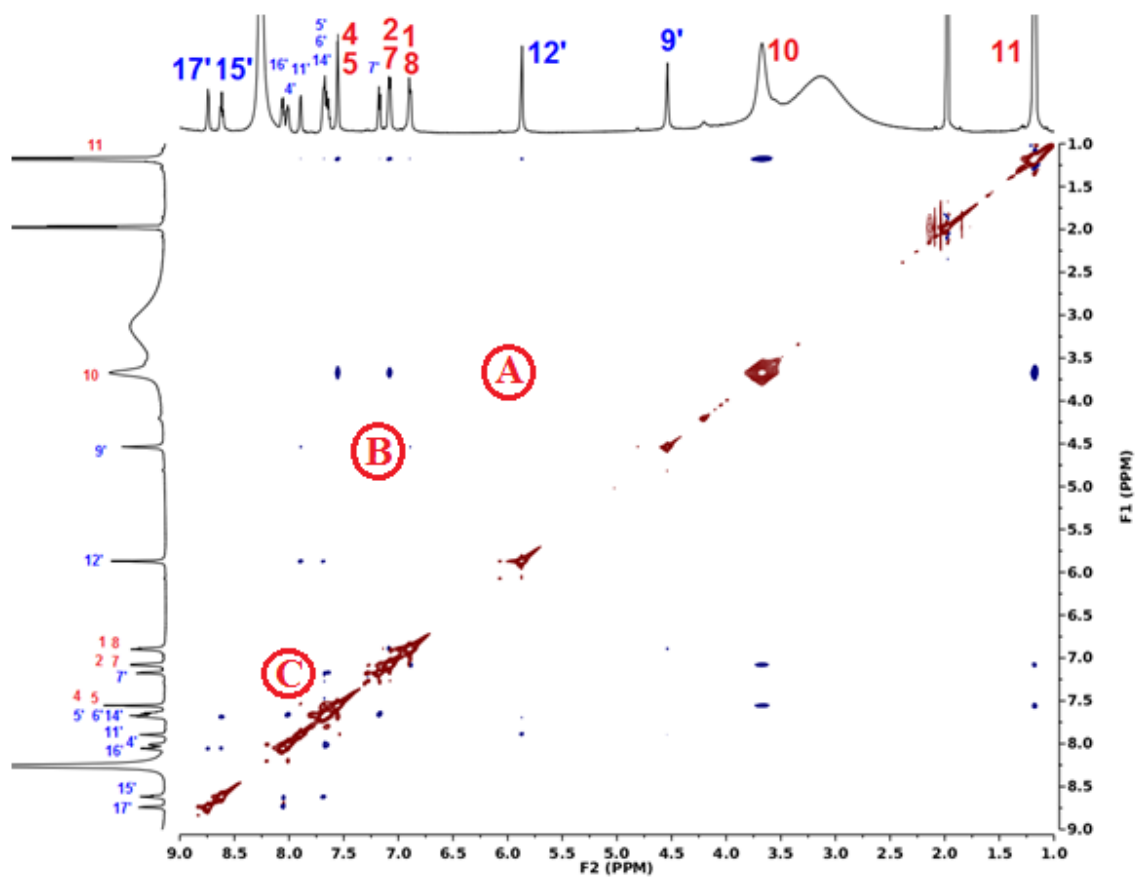


Figure 5.25. ROSEY of complex of compound **5.12** (10 mM) with five equivalents  $Al(ClO_4)_3$  in  $CD_3CN$ . The cross peak labelled as (A), (B), and (C) were absent in the complex.

2D NMR of the compounds **5.11** with  $\text{Al}(\text{ClO}_4)_3$  is also studied in detail and supports the conclusion that pendent arm is far away from the xanthene ring upon coordination of metal ion. 2D NMR of the compounds **5.13** with  $\text{Al}(\text{ClO}_4)_3$  is under study.

#### IR Study of Molecular Probe **5.12**

The  $^{13}\text{C}$  NMR of the complex **5.12** clearly showed the coordination of metal ion by carbonyl oxygen atoms of the lactam group. The coordination of metal ion by carbonyl group of lactam can further be verified by studies of IR-spectrum as the carbonyl group of lactam has characteristic IR stretching bands. A change in either the intensity or shift in the stretching band of carbonyl groups further verifies the involvement in the coordination of  $\text{Fe}^{3+}$  ion.

Therefore, the coordination of compound **5.12** with  $\text{Fe}(\text{ClO}_4)_3$  is studied by IR-spectroscopy. The infrared spectrum of free receptor **5.12** was recorded as a solid using an ATR-IR and showed the characteristic IR bands for the lactam functional group. The lactam carbonyl stretching band appears at  $1681\text{ cm}^{-1}$  (Figure 5.26). For the metal complex needed for the IR study, the compound **5.12** and  $\text{Fe}(\text{ClO}_4)_3$  was prepared in 1:1 stoichiometry by refluxing the metal salt and the molecular probe in  $\text{CH}_3\text{CN}$  overnight and evaporated to dryness and left to air dry over several days. The dried pink red solid was used to take an IR spectrum for the complex. The IR-spectrum of the complex showed that stretching band of the carbonyl group is almost completely reduced and broad at  $1681\text{ cm}^{-1}$  (Figure 5.26). The reduced peak for the carbonyl group indicates that it should involve coordination with the  $\text{Fe}^{3+}$  ion. This is because on coordination of  $\text{Fe}^{3+}$  ion with the oxygen atoms of the carbonyl group, the double bond character of the carbonyl



group is reduced. Further, the carbonyl group is in conjugation once the lactam ring is opened to bind the metal ion (Chapter I). Also, a broad band is seen at 3300-3600  $\text{cm}^{-1}$ . It could be either the water molecule coordinated to the metal ion or the hydroxyl group formed from the carbonyl group of the lactam ring after opening the ring. It is possible that the negative carbonyl oxygen atom may pick the hydrogen and form a hydroxyl group.

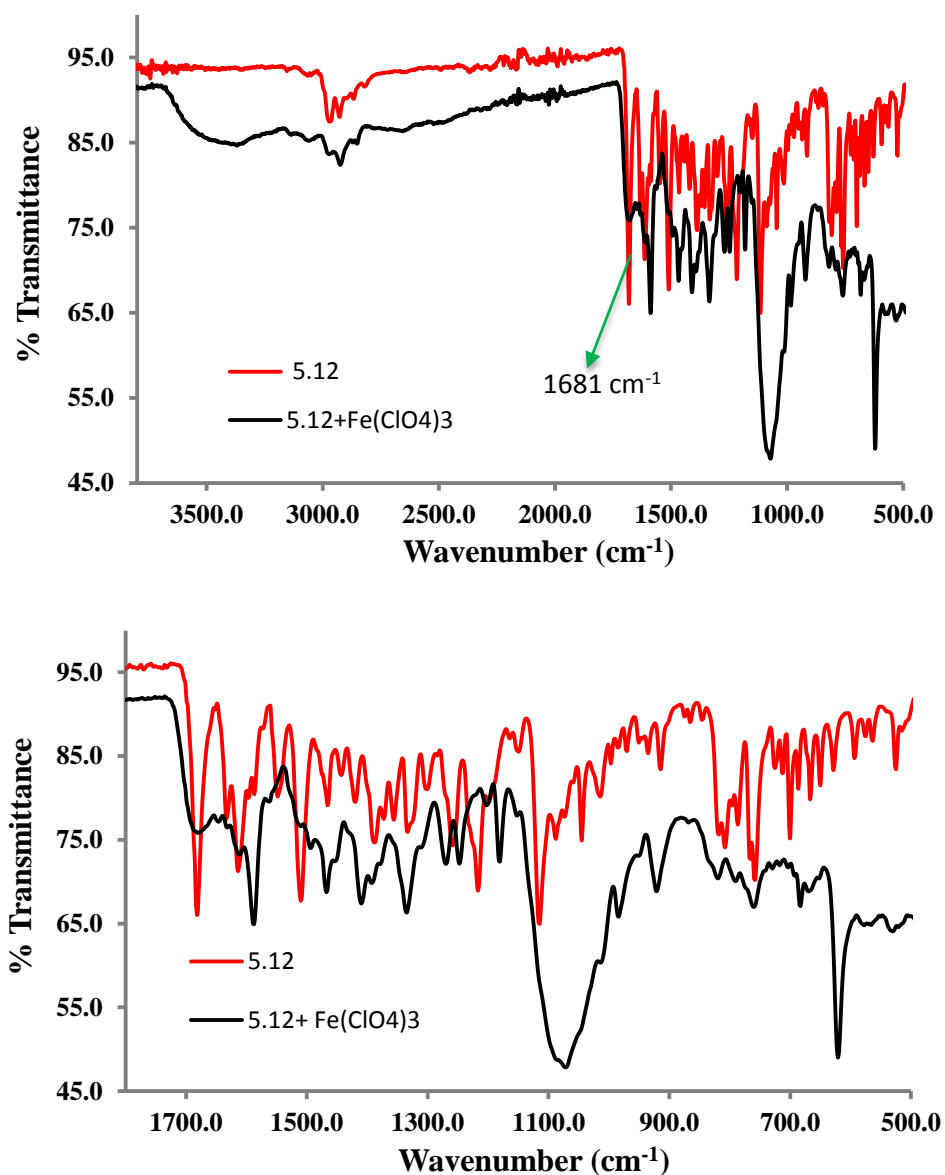


Figure 5.26. ATR-IR data of compound **5.12** on the addition of  $\text{Fe}(\text{ClO}_4)_3$ .

### Reversibility of Molecular Probes **5.11**, **5.12** and **5.13**

As discussed in Chapter II, the reversibility of the chemosensors for binding a target ion is a very important aspect of practical application. The reversibility of **5.11**, **5.12**, and **5.13** with both  $\text{Fe}^{3+}$  or  $\text{Al}^{3+}$  ions is studied by simply adding DFB (deferoxamine) in an aqueous ethanol solution of 1:1 (EtOH:H<sub>2</sub>O) at pH 7.1 to the desired probe. The DFB molecule is a siderophore which has a high affinity for iron. The addition of three equivalents of DFB to the solution of complex with  $\text{Fe}^{3+}$  or  $\text{Al}^{3+}$  (three equivalents of  $\text{Fe}^{3+}$  or  $\text{Al}^{3+}$  to 10  $\mu\text{M}$  solution) ions decreased the fluorescence intensity nearly to the initial fluorescence intensity (blue line spectrum in Figure 5.27 and 5.28) indicating the solution returned to original lactam state. The addition of more than three equivalents of DFB might completely 'strip' out the  $\text{Fe}^{3+}$  or  $\text{Al}^{3+}$  ions from the complex, and the fluorescence might return to initial stage. When high concentrations of  $\text{Fe}^{3+}$  or  $\text{Al}^{3+}$  ions were added to the system again, the fluorescence of solution was enhanced again. This confirms that the reversibility is due to the chelation-induced ring opening of rhodamine spirolactam rather than other possible reactions. Figures 5.27 and 5.28 showed the reversibility of compound **5.12** with  $\text{Fe}(\text{ClO}_4)_3$  and  $\text{Al}(\text{ClO}_4)_3$  with DFB.

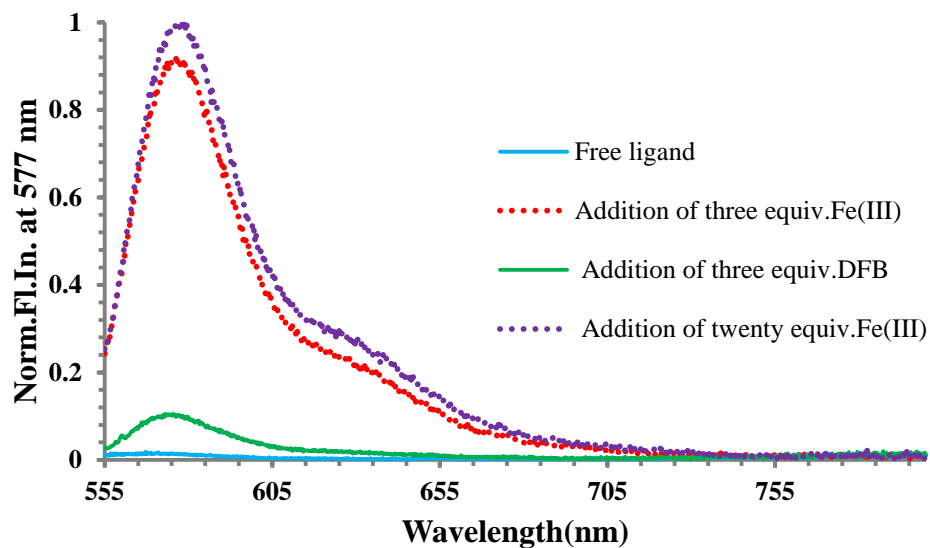


Figure 5.27. Reversibility test: [5.12] = 10  $\mu\text{M}$ ; Fe (III) = 100  $\mu\text{M}$ ; DFB = 100  $\mu\text{M}$  in EtOH: H<sub>2</sub>O (1:1).

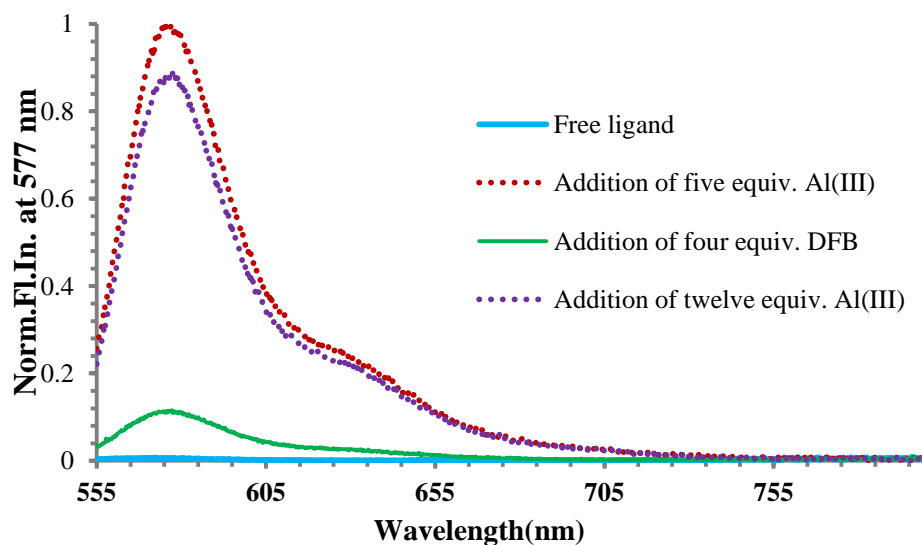


Figure 5.28. Reversibility test: [5.12] = 10  $\mu\text{M}$ ; Al (III) = 100  $\mu\text{M}$ ; DFB = 100  $\mu\text{M}$  in EtOH: H<sub>2</sub>O (1:1).

#### Detection Limit of Molecular Probe 5.12 and 5.13

It is important for the probes to detect Fe<sup>3+</sup> and Al<sup>3+</sup> ions in low concentrations.

The limit of detection was calculated by titrating 10  $\mu\text{M}$  of compound 5.12 with 100  $\mu\text{M}$  Fe(ClO<sub>4</sub>)<sub>3</sub> in 1:1 (EtOH : H<sub>2</sub>O) (Figure 5.29). For compound 5.13, 5  $\mu\text{M}$  of compound

**5.13** is titrated with 50  $\mu\text{M}$   $\text{Fe}(\text{ClO}_4)_3$  in 1:1 (EtOH :  $\text{H}_2\text{O}$ ). The solution is stirred for a few minutes after addition of metal salts before taking the fluorescence reading. The fluorescence intensity at 577 nm is increased upon the addition of  $\text{Fe}(\text{ClO}_4)_3$ . The limit of detection was calculated by using the method of least squares as described in Chapter II. The limit of detection of compound **5.12** and **5.13** for  $\text{Fe}^{3+}$  ion was calculated to be 1.15  $\mu\text{M}$  (64 ppb) and 0.59  $\mu\text{M}$  (33 ppb) (Figure 5.30).

In the United States, iron in drinking water is considered as secondary contaminant which does not pose a danger to human health. Therefore, iron is not considered “toxic;” however, its concentration greater than recommended limit changes the color and taste of water. Excess iron can cause yellow/orange/brown staining on skins, teeth and cloths. The recommended limits of iron in drinking water is 0.1 mg/L (100 ppb) and 0.3 mg/L (300 ppb) by the World Health organization and the U.S. Environmental Protection Agency, respectively.<sup>209</sup> The detection limit of molecular probes **5.12** and **5.13** are below the limits set up by the WHO and the U. S. EPA.

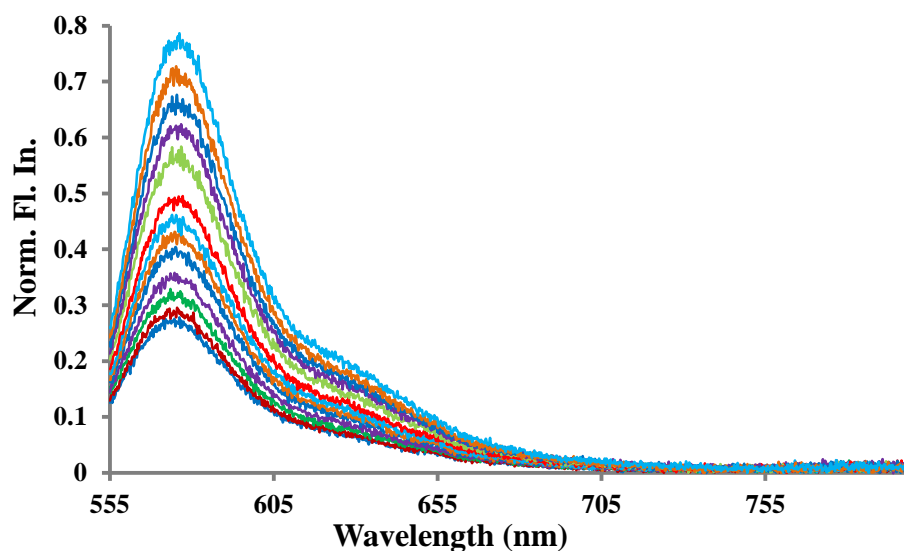


Figure 5.29. Fluorescence chart of **5.12** (10  $\mu\text{M}$ ) with 100  $\mu\text{M}$   $\text{Fe}(\text{ClO}_4)_3$  used to calculate LOD.

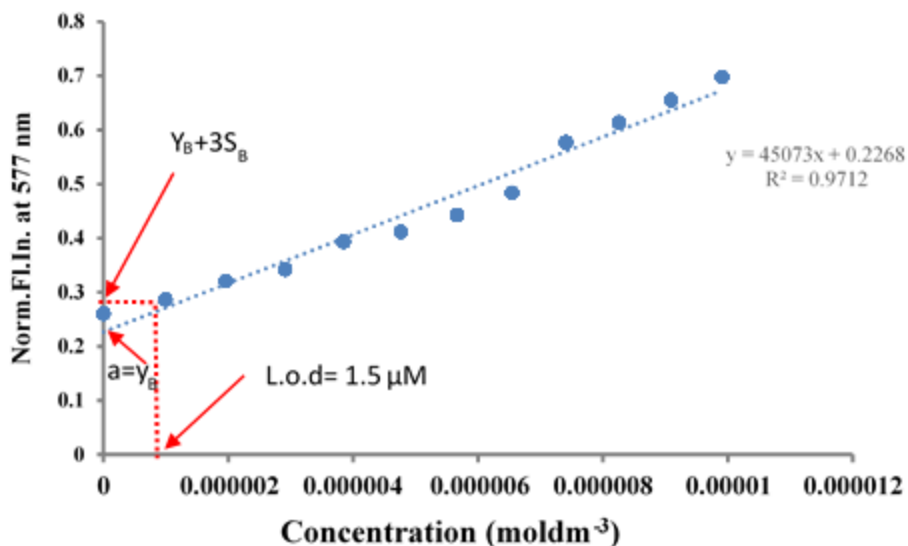


Figure 5.30. Calibration curve used to calculate the LoD for Fe<sup>3+</sup> with **5.12**.

#### Protocols to Distinguish Fe<sup>3+</sup> and Al<sup>3+</sup> Ions

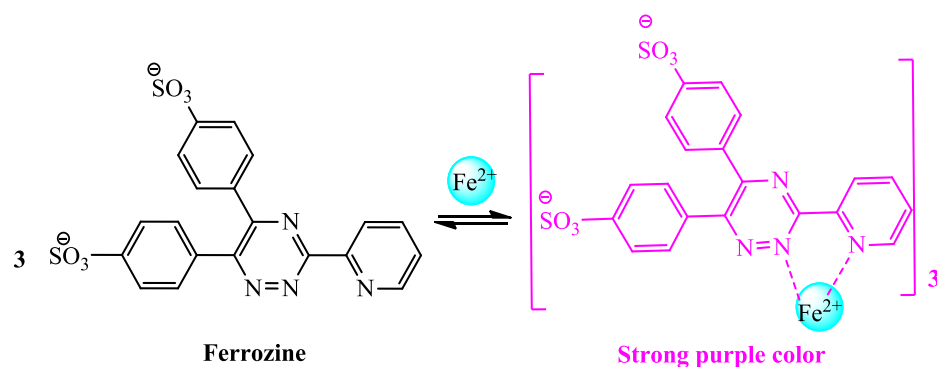
The molecular probes developed so far for the detection of Fe<sup>3+</sup> ions suffer from cross sensitivity towards competitive metal ions such as Al<sup>3+</sup> and Cr<sup>3+</sup> ions (to less extent).<sup>180, 210, 211</sup> Upon the review of literature, many of the published work omit these two cations. Therefore, this brings into questions how selective these in the other molecular sensors.<sup>109, 179</sup> In particular, the Al<sup>3+</sup> ion gives almost identical response to Fe<sup>3+</sup> ions. This is a double edge sword because on the one hand, Al<sup>3+</sup> ion can aid our understanding in the coordination environment by using NMR but, yet Al<sup>3+</sup> ion can also interfere and compete with the molecular probe when targeting the Fe<sup>3+</sup> ions. This is not surprising as the Al<sup>3+</sup> ion has almost the same properties as Fe<sup>3+</sup> ions. For example, both Al<sup>3+</sup> and Fe<sup>3+</sup> ions have the same charges (+3) and are almost of the same ionic sizes. The Al<sup>3+</sup> ion has the size of (0.53 Å for tetrahedral and 0.68 Å for octahedral) while the size of Fe<sup>3+</sup> ion is (0.69 Å for low spin and octahedral, 0.79 Å for high spin and octahedral, 0.63 Å for high spin and tetrahedral).<sup>212</sup> Both Al<sup>3+</sup> and Fe<sup>3+</sup> ions are considered hard

Lewis acid and hence prefer to bind with a hard Lewis base such as oxygen atom.<sup>213</sup> Aluminium mostly exists as  $\text{Al}^{3+}$  ions while iron exists in both  $\text{Fe}^{3+}$  and  $\text{Fe}^{2+}$  ions.<sup>214</sup> The size of  $\text{Fe}^{2+}$  ion is 0.77 Å. Therefore, it is a challenge to make a sensor that is selective to  $\text{Fe}^{3+}$  ions over the  $\text{Al}^{3+}$  ion. Hence there is a need for methods that can distinguish  $\text{Fe}^{3+}$  and  $\text{Al}^{3+}$  ions. One way to distinguish  $\text{Fe}^{3+}$  and  $\text{Al}^{3+}$  ions is  $\text{Fe}^{3+}$  ion can be reduced to  $\text{Fe}^{2+}$  ion while  $\text{Al}^{3+}$  ion cannot be reduced to the  $\text{Al}^{2+}$  ion. There are a number of chemical means to reduce the  $\text{Fe}^{3+}$  ion to the  $\text{Fe}^{2+}$  ion for example, sodium ascorbate, hydroxylamine hydrochloride, sodium sulphite, zinc powder, and hydroquinone. Once  $\text{Fe}^{3+}$  ion is reduced to  $\text{Fe}^{2+}$  ions, it is known that particular reagents such as ferrozine and 1, 10-phenanthroline can be used to monitor the  $\text{Fe}^{2+}$  ion as these reagents give strong color upon the coordination with  $\text{Fe}^{2+}$  ion but not with the  $\text{Fe}^{3+}$  ion.

Based on the redox chemistry, we have developed two protocols using ferrozine and 1, 10- phenanthroline to distinguish between  $\text{Fe}^{3+}$  and  $\text{Al}^{3+}$  ions which are discussed detail below.

#### Protocol to Distinguish $\text{Fe}^{3+}$ and $\text{Al}^{3+}$ Ions Using Ferrozine

Ferrozine (3-(2-Pyridyl)-5,6-diphenyl-1,2,4-triazine-4',4''-disulfonic acid sodium salt) is a bidentate ligand that binds to  $\text{Fe}^{2+}$  ion in a 3:1. Upon the coordination of the  $\text{Fe}^{2+}$  ion, a strong purple color is seen (Scheme 5.8).<sup>215</sup> The molar absorption coefficient of ferrozine complex is  $30,000 \text{ L mol}^{-1} \text{ cm}^{-1}$ . The two sulfite groups ( $-\text{SO}_3^-$ ) on each ferrozine molecule keep the resulting complex soluble in water. The absorption band is seen in the visible region with  $\lambda_{\text{max}}=562 \text{ nm}$  (Figure 5.31).<sup>216, 217</sup> Ferrozine has previously been used to monitor  $\text{Fe}^{2+}$  ion in an aqueous system.



*Scheme 5.8.* Structures of ferrozine and its complex with  $\text{Fe}^{2+}$  ion (counter ion  $\text{Na}^+$ ).

The intense color of ferrozine complex with  $\text{Fe}^{2+}$  ion is due to the formation of a charge transfer complex which is defined as an association of two or more molecules in which the electronic charge from the  $d$ -orbitals is transferred to the empty  $\pi^*$ -orbitals of the ligand. There are two types of charge transfer complexes: metal to ligand charge transfer (MLCT) complexes such as  $\text{MnO}_4^-$ ,  $\text{CrO}_4^-$  and ligand to metal charge transfer complex (LMCT) complexes such as  $[\text{PtCl}_4]^{2-}$ . The charge transfer transitions are both spin-allowed ( $\Delta S = 0$ ) and laporte-allowed ( $\Delta l = \pm 1$ ) and hence intense-absorption bands are observed. Ferrozine complex with  $\text{Fe}^{2+}$  ions is classified as a metal to ligand charge transfer complex (MLCT) in which the electronic charge shifts from the molecular orbital with metal-like character ( $\text{Fe}^{2+}$  ion) to the antibonding ligand orbital of ferrozine.<sup>38, 218</sup>

One important criteria for MLCT transitions is that it needs a ligand with a high energy antibonding orbitals for examples strong field ligands ( $\text{CO}$ ,  $\text{CN}^-$  and  $\text{PR}_3$ ). Ligands with delocalized  $\pi$  orbitals such as 1,10-phenanthroline and bipyridine also provide suitable  $\pi^*$  orbitals.<sup>38, 219</sup>

In MLCT, the metal is formally oxidized (loses electron) while ligand is reduced (gains electron). Therefore, the more reducing the metal is and more oxidizing the ligand, the less energy the corresponding CT band will have and appears in the visible region. A

$\text{Fe}^{2+}$  ion complex will yield MLCT bands of lower energy than those of a  $\text{Fe}^{3+}$  ion complex.  $\text{Fe}^{2+}$  ion can be easily oxidized to  $\text{Fe}^{3+}$  ion whereas  $\text{Fe}^{3+}$  ion is not readily oxidized to  $\text{Fe}^{4+}$  ion. Therefore, in comparison to  $\text{Fe}^{2+}$  ion,  $\text{Fe}^{3+}$  ion does not give strong color with ferrozine and does not absorb in the visible region (Figure 5.31).<sup>219</sup>

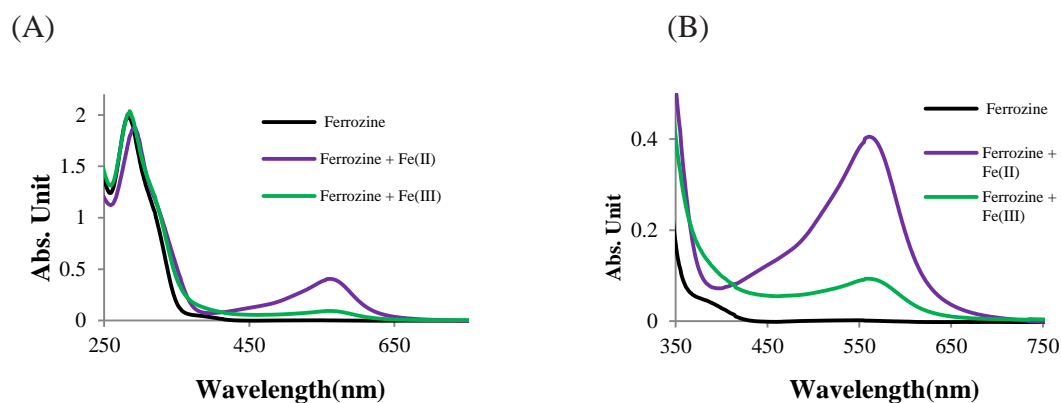
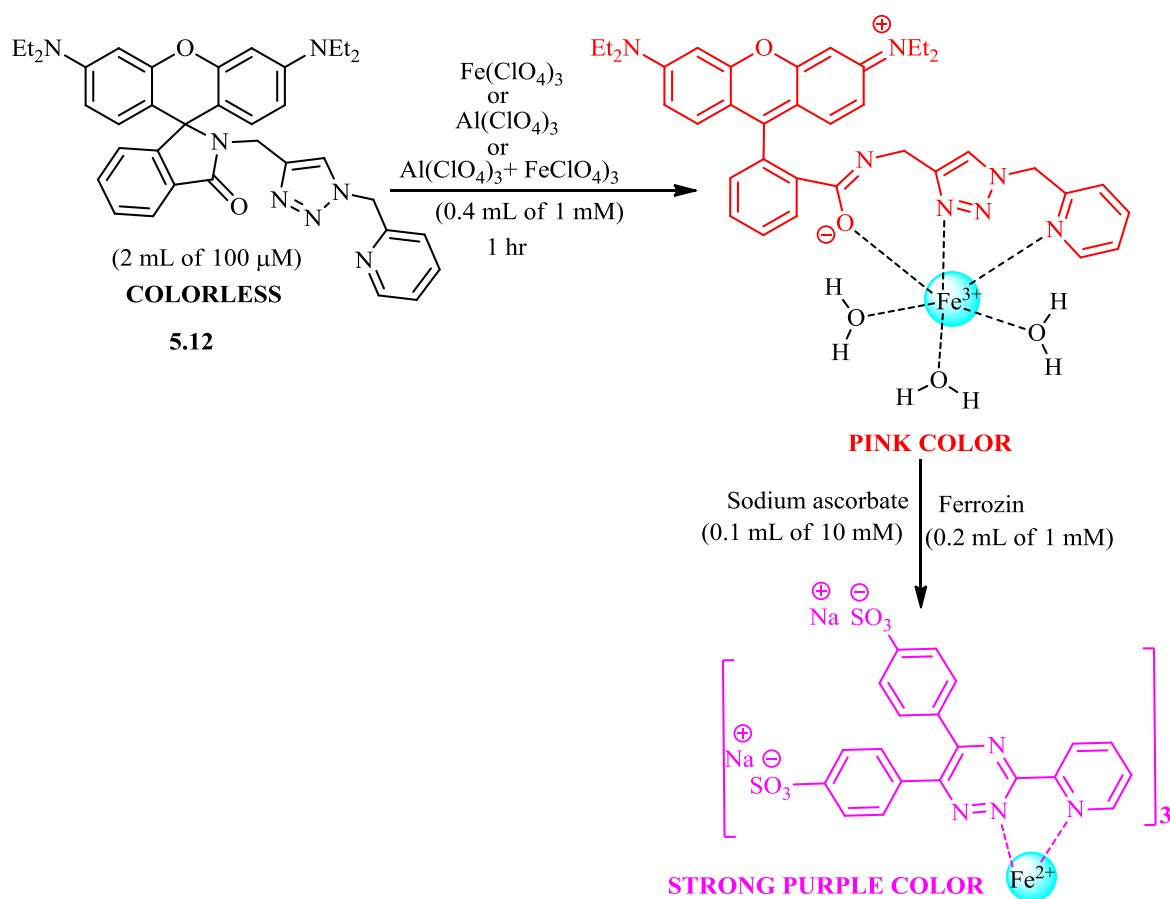


Figure 5.31. (A) UV-Vis spectrum of ferrozine (50  $\mu\text{M}$ ), its complex with  $\text{Fe}^{2+}$  (0.5 mM) and  $\text{Fe}^{3+}$  (0.5 mM) ions in 1:1 (EtOH:H<sub>2</sub>O) and (B) its UV-Vis absorbance from 350-750 nm.

### Protocol

The protocol is applied separately with each of  $\text{Fe}(\text{ClO}_4)_3$ ,  $\text{Al}(\text{ClO}_4)_3$  and for mixture of  $\text{Fe}(\text{ClO}_4)_3$  and  $\text{Al}(\text{ClO}_4)_3$  in three different ratios (3:1, 1:1, and 1:3) with compound **5.12** as discussed below.





Scheme 5.9. Representation of protocol using ferrozine to distinguish Fe<sup>3+</sup> and Al<sup>3+</sup> ions.

#### Addition of Fe(ClO<sub>4</sub>)<sub>3</sub>

The absorbance of the free ligand **5.12** (2 mL of 100 μM) prepared in 1:1 (EtOH:H<sub>2</sub>O) was recorded; there is a low absorbance band at 560 nm as shown by green spectrum in Figure 5.32. Then two equivalents of Fe(ClO<sub>4</sub>)<sub>3</sub> (400 μL of 1 mM Fe(ClO<sub>4</sub>)<sub>3</sub>) prepared in 1:1 (EtOH:H<sub>2</sub>O) was added into it. The solution turns pink red in color, and its absorbance was taken after one hour (shown by red spectrum in Figure 5.32). The pink red color is due to the formation of rhodamine complex with Fe<sup>3+</sup> ion as shown in Scheme 5.9.

In the next step, 100 μL of 10 mM sodium ascorbate prepared in H<sub>2</sub>O and 200 μL of one mM ferrozine prepared in H<sub>2</sub>O were added simultaneously into the solution. Sodium

ascorbate reduced  $\text{Fe}^{3+}$  ion to  $\text{Fe}^{2+}$  ion which then reacts with the ferrozine to form the ferrozine complex  $[\text{Fe}(\text{ferrozine})_3]^{2+}$  (Scheme 5.9). The change of color from pink to purple indicates the formation of ferrozine complex which is shown by the development of the purple color spectrum in Figure 5.32. The absorbance of the purple band is measured with increasing time interval of a few minutes until the color becomes constant as shown in Figure 5.32. The purple band has the same absorbance maximum as the rhodamine absorbance band however, the purple band is broad and ranges from 400-700nm.

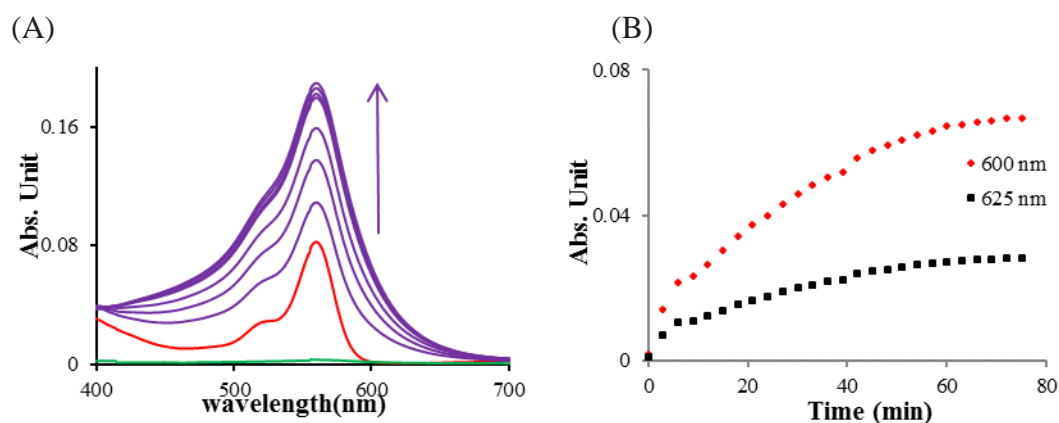


*Figure 5.32.* Ferrozine protocol with  $\text{Fe}(\text{ClO}_4)_3$  in 1:1 (EtOH:  $\text{H}_2\text{O}$ ). (A) UV-Vis absorbance of **5.12** ( $100 \mu\text{M}$ ) on addition of  $\text{Fe}(\text{ClO}_4)_3$  (1 mM), sodium ascorbate (10 mM), and ferrozine (1 mM) and (B) absorbance with increasing time interval.

#### *Addition of $\text{Al}(\text{ClO}_4)_3$*

The same experiment is repeated for  $\text{Al}(\text{ClO}_4)_3$ . In the case of  $\text{Al}(\text{ClO}_4)_3$ , the pink color did not change into purple color after addition of sodium ascorbate and ferrozine (Figure 5.33). This is reasonable as there is no  $\text{Fe}^{3+}$  ion in the solution.

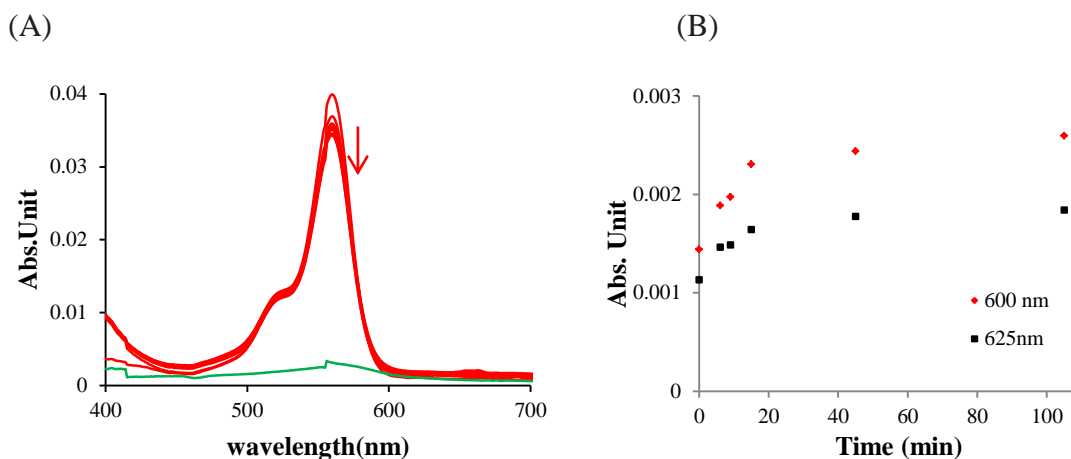


Figure 5.33. Ferrozine protocol with  $\text{Fe}(\text{ClO}_4)_3$  in 1:1 (EtOH:  $\text{H}_2\text{O}$ ). (A) UV-Vis absorbance of **5.12** (100  $\mu\text{M}$ ) on addition of  $\text{Al}(\text{ClO}_4)_3$  (1 mM), sodium ascorbate (10 mM), and ferrozine (1 mM) and (B) absorbance with increasing time interval.

#### Addition of $\text{Fe}(\text{ClO}_4)_3$ and $\text{Al}(\text{ClO}_4)_3$

Once it was established that the color is only turned on upon the reduction of  $\text{Fe}^{3+}$  to  $\text{Fe}^{2+}$ , we then looked at a mixed system. Three different ratios of  $\text{Al}(\text{ClO}_4)_3:\text{Fe}(\text{ClO}_4)_3$  (3:1, 1:1, or 1:3) were used for the study. The purple color is produced in all three different ratios. Figure 5.34 shows UV-Vis absorbance with 1:3 ( $\text{Fe}(\text{ClO}_4)_3:\text{Al}(\text{ClO}_4)_3$ ). However, the intensity of color is different which is reflected by the intensity of broad ferrozine band (purple color) from 400-700 nm. The intensity of ferrozine band is small when the  $\text{Fe}^{3+}$  ion is present in low amount in the mixture and vice versa. Hence, the intensity of broad ferrozine band can be used as the good indication for presence of  $\text{Fe}^{3+}$  ion amount in the solution. However, when  $\text{Al}^{3+}$  ion is present in low concentration in the mixture, this method is not good enough to indicate the presence of  $\text{Al}^{3+}$  ion.

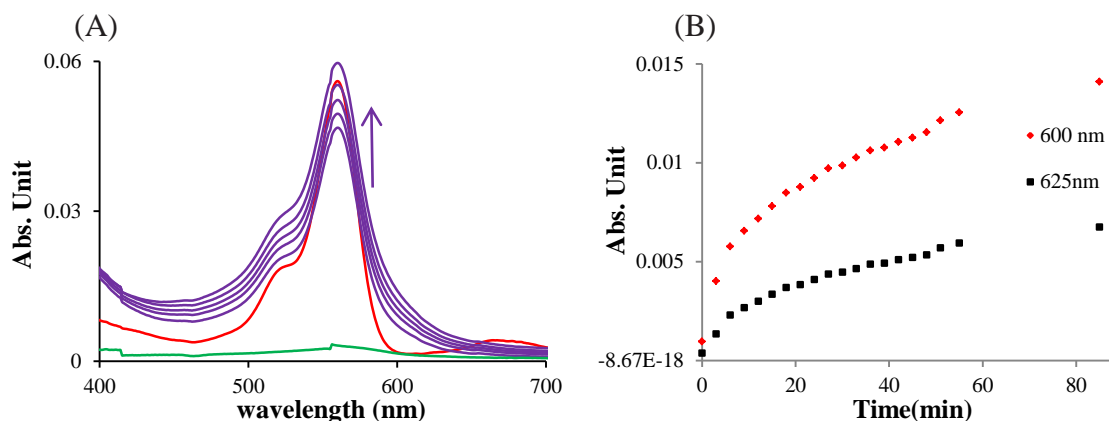


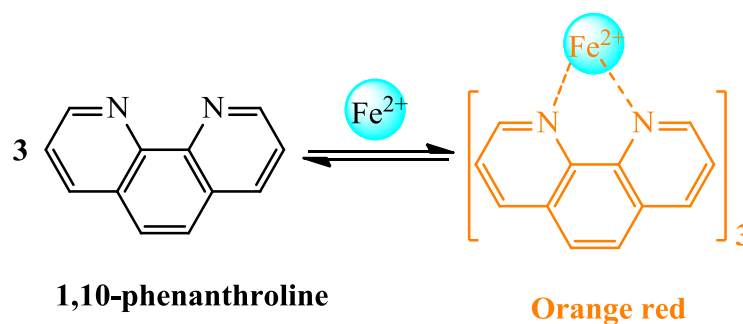
Figure 5.34. Ferrozine protocol with 1:3 ( $\text{Fe}(\text{ClO}_4)_3:\text{Al}(\text{ClO}_4)_3$  in 1:1 (EtOH:  $\text{H}_2\text{O}$ ). (A) UV-Vis absorbance of **5.12** ( $100\ \mu\text{M}$ ) on addition of 1:3 ( $\text{Fe}(\text{ClO}_4)_3:\text{Al}(\text{ClO}_4)_3$  ( $1\ \text{mM}$ ), sodium ascorbate ( $10\ \text{mM}$ ), and ferrozine ( $1\ \text{mM}$ ) and (B) absorbance with increasing time interval.

In summary, ferrozine can be used to distinguish  $\text{Fe}^{3+}$  and  $\text{Al}^{3+}$  ions as ferrozine produces strong purple color with  $\text{Fe}^{2+}$  ion which is formed by reduction of  $\text{Fe}^{3+}$  but not with  $\text{Al}^{3+}$  ion. One major disadvantage of this protocol is both ferrozine and rhodamine have the same absorbance maximum at  $560\ \text{nm}$  in UV-Vis spectroscopy. Though, ferrozine complex has broad band from  $400\text{--}700\ \text{nm}$  in comparison to  $500\text{--}600\ \text{nm}$  of rhodamine complex. The purple color of ferrozine complex is clearly distinguishable from the red color of rhodamine complex.

#### Protocol to Distinguish $\text{Fe}^{3+}$ and $\text{Al}^{3+}$ Ions Using 1, 10-Phenanthroline

Due to overlap of the absorption spectra, a different chromophore was used to shift the absorption band. A slightly modified protocol is developed; this time a 1, 10-phenanthroline indicator is used which also produces a strong orange red color with  $\text{Fe}^{2+}$  ion but not with  $\text{Fe}^{3+}$  ion (Scheme 5.10). The maximum absorbance of 1, 10-phenanthroline complex of  $\text{Fe}^{2+}$  ion is  $508\ \text{nm}$  which is clearly different from the rhodamine maximum absorbance at  $560\ \text{nm}$  (Figure 5.35). The molar absorptivity ( $\epsilon$ ) of the  $\text{Fe}^{2+}$  complex is  $11,100\ \text{Lmol}^{-1}\ \text{cm}^{-1}$  which indicates that the complex absorbs very

strongly. The intensity of the color is independent of pH in the range of 2-9. The complex is very stable, and the color intensity does not change appreciably long periods of time (Scheme 5.10).<sup>38, 220</sup>



Scheme 5.10. Structures of 1,10-phenanthroline and its complex with  $\text{Fe}^{2+}$  ion.

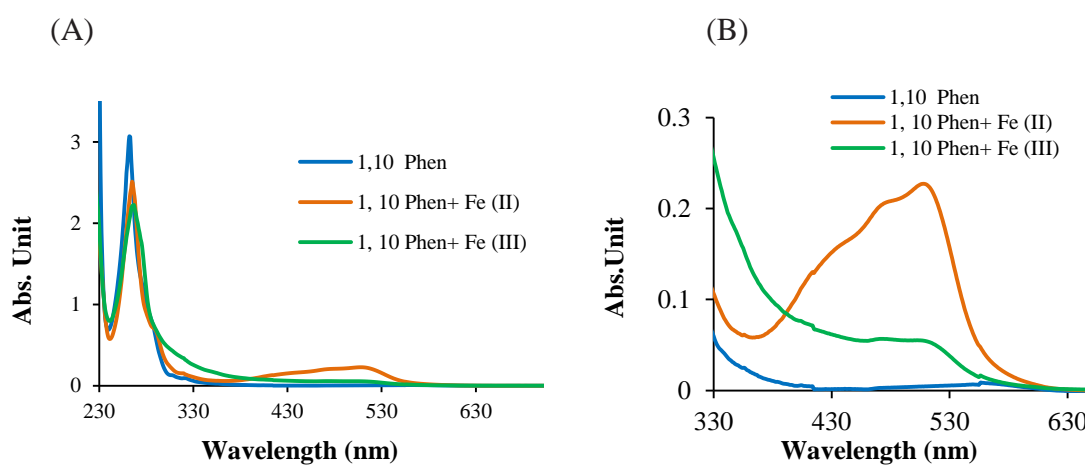
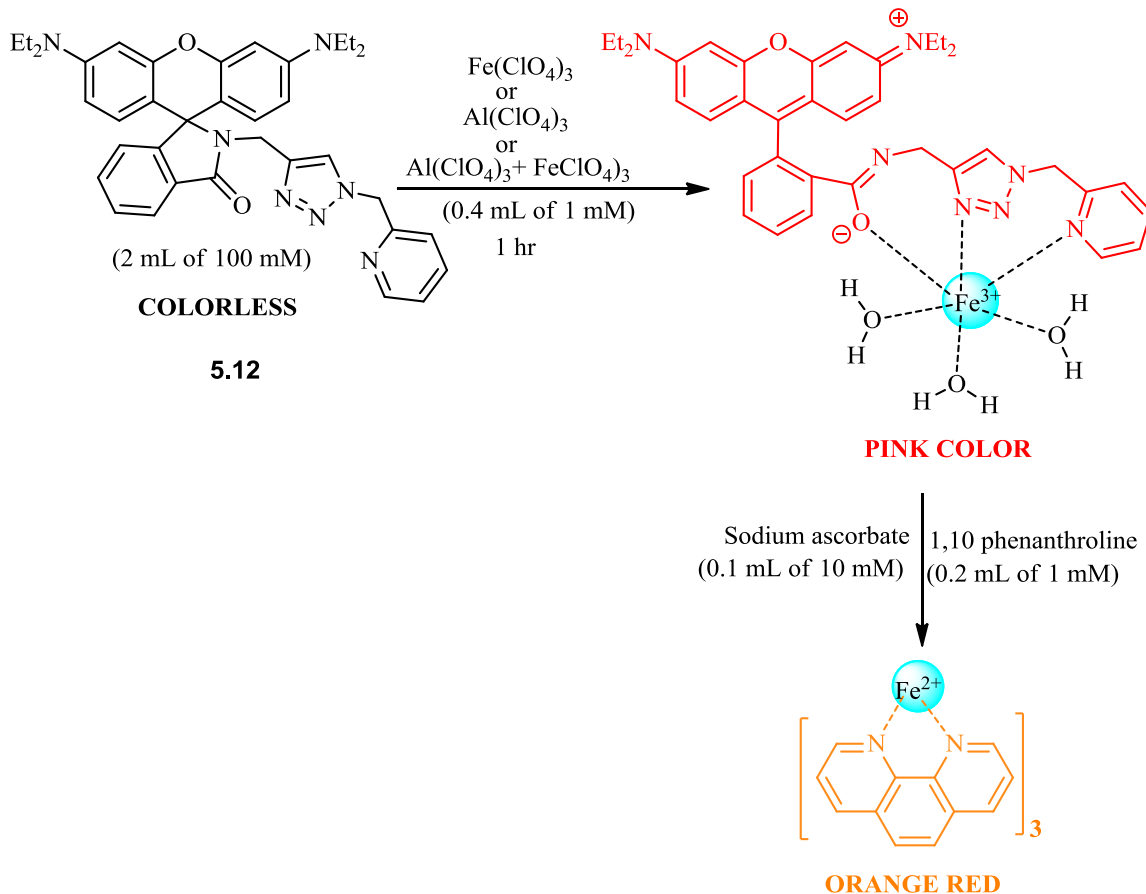


Figure 5.35. (A) UV-Vis spectrum of 1,10phenanthroline ( $50 \mu\text{M}$ ), its complex with  $\text{Fe}^{2+}$  ( $0.5 \text{ mM}$ ), and  $\text{Fe}^{3+}$  ( $0.5 \text{ Mm}$ ) ions in 1:1 (EtOH: $\text{H}_2\text{O}$ ) and (B) its UV-Vis absorbance from 330-630 nm.

## Protocol



*Scheme 5.11.* Representation of protocol using 1, 10-phenanthroline to distinguish  $\text{Fe}^{3+}$  and  $\text{Al}^{3+}$  ions.

This protocol is the same as the previous protocol described for the ferrozine (Scheme 5.11). The only difference is the use of 1, 10-phenanthroline instead of ferrozine. In this protocol, the pink color is slowly changed into orange red color upon addition of sodium ascorbate and 1,10-phenanthroline. Formation of orange red color indicates that 1,10-phenanthroline reacts with the  $\text{Fe}^{2+}$  ion produced by the reduction of  $\text{Fe}^{3+}$  ion with sodium ascorbate (Scheme 5.11). The orange red color band absorbs at 512 nm as shown in Figure 5.36 for protocol with  $\text{Fe}(\text{ClO}_4)_3$ . In case of protocol with  $\text{Al}(\text{ClO}_4)_3$ , the pink color is not changed into orange red color after addition of sodium

ascorbate and 1,10-phenanthroline (Figure 5.37). Therefore, there is no any absorbance band at 512 nm.

In the case of mixed protocol, the result is the same as the protocol for the mixture based on ferrozine except the difference in the color that is being formed. Figure 5.38 shows the UV-Vis absorbance with 1:1 ( $\text{Fe}(\text{ClO}_4)_3:\text{Al}(\text{ClO}_4)_3$ ). The intensity of orange red color band at 512 nm is small when  $\text{Fe}^{3+}$  ion is present in low concentration in the mixture and vice versa. Hence, the intensity of orange red band at 512 nm can be used as the good indication for presence of  $\text{Fe}^{3+}$  ion amount in the solution. However, when  $\text{Al}^{3+}$  ion is present in small amount in the mixture, this method is not good enough to indicate the presence of  $\text{Al}^{3+}$  ion.

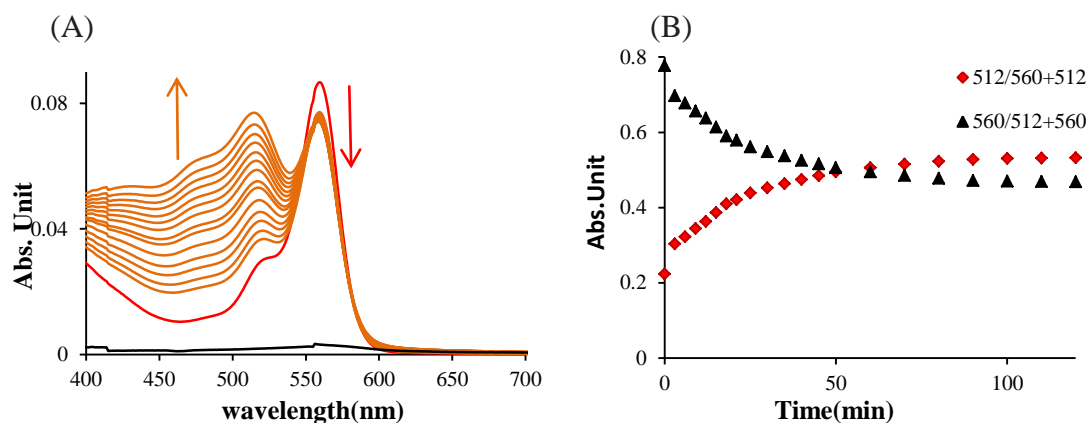


Figure 5.36. 1, 10-phenanthroline protocol with  $\text{Fe}(\text{ClO}_4)_3$  in 1:1 (EtOH:  $\text{H}_2\text{O}$ ). (A) UV-Vis absorbance of **5.12** ( $100 \mu\text{M}$ ) on addition of  $\text{Fe}(\text{ClO}_4)_3$  (1 mM), sodium ascorbate (10 mM), and 1, 10-phenanthroline (1 mM), and (B) absorbance with increasing time interval.

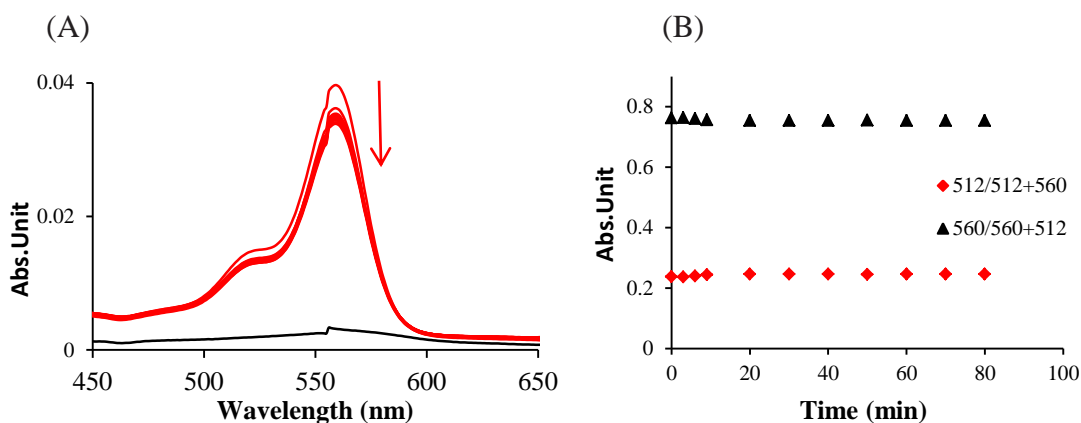


Figure 5.37. 1, 10-phenanthroline protocol with Al(ClO<sub>4</sub>)<sub>3</sub> in 1:1 (EtOH: H<sub>2</sub>O). (A) UV-Vis absorbance of **5.12** (100 μM) on addition of Al(ClO<sub>4</sub>)<sub>3</sub> (1 mM), sodium ascorbate (10 mM), and 1, 10-phenanthroline (1 mM), and (B) absorbance with increasing time interval.

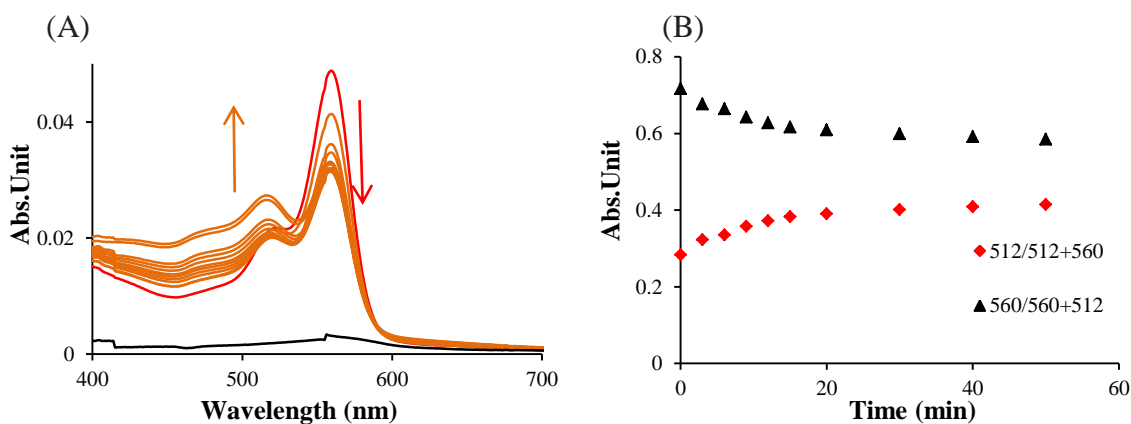


Figure 5.38. 1, 10-phenanthroline protocol with 1:1 (Fe(ClO<sub>4</sub>)<sub>3</sub>:Al(ClO<sub>4</sub>)<sub>3</sub>) in 1:1 (EtOH: H<sub>2</sub>O). (A) UV-Vis absorbance of **5.12** (100 μM) on addition of 1:1 (Fe(ClO<sub>4</sub>)<sub>3</sub>:Al(ClO<sub>4</sub>)<sub>3</sub>) (1 mM), sodium ascorbate (10 mM), and 1, 10-phenanthroline (1 mM), and (B) absorbance with increasing time interval.

In summary, 1,10-phenanthroline can be used to distinguish Fe<sup>3+</sup> and Al<sup>3+</sup> ions as 1,10-phenanthroline produces strong orange red color with Fe<sup>2+</sup> ion which is formed by reduction of Fe<sup>3+</sup> but not with Al<sup>3+</sup> ion. One advantage of this protocol is that orange red color gives the absorbance at 512 nm which is clearly different from the rhodamine maximum absorbance. However, both protocols can work only in UV-Vis spectroscopy.



Though they produce strong color with  $\text{Fe}^{2+}$  ion, their fluorescence is quenched and hence cannot be used to distinguish on the basis of fluorescence spectroscopy.

#### Cell imaging Studies of Molecular Probe **5.12** in Vero Cells

The importance of  $\text{Fe}^{3+}$  ion has previously been discussed (Chapter I). It is very important to know the concentration of metal ions, its speciation (what chemical form they are in?), and location in the cells and organism to understand the consequences of diseases, or any metal ion related biological process.<sup>221</sup> One way of obtaining this information is through live cell imaging which is the study of living cells using images acquired from microscopy (time-lapse microscopy, phase contrast microscopy, and fluorescent microscopy).<sup>222</sup> Live cell imaging allows for the study of dynamical physiological processes in living cells by giving a snapshot of the cells current state, and overtime can produce images from a single snap shot to a movie by combining the individual “snapshots.”<sup>223</sup> Live-cell imaging provides spatial and temporal information of dynamic molecular events in singles cells, cellular network (in situ), or even whole organisms (in vivo).<sup>224, 225</sup> Live-cell imaging is typically carried out with cultured cell lines (e.g., HeLa cells), primary cell cultures (e.g., skin cells, neural cells), acute slice preparations (e.g., brain slices), or whole organs or organism. HeLa cells is the most common type of cells used and frequently studied to show that a particular molecular probe works in a cell environment. However, different cells are needed to investigate a specific disease. One of the major proble is to keep cells alive and functioning as naturally as possible for duration of the experiment as the cells suffer from phototoxicity.<sup>226, 227</sup> Besides, false positives are commonly seen in the cell imaging

experiments. In particular with the imaging of free  $\text{Fe}^{3+}$  ion in the cells as all the cells need iron to grow.

Molecular probe **5.12** was studied for the detection of free intracellular  $\text{Fe}^{3+}$  ions in the living cells in Vero cell line cultures. The Vero cell line cultures were first grown overnight in 100 mL of basal media (BME). The cells were then grown in the microtiter plate until it reached a >90% confluent monolayer. Iron (III) chloride (100  $\mu\text{M}$ ) was added in the wells designated as test wells, and BME media is added in the separate well designated as negative control (no additional  $\text{FeCl}_3$ ). The plate was further incubated for 30 minutes. The cells were washed two times with sterile double distilled water, and 500  $\mu\text{L}$  of 100  $\mu\text{M}$  of **5.12** was added in each wells and further incubated for 30 min at 37  $^\circ\text{C}$ . The cells were then visualized by confocal microscopy. Phase contrast image was first taken to visualize the cells, and the same field was laser scanned in cy3/rhodamine settings which has an emission and excitation wavelength of 550 nm and 580 nm, respectively, to detect the fluorescence. Results from the confocal images showed that in absence of additional iron, compound **5.12** did not show any fluorescence; whereas in presence of additional iron, the cells were fluoresce red (Figure 5.39). Phase contrast images showed the presence of fairly equal number of cells in both test and negative control, which suggests the possibility that this compound has least toxicity towards the living cells; however a separate cell toxicity test will confirm this result. These results demonstrated that **5.12** can be used for detection of free intracellular  $\text{Fe}^{3+}$  ions in living cells.

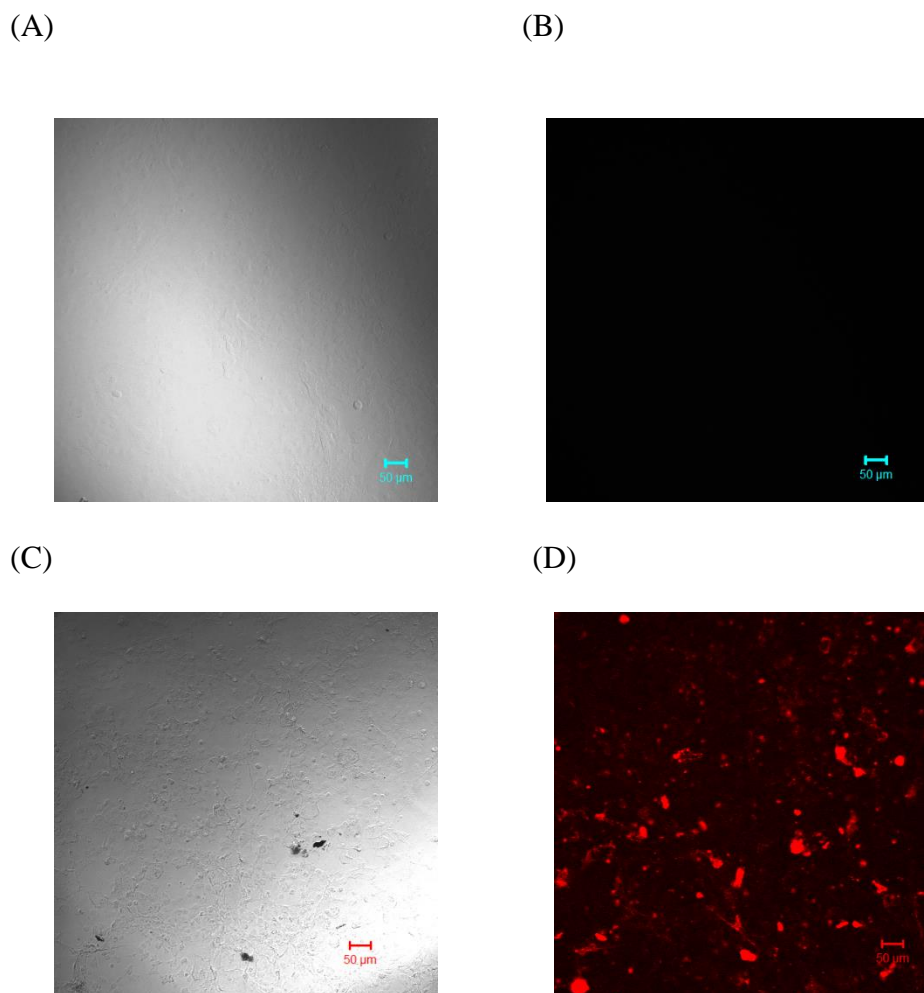


*Figure 5.39.* Confocal microscopy for detecting intracellular free iron using probe **5.12**. Phase contrast images (A and C) and fluorescence images (B and D) of Vero cells. The upper panel is negative control and the lower panel is the test with an additional iron.

#### Cell Imaging Studies of Molecular Probe **5.12** in Bacterial Cells

Iron also plays numerous diverse functions in bacterial cells.<sup>228</sup> The growth of many bacteria such as *Neisseria meningitides* depends on the availability of iron.<sup>229</sup> Iron influences cell composition, metabolism, enzyme activity, and host cell interaction which would include pathogenicity. The main functions of iron are catalytic rather than of a regulatory role. Iron, besides being co-factors for various proteins, can influence other components for the cells. For example, under iron-deficient conditions *Mycobacterium smegmatis* shows decreased DNA and RNA levels.<sup>228</sup>

A number of diseases are caused by the bacteria in humans. For example, cystic fibrosis is caused by the *Pseudomonas aeruginosa*<sup>230</sup> while *N. meningitidis* causes two serious human diseases, pyogenic meningitis and meningococcal septicemia.<sup>229</sup> Imaging of bacterial cell can help understand the diseases caused by them.

Therefore, molecular probe 5.12 was also tested for its ability to detect the free intracellular iron in the bacterial cells. The gram positive bacterium, *Staphylococcus aureus*, was used in this study as this bacterium has the ability to sequester and use intracellular iron as one of its virulent factor. *Staphylococcus aureus* causes a number of diseases in humans such as pneumonia (infections of the lungs) and bacteremia (bloodstream infection). It is the leading causes of skin and soft tissues infections such as abscesses (boils), furuncles, and cellulitis.<sup>231</sup>

As previously described, 100  $\mu\text{M}$   $\text{FeCl}_3$  was added in the over nightly grown cells and incubated for additional 30 min. The bacterial cells were collected by centrifugation and washed two times with sterile double distilled water. The cells were then suspended in 100  $\mu\text{L}$  of 100 mM probe **5.12**. 10  $\mu\text{L}$  of the bacterial suspension was added in the slide, covered with the lifter slide, and then images were taken by confocal microscope. The bacterial cells suspension without any additional iron was used as a negative control. Phase contrast image of the bacterial cell was first taken to visualize the cells, and the same field was laser scanned in cy3/rhodamine settings which has an emission and excitation wavelength of 550 nm and 580 nm, respectively, to detect the presence of any fluorescence. The preliminary data shows that the confocal images highlights that the bacterial cells in absence of any additional iron did not show any fluorescence; whereas in presence of additional iron, the bacterial cells were fluoresced red (Figure 5.40). Phase

contrast images, besides showing the presence of bacteria, also showed the presence of fairly equal number of cells in both test and negative control, which suggests that the fluoresces produced in the test is due to presence of free intracellular detected by the probe and not due to any background fluoresce. These results showed that this probe can be used to detect intracellular iron in the eukaryotic living cells as shown previously by many researchers, but this compound can also be used to detect the intracellular iron in the prokaryotic cells like bacteria.

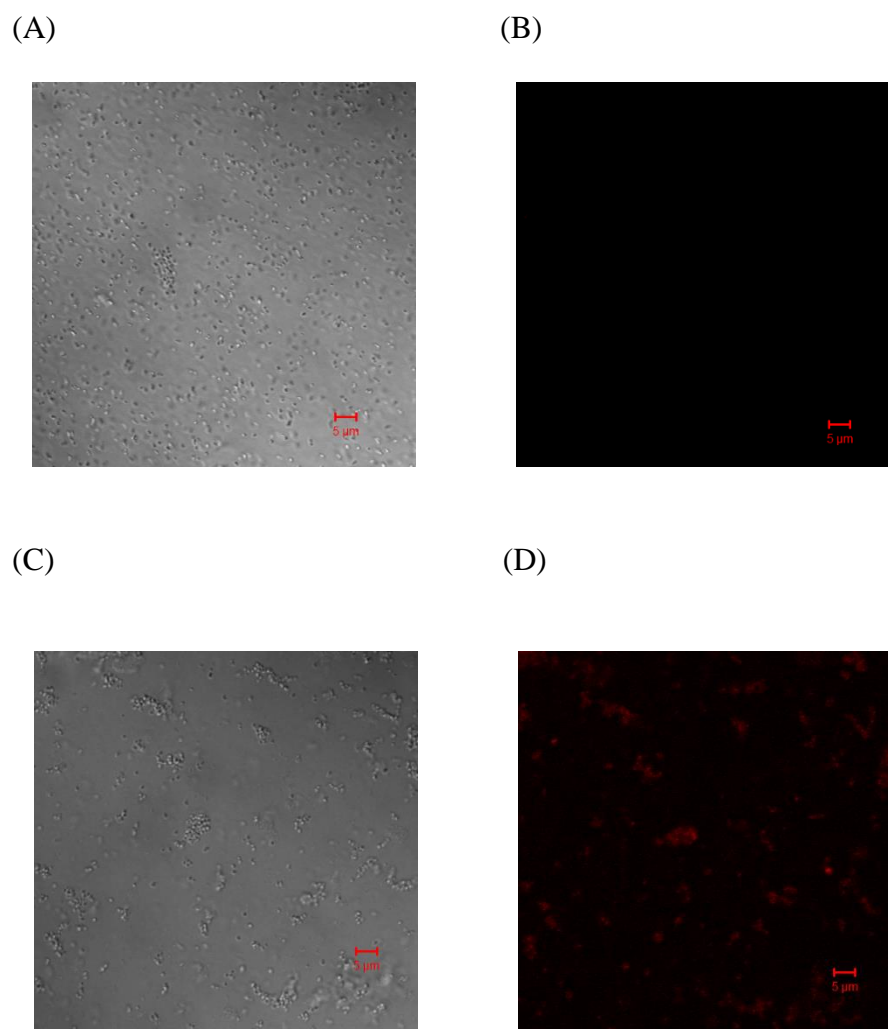


*Figure 5.40.* Confocal microscopy for detecting intracellular free iron using probe **5.12**. Phase contrast images (A and C) and fluorescence images (B and D) of gram positive bacterium, *Staphylococcus aureus*. The upper panel is negative control and the lower panel is the test with an additional iron.

To further verify the results from the confocal microscopy, the fluorescence, produced from the bacterial cells after addition of excess iron ( $100\ \mu\text{M}$ ) and in presence of probe ( $100\ \mu\text{M}$ ), was also analyzed by using the fluorometer. The result of the test samples (bacterial cells with different source of excess iron and probes **5.12**) showed the enhancement of fluorescence compared to those of controls (probes **5.12** only, bacterial cells only, bacterial cells with probes **5.12** and bacterial cells without excess iron) (Figure 5.41). This suggests that the increased fluorescence produced in the test is because of the presence of increased concentration of free intracellular iron in the bacterial cells grown in the presence of excess free iron, and not just because of background and/or contamination of any residual iron concentration from the growth media.

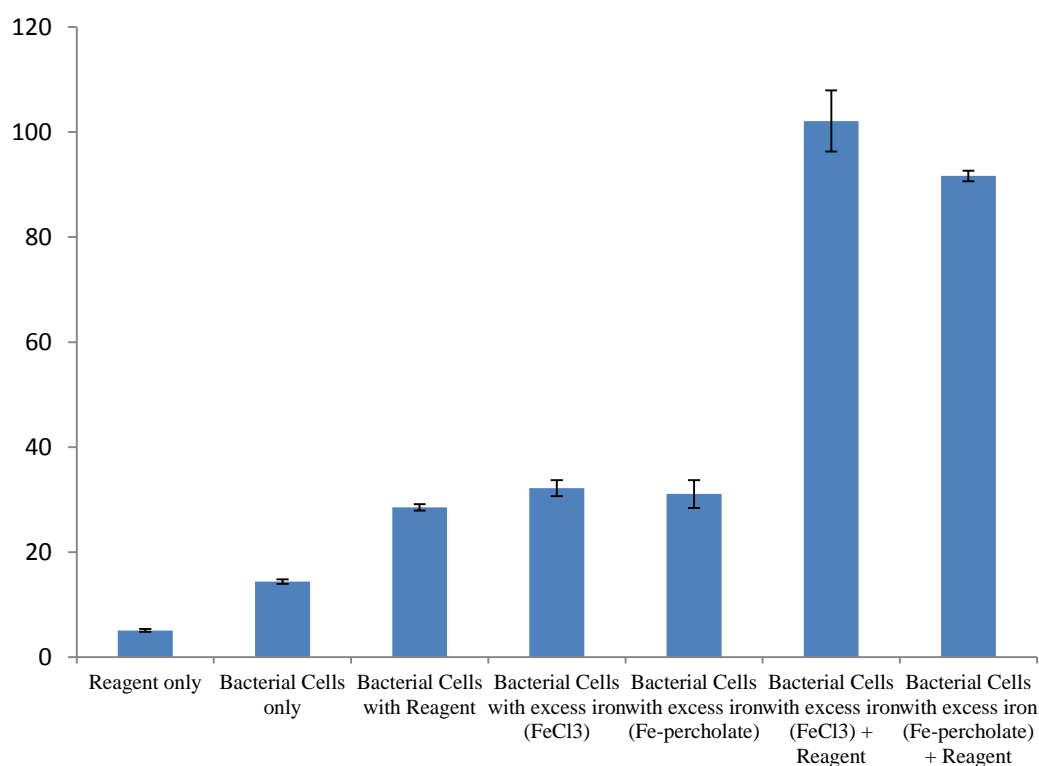


*Figure 5.41.* Fluorescence of bacterial cells showing enhancement upon addition of additional  $\text{FeCl}_3$  or  $\text{Fe}(\text{ClO}_4)_3$ .

## Summary

In summary, a rhodamine-based triazole chemosensors were synthesized by azide-alkyne Huisgen cycloaddition reaction between 3', 6'-bis(diethylamino)-2-(prop-2-ynyl)spiro [isoindoline-1,9'-xanthen]-3-one (**5.7**) and benzy azide (**5.8**) or picolyl azide(**5.9**) or methyl 2, 3, 4-tri-*O*-acetyl-6-azido-6-deoxy- $\alpha$ -D-glucopyranoside (**5.10**). The structure of compounds **5.11** and **5.12** were also confirmed by X-ray crystal structures which showed that xanthen ring and spirolactam ring was orthogonal to each other. The UV-Vis and fluorescence studies of compound **5.11**, **5.12**, and **5.13** with different metal ions showed the high selectivity for  $\text{Fe}^{3+}$  and  $\text{Al}^{3+}$  ions in aqueous ethanol solution of 1:1 (EtOH :H<sub>2</sub>O) at pH 7.1. Job's plot and Benesi-Hildebrand plot showed that the compound **5.12** and **5.13** was binding with  $\text{Fe}^{3+}$  or  $\text{Al}^{3+}$  ions in a 1:1 stoichiometry.

Binding of compounds **5.11**, **5.12**, and **5.13** with  $\text{Al}(\text{ClO}_4)_3$  is also supported by 1D (<sup>1</sup>H NMR and <sup>13</sup>C NMR) and 2D NMR spectroscopy with the  $\text{Al}^{3+}$  ion coordinated by carbonyl oxygen and triazole nitrogen atoms. This is further supported by the reduction of carbonyl group stretching band on IR spectrum. Detection limit was in the ppb range. The confocal microscopy experiment showed that the compound **5.12** could be used to detect the intracellular  $\text{Fe}^{3+}$  in live Vero and bacterial (*Staphylococcus aureus*) cells.

## Experimental

### *General procedure for UV-Vis and fluorescence experiments*

A stock solution of all compounds was prepared in EtOH. Final concentration of solution (50  $\mu\text{M}$  for UV-Vis and 20  $\mu\text{M}$  for Fluorescence experiment) was prepared by diluting the stock solution with deionized H<sub>2</sub>O to make final 1:1 (EtOH:H<sub>2</sub>O) solution.

The solution was excited at  $\lambda = 550$  nm and scanned from  $\lambda = 555$ -800 nm with slit widths set to 0.5 nm. A ten times more concentrated solution of the metal salt was prepared in 1:1 (EtOH:H<sub>2</sub>O), and 20  $\mu$ L (20  $\mu$ L = 0.1 equivalent of metal salt) aliquots were added to compound. Fluorescence spectra were recorded after each addition. Dilution factors were taken into consideration upon binding study determination. The binding constants were determined from fluorescence titrations using HypSpec 2006.<sup>116</sup>

#### *General procedure for <sup>1</sup>H NMR experiment*

A solution of 9.77 mM for **5.12** or **5.13** was prepared by dissolving 3 mg in 0.5 mL CD<sub>3</sub>CN. A ten times more concentrated solution of Al(ClO<sub>4</sub>)<sub>3</sub> was prepared in CD<sub>3</sub>CN and 5  $\mu$ L (5  $\mu$ L = 0.1 equivalent of metal salt) aliquot was added to compound, and the <sup>1</sup>H NMR spectrum recorded after each addition. The binding studies were pursued by <sup>1</sup>H NMR titrations using HypNMR 2008.<sup>141</sup>

#### General Procedure for the Synthesis

##### *Preparation of picolyl azide (5.9)<sup>201</sup>*

In a round bottom flask, picolylhydrochloride (505 mg, 2mmol), 18-Crown-6 (1-2 mg, as catalyst), and TBAI (1-2 mg, as catalyst) were dissolved in 10 mL DMF. DIPEA (0.34 mL) was added to this stirred solution. Lastly, NaN<sub>3</sub> was added, and the solution was stirred for overnight. Then the solution was diluted with EtOAc (100mL), rinsed with basic brine (made by adding some pellets of NaOH to saturated NaCl and then pH is measured, pH $\geq$ 10), followed by washing with NH<sub>4</sub>Cl (50 mL, 2 times). The organic layer was then dried over Na<sub>2</sub>SO<sub>4</sub>, and the solvent removed to afford the pure product as yellow oil (80 % yield).



$^1\text{H}$  NMR (300 K,  $\text{CDCl}_3$ , 400MHz):  $\delta$  8.62(d,  $J=4.3\text{Hz}$ , 1H), 7.73(td,  $J=1.8$  and  $7.7\text{Hz}$ , 1H), 8.62(d,  $J=4.3\text{Hz}$ , 1H), 7.35(d,  $J=7.8\text{Hz}$ , 1H), 7.26(m,  $J=1\text{H}$ ), 4.5(s, 2H)

*Preparation of 3',6'-bis(diethylamino)-2-(prop-2-ynyl)spiro [isoindoline-1,9'-xanthen]-3-one (5.7)*<sup>200</sup>

To a solution of Rhodamine B (958 mg, 2mmol) in 20mL of anhydrous dichloromethane was sequentially added HoBt (406mg, 3mmol), EDC (531  $\mu\text{L}$ , 3mmol), and propargylamine (192.13  $\mu\text{L}$ , 3mmol). The reaction mixture was stirred at room temperature for 2 days under anhydrous condition. The reaction mixture was diluted with dichloromethane and washed with sodium bicarbonate, brine, and water. The combined organic layers were dried over anhydrous sodium sulfate, filtered, and evaporated under reduced pressure to get the crude residue which was dissolved in a small amount of dichloromethane and left in a hood for overnight. A pink white solid is crystallized from it which is filtered by washing with hexane only. The pink white solid was then column chromatographed using 2:8 (Ethyl acetate: Hexane) to get 3', 6'-bis (diethylamino)-2-(prop-2-ynyl) spiro [isoindoline-1,9'-xanthen]-3-one (**5.7**) as pure white solid in 80% yield.

$^1\text{H}$  NMR (300 K,  $\text{CDCl}_3$ , 400MHz):  $\delta$  7.92 (m, 1H), 7.42(m, 2H), 7.10 (m, 1H), 6.46 (d,  $J=8.8\text{Hz}$ , 2H), 6.39 (d,  $J=2.48\text{Hz}$ , 2H), 6.27 (dd,  $J=9$  Hz, 2.5, 2H), 3.95 (d, $J=2.55\text{Hz}$ , 2H), 3.34 (q,  $J=7\text{Hz}$ , 8H), 1.75 (t,  $J=2.5\text{Hz}$ ,1H), 1.14 (t,  $J=7\text{Hz}$ ,12H)

$^{13}\text{C}$  NMR (300 K,  $\text{CDCl}_3$ , 400MHz):  $\delta$ 167.36, 153.76, 153.49, 148.87, 132.61, 130.44, 129.04, 127.98, 127.98, 123.78, 123.03, 108.02, 105.13, 97.82, 78.3, 70.01, 64.78, 44.37, 28.51, 12.57

IR (ATR solid); 3299  $\nu_{\text{C}=\text{CH}}$  (m), 3053  $\nu_{\text{C}=\text{CH}}$  (w), 2966, 2929, 2892  $\nu_{\text{C-H}}$  (w), 1693  $\nu_{\text{C}=\text{O}}$  (vs)  $\text{cm}^{-1}$ .

*General procedure for preparation of compounds 5.11, 5.12 and 5.13*<sup>190, 200</sup>

Compound **5.7** (480 mg, 1 mmol), picolyl azide **5.9** (135 mg, 1 mmol), copper (II) sulfate (13 mg, 0.05 mmol), and sodium ascorbate (20 mg, 0.1 mmol) were dissolved in a mixture of tertiary butanol and water solution (1:1, 20-30 mL) and refluxed for overnight. TLC of the reaction mixture was checked to see the completion of reaction. Then, the reaction mixture was cooled, poured into ice cold water, and extracted with ethyl acetate (3x30 mL). The combined ethyl acetate was dried over magnesium sulphate, filtered and evaporated to get the residue which was column chromatographed to get the pure compound (70% yield).

Characterization of **5.11**:

<sup>1</sup>H NMR (300 K, CDCl<sub>3</sub>, 400MHz):  $\delta$ 7.86 (m, 1H), 7.52(m, 2H), 7.33-7.41(m, 3H), 7.21 (d,  $J=6.6\text{Hz}$ , 2H), 7.14 (s, 1H), 6.98-7.04(m, 1H), 6.36 (d,  $J=2.3\text{Hz}$ , 2H), 6.28 (d,  $J=8.9\text{Hz}$ , 2H), 6.23 (dd,  $J=2.5\text{ Hz}$ , 2H), 5.29 (s, 2H), 4.33 (s,2H), 3.36 (q,  $J=7\text{Hz}$ , 8H), 1.15 (t,  $J=7\text{Hz}$ ,12H)

<sup>13</sup>C NMR (300 K, CDCl<sub>3</sub>, 400MHz):  $\delta$ 168.37, 155.04, 154.28, 149.88, 145.25, 136.90, 133.73, 131.73, 129.87, 129.74, 129.30, 128.93, 124.47, 123.84, 123.56, 109.09, 106.17, 98.39, 65.58, 54.19, 44.04, 35.94, 12.89

IR (ATR solid): 2968 $\nu_{\text{C-H}}$  (w), 1685  $\nu_{\text{C}=\text{O}}$  (vs)  $\text{cm}^{-1}$ .

Anal. Calcd for C<sub>38</sub>H<sub>40</sub>N<sub>6</sub>O<sub>2</sub>: H 6.57 %; N 13.71 %; C; 74.48 %

Anal. Recalcd for C<sub>38</sub>H<sub>40</sub>N<sub>6</sub>O<sub>2</sub>·0.5H<sub>2</sub>O: H 6.64 %; N 13.51 %; C; 73.40 %

Found for C<sub>38</sub>H<sub>40</sub>N<sub>6</sub>O<sub>2</sub>·0.5H<sub>2</sub>O: H 6.63 %; N 13.39 %; C; 73.67 %

Characterization of **5.12**:

$^1\text{H}$  NMR (300 K,  $\text{CDCl}_3$ , 400MHz):  $\delta$  8.54 (d,  $J=4.79\text{Hz}$ , 1H), 7.92 (m, 1H), 7.59 (m, 1H), 7.44 (m, 2H), 7.19 (m, 1H), 7.15 (s, 1H), 7.09 (m, 1H), 6.89 (d,  $J=7.8\text{Hz}$ , 1H), 6.34 (d,  $J=2.56\text{Hz}$ , 2H), 6.29 (d,  $J=8.85\text{Hz}$ , 2H), 6.14 (dd,  $J=8.9\text{ Hz}$ , 2.6, 2H), 5.39 (s, 2H), 4.48 (s, 2H), 3.30 (q,  $J=7\text{Hz}$ , 8H), 1.14 (t,  $J=7\text{Hz}$ , 12H)

$^{13}\text{C}$  NMR (300 K,  $\text{CDCl}_3$ , 400MHz):  $\delta$  167.88, 154.94, 153.44, 149.50, 148.73, 144.90, 137.08, 132.52, 130.96, 128.74, 128.03, 123.05, 122.90, 121.71, 107.83, 105.34, 97.92, 65.03, 55.11, 44.35, 35.35, 12.61

IR (ATR solid): 2968  $\nu_{\text{C-H}}$  (w), 1685  $\nu_{\text{C=O}}$  (vs)  $\text{cm}^{-1}$ .

Anal. Calcd for  $\text{C}_{37}\text{H}_{39}\text{N}_7\text{O}_2$ : H 6.40 %; N 15.97 %; C; 72.40 %

Anal. Recalcd for  $\text{C}_{37}\text{H}_{39}\text{N}_7\text{O}_2 \cdot 0.5\text{H}_2\text{O}$ : H 6.47 %; N 15.74 %; C; 71.36 %

Found for  $\text{C}_{37}\text{H}_{39}\text{N}_7\text{O}_2 \cdot 0.5\text{H}_2\text{O}$ : H 6.43 %; N 15.75 %; C; 71.61 %

Characterization of **5.13**:

$^1\text{H}$  NMR (300 K,  $\text{CD}_3\text{CN}$ , 400MHz):  $\delta$  7.83 (m, 1H), 7.85 (m, 1H), 7.08 (s, 1H), 7.00 (m, 1H), 6.33 (d,  $J=1.2\text{Hz}$ , 2H), 6.26 (d,  $J=1.8\text{Hz}$ , 2H), 6.23 (d,  $J=1.8\text{Hz}$ , 2H), 5.30 (m, 1H), 4.78 (m, 3H), 4.30 (m, 3H), 4.12 (m, 1H), 4.01 (m, 1H), 3.33 (q,  $J=7\text{Hz}$ , 8H), 3.06 (s, 3H,  $\text{CH}_3$ ), 2.00 (s, 3H,  $\text{CH}_3$ ), 1.97 (s, 3H,  $\text{CH}_3$ ), 1.94 (s, 3H,  $\text{CH}_3$ ), 1.12 (t,  $J=7\text{Hz}$ , 12H)

$^{13}\text{C}$  NMR (300 K,  $\text{CD}_3\text{CN}$ , 400MHz):  $\delta$  171.01, 170.92, 170.69, 168.23, 154.88, 154.32, 149.88, 144.85, 133.72, 131.89, 129.81, 129.79, 129.31, 124.87, 124.51, 123.52, 109.12, 109.08, 106.27, 98.35, 98.32, 97.58, 71.30, 70.63, 70.46, 68.79, 66.57, 56.88, 50.98, 45.07, 35.86, 21.02, 20.91, 20.86, 12.92

IR (ATR solid) 2965  $\nu_{\text{C-H}}$  (w), 1746  $\nu_{\text{C=O}}$  (vs) 1685  $\nu_{\text{C=O}}$  (vs)  $\text{cm}^{-1}$ .

Anal. Calcd for  $\text{C}_{44}\text{H}_{52}\text{N}_6\text{O}_{10}$ : H 6.35 %; N 10.18 %; C; 64.06 %

Anal. Recalcd for  $\text{C}_{44}\text{H}_{52}\text{N}_6\text{O}_{10} \cdot 0.5\text{H}_2\text{O}$ : H 6.40 %; N 10.07 %; C; 63.37 %

Found for  $C_{37}H_{39}N_7O_2 \cdot 0.5H_2O$ : H 6.36 %; N 9.80 %; C; 63.38 %

#### Protocol for Bacterial Cell Imaging

Bacterial cells were grown in a Tryptic Soy Agar (TSA) plate from the  $-80^{\circ}C$  freezer stock culture. A loopful of bacterial cells were inoculated into 5 ml of Tryptic soy Broth (TSB) and incubated overnight at  $37^{\circ}C$  with shaking at 200 rpm. The overnight culture was diluted 1:10 in 4 ml of pre-warmed TSB and further incubated at  $37^{\circ}C$  with shaking at 200 rpm for three hours. After incubation, 400  $\mu L$  of  $FeCl_3$  (1 mM) was added in the culture (Final Fe concentration, 100  $\mu M$ ) and further incubated for 30 min. In the negative control, 400  $\mu L$  of pre-warmed TSB was added. One mL of cells was aliquot in 1.5 mL microfuge tube and centrifuged at 10000 x g for 5 min to harvest the cells. The cells were washed twice with sterile distilled water. The supernatants were removed completely and discarded in each of the washing steps. The cells were resuspended in 100  $\mu L$  of 1 mM **5.12**, and 20  $\mu L$  of bacteria was spotted in the clean glass slide, covered with the lifter slide, and edges were sealed. Confocal microscopy images were taken in 100 X/0.63 oil immersions. Phase contrast images were taken to visualize the cells, and the same field was laser scanned in cy3/rhodamine settings with emission at 550 nm and excitation at 580 nm. The same settings were used to scan both control and experimental (iron supplemented condition) for taking images, and the experiment was performed at least three times to verify the result.

#### Protocol for Vero Cell Line Imaging

Growth and maintenance of Vero cell lines were performed as previously described by Ammerman et al. 2008. In brief, the cells were quickly thawed from the stock cryovial in 10 ml of DMEM media supplemented with FBS. The cells were grown

overnight with shaking at 37°C with 5% CO<sub>2</sub>. The cells were pelleted by centrifugation at 200 x g for 5 min. Approximately 4×10<sup>5</sup> cells were inoculated in 24-well sterile corsar microtiter plate with 500 μL of basal BME media and incubated further for 2-3 days until they reached a >90% confluent monolayer. 50 μL of FeCl<sub>3</sub> (1 mM) pre-warmed at 37°C was added in the media and further incubated for 30 min. In control, 50 μL of fresh media was added. After 30 min incubation, the media was aspirated completely and washed twice with sterile double distilled water. 200 μL of **5.12** (100 μM) reagent was added, and confocal microscopy images were taken. Phase contrast images were taken to visualize the cells, and the same field was laser scanned to visualize the fluorescence with emission and excitation wavelength of 550 nm and 580 nm, respectively (cy3/rhodamine). Same settings were used to scan both control and iron supplemented cells. The experiment was performed at least three times to confirm the result.

## CHAPTER VI

RHODAMINE BASED TWEEZERS FOR DETECTION OF  $\text{Fe}^{3+}$  AND  $\text{Al}^{3+}$  IONS

## Introduction

In Chapter V, rhodamine based molecular probes containing only one rhodamine unit were discussed for the detection of  $\text{Fe}^{3+}$  and  $\text{Al}^{3+}$  ions. In these systems for all three probes, both of the ions showed the same response regardless of the probes **5.11**, **5.12**, and **5.13**. These molecular probes do not have a definite binding pocket or cavity for these metal ions. It might be possible that the molecular probes have the correct binding pocket to selectively bind  $\text{Fe}^{3+}$  ion over  $\text{Al}^{3+}$  ion. Moreover, molecular probes containing multiple binding sites bind the metal ion more thermodynamically stable due to the chelate effect. Therefore, molecular probes containing two rhodamine units in the form of molecular cleft are designed and synthesized for the detection of  $\text{Fe}^{3+}$  ions. Furthermore, the molecular clefts are more preorganized (rigid) than the probes with only one rhodamine unit and hence bind the target metal ion stronger.

Yoon et al. synthesized two rhodamine compounds **6.1** and **6.2** bearing urea groups for detection of  $\text{Hg}^{2+}$  ion (Figure 6.1).<sup>232</sup> Compound **6.2** is synthesized as a molecular cleft with two pendent arms *meta* to each other. Compound **6.1** has only one rhodamine group and is synthesized as a model compound for compound **6.2**. The perchlorate salts of  $\text{Na}^+$ ,  $\text{K}^+$ ,  $\text{Li}^+$ ,  $\text{Ag}^+$ ,  $\text{Cs}^+$ ,  $\text{Mg}^{2+}$ ,  $\text{Ca}^{2+}$ ,  $\text{Hg}^{2+}$ ,  $\text{Zn}^{2+}$ ,  $\text{Mn}^{2+}$ ,  $\text{Cd}^{2+}$ ,  $\text{Ni}^{2+}$ ,  $\text{Co}^{2+}$ , and  $\text{Pb}^{2+}$  were used to evaluate the metal ion binding properties in  $\text{CH}_3\text{CN}$ . Model compound **6.1** showed large CHEF effects with  $\text{Hg}^{2+}$  and  $\text{Pb}^{2+}$  ions and relatively small CHEF effects with  $\text{Zn}^{2+}$  and  $\text{Cd}^{2+}$  ions. However, compound **6.2** showed a highly selective CHEF effect with  $\text{Hg}^{2+}$  ion with a little interference from  $\text{Zn}^{2+}$  ion. These could

be explained by the coordination of the oxygen atom in the carbonyl groups of urea and lactam which form a binding pocket for  $\text{Hg}^{2+}$  ions. Fluorescence emission and UV-Vis absorption of compound **6.2** was increased by more than 100 folds upon addition of 100 equivalents of  $\text{Hg}^{2+}$  ions. The association constants of **6.1** and **6.2** were calculated to be  $2.9 \times 10^4$  and  $3.2 \times 10^5 \text{ M}^{-1}$ , respectively, from fluorescence titration. Addition of excess 1,10-diaza-4,7,14,17-tetrathiacyclooctadecane decreases both fluorescence and absorption of the complex indicating the binding process is reversible. The spiro-carbon signal at 64.9 ppm in  $^{13}\text{C}$  NMR spectrum was disappeared in the presence of  $\text{Hg}^{2+}$  ion which further confirms the ring opening process of **6.2** (Scheme 6.1). However, they did not carry out any molecular modeling, IR and  $^1\text{H}$  NMR studies to confirm the geometry of the complex.

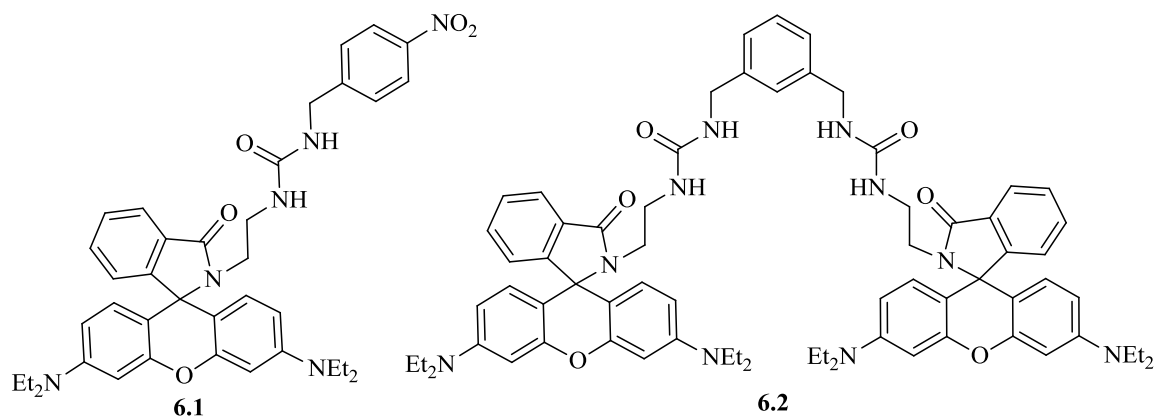
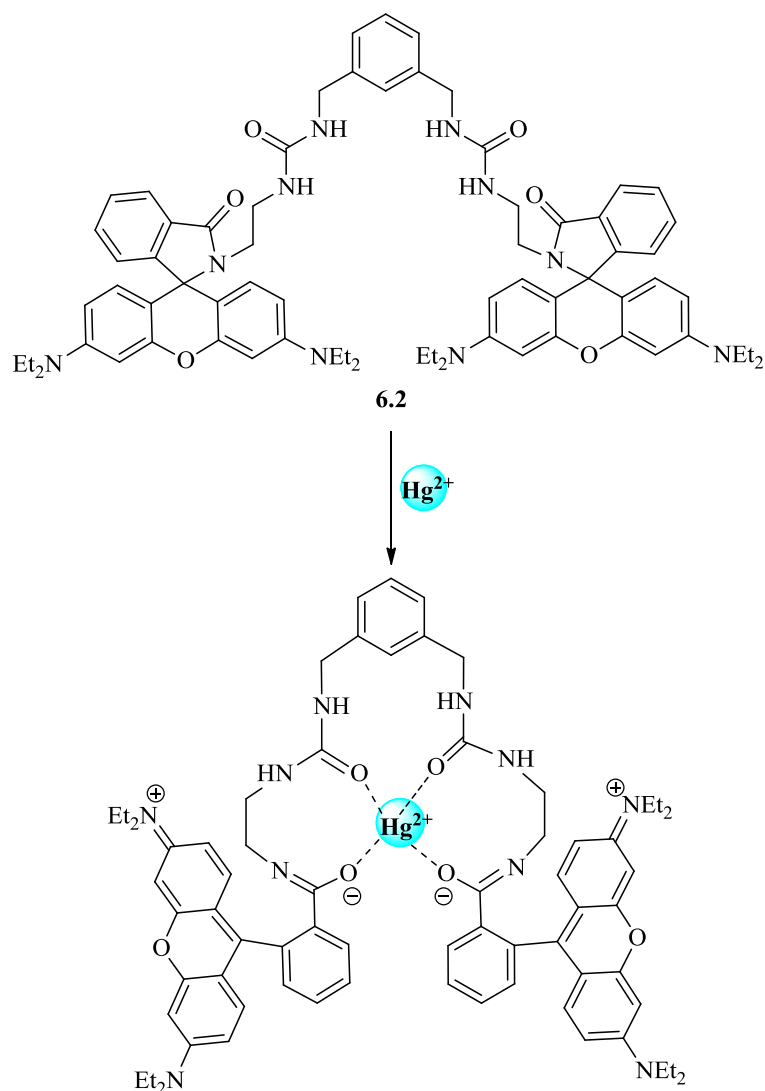


Figure 6.1. Structure of model compound **6.1** and molecular cleft **6.2**.



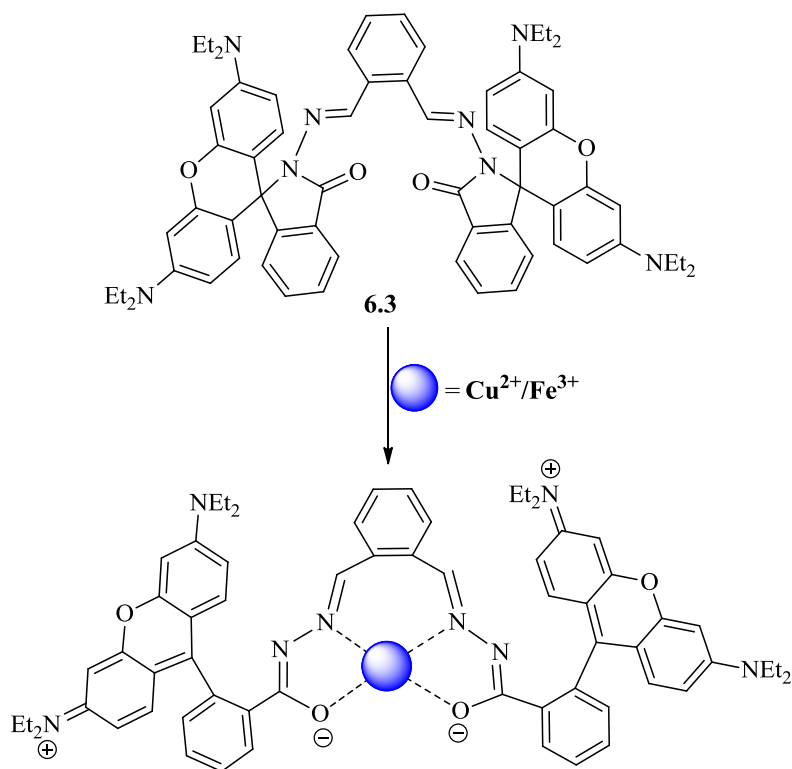
*Scheme 6.1.* Proposed structure for binding  $\text{Hg}^{2+}$  ion by compound **6.2**.<sup>232</sup>

Sinn et al. developed molecular cleft **6.3** with two rhodamine groups *ortho* to each other for detection of  $\text{Cu}^{2+}$  and  $\text{Fe}^{3+}$  ions.<sup>233</sup> The compound **6.3** was synthesized by refluxing rhodamine B hydrazide with phthalaldehyde in ethanol. The compound was designed to bind metal ions between two rhodamine groups through two carbonyl oxygen and imine nitrogen atoms. The spectroscopic properties were carried out in a 3:1 solution of  $\text{CH}_3\text{CN}$ : Tris-HCl (10 mM) buffer at pH 7.0. The compound **6.3** has no absorption band at 551 nm but showed a significant enhancement (180-folds) upon addition of 40



equivalents of  $\text{Cu}^{2+}$  ion. Interestingly, addition of  $\text{Fe}^{3+}$  ion also gave absorption band but at 562 nm with low (80 folds) enhancement compared to  $\text{Cu}^{2+}$  ion. Hypsochromic shift of the absorption band with  $\text{Cu}^{2+}$  ion could be due to the formation of H-aggregates.<sup>202</sup> It is well known that rhodamine dyes can aggregate in solution causing a bathochromic (J-type) or hypsochromic (H-type) shift in their absorption band. Other metal ions such as  $\text{Na}^+$ ,  $\text{K}^+$ ,  $\text{Zn}^{2+}$ ,  $\text{Cd}^{2+}$ ,  $\text{Hg}^{2+}$ ,  $\text{Pb}^{2+}$ ,  $\text{Ca}^{2+}$ ,  $\text{Mn}^{2+}$ ,  $\text{Co}^{2+}$ , and  $\text{Fe}^{2+}$  were also tested but found no effect on the absorbance. However, the authors did not mention the effect of  $\text{Al}^{3+}$  ion in their studies which has similar chemical properties with  $\text{Fe}^{3+}$  and  $\text{Cr}^{3+}$  ions. The compound **6.3** has weak fluorescence at 570 nm. Upon addition of 40 equivalents of  $\text{Fe}^{3+}$  ions, the fluorescence emission at 580 nm was enhanced by more than 13 folds. The fluorescence enhancement was much weaker than that of absorbance possibly due to a paramagnetic nature of  $\text{Fe}^{3+}$  ion. Interestingly,  $\text{Cu}^{2+}$  and  $\text{Cr}^{3+}$  ions increase the intensity by two and three folds, respectively, while other metal ions showed no enhancement. The emission enhancement of **6.3** with  $\text{Cu}^{2+}$  ion is negligible in comparison to that of its absorption. The weak fluorescence emission with  $\text{Cu}^{2+}$  could be due to the formation of H-aggregate which is non fluorescent on the basis of the exciton theory.<sup>234, 235</sup> The binding constant ( $K_{11}$ ) for  $\text{Cu}^{2+}$  ion was calculated to be  $1.6 \times 10^3 \text{ M}^{-1}$  by the Benesi-Hildebrand method in UV-Vis absorbance. While the binding constant ( $K_{11}$ ) was  $9.75 \times 10^2 \text{ M}^{-1}$  for  $\text{Fe}^{3+}$  ion in fluorescence. The detection limit was calculated based on absorption data and was found to be 69  $\mu\text{M}$  (4 ppm) for  $\text{Cu}^{2+}$  ion and 100  $\mu\text{M}$  (6 ppm) for  $\text{Fe}^{3+}$  ion.  $^1\text{H}$  NMR titration was carried out in  $\text{CD}_3\text{CN}$  to clarify the binding mechanism of  $\text{Cu}^{2+}$  ion. Addition of one equivalent of  $\text{Cu}^{2+}$  ion broadened and shifted the imine signal at 9.64 ppm in downfield direction indicating the involvement of imine

group in the coordination of  $\text{Cu}^{2+}$  ion. This suggests a decrease in electron density at imine nitrogen resulting from direct coordination with  $\text{Cu}^{2+}$  ion (Scheme 6.2).



Scheme 6.2. Proposed structure for binding  $\text{Cu}^{2+}/\text{Fe}^{3+}$  ions by compound **6.3**.<sup>233</sup>

There are only a handful of molecular probes that contain bisrhodamine system. Here, we report the synthesis of three rhodamine based molecular probes for detection of  $\text{Fe}^{3+}$  ion using triazole as the coordination sites with benzene and pyridine as scaffolds. The molecular clefts are analogous to the pyrene based molecular clefts in Chapter II except the sensing motifs rhodamine is used instead of pyrene. It was anticipated that this functional group will aid into water solubility. The coordination motifs such as triazole and amide groups remain same.

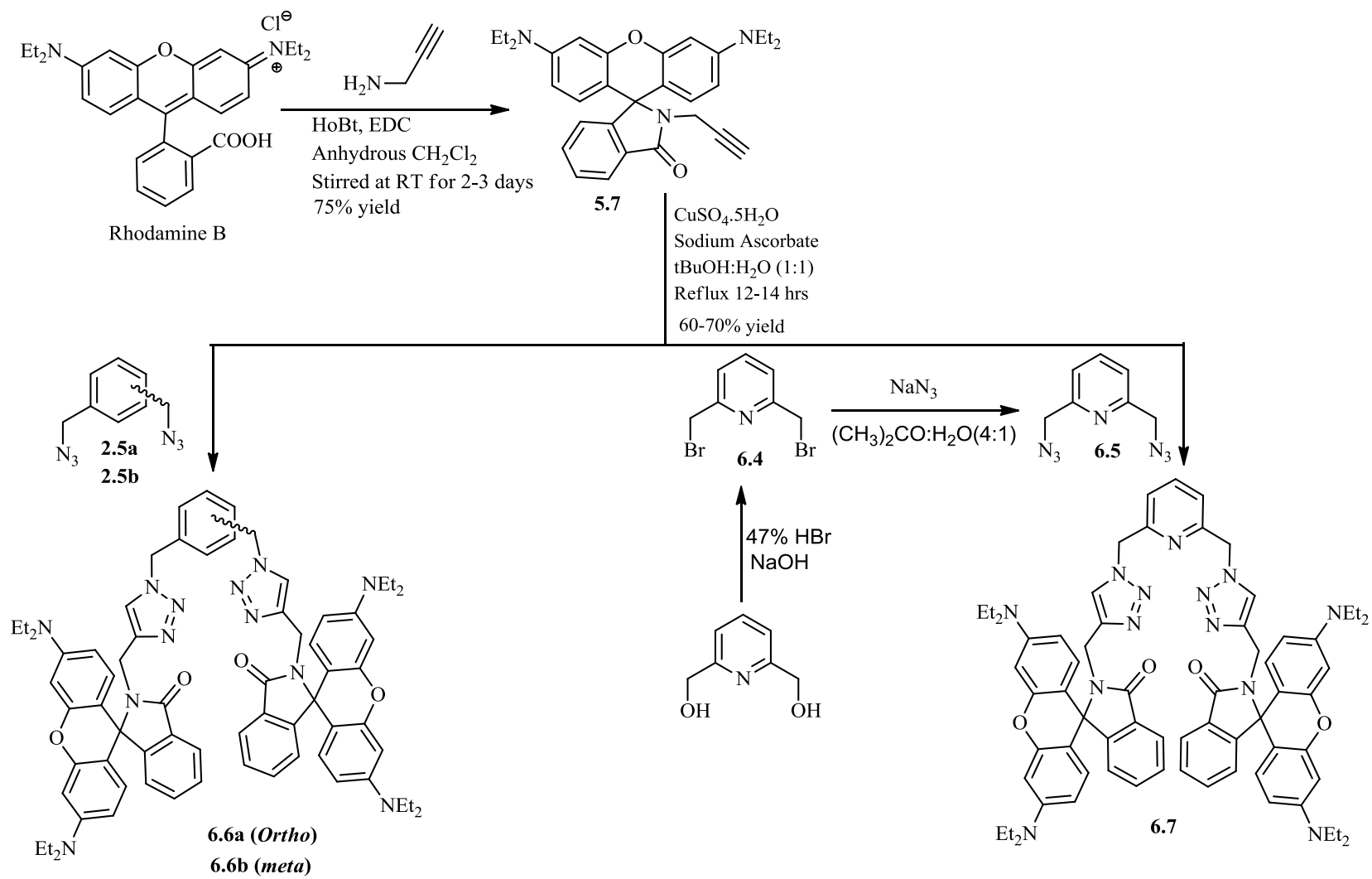
Two molecular probes are synthesized as *ortho* and *meta* isomer whereby the bite angle is different between the pendent arms. It is expected that one isomer binds the  $\text{Fe}^{3+}$  ion more thermodynamically favorable than the other isomer. To increase the binding

affinity, a third molecular probe is synthesized. This probe introduces pyridine group as scaffold at 2, 6 positions to aid in the coordination of the metal ion. Hence, it improves the selectivity and binding affinity. As in Chapter V, it is expected that molecular clefts will have low absorbance and fluorescence and should increase upon binding with the target metal ion. It is proposed that metal ions will be coordinated by the oxygen and nitrogen atoms of lactam and triazole groups within the cleft of the molecular probes.

#### Synthesis of Molecular Probes **6.6a**, **6.6b**, and **6.7**

3',6'-Bis(diethylamino)-2-(prop-2-ynyl)spiro [isoindoline-1,9'-xanthen]-3-one (**5.7**) is prepared from rhodamine B by the same procedure as discussed in Chapter V. 2,6-Bis (azidomethyl)pyridine (**6.5**) is prepared from 2,6-bis(hydroxymethyl) pyridine. 2,6-Bis(bromomethyl) pyridine (**6.4**) is first prepared from 2,6-bis(hydroxymethyl) pyridine in 80% yield by refluxing in 47% hydrobromic acid overnight. The product is confirmed by the disappearance of the hydroxyl group signal in the  $^1\text{H}$  NMR and OH stretching bands in the IR-spectrum, and its spectroscopic data ( $^1\text{H}$  NMR,  $^{13}\text{C}$  NMR and IR) also agreed with the published procedure.<sup>236</sup> 2,6-Bis(bromomethyl) pyridine (**6.4**) is then reacted with sodium azide in 4:1(( $\text{CH}_3$ ) $_2\text{CO}$ :  $\text{H}_2\text{O}$ ) to prepare 2,6-bis (azidomethyl) pyridine in 80 % yield(**6.5**). The azide molecule (**6.5**) was confirmed by its characteristic strong stretching bands at  $2090\text{ cm}^{-1}$  in IR spectrum, and its spectroscopic data ( $^1\text{H}$  NMR,  $^{13}\text{C}$  NMR and IR) also agreed with the published procedure.<sup>114</sup> Finally, **5.7** was then reacted with *ortho* or *meta* bis(azidomethyl) benzene (**2.5a** or **2.5b**) or 2,6-bis (azidomethyl)pyridine (**6.5**) via the click reaction.<sup>114</sup> Pure products are obtained in all three cases in 60-70% yields by column chromatography [Hexane (2): ethyl acetate (8)] of the ethyl acetate extracts of the reaction mixture. The product is confirmed by the

signal of triazole proton at  $\delta$  7.04 ppm ( $\text{CD}_3\text{CN}$ ). The compounds were fully characterized by  $^1\text{H}$  NMR,  $^{13}\text{C}$  NMR, IR, ESI mass spectrum, elemental analysis, and by X-ray crystallography (scheme 6.3).



Scheme 6.3. Synthesis of molecular probes **6.6a**, **6.6b**, and **6.7**.

### X-ray Crystallographic Study of Molecular Probes **6.7**

The crystal for compound **6.7** was grown by slow evaporation of its saturated solution in a mixture of  $\text{CHCl}_3$  and  $\text{CH}_3\text{OH}$ . As shown in Figure **6.2**, crystal structure is in spiro lactam configuration which explains its low absorption and fluorescence. Xanthene ring is orthogonal to the spiro lactam ring.

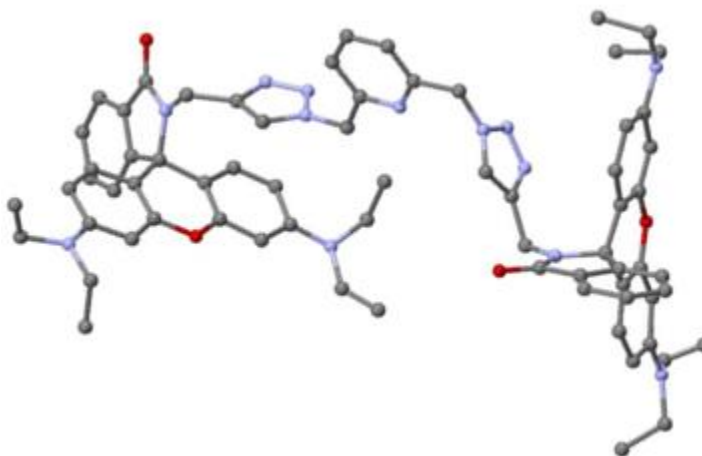
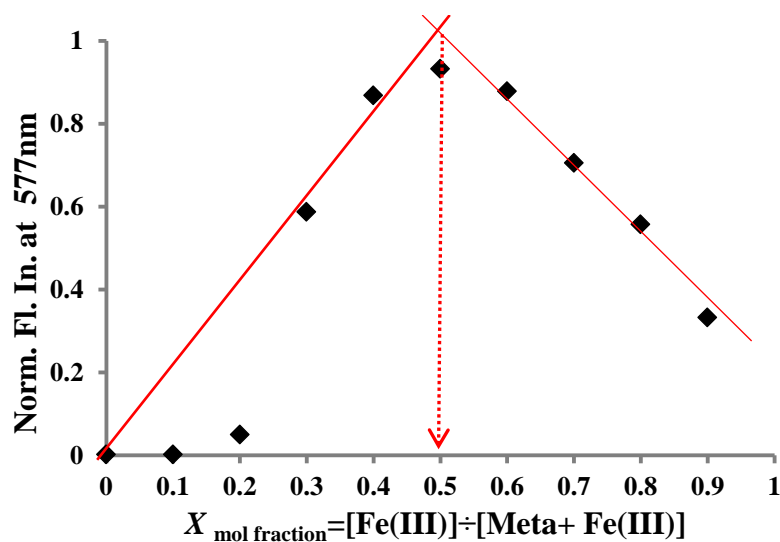


Figure 6.2. X-ray crystal structure of compound **6.7**.

### Job's Plot Studies of Molecular Probes **6.6a**, **6.6b**, and **6.7**

The binding stoichiometry of compound **6.6a**, **6.6b**, and **6.7** with  $\text{Fe}(\text{ClO}_4)_3$  is confirmed by Job's plot analysis. A  $1 \times 10^{-4}$  M solution is prepared for each of compound (**6.6a** or **6.6b** or **6.7**) and  $\text{Fe}(\text{ClO}_4)_3$  in 1:1 (EtOH:H<sub>2</sub>O). Both solutions are then mixed in different ratios to get the solutions having mole fractions from 0 to 1; each of which have the same total molar concentration i.e.,  $1 \times 10^{-4}$  M. Fluorescence was measured for each mole fraction, and the fluorescence intensity at 577 nm was plotted against the mole fraction of  $\text{Fe}(\text{ClO}_4)_3$  or  $\text{Al}(\text{ClO}_4)_3$ . The apex of the curve lies at 0.5 mole fraction which corresponds to 1:1 (Ligand: metal) stoichiometry. Figure 6.3 shows the Job's plot of compound **6.6b** with  $\text{Fe}(\text{ClO}_4)_3$ . As explained in Chapter V, the fluorescence of the 0.1 and 0.2 mole fractions have low fluorescence.



*Figure 6.3.* Job's plot of compound **6.6b** with  $\text{Fe}(\text{ClO}_4)_3$  obtained by fluorescence measurements in 1:1 (EtOH :H<sub>2</sub>O). The total concentration of **6.6b** and  $\text{Fe}(\text{ClO}_4)_3$  is 100  $\mu\text{M}$  where  $X \approx 0.5$  (1:1 ligand:metal ratio). The red lines are for visual interpretation only.

#### pH Studies on the Molecular Probes **6.6a**, **6.6b**, and **6.7**

As discussed previously in Chapter I and V, rhodamine based sensors are acid sensitive, and its spirolactam ring can open in the presence of acid to give ring open amide form which is red color and highly fluorescent. Therefore, the fluorescence response of all three probes (**6.6a**, **6.6b**, and **6.7**) was evaluated at different pH to find the working pH range. The fluorescence emission of compounds (**6.6a** or **6.6b** or **6.7**) is low and changes very little from pH 4 to pH 10 but shows high fluorescence below pH 2. This suggests that the spirolactam ring is stable and does not open in the pH range of 4-10 but opens below pH 4. As a consequence, compound (**6.6a**, **6.6b**, and **6.7**) cannot be used for detection of metal ions below pH 4. Upon addition of five equivalents of  $\text{Fe}^{3+}$  and  $\text{Al}^{3+}$  ions in the above solutions, a significant enhancement in fluorescence was observed which is attributed to opening of the rhodamine ring. This data demonstrate that

compounds (**6.6a**, **6.6b**, and **6.7**) could act as a fluorescent probe for  $\text{Fe}^{3+}$  ions in the pH range of pH 4-10 (Figure 6.4).

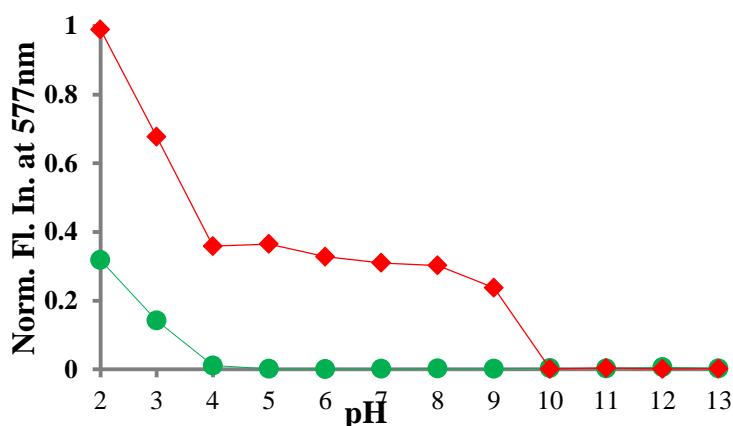


Figure 6.4. pH profile of compound **6.6b** (20  $\mu\text{M}$ ) with pH from 1-14 (bottom green circle) and upon the addition of five equivalents of  $\text{Fe}(\text{III})$  (upper red diamond) in 1:1 ( $\text{EtOH}:\text{H}_2\text{O}$ ).

#### Optical Studies of the Molecular Probes **6.6a**, **6.6b**, and **6.7**

##### *UV-Vis spectroscopy*

As discussed in Chapter V, the metal ions can trigger the spirolactam ring to open to form the intense red color which is highly fluorescent. Therefore, molecular clefts (**6.6a**, **6.6b**, and **6.7**) are first studied towards various metal ions by UV-Vis spectroscopy. The 1:1 ratio of  $\text{EtOH}$  and  $\text{H}_2\text{O}$  is selected as the solvent system for the UV-Vis studies as explained in Chapter V.

All compounds **6.6a**, **6.6b**, and **6.7** (100  $\mu\text{M}$ ) do not show any characteristic absorption bands of the rhodamine moiety around 550 nm in aqueous ethanol solution ( $\text{EtOH}:\text{H}_2\text{O} = 1:1$ ) at pH 7.1. This suggests that the compounds are in spirolactam configurations. A new absorption band appears at 550 nm upon addition of one equivalent of  $\text{Fe}^{3+}$  or  $\text{Al}^{3+}$  ions (500  $\mu\text{L}$  of 200  $\mu\text{M}$ ) to **6.6a** or **6.6b** or **6.7** (100  $\mu\text{M}$ ) with a color change from colorless to pink. This can be explained by the formation of the ring



opened amide forms as a result of  $\text{Fe}^{3+}$  or  $\text{Al}^{3+}$  ions coordinates to the molecular receptors. The intensity of absorption band on the addition of  $\text{Fe}^{3+}$  ion is two times greater than  $\text{Al}^{3+}$  ion. The absorption spectrum of compounds (**6.6a** or **6.6b** or **6.7**) did not change upon addition of other metal ions such as  $\text{Na}^+$ ,  $\text{K}^+$ ,  $\text{Ca}^{2+}$ ,  $\text{Mg}^{2+}$ ,  $\text{Cr}^{3+}$ ,  $\text{Fe}^{3+}$ ,  $\text{Fe}^{2+}$ ,  $\text{Zn}^{2+}$ ,  $\text{Cd}^{2+}$ ,  $\text{Co}^{2+}$ , and  $\text{Hg}^{2+}$ .

This suggests that compounds **6.6a** or **6.6b** or **6.7** could serve as “naked-eye” chemosensors for  $\text{Fe}^{3+}$  or  $\text{Al}^{3+}$  ions in aqueous ethanol solution (Figure 6.5). The comparison for selectivity of compounds **6.6a**, **6.6b**, and **6.7** to  $\text{Fe}^{3+}$  and  $\text{Al}^{3+}$  ions is shown in Figure 6.6. All compounds showed more intense absorption bands for the  $\text{Fe}^{3+}$  ion in comparison to  $\text{Al}^{3+}$  ions. This showed that molecular clefts are more selective to a  $\text{Fe}^{3+}$  ion than  $\text{Al}^{3+}$  ion in comparison to the molecular probes containing only one rhodamine unit in Chapter V. The intensity of absorbance band for either  $\text{Fe}^{3+}$  or  $\text{Al}^{3+}$  ions are almost the same in all compounds suggesting the binding pocket between the pendent arms of the *ortho* and *meta* isomer do not play a significant role in the selectivity of the metal ions.

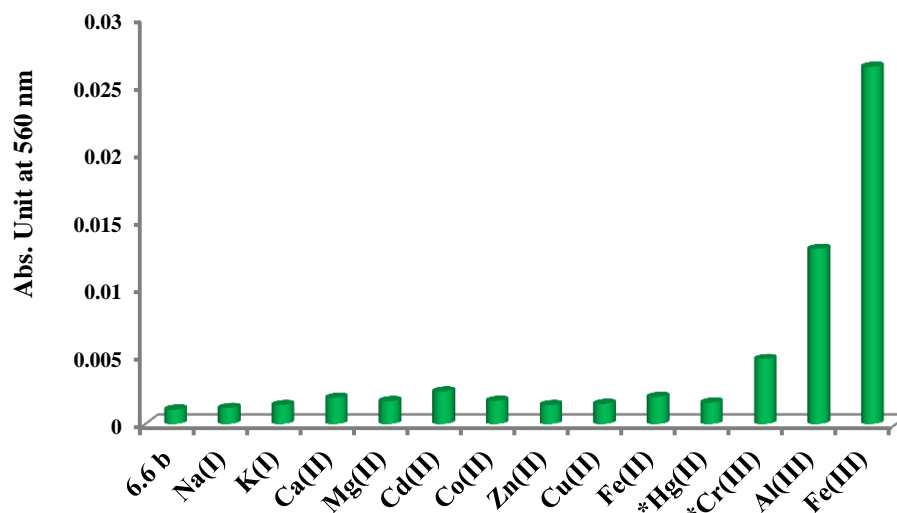


Figure 6.5. UV-Vis selectivity chart of compound **6.6b** (100  $\mu\text{M}$ ) in 1:1 (EtOH:H<sub>2</sub>O), at pH=7.1, upon the addition of one equivalents of metal ions as their ClO<sub>4</sub><sup>-</sup> salts (\*Cl<sup>-</sup> salt).

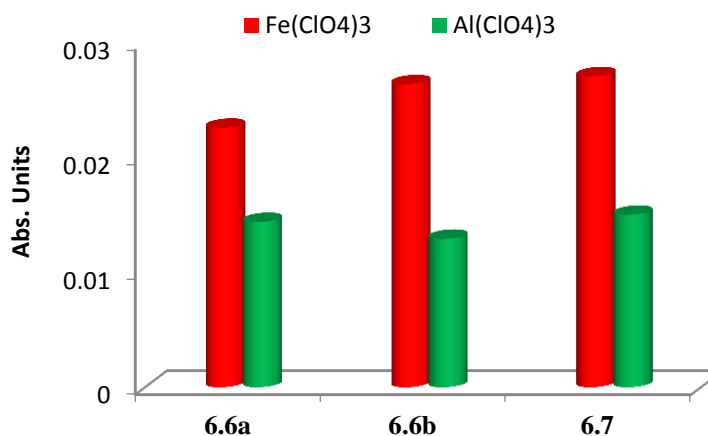


Figure 6.6. Comparison of UV-Vis selectivity chart of compounds **6.6a**, **6.6b**, and **6.7** (100  $\mu\text{M}$ ) in 1:1 (EtOH:H<sub>2</sub>O), pH 7.1, upon addition of one equivalents of Fe<sup>3+</sup> and Al<sup>3+</sup> ions as their ClO<sub>4</sub><sup>-</sup> salts.

In order to study the binding in detail, UV-Vis titration of compounds **6.6a** or **6.6b** or **6.7** (50  $\mu\text{M}$ ) was carried out with Fe(ClO<sub>4</sub>)<sub>3</sub> and Al(ClO<sub>4</sub>)<sub>3</sub> in aqueous ethanol solution 1:1 (EtOH:H<sub>2</sub>O) at pH 7.1. For example, the UV-Vis titration of compound **6.6b** with Fe(ClO<sub>4</sub>)<sub>3</sub> and Al(ClO<sub>4</sub>)<sub>3</sub> are shown in Figures 6.7 and 6.8. Addition of Fe(ClO<sub>4</sub>)<sub>3</sub> or Al(ClO<sub>4</sub>)<sub>3</sub> increases the UV-Vis absorption band with the maximum at 560 nm. The

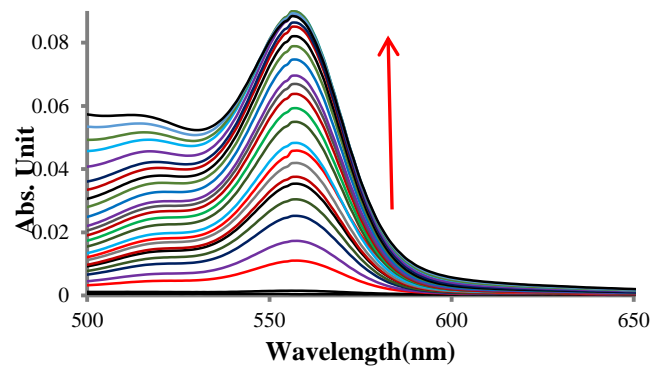
absorbance bands plateaued after 20 equivalents for both  $\text{Fe}^{3+}$  and  $\text{Al}^{3+}$  ions. Data obtained during UV-Vis titration is analysed using the Benesi-Hildebrand method and HypSpec program.<sup>116</sup> The binding constants calculated by these two methods are shown in Table 6.1 and are in good agreement. Both methods showed that compounds **6.6a**, **6.6b**, and **6.7** are binding with  $\text{Fe}^{3+}$  or  $\text{Al}^{3+}$  ion in 1:1 stoichiometry.

Table 6.1

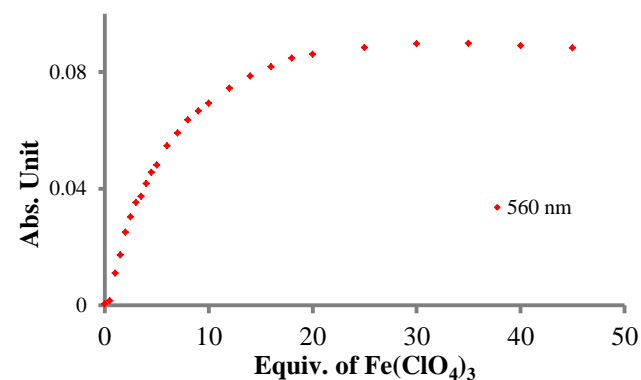
*Binding constant ( $K_{11}$ ) calculated for UV-Vis titrations of **6.6a**, **6.6b** and **6.7** (50  $\mu\text{M}$ ) with  $\text{Fe}(\text{ClO}_4)_3$  and  $\text{Al}(\text{ClO}_4)_3$  (5 mM) in 1:1 (EtOH:  $\text{H}_2\text{O}$ ) using Benesi-Hildebrand and HypSpec program<sup>116</sup>*

Compounds	salts	Benesi-Hilder brand( $K_{11}, \text{M}^{-1}$ )	HypSpec ( $K_{11}, \text{M}^{-1}$ )
<b>6.6a</b>	$\text{Fe}(\text{ClO}_4)_3$	$2.8 \times 10^3$	$5.5 \times 10^3$
	$\text{Al}(\text{ClO}_4)_3$	$6.0 \times 10^3$	$6.4 \times 10^3$
<b>6.6b</b>	$\text{Fe}(\text{ClO}_4)_3$	$2.6 \times 10^3$	$2.9 \times 10^3$
	$\text{Al}(\text{ClO}_4)_3$	$5 \times 10^3$	$1.3 \times 10^4$
<b>6.7</b>	$\text{Fe}(\text{ClO}_4)_3$	$1.4 \times 10^3$	$8.3 \times 10^2$
	$\text{Al}(\text{ClO}_4)_3$	$5.6 \times 10^3$	$1.4 \times 10^4$

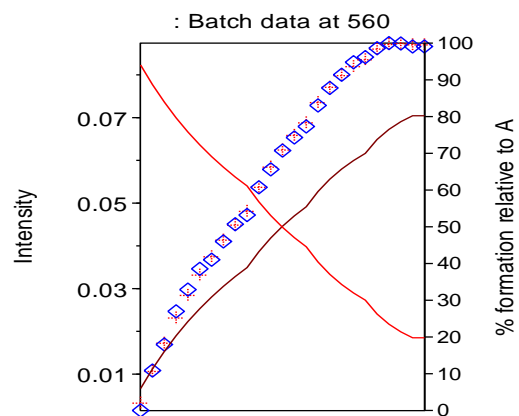
(A)



(B)



(C)



(D)

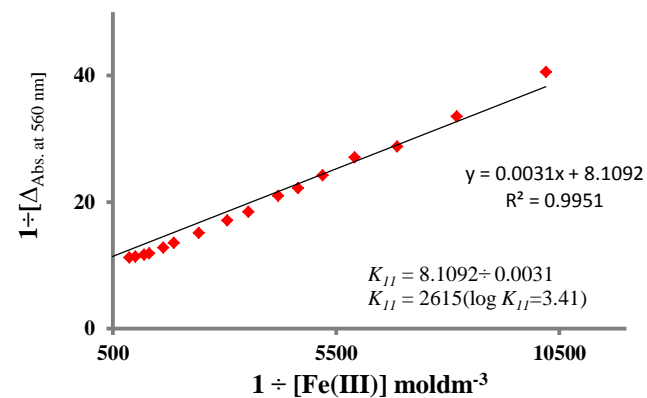
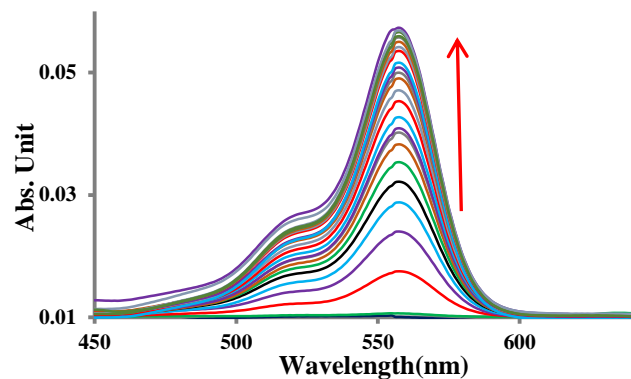
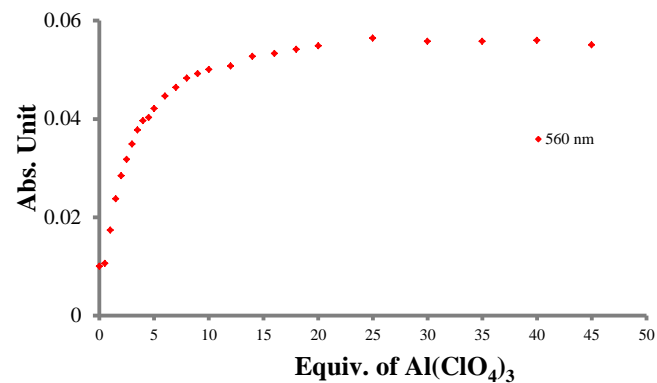


Figure 6.7. (A) UV-Vis spectrum of compound **6.6b** (50  $\mu\text{M}$ ) upon addition of  $\text{Fe}(\text{ClO}_4)_3$ , (B) its binding isotherm in 1:1 (EtOH:H<sub>2</sub>O) pH=7.1, (C) binding isotherm for HypSpec program,<sup>116</sup> and (D) Benesi-Hildbrand plot.

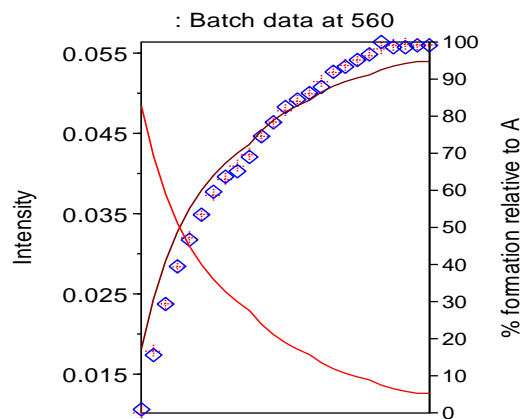
(A)



(B)



(C)



(D)

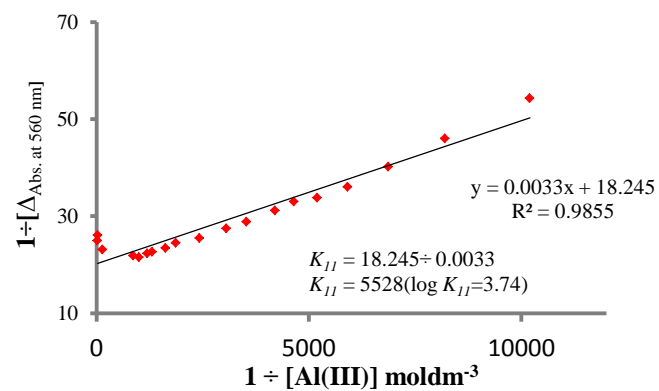


Figure 6.8. (A) UV-Vis spectrum of compound **6.6b** (50  $\mu\text{M}$ ) upon addition of  $\text{Al}(\text{ClO}_4)_3$ , (B) its binding isotherm in 1:1 (EtOH:H<sub>2</sub>O), pH =7.1, (C) binding isotherm for HypSpec program,<sup>116</sup> and (D) Benesi-Hildbrand plot.

### *Fluorescence spectroscopy*

After the UV-Vis studies, I turned my attention to fluorescence as this is more sensitive technique. Therefore, it was anticipated that selectivity might be changed in the fluorescence. Besides, color produced by the quenching metal ions such as  $\text{Hg}^{2+}$ ,  $\text{Cu}^{2+}$ , and  $\text{Fe}^{3+}$  ions could have low fluorescence. Therefore, compounds **6.6a**, **6.6b**, and **6.7** are studied by fluorescence towards different metal ions such as  $\text{Na}^+$ ,  $\text{K}^+$ ,  $\text{Ca}^{2+}$ ,  $\text{Mg}^{2+}$ ,  $\text{Cr}^{3+}$ ,  $\text{Al}^{3+}$ ,  $\text{Fe}^{3+}$ ,  $\text{Fe}^{2+}$ ,  $\text{Zn}^{2+}$ ,  $\text{Cd}^{2+}$ ,  $\text{Co}^{2+}$ , and  $\text{Hg}^{2+}$  ions in the same solvent system 1:1 (EtOH:H<sub>2</sub>O) at pH 7.1.

Compound **6.6a**, **6.6b**, and **6.7** (10  $\mu\text{M}$ ) all have a low fluorescence intensity at 577 nm ( $\lambda_{\text{ex}}=550$  nm). A strong fluorescence emission band at 577 nm was produced with a color change from colorless to pink upon addition of five equivalents of  $\text{Fe}^{3+}$  or  $\text{Al}^{3+}$  ions. Fluorescence produced by  $\text{Al}^{3+}$  ions is two times lower than fluorescence by  $\text{Fe}^{3+}$  ions. In Chapter V, the fluorescence signal produced by the  $\text{Al}^{3+}$  ions is almost the same in intensity as  $\text{Fe}^{3+}$  ions. Therefore, low fluorescence intensity by  $\text{Al}^{3+}$  ions in comparison to  $\text{Fe}^{3+}$  could be either due to a chelate effect or having a right binding pocket for  $\text{Fe}^{3+}$  ions. However, there is almost no change in the fluorescence and color upon addition of the above mentioned metal ions. For example, the bar chart selectivity of compound **6.6b** with different metal ions is shown in Figure 6.9. This showed that compounds **6.6a**, **6.6b**, or **6.7** can be used as potential fluorescent chemosensors selective to  $\text{Fe}^{3+}$  or  $\text{Al}^{3+}$  ions. The comparison chart of compounds **6.6a**, **6.6b**, and **6.7** for  $\text{Al}^{3+}$  and  $\text{Fe}^{3+}$  ions is shown in Figure 6.10. All compounds showed almost the same fluorescent intensity for both  $\text{Fe}^{3+}$  and  $\text{Al}^{3+}$  ions. However, the fluorescent intensity for the  $\text{Al}^{3+}$  ion is almost half of the fluorescence of  $\text{Fe}^{3+}$  ion. This result is in complete agreement with the

result from UV-Vis absorption and supports that molecular clefts are more selective to the  $\text{Fe}^{3+}$  ion than the  $\text{Al}^{3+}$  ion.

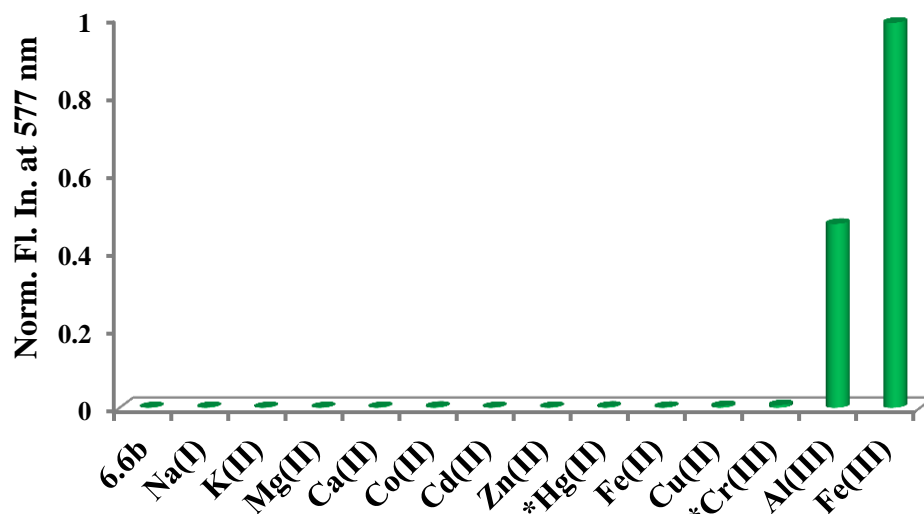


Figure 6.9. Fluorescence selectivity chart of compound **6.6b** ( $10\mu\text{M}$ ) in 1:1 (EtOH:H<sub>2</sub>O), at pH=7.1, upon the addition of metal ions (five equivalents) as their  $\text{ClO}_4^-$  salts (\* $\text{Cl}^-$  salt).  $\lambda_{\text{ex}}=550\text{ nm}$

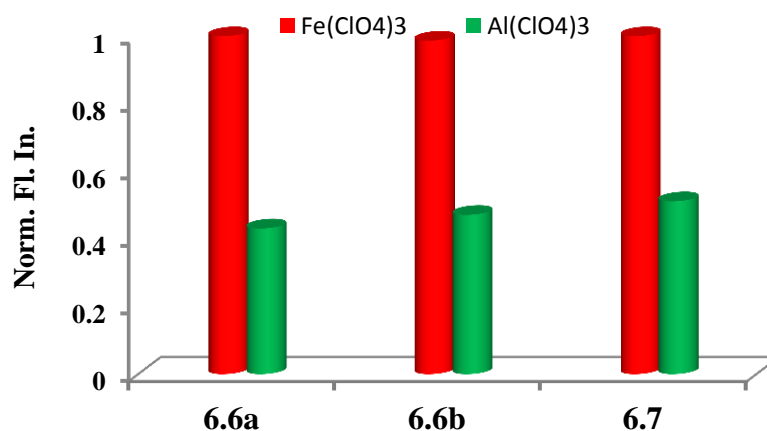


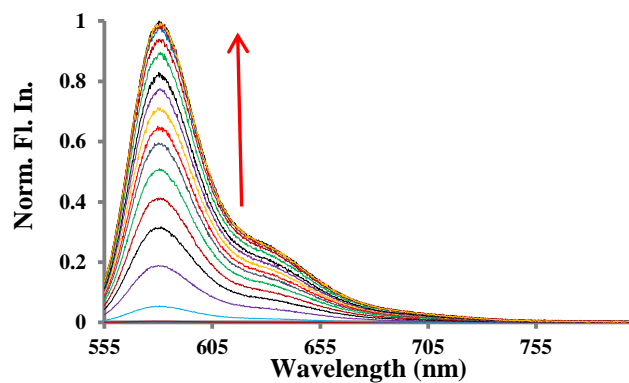
Figure 6.10. Comparison of UV-Vis selectivity chart of compounds **6.6a**, **6.6b**, and **6.7** ( $10\mu\text{M}$ ) in 1:1 (EtOH:H<sub>2</sub>O), pH 7.1, upon addition of one equivalents of  $\text{Fe}^{3+}$  and  $\text{Al}^{3+}$  ions as their  $\text{ClO}_4^-$  salts.

Fluorescence titrations were carried out in 1:1 (EtOH:H<sub>2</sub>O) in order to further investigate the binding of **6.6a**, **6.6b**, and **6.7** with  $\text{Fe}^{3+}$  and  $\text{Al}^{3+}$  ions. Figures 6.11 and

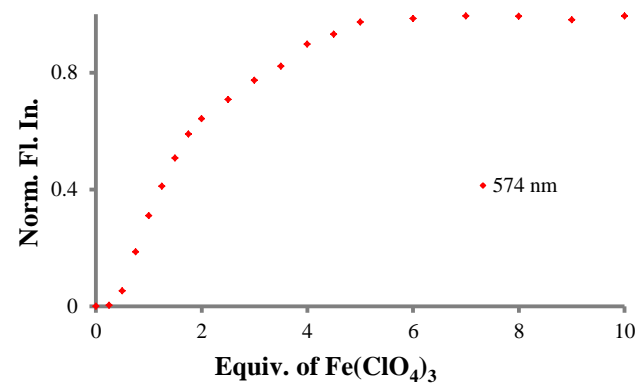
6.12 show the fluorescence titration of compound **6.6b** with  $\text{Fe}(\text{ClO}_4)_3$  and  $\text{Al}(\text{ClO}_4)_3$ . The fluorescence intensity of compound **6.6b** at 577 nm was increased gradually on addition of increasing concentrations of  $\text{Fe}^{3+}$  or  $\text{Al}^{3+}$  ions. The fluorescence was plateaued after five equivalents of  $\text{Fe}^{3+}$  or  $\text{Al}^{3+}$  ions. Binding constants were calculated by the Benesi-Hildebrand method and HypSpec program which are shown in Table 6.2. Both methods showed the binding stoichiometry is 1:1. The binding constants calculated from the HypSpec program are of magnitudes greater than those calculated from the Benesi-Hildebrand method. As explained in Chapter V, calculation of binding constant in the Benesi-Hildebrand involves fewer data in order to satisfy the conditions i.e., one of the reactant (host or guest) should be excess to another reactant.



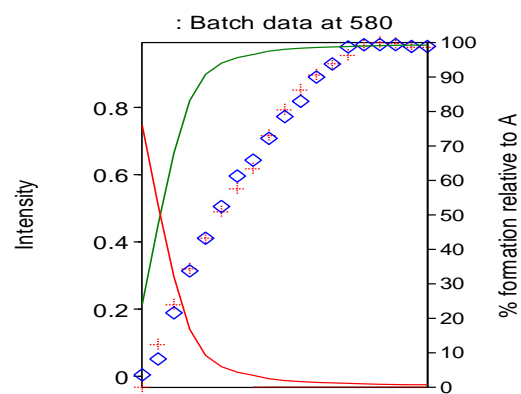
(A)



(B)



(C)



(D)

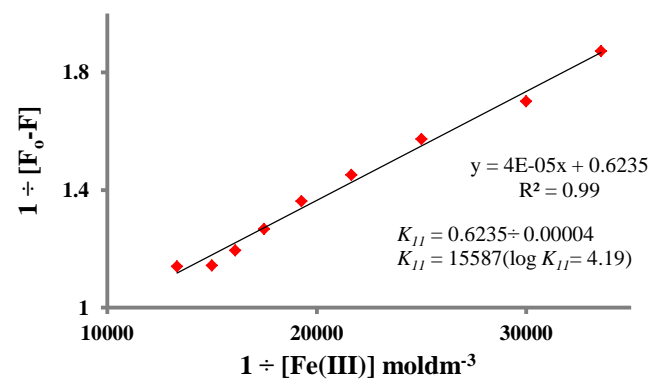
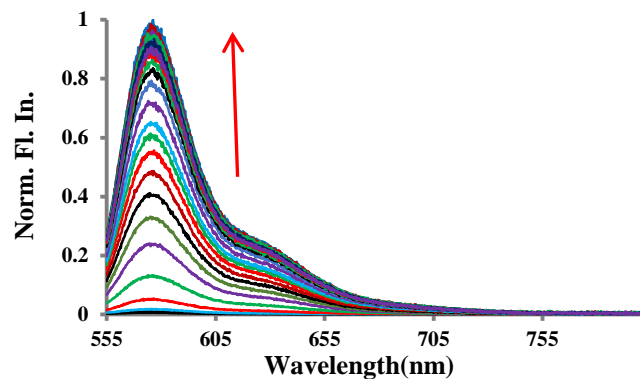
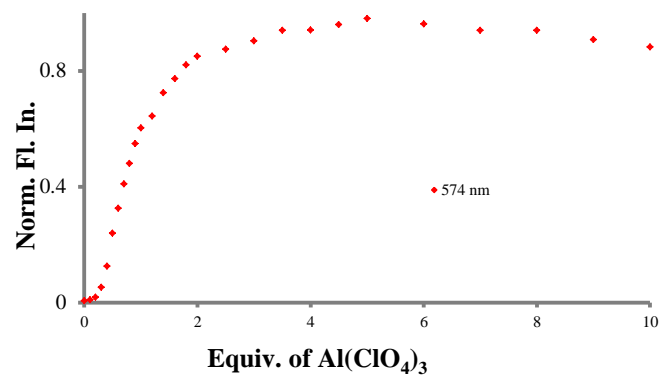


Figure 6.11. (A) Fluorescence spectrum of compound **6.6b** (20  $\mu\text{M}$ ) upon addition of  $\text{Fe}(\text{ClO}_4)_3$ , (B) its binding isotherm in 1:1 (EtOH:H<sub>2</sub>O), pH=7.1, (C) binding isotherm for HypSpec program,<sup>116</sup> and (D) Benesi-Hildbrand plot.

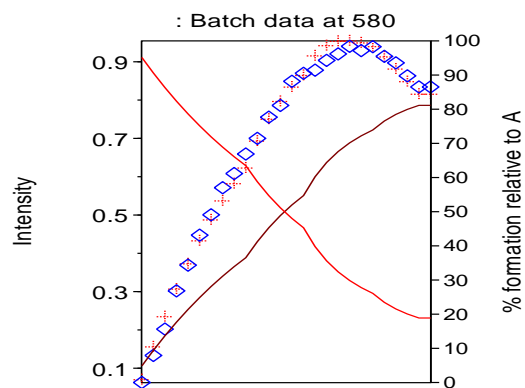
(A)



(B)



(C)



(D)

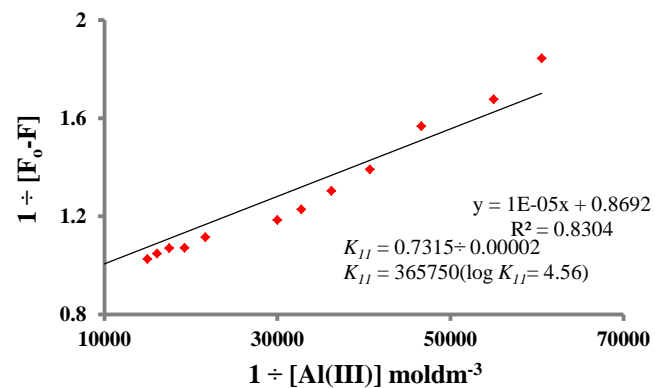


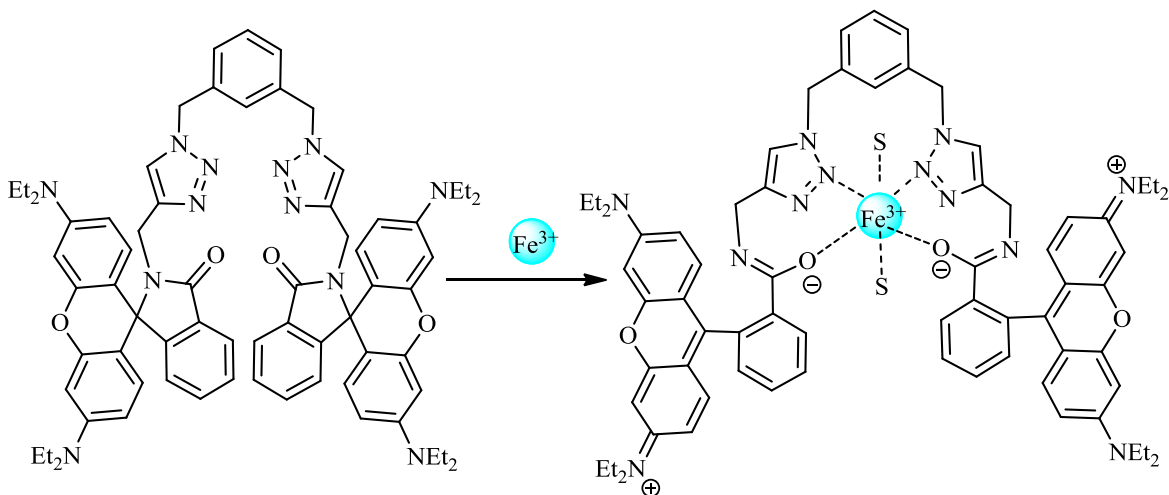
Figure 6.12. (A) Fluorescence spectrum of compound **6.6b** (20  $\mu\text{M}$ ) upon addition of  $\text{Al}(\text{ClO}_4)_3$ , (B) its binding isotherm in 1:1 (EtOH:H<sub>2</sub>O), pH=7.1, (C) binding isotherm for HypSpec program,<sup>116</sup> and (D) Benesi-Hildbrand plot.

Table 6.2

Binding constant ( $K_{11}$ ) calculated for fluorescence titrations of **6.6a**, **6.6b**, and **6.7** with  $\text{Fe}(\text{ClO}_4)_3$  and  $\text{Al}(\text{ClO}_4)_3$  using Benesi-Hilderbrand and HypSpec program<sup>116</sup>

Compounds	salts	Benesi-Hilder brand( $K_{11} \text{ M}^{-1}$ )	HypSpec ( $K_{11}, \text{M}^{-1}$ )
<b>6.6a</b>	$\text{Fe}(\text{ClO}_4)_3$	$1.4 \times 10^3$	$2.3 \times 10^6$
	$\text{Al}(\text{ClO}_4)_3$	$6.0 \times 10^3$	$5.7 \times 10^5$
<b>6.6b</b>	$\text{Fe}(\text{ClO}_4)_3$	$1.5 \times 10^4$	$2.8 \times 10^6$
	$\text{Al}(\text{ClO}_4)_3$	$3.6 \times 10^4$	$5.0 \times 10^5$
<b>6.7</b>	$\text{Fe}(\text{ClO}_4)_3$	$2.0 \times 10^4$	XX
	$\text{Al}(\text{ClO}_4)_3$	$2.2 \times 10^4$	$2.6 \times 10^5$

Based upon the UV-Vis and fluorescence result, it is assumed that  $\text{Fe}^{3+}$  or  $\text{Al}^{3+}$  ions could be coordinated by the carbonyl oxygen atom of lactam and nitrogen atoms of the triazole ring within the cleft of the molecular probes (Scheme 6.4).



Scheme 6.4. Proposed binding mode of compound **6.6b** with  $\text{Fe}^{3+}$  ion on the basis of UV-Vis and fluorescence results (S= solvent).

Reversibility of Molecular Probes **6.6a**, **6.6b**, and **6.7**

DFB (deferoxamine), a siderophore, is again used to test the reversibility of compounds **6.6a**, **6.6b**, and **6.7** with  $\text{Fe}^{3+}$  ions in aqueous ethanol solution. Figure 6.13 shows the reversibility test of compound **6.6b**. The fluorescence intensity of compound **6.6b** with  $\text{Fe}^{3+}$  ions (two equivalents  $\text{Fe}^{3+}$  ions to  $10\ \mu\text{M}$  solution) is quenched upon addition of two equivalents of DFB because DFB, due to its high binding affinity with iron, stripped off the  $\text{Fe}^{3+}$  ions from the complex of compound **6.6b**. The quenching of fluorescence indicates that compound **6.6b** is returned to its original lactam state. The fluorescence of the solution was enhanced again upon addition of high concentration of  $\text{Fe}^{3+}$  ions (two equivalents of  $2\ \text{mM}$   $\text{Fe}^{3+}$  ions) to it. This confirms that compound **6.6b** is a reversible fluorescent probe for  $\text{Fe}^{3+}$  ions, and the spectral response of compound **6.6b** to  $\text{Fe}^{3+}$  ions is due to the chelation-induced ring opening of rhodamine spirolactam rather than other possible reactions.

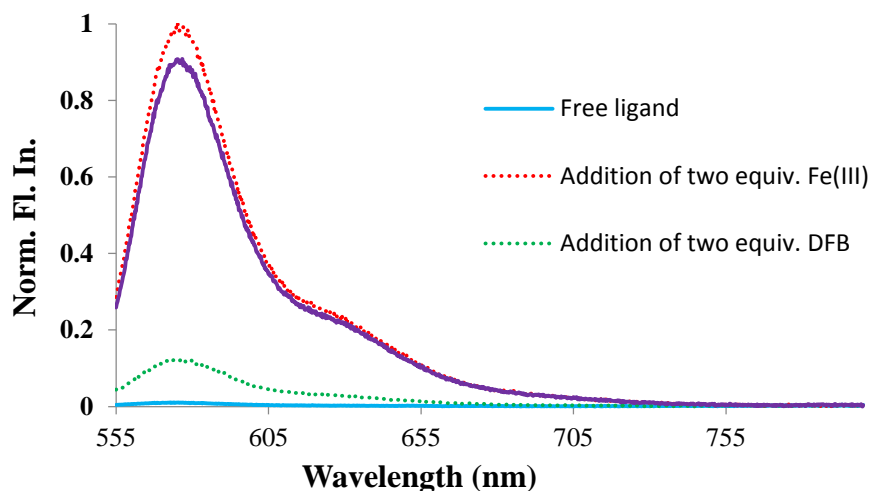
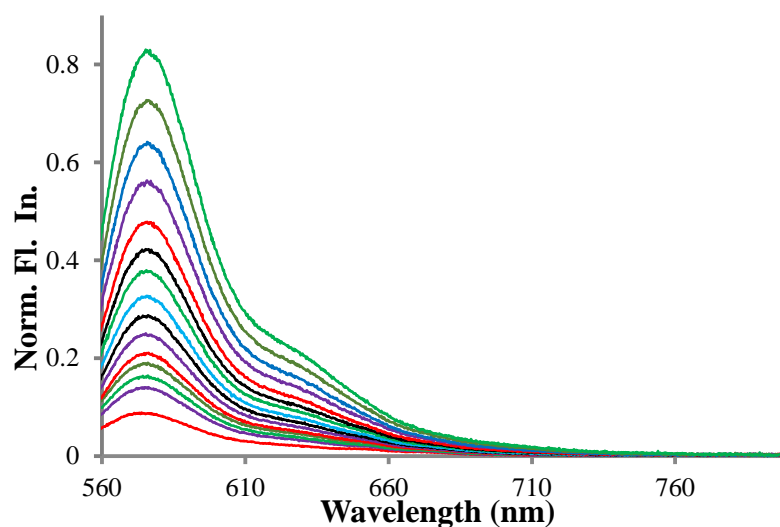


Figure 6.13. Reversibility test: [**6.6b**] =  $10\ \mu\text{M}$ ; Fe (III) =  $100\ \mu\text{M}$ ; DFB =  $100\ \mu\text{M}$  in EtOH:  $\text{H}_2\text{O}$  (1:1).

### Detection limit of Molecular Probes **6.6a** and **6.6b**

It is important to have the sensors with the low limit of detection as the  $\text{Fe}^{3+}$  is present in a very small amount in the environment and biology. The limit of detection was calculated by titrating  $20\ \mu\text{M}$  of Compounds **6.6a** or **6.6b** with  $50\ \mu\text{M}$   $\text{Fe}(\text{ClO}_4)_3$  in 1:1 (EtOH:H<sub>2</sub>O) (Figure 6.14). The limit of detection was calculated by using the method of least squares as described in previous Chapter II. The limit of detection for compounds **6.6a** and **6.6b** for  $\text{Fe}^{3+}$  ion was calculated to be  $3\ \mu\text{M}$  (163 ppb) and  $0.5\ \mu\text{M}$  (28 ppb), respectively (Figure 6.15). The detection limit of molecular probe **6.6b** is below the limit set up for  $\text{Fe}^{3+}$  ion in drinking water by the WHO (100 ppb) and the EPA (300 ppb).



*Figure 6.14.* Fluorescence chart of **6.6b** ( $20\ \mu\text{M}$ ) with  $\text{Fe}(\text{ClO}_4)_3$  ( $50\ \mu\text{M}$ ) used to calculate L.o.D in 1:1 (EtOH:H<sub>2</sub>O).

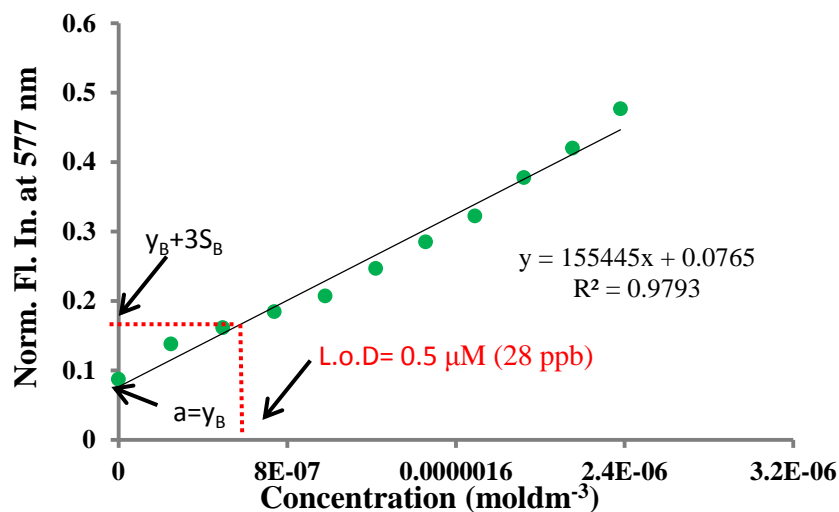


Figure 6.15. Calibration curve used to calculate the LoD for Fe<sup>3+</sup> ion with **6.6b**.

### Summary

In summary, rhodamine-based molecular clefts **6.6a**, **6.6b**, and **6.7** were synthesized by an azide-alkyne Huisgen cycloaddition reaction of 3', 6'-bis(diethylamino)-2-(prop-2-ynyl)spiro [isoindoline-1, 9'-xanthen]-3-one (**5.7**) with *ortho* or *meta* bis(azidomethyl)benzene (**2.5a** or **2.5b**) or 2,6-bis(azidomethyl)pyridine (**6.5**).

The structure of compound **6.7** was also confirmed by X-ray crystal structures which showed that the free compound is in spiro lactam configuration. The UV-Vis and fluorescence studies of compounds **6.6a**, **6.6b**, and **6.7** showed the high selectivity for Fe<sup>3+</sup> and Al<sup>3+</sup> ions in aqueous ethanol solution of 1:1 (EtOH :H<sub>2</sub>O) at pH 7.1. Job's plot and the Benesi-Hildebrand plot showed that the compounds **6.6a**, **6.6b**, and **6.7** is binding with Fe<sup>3+</sup> or Al<sup>3+</sup> ions in a 1:1 stoichiometry.

### Experimental

#### *General procedure for UV-Vis and fluorescence experiments*

A stock solution of all compounds was prepared in EtOH. Final concentration of solution (50 μM for UV-Vis and 20 μM for Fluorescence experiment) is prepared by

diluting the stock solution with deionized H<sub>2</sub>O to make final 1:1 (EtOH:H<sub>2</sub>O) solution. The solution was excited at  $\lambda = 550$  nm and scanned from  $\lambda = 555$ -800 nm with slit widths set to 0.5 nm. A ten times more concentrated solution of the metal salt was prepared in 1:1 (EtOH:H<sub>2</sub>O), and 20  $\mu$ L (20  $\mu$ L = 0.1 equivalent of metal salt) aliquots were added to compound. Fluorescence spectra were recorded after each addition. Dilution factors were taken into consideration upon binding study determination. The binding constants were determined from fluorescence titrations using HypSpec 2006.<sup>116</sup>

#### General Procedure for Synthesis

##### *Preparation of 2,6-bis(bromomethyl)pyridine(6.4)*<sup>236</sup>

A solution of 2,6-bis(hydroxymethyl) pyridine (0.278 g, 2 mmol) in 47% HBr (4 mL) was heated overnight under reflux. After the reaction was cooled to room temperature, the mixture was poured into ice and neutralized with saturated NaOH. The resulting precipitate was collected, washed by water, and dried to get the pure product (80 % yield).

<sup>1</sup>H NMR (300 K, CD<sub>3</sub>Cl, 400 MHz):  $\delta$  7.72 (*t*, 1H,  $J = 7.7$ Hz, CH<sub>Ar</sub>), 7.39 (*d*, 2H,  $J = 7$ Hz, CH<sub>Ar</sub>), 4.56(*s*, 4H, CH<sub>2</sub>).

<sup>13</sup>C NMR (300 K, DMSO, 400 MHz):  $\delta$  156, 138, 122, 33

##### *Preparation of 2,6-bis(azidomethyl) pyridine (6.5)*<sup>114</sup>

The 2,6-bis(bromomethyl) pyridine (0.53 g, 2.0 mmol) and sodium azide (0.39 g, 6 mmol) were dissolved in a 4:1 mixture of acetone and water (30 mL) and stirred at room temperature for 24 h. A mixture of dichloromethane (25 mL) and water (25 mL) was then added to the reaction mixture and stirred for 10 mins. The organic layer was

separated and washed three times with water (50 mL), dried over magnesium sulfate, filtered and the solvent removed to produce a yellowish oil (80 % yield).

$^1\text{H}$  NMR (300 K,  $\text{CD}_3\text{Cl}$ , 400 MHz):  $\delta$  7.77 (*t*, 1H,  $J = 7.7\text{Hz}$ ,  $\text{CH}_{\text{Ar}}$ ), 7.31 (*d*, 2H,  $J = 7.7\text{Hz}$ ,  $\text{CH}_{\text{Ar}}$ ), 4.49(*s*, 4H,  $\text{CH}_2$ ).

IR (ATR solid): 2928  $\nu_{\text{C-H}}$  (w), 2090  $\nu_{\text{N=N}}$  (vs)  $\text{cm}^{-1}$ .

*General procedure for preparation of compounds 6.6a, 6.6b, and 6.7*<sup>14</sup>

Compound **5.7** (480 mg, 1 mmol), *meta* bis(azidomethyl) benzene **2.5b** (95 mg, 0.5 mmol), copper (II) sulfate (13 mg, 0.05 mmol), and sodium ascorbate (20 mg, 0.1 mmol) were dissolved in a mixture of tertiary butanol and water solution (1:1, 20-30 mL) and refluxed overnight. TLC of the reaction mixture was checked to see the completion of the reaction. Then, the reaction mixture was cooled, poured into ice cold water, and extracted with ethyl acetate (3x30 mL). The combined ethyl acetate is dried over magnesium sulphate, filtered, and evaporated to get the residue which was column chromatographed [hexane(8):ethyl acetate(2)] to get the pure compound (70% yield).

Characterization of compound 6.6a:

$^1\text{H}$  NMR (300 K,  $\text{CD}_3\text{CN}$ , 400MHz):  $\delta$ 7.78 (m, 2H), 7.40-7.51(m, 4H), 7.26-7.35 (m, 2H), 6.99-7.05 (m, 2H), 6.96 (*t*,  $J=4.0\text{Hz}$ , 4H), 6.32 (*d*,  $J=2.4\text{Hz}$ , 4H), 6.22-6.27 (m, 4H), 6.19 (*dd*,  $J=8.9,2.4\text{ Hz}$ , 4H), 5.31 (*s*, 4H), 4.27 (*s*,4H), 3.30 (*q*,  $J=7\text{Hz}$ , 16H), 1.08 (*t*,  $J=7\text{Hz},24\text{H}$ )

$^{13}\text{C}$  NMR (300 K,  $\text{CDCl}_3$ , 400MHz):  $\delta$ 166.97, 153.67, 152.89, 148.51, 143.99, 133.55, 132.34, 130.31, 129.29, 128.79, 128.39, 127.89, 123.09, 122.55, 122.21, 107.74, 104.76, 97.05, 64.20, 49.85, 43.68, 34.54, 11.55

Anal. Calcd for  $\text{C}_{70}\text{H}_{74}\text{N}_{12}\text{O}_4$ : H 6.50 %; N 14.64 %; C; 73.27 %



Anal. Recalcd for  $C_{70}H_{74}N_{12}O_4 \cdot 1.5H_2O \cdot CH_3CO_2CH_2CH_3$ : H 6.66 %; N 13.89 %; C; 71.4 %

Found for  $C_{70}H_{74}N_{12}O_4 \cdot 1.5H_2O \cdot CH_3CO_2CH_2CH_3$ : H 6.7 %; N 13.77 %; C; 71.39 %

Characterization of compound **6.6b**:

$^1H$  NMR (300 K,  $CD_3CN$ , 400MHz):  $\delta$ 7.78-7.84 (m, 2H), 7.42-7.51(m, 4H), 7.30 (t,  $J=7.5Hz$ , 1H), 7.07 (d,  $J=8.0Hz$ , 3H), 7.04 (s, 2H), 6.93-7.00(m, 2H), 6.31 (d,  $J=8.9Hz$ , 4H), 6.23 (d,  $J=8.9Hz$ , 4H), 6.17 (dd,  $J=8.9, 2.4 Hz$ , 4H), 5.20 (s, 4H), 4.26 (s, 4H), 3.20-3.36 (q,  $J=7Hz$ , 16H), 1.08 (t,  $J=7Hz, 24H$ )

$^{13}C$  NMR (300 K,  $CDCl_3$ , 400MHz):  $\delta$ 166.90, 153.58, 152.90, 148.48, 143.79, 136.15, 132.34, 130.41, 129.05, 128.39, 127.91, 127.37, 127.04, 123.10, 122.54, 122.20, 107.72, 104.81, 97.02, 64.17, 52.45, 43.66, 34.46, 11.53

Anal. Calcd for  $C_{70}H_{74}N_{12}O_4$ : H 6.50 %; N 14.64 %; C; 73.27 %

Anal. Recalcd for  $C_{70}H_{74}N_{12}O_4 \cdot 1.5H_2O \cdot CH_3CO_2CH_2CH_3$ : H 6.7 %; N 13.79 %; C; 70.97 %

Found for  $C_{70}H_{74}N_{12}O_4 \cdot 1.5H_2O \cdot CH_3CO_2CH_2CH_3$ : H 6.69 %; N 13.53 %; C; 71.26 %

Characterization of compound **6.7**:

$^1H$  NMR (300 K,  $CD_3CN$ , 400MHz):  $\delta$ 7.81-7.85 (m, 2H), 7.68 (t,  $J=7.8Hz$ , 1H), 7.44-7.52(m, 4H), 7.07 (s, 2H), 6.98-7.00 (m, 2H), 6.96 (d,  $J=7.8Hz$ , 2H), 6.32 (d,  $J=2.5Hz$ , 4H), 6.24 (d,  $J=8.9Hz$ , 4H) 6.17 (dd,  $J=8.9, 2.6 Hz$ , 4H), 5.28 (s, 4H), 4.31 (s, 4H), 3.21-3.36 (q,  $J=7Hz$ , 16H), 1.08 (t,  $J=7Hz, 24H$ )

$^{13}C$  NMR (300 K,  $CDCl_3$ , 500MHz):  $\delta$ 168.26, 156.03, 154.94, 154.20, 149.87, 145.03, 139.62, 133.72, 131.84, 129.79, 129.29, 124.48, 123.59, 122.24, 109.11, 106.14, 98.41, 64.00, 55.46, 45.03, 35.79, 12.78

Anal. Calcd for  $C_{69}H_{73}N_{13}O_4$ : H 6.40 %; N 15.85 %; C; 72.16 %

Anal. Recalcd for  $C_{69}H_{73}N_{13}O_4 \cdot 1.5H_2O$ : H 6.51 %; N 15.49 %; C; 70.50 %

Found for  $C_{69}H_{73}N_{13}O_4 \cdot 1.5H_2O$ : H 6.49 %; N 15.23 %; C; 70.62 %

## CHAPTER VII

## CONCLUSION

## Conclusion of Chapters II, III, and IV

Pyrene based molecular probes (**2.6a**, **2.6b**, **3.6**, and **4.7**) were synthesized in good yields by an azide-alkyne Huisgen cycloaddition reaction of N-(prop-2-ynyl) pyrene-1-carboxamide (**2.4**) with *ortho* and *meta* bis azidomethyl benzene (**2.5a**, and **2.5b**), benzyl azide (**3.5**), and methyl 2, 3, 4-tri-*O*-acetyl-6-azido-6-deoxy- $\alpha$ -D-glucopyranoside (**4.6**). Formation of excimer or monomer-excimer equilibrium is used as a sensing mechanism for the detection of metal ions. Molecular probes **2.6a** and **2.6b** were found to be selective for the  $\text{Zn}^{2+}$  ion, which showed a significant hypsochromic shift in the excimer band from 495 to 400 nm upon addition of  $\text{Zn}^{2+}$  ions. The fluorescence intensity at 400 nm was found to be more intense for **2.6b** than **2.6a**, upon addition of  $\text{Zn}(\text{ClO}_4)_2$ . The molecular probe was found to be reversible with a detection limit for the  $\text{Zn}^{2+}$  ion in the nanomolar range. Molecular modelling calculations (DFT), 2D NMR, and IR studies support the proposed structure of the complexes: unfortunately, these compounds were very insoluble in polar solvents due to the hydrophobic nature of the pyrene units. Therefore, their biological applications were not studied. However, this is one of the first reported systems whereby a hypsochromic excimer formation is seen rather than the bathochromic shift normally reported.

Molecular probe **3.6** acts as a self-assembled simultaneous cation and anion binding molecular probe. This was one of the first examples that utilizes an ion-pair to switch on the excimer formation with  $\text{ZnCl}_2$  in  $\text{CH}_3\text{CN}$ . The excimer was most intense with  $\text{ZnCl}_2$  and binds exclusively in a 2:1(ligand:metal) ratio in a tetrahedral fashion. The

tetrahedral geometry of the complex  $[\text{ZnCl}_2(\mathbf{3.6})_2]$  is supported by  $^1\text{H}$  NMR titration, 2D NMR, and DFT calculations.

Molecular probe **4.7** is shown to self-assemble in presence of the  $\text{Fe}^{3+}$  ion. The most intense excimer signal is produced by  $\text{Fe}(\text{ClO}_4)_3$  and binds the compound **4.7** in 1:2 stoichiometric ratio. Binding is further supported by  $^1\text{H}$  NMR titration studies with  $\text{Al}(\text{ClO}_4)_3$ . Electrogenerated chemiluminescence studies show for the first time an enhancement in ECL intensity upon addition of  $\text{Fe}^{3+}$  ion.

#### Conclusion of Chapters V and VI

Several rhodamine based molecular probes have been synthesized (**5.11**, **5.12**, **5.13**, **6.6a**, **6.6b**, and **6.7**) in good yields by an azide-alkyne Huisgen cycloaddition reaction. The ring opening of spirolactam to the open amide form is used as the sensing mechanism for the detection of metal ions. All rhodamine based molecular probes were found to bind both  $\text{Fe}^{3+}$  and  $\text{Al}^{3+}$  ions in 1:1(EtOH:H<sub>2</sub>O) at pH 7.1 in both UV-Vis and fluorescence.

The limit of detection for  $\text{Fe}^{3+}$  ions is calculated in the range of 0.5-3  $\mu\text{M}$  (28-163 ppb). 1D NMR ( $^1\text{H}$  NMR,  $^{13}\text{C}$  NMR), 2D NMR (ROESY), and IR-studies support the proposed structures of the complexes.

Several protocols are developed for the first time to distinguish  $\text{Fe}^{3+}$  and  $\text{Al}^{3+}$  ions in aqueous ethanol system. The protocol is based on the reduction of  $\text{Fe}^{3+}$  to  $\text{Fe}^{2+}$  ions which then react with ferrozine and 1, 10-phenanthroline to give an intense purple and orange red color, respectively.

The rhodamine molecular probe **5.12** was successfully applied for the cell imaging of free intracellular  $\text{Fe}^{3+}$  ions in the live Vero cell lines and in bacterial cells.

## REFERENCES

1. Callender, E.; Rice, K. C., "The Urban Environmental Gradient: Anthropogenic Influences on the Spatial and Temporal Distributions of Lead and Zinc in Sediments." *Environ. Sci. Technol.* **2000**, *34*, 232-238.
2. Lieu, P. T.; Heiskala, M.; Peterson, P. A.; Yang, Y., "The roles of iron in health and disease." *Mol. Aspects Med.* **2001**, *22*, 1-87.
3. Rink, L.; Gabriel, P., "Zinc and the immune system." *Proc. Nutr. Soc.* **2000**, *59*, 541-552.
4. Berg, J. M.; Shi, Y., "The galvanization of biology: a growing appreciation for the roles of zinc." *Science* **1996**, *271*, 1081-1085.
5. Vallee, B. L.; Falchuk, K. H., "The biochemical basis of zinc physiology." *Physiol. Rev.* **1993**, *73*, 79-118.
6. Sensi, S. L.; Canzoniero, L. M. T.; Yu, S. P.; Ying, H. S.; Koh, J.-Y.; Kerchner, G. A.; Choi, D. W., "Measurement of intracellular free zinc in living cortical neurons: routes of entry." *J. Neurosci.* **1997**, *17*, 9554-9564.
7. Coleman, J. E., "Zinc enzymes." *Curr. Opin. Chem. Biol.* **1998**, *2*, 222-234.
8. Bush, A. I., "Metals and neuroscience." *Curr. Opin. Chem. Biol.* **2000**, *4*, 184-191.
9. Jiang, P.; Guo, Z., "Fluorescent detection of zinc in biological systems: recent development on the design of chemosensors and biosensors." *Coord. Chem. Rev.* **2004**, *248*, 205-229.
10. Frederickson, C. J., "Neurobiology of zinc and zinc-containing neurons." *Int. Rev. Neurobiol.* **1989**, *31*, 145-238.

11. Que, E. L.; Domaille, D. W.; Chang, C. J., "Metals in Neurobiology: Probing Their Chemistry and Biology with Molecular Imaging." *Chem. Rev.* **2008**, *108*, 1517-1549.
12. Sladek, R.; Rocheleau, G.; Rung, J.; Dina, C.; Shen, L.; Serre, D.; Boutin, P.; Vincent, D.; Belisle, A.; Hadjadj, S.; Balkau, B.; Heude, B.; Charpentier, G.; Hudson Thomas, J.; Montpetit, A.; Pshezhetsky Alexey, V.; Prentki, M.; Posner Barry, I.; Balding David, J.; Meyre, D.; Polychronakos, C.; Froguel, P., "A genome-wide association study identifies novel risk loci for type 2 diabetes." *Nature* **2007**, *445*, 881-885.
13. Crichton, R. R.; Dexter, D. T.; Ward, R. J., "Metal based neurodegenerative diseases. From molecular mechanisms to therapeutic strategies." *Coord. Chem. Rev.* **2008**, *252*, 1189-1199.
14. Cuajungco, M. P.; Lees, G. J., "Zinc and Alzheimer's disease: is there a direct link?" *Brain Res. Rev.* **1997**, *23*, 219-236.
15. Smith, J. L.; Xiong, S.; Markesbery, W. R.; Lovell, M. A., "Altered expression of zinc transporters-4 and -6 in mild cognitive impairment, early and late Alzheimer's disease brain." *Neuroscience* **2006**, *140*, 879-888.
16. Lu, M.; Fu, D., "Structure of the Zinc Transporter YiiP." *Science* **2007**, *317*, 1746-1748.
17. Kimura, E.; Aoki, S.; Kikuta, E.; Koike, T., "A macrocyclic zinc(II) fluorophore as a detector of apoptosis." *Proc. Natl. Acad. Sci.* **2003**, *100*, 3731-3736.

18. Wallace, K. J., "Molecular dyes used for the detection of biological and environmental heavy metals: Highlights from 2004 to 2008." *Supramol. Chem.* **2009**, *21*, 89-102.
19. Sahoo, S. K.; Sharma, D.; Bera, R. K.; Crisponi, G.; Callan, J. F., "Iron(III) selective molecular and supramolecular fluorescent probes." *Chem. Soc. Rev.* **2012**, *41*, 7195-7227.
20. Aisen, P.; Wessling-Resnick, M.; Leibold, E. A., "Iron metabolism." *Curr. Opin. Chem. Biol.* **1999**, *3*, 200-206.
21. Halliwell, B.; Gutteridge, J. M. C., "Role of free radicals and catalytic metal ions in human disease: an overview." *Methods Enzymol.* **1990**, *186*, 1-85.
22. Halliwell, B.; Gutteridge, J. M. C., "Biologically relevant metal ion-dependent hydroxyl radical generation. An update." *FEBS Lett.* **1992**, *307*, 108-12.
23. Crichton, R., *Inorganic Biochemistry of Iron Metabolism: From Molecular Mechanisms to Clinical Consequences, Second Edition*. John Wiley & Sons: Chichester, 2001; p 1-321.
24. Rivera-Mancia, S.; Perez-Neri, I.; Rios, C.; Tristan-Lopez, L.; Rivera-Espinosa, L.; Montes, S., "The transition metals copper and iron in neurodegenerative diseases." *Chem. Biol. Interact.* **2010**, *186*, 184-199.
25. Thompson, K. J.; Shoham, S.; Connor, J. R., "Iron and neurodegenerative disorders." *Brain Res. Bull.* **2001**, *55*, 155-164.
26. Kozłowski, H.; Janicka-Kłos, A.; Brasun, J.; Gaggelli, E.; Valensin, D.; Valensin, G., "Copper, iron, and zinc ions homeostasis and their role in neurodegenerative

- disorders (metal uptake, transport, distribution and regulation)."*Coord. Chem. Rev.* **2009**, *253*, 2665-2685.
27. Zatta, P.; Drago, D.; Bolognin, S.; Sensi, S. L., "Alzheimer's disease, metal ions and metal homeostatic therapy."*Trends Pharmacol. Sci.* **2009**, *30*, 346-355.
28. Esposito, B. P.; Epsztejn, S.; Breuer, W.; Cabantchik, Z. I., "A review of fluorescence methods for assessing labile iron in cells and biological fluids."*Anal. Biochem.* **2002**, *304*, 1-18.
29. Emsley, J., *The Oxford Book of the Elements*. Oxford University Oxford, 2001; p 1-448.
30. Ayres, R. U., "Toxic heavy metals: materials cycle optimization."*Proc. Natl. Acad. Sci* **1992**, *89*, 815-820.
31. Byrne, R. H.; Kester, D. R., "Solubility of hydrous ferric oxide and iron speciation in sea water."*Mar. Chem.* **1976**, *4*, 255-274.
32. Moiescu, C.; Bonneville, S.; Staniland, S.; Ardelean, I.; Benning, L. G., "Iron Uptake Kinetics and Magnetosome Formation by *Magnetospirillum gryphiswaldense* as a Function of pH, Temperature and Dissolved Iron Availability."*Geomicrobiol. J.* **2011**, *28*, 590-600.
33. Boyd, P. W.; Law, C. S.; Wong, C. S.; Nojiri, Y.; Tsuda, A.; Levasseur, M.; Takeda, S.; Rivkin, R.; Harrison, P. J.; Strzepek, R.; Gower, J.; McKay, R. M.; Abraham, E.; Arychuk, M.; Barwell-Clarke, J.; Crawford, W.; Crawford, D.; Hale, M.; Harada, K.; Johnson, K.; Kiyosawa, H.; Kudo, I.; Marchetti, A.; Miller, W.; Needoba, J.; Nishioka, J.; Ogawa, H.; Page, J.; Robert, M.; Saito, H.; Sastri, A.; Sherry, N.; Soutar, T.; Sutherland, N.; Taira, Y.; Whitney, F.; Wong, S.-K. E.;



- Yoshimura, T., "The decline and fate of an iron-induced subarctic phytoplankton bloom." *Nature* **2004**, *428*, 549-553.
34. Boyd, P. W.; Watson, A. J.; Law, C. S.; Abraham, E. R.; Trull, T.; Murdoch, R.; Bakker, D. C. E.; Bowie, A. R.; Buesseler, K. O.; Chang, H.; Charette, M.; Croot, P.; Downing, K.; Frew, R.; Gall, M.; Hadfield, M.; Hall, J.; Harvey, M.; Jameson, G.; LaRoche, J.; Liddicoat, M.; Ling, R.; Maldonado, M. T.; McKay, R. M.; Nodder, S.; Pickmere, S.; Pridmore, R.; Rintoul, S.; Safi, K.; Sutton, P.; Strzepek, R.; Tanneberger, K.; Turner, S.; Waite, A.; Zeldis, J., "A mesoscale phytoplankton bloom in the polar Southern Ocean stimulated by iron fertilization." *Nature* **2000**, *407*, 695-702.
35. Wells, M. L.; Mayer, L. M., "Variations in the chemical lability of iron in estuarine, coastal and shelf waters and its implications for phytoplankton." *Mar. Chem.* **1991**, *32*, 195-210.
36. Wells, M. L.; Mayer, L. M.; Guillard, R. R. L., "Evaluation of iron as a triggering factor for red tide blooms." *Mar. Ecol.: Prog. Ser.* **1991**, *69*, 93-102.
37. Sneddon, J., Atomic absorption spectrometry. In *Handbook of Instrumental Techniques for Analytical Chemistry*, Settle, F. A., Ed. Prentice Hall: Upper Saddle River, New Jersey, 1997; pp 373-393.
38. Skoog, D. A.; Hollar, F. J.; Nieman, T. A., *Principles of Instrumental Analysis*. 5 ed.; Harcourt College Publishing: FortWorth, 1998; p 1-1048.
39. Varnes, A. W., Inductively coupled plasma mass spectrometry. In *Handbook of Instrumental Techniques for Analytical Chemistry*, Settle, F. A., Ed. Prentice Hall: Upper Saddle River, New Jersey, 1997; pp 419-439.

40. Kounaves, S. P., Voltammetric techniques. In *Handbook of Instrumental Techniques for Analytical Chemistry*, Settle, F. A., Ed. Prentice Hall: Upper Saddle River, New Jersey, 1997; pp 709-725.
41. Havrilla, G. J., X-ray fluorescence spectrometry. In *Handbook of Instrumental Techniques for Analytical Chemistry*, Settle, F. A., Ed. Prentice Hall: Upper Saddle River, New Jersey, 1997; pp 459-479.
42. Wehry, E. L., Molecular fluorescence and phosphorescence spectrometry. In *Handbook of Instrumental Techniques for Analytical Chemistry*, Settle, F. A., Ed. Prentice Hall: Upper Saddle River, New Jersey, 1997; pp 507-539.
43. Valeur, B., *Molecular Fluorescence: Principles and Applications*. Wiley-VCH Weinheim, 2001; p 1-383.
44. Fereja, T. H.; Hymete, A.; Gunasekaran, T., "A recent review on chemiluminescence reaction, principle and application on pharmaceutical analysis." *ISRN Spectrosc.* **2013**, 2013, 1-12.
45. Jimenez, A. M.; Navas, M. J., "Chemiluminescence methods (present and future)." *Grasas Aceites* **2002**, 53, 64-75.
46. Kricka, L. J., "Chemiluminescent and bioluminescent techniques." *Clin. Chem.* **1991**, 37, 1472-1481.
47. Nieman, T. A., Chemiluminescence In *Handbook of Instrumental Techniques for Analytical Chemistry*, Settle, F. A., Ed. Prentice Hall: Upper Saddle River, New Jersey, 1997; pp 541-559.

48. Howell, J. A., Ultraviolet and visible molecular absorption spectrometry. In *Handbook of Instrumental Techniques for Analytical Chemistry*, Settle, F. A., Ed. Prentice Hall: Upper Saddle River, New Jersey, 1997; pp 481-506.
49. Bell, T. W.; Hext, N. M., "Supramolecular optical chemosensors for organic analytes." *Chem. Soc. Rev.* **2004**, *33*, 589-598.
50. de Silva, A. P.; Gunaratne, H. Q. N.; Gunnlaugsson, T.; Huxley, A. J. M.; McCoy, C. P.; Rademacher, J. T.; Rice, T. E., "Signaling recognition events with fluorescent sensors and switches." *Chem. Rev.* **1997**, *97*, 1515-1566.
51. Yang, R.-H.; Chan, W.-H.; Lee, A. W. M.; Xia, P.-F.; Zhang, H.-K.; Li, K. A., "A Ratiometric Fluorescent Sensor for AgI with High Selectivity and Sensitivity." *J. Am. Chem. Soc.* **2003**, *125*, 2884-2885.
52. Nishizawa, S.; Kato, Y.; Teramae, N., "Fluorescence Sensing of Anions via Intramolecular Excimer Formation in a Pyrophosphate-Induced Self-Assembly of a Pyrene-Functionalized Guanidinium Receptor." *J. Am. Chem. Soc.* **1999**, *121*, 9463-9464.
53. Manandhar, E.; Wallace, K. J., "Host-guest chemistry of pyrene-based molecular receptors." *Inorg. Chim. Acta* **2012**, *381*, 15-43.
54. Wang, H.-F.; Wu, S.-P., "A pyrene-based highly selective turn-on fluorescent sensor for copper(II) ions and its application in living cell imaging." *Sens. Actuators, B* **2013**, *181*, 743-748.
55. Das, S.; Sahana, A.; Banerjee, A.; Lohar, S.; Safin, D. A.; Babashkina, M. G.; Bolte, M.; Garcia, Y.; Hauli, I.; Mukhopadhyay, S. K.; Das, D., "Ratiometric fluorescence sensing and intracellular imaging of Al<sup>3+</sup> ions driven by an

- intramolecular excimer formation of a pyrimidine-pyrene scaffold." *Dalton Trans.* **2013**, *42*, 4757-4763.
56. Baek, K.; Eom, M. S.; Kim, S.; Han, M. S., "Metal ion-prompted pyrene-excimer formation via an anion-mediated process and its application for a ratiometric Zn<sup>2+</sup> chemosensor with high selectivity over Cd<sup>2+</sup>." *Tetrahedron Lett.* **2013**, *54*, 1654-1657.
57. Birks, J. B., "Excimers." *Rep. Prog. Phys.* **1975**, *38*, 903-974.
58. Karuppanan, S.; Chambron, J.-C., "Supramolecular Chemical Sensors Based on Pyrene Monomer-Excimer Dual Luminescence." *Chem. Asian J.* **2011**, *6*, 964-984.
59. Kim, H. J.; Hong, J.; Hong, A.; Ham, S.; Lee, J. H.; Kim, J. S., "Cu<sup>2+</sup>-Induced Intermolecular Static Excimer Formation of Pyrenealkylamine." *Org. Lett.* **2008**, *10*, 1963-1966.
60. Yang, J.-S.; Lin, C.-S.; Hwang, C.-Y., "Cu<sup>2+</sup>-Induced Blue Shift of the Pyrene Excimer Emission: A New Signal Transduction Mode of Pyrene Probes." *Org. Lett.* **2001**, *3*, 889-892.
61. Winnik, F. M., "Photophysics of preassociated pyrenes in aqueous polymer solutions and in other organized media." *Chem. Rev.* **1993**, *93*, 587-614.
62. Birks, J. B.; Dyson, D. J.; Munro, I. H., "'Excimer' Fluorescence. II. Lifetime Studies of Pyrene Solutions." *Proceedings of the Royal Society of London. Series A. Mathematical and Physical Sciences* **1963**, *275*, 575-588.
63. Ferreira, J. A. B.; Costa, S. M. B.; Ferreira, L. F. V., "Activated Radiationless Decay of Rhodamine 3B: Polarity and Friction Effects." *J. Phys. Chem. A* **2000**, *104*, 11909-11917.

64. Casey, K. G.; Quitevis, E. L., "Effect of solvent polarity on nonradiative processes in xanthene dyes: Rhodamine B in normal alcohols." *J. Phys. Chem.* **1988**, *92*, 6590-6594.
65. Karstens, T.; Kobs, K., "Rhodamine B and rhodamine 101 as reference substances for fluorescence quantum yield measurements." *J. Phys. Chem.* **1980**, *84*, 1871-1872.
66. Lopez Arbeloa, T.; Lopez Arbeloa, F.; Hernandez Bartolome, P.; Lopez Arbeloa, I., "On the mechanism of radiationless deactivation of rhodamines." *Chem. Phys.* **1992**, *160*, 123-130.
67. Beija, M.; Afonso, C. A. M.; Martinho, J. M. G., "Synthesis and applications of Rhodamine derivatives as fluorescent probes." *Chem. Soc. Rev.* **2009**, *38*, 2410-2433.
68. Ramette, R. W.; Sandell, E. B., "Rhodamine B equilibria." *J. Am. Chem. Soc.* **1956**, *78*, 4872-4878.
69. Kim, H. N.; Lee, M. H.; Kim, H. J.; Kim, J. S.; Yoon, J., "A new trend in rhodamine-based chemosensors: application of spirolactam ring-opening to sensing ions." *Chem. Soc. Rev.* **2008**, *37*, 1465-1472.
70. Steed, J. W.; Turner, D. R.; Wallace, K. J., *Core Concepts in supramolecular Chemistry and Nanochemistry*. John Wiley & Sons: Chichester, 2007; p 1-297.
71. Hancock, R. D., "Chelate ring size and metal ion selection: the basis of selectivity for metal ions in open-chain ligands and macrocycles." *J. Chem. Educ.* **1992**, *69*, 615-621.

72. Cram, D. J., "Preorganization—From Solvents to Spherands." *Angew. Chem., Int. Ed. Engl.* **1986**, *25*, 1039-1057.
73. Steed, J. W.; Atwood, J. L., *Supramolecular Chemistry, Second Edition*. John Wiley & Sons: Chichester, 2009; p 1-941.
74. Lau, Y. H.; Rutledge, P. J.; Watkinson, M.; Todd, M. H., "Chemical sensors that incorporate click-derived triazoles." *Chem. Soc. Rev.* **2011**, *40*, 2848-2866.
75. Kolb, H. C.; Finn, M. G.; Sharpless, K. B., "Click chemistry: diverse chemical function from a few good reactions." *Angew. Chem., Int. Ed.* **2001**, *40*, 2004-2021.
76. Xu, Z.; Yoon, J.; Spring, D. R., "Fluorescent chemosensors for Zn<sup>2+</sup>." *Chem. Soc. Rev.* **2010**, *39*, 1996-2006.
77. Kolb, H. C.; Sharpless, K. B., "The growing impact of click chemistry on drug discovery." *Drug Discovery Today* **2003**, *8*, 1128-1137.
78. Angell, Y.; Burgess, K., "Base dependence in copper-catalyzed Huisgen reactions: efficient formation of bistriazoles." *Angew. Chem., Int. Ed.* **2007**, *46*, 3649-3651.
79. Mindt, T. L.; Struthers, H.; Brans, L.; Anguelov, T.; Schweinsberg, C.; Maes, V.; Tourwe, D.; Schibli, R., "'Click to Chelate': Synthesis and Installation of Metal Chelates into Biomolecules in a Single Step." *J. Am. Chem. Soc.* **2006**, *128*, 15096-15097.
80. Li, Y.; Flood, A. H., "Strong, Size-Selective, and Electronically Tunable C-H···Halide Binding with Steric Control over Aggregation from Synthetically Modular, Shape-Persistent [3<sub>4</sub>]Triazolophanes." *J. Am. Chem. Soc.* **2008**, *130*, 12111-12122.

81. Li, Y.; Flood, A. H., "Pure C-H hydrogen bonding to chloride ions: a preorganized and rigid macrocyclic receptor." *Angew. Chem., Int. Ed.* **2008**, *47*, 2649-2652.
82. Juwarker, H.; Lenhardt, J. M.; Pham, D. M.; Craig, S. L., "1,2,3-Triazole CH $\cdots$ Cl $^-$  contacts guide anion binding and concomitant folding in 1,4-diaryl triazole oligomers." *Angew. Chem., Int. Ed.* **2008**, *47*, 3740-3743.
83. Michaels, H. A.; Murphy, C. S.; Clark, R. J.; Davidson, M. W.; Zhu, L., "2-Anthryltriazolyl-Containing Multidentate Ligands: Zinc-Coordination Mediated Photophysical Processes and Potential in Live-Cell Imaging Applications." *Inorg. Chem.* **2010**, *49*, 4278-4287.
84. Valeur, B.; Leray, I., "Design principles of fluorescent molecular sensors for cation recognition." *Coord. Chem. Rev.* **2000**, *205*, 3-40.
85. Fabbrizzi, L.; Licchelli, M.; Pallavicini, P.; Sacchi, D.; Taglietti, A., "Sensing of transition metals through fluorescence quenching or enhancement." *Analyst* **1996**, *121*, 1763-1768.
86. Lim, N. C.; Schuster, J. V.; Porto, M. C.; Tanudra, M. A.; Yao, L.; Freake, H. C.; Brueckner, C., "Coumarin-based chemosensors for zinc(II): Toward the determination of the design algorithm for CHEF-type and ratiometric probes." *Inorg. Chem.* **2005**, *44*, 2018-2030.
87. Jana, S. K.; Bera, M.; Puschmann, H.; Dalai, S., "Sensing of Zn $^{2+}$  ion by N-Furfurylsalicylaldehyde Based on CHEF Process." *J. Fluoresc.* **2014**, *24*, 1245-1251.

88. Formica, M.; Fusi, V.; Giorgi, L.; Micheloni, M., "New fluorescent chemosensors for metal ions in solution." *Coord. Chem. Rev.* **2012**, *256*, 170-192.
89. Jang, Y. J.; Moon, B.-S.; Park, M. S.; Kang, B.-G.; Kwon, J. Y.; Hong, J. S. J.; Yoon, Y. J.; Lee, K. D.; Yoon, J., "New cavitand derivatives bearing four coumarin groups as fluorescent chemosensors for Cu<sup>2+</sup> and recognition of dicarboxylates utilizing Cu<sup>2+</sup> complex." *Tetrahedron Lett.* **2006**, *47*, 2707-2710.
90. Ni, X.-L.; Wu, Y.; Redshaw, C.; Yamato, T., "Direct evidence of a blocking heavy atom effect on the water-assisted fluorescence enhancement detection of Hg<sup>2+</sup> based on a ratiometric chemosensor." *Dalton Trans.* **2014**, *43*, 12633-12638.
91. Kim, J. S.; Quang, D. T., "Calixarene-Derived Fluorescent Probes." *Chem. Rev.* **2007**, *107*, 3780-3799.
92. Lu, Y.; Huang, S.-S.; Liu, Y.-Y.; He, S.; Zhao, L.-C.; Zeng, X.-S., "Highly Selective and Sensitive Fluorescent Turn-on Chemosensor for Al<sup>3+</sup> Based on a Novel Photoinduced Electron Transfer Approach." *Org. Lett.* **2011**, *13*, 5274-5277.
93. Chae, M. Y.; Czarnik, A. W., "Fluorometric chemodosimetry. Mercury(II) and silver(I) indication in water via enhanced fluorescence signaling." *J. Am. Chem. Soc.* **1992**, *114*, 9704-9705.
94. Desvergne, J. P.; Czarnik, A. W., *Chemosensors of Ion and Molecule Recognition*. Kluwer: Dordrecht, **1997**; p 1-245
95. Loehr, H. G.; Voegtle, F., "Chromo- and fluoroionophores. A new class of dye reagents." *Acc. Chem. Res.* **1985**, *18*, 65-72.



96. Prodi, L.; Bolletta, F.; Montalti, M.; Zaccheroni, N., "Luminescent chemosensors for transition metal ions." *Coord. Chem. Rev.* **2000**, *205*, 59-83.
97. Hanaoka, K.; Muramatsu, Y.; Urano, Y.; Terai, T.; Nagano, T., "Design and Synthesis of a Highly Sensitive Off-On Fluorescent Chemosensor for Zinc Ions Utilizing Internal Charge Transfer." *Chem. Eur. J.* **2010**, *16*, 568-572.
98. Park, S. Y.; Yoon, J. H.; Hong, C. S.; Souane, R.; Kim, J. S.; Matthews, S. E.; Vicens, J., "A Pyrenyl-Appended Triazole-Based Calix[4]arene as a Fluorescent Sensor for Cd<sup>2+</sup> and Zn<sup>2+</sup>." *J. Org. Chem.* **2008**, *73*, 8212-8218.
99. Albini, A.; Fasani, E.; Faiardi, D., "Charge-transfer and exciplex pathway in the photocycloaddition of 9-anthracenecarbonitrile with anthracene and naphthalenes." *J. Org. Chem.* **1987**, *52*, 155-7.
100. Zhou, Y.; Zhu, C.-Y.; Gao, X.-S.; You, X.-Y.; Yao, C., "Hg<sup>2+</sup>-Selective Ratiometric and "Off-On" Chemosensor Based on the Azadiene-Pyrene Derivative." *Org. Lett.* **2010**, *12*, 2566-2569.
101. Banerjee, A.; Sahana, A.; Guha, S.; Lohar, S.; Hauli, I.; Mukhopadhyay, S. K.; Sanmartin Matalobos, J.; Das, D., "Nickel(II)-Induced Excimer Formation of a Naphthalene-Based Fluorescent Probe for Living Cell Imaging." *Inorg. Chem.* **2012**, *51*, 5699-5704.
102. Nandy, R.; Subramoni, M.; Varghese, B.; Sankararaman, S., "Intramolecular  $\pi$ -Stacking Interaction in a Rigid Molecular Hinge Substituted with 1-(Pyrenylethynyl) Units." *J. Org. Chem.* **2007**, *72*, 938-944.

103. Yuan, L.; Lin, W.; Zheng, K.; Zhu, S., "FRET-Based Small-Molecule Fluorescent Probes: Rational Design and Bioimaging Applications." *Acc. Chem. Res.* **2013**, *46*, 1462-1473.
104. Fan, J.; Hu, M.; Zhan, P.; Peng, X., "Energy transfer cassettes based on organic fluorophores: construction and applications in ratiometric sensing." *Chem. Soc. Rev.* **2013**, *42*, 29-43.
105. Chereddy, N. R.; Thennarasu, S.; Mandal, A. B., "A highly selective and efficient single molecular FRET based sensor for ratiometric detection of Fe<sup>3+</sup> ions." *Analyst* **2013**, *138*, 1334-1337.
106. Hardouin-Lerouge, M.; Hudhomme, P.; Salle, M., "Molecular clips and tweezers hosting neutral guests." *Chem. Soc. Rev.* **2011**, *40*, 30-43.
107. Cao, Q.-Y.; Han, Y.-M.; Wang, H.-M.; Xie, Y., "A new pyrenyl-appended triazole for fluorescent recognition of Hg<sup>2+</sup> ion in aqueous solution." *Dyes Pigm.* **2013**, *99*, 798-802.
108. Kumar, M.; Kumar, R.; Bhalla, V., "A reversible fluorescent Hg<sup>2+</sup>/K<sup>+</sup> switch that works as keypad lock in the presence of F<sup>-</sup> ion." *Chem. Commun.* **2009**, 7384-7386.
109. Wu, Y.-S.; Li, C.-Y.; Li, Y.-F.; Tang, J.-L.; Liu, D., "A ratiometric fluorescent chemosensor for Cr<sup>3+</sup> based on monomer–excimer conversion of a pyrene compound." *Sensors and Actuators B: Chemical* **2014**, *203*, 712-718.
110. Zayed, A. M.; Terry, N., "Chromium in the environment: factors affecting biological remediation." *Plant Soil* **2003**, *249*, 139-156.

111. Martinez, R.; Espinosa, A.; Tarraga, A.; Molina, P., "New Hg<sup>2+</sup> and Cu<sup>2+</sup> Selective Chromo- and Fluoroionophore Based on a Bichromophoric Azine." *Org. Lett.* **2005**, *7*, 5869-5872.
112. Wang, F.; Nandhakumar, R.; Moon, J. H.; Kim, K. M.; Lee, J. Y.; Yoon, J., "Ratiometric fluorescent chemosensor for silver ion at physiological pH." *Inorg. Chem.* **2011**, *50*, 2240-2245.
113. Hasegawa, T.; Umeda, M.; Numata, M.; Li, C.; Bae, A.-H.; Fujisawa, T.; Haraguchi, S.; Sakurai, K.; Shinkai, S., "'Click chemistry' on polysaccharides: a convenient, general, and monitorable approach to develop (1-->3)- $\beta$ -D-glucans with various functional appendages." *Carbohydr. Res.* **2006**, *341*, 35-40.
114. Ramirez-Lopez, P.; de la Torre, M. C.; Montenegro, H. E.; Asenjo, M.; Sierra, M. A., "A Straightforward Synthesis of Tetrameric Estrone-Based Macrocycles." *Org. Lett.* **2008**, *10*, 3555-3558.
115. Thordarson, P., "Determining association constants from titration experiments in supramolecular chemistry." *Chem. Soc. Rev.* **2011**, *40*, 1305-1323.
116. Gans, P. *HypSpec*, Protonic Software: Leeds, 2006.
117. Shoji, O.; Nakajima, D.; Annaka, M.; Yoshikuni, M.; Nakahira, T., "Highly controlled side chain chromophore orientation in poly[N5-1-(1-pyrenyl)ethyl-L-glutamines]." *Polymer* **2002**, *43*, 1711-1714.
118. Collart, P.; Demeyer, K.; Toppet, S.; De Schryver, F. C., "intramolecular excimer formation in diastereoisomeric Bis[1-(1-pyrenyl)ethyl]ethers." *Macromolecules* **1983**, *16*, 1390-1391.

119. Hynes, M. J., "EQNMR: a computer program for the calculation of stability constants from nuclear magnetic resonance chemical shift data." *J. Chem. Soc., Dalton Trans.* **1993**, 311-312.
120. Gans, P.; Sabatini, A.; Vacca, A., "Investigation of equilibria in solution. Determination of equilibrium constants with the HYPERQUAD suite of programs." *Talanta* **1996**, *43*, 1739-53.
121. Pastor, A.; Martinez-Viviente, E., "NMR spectroscopy in coordination supramolecular chemistry: A unique and powerful methodology." *Coord. Chem. Rev.* **2008**, *252*, 2314-2345.
122. Rosenthal, M. R., "The Myth of the non-coordinating Anion." *J. Chem. Ed.* **1973**, *50*, 331-335.
123. Armstrong, R. D.; Porter, D. F.; Thirsk, H. R., "Passivation of mercury in sulfide ion solutions." *J. Phys. Chem.* **1968**, *72*, 2300-2306.
124. Goldin, A. S.; Velten, R. J.; Frishkorn, G. W., "Determination of radioactive strontium." *Anal. Chem.* **1959**, *31*, 1490-1492.
125. Kumar, Y. P.; King, P.; Prasad, V. S. R. K., "Adsorption of zinc from aqueous solution using marine green algae-Ulva fasciata sp." *Chem. Eng. J.* **2007**, *129*, 161-166.
126. Duruibe, J. O.; Ogwuegbu, M. O. C.; Ekwurugwu, J. N., "Heavy metal pollution and human biotoxic effects." *Int. J. Phys. Sci.* **2007**, *2*, 112-118.
127. Wang, B.; Anslyn, E. V., *Chemosensors: Principles, Strategies, And Applications*. John Wiley & Sons: Hoboken, New Jersey, 2011; p 1-497.

128. Lakowicz, J. R., *Principles of Fluorescence Spectroscopy*. 3rd ed.; Springer: Spring street, New York, 2006; p 1-923.
129. Leininger, S.; Olenyuk, B.; Stang, P. J., "Self-Assembly of Discrete Cyclic Nanostructures Mediated by Transition Metals." *Chem. Rev.* **2000**, *100*, 853-907.
130. Zhang, B.; Sun, J.; Bi, C.; Yin, G.; Pu, L.; Shi, Y.; Sheng, L., "A highly selective ratiometric fluorescent chemosensor for Ag<sup>+</sup> based on a rhodanine acetic acid-pyrene derivative." *New J. Chem.* **2011**, *35*, 849-853.
131. Romero, T.; Caballero, A.; Tarraga, A.; Molina, P., "A Click-Generated Triazole Tethered Ferrocene-Pyrene Dyad for Dual-Mode Recognition of the Pyrophosphate Anion." *Org. Lett.* **2009**, *11*, 3466-3469.
132. Bodenant, B.; Fages, F.; Delville, M.-H., "Metal-Induced Self-Assembly of a Pyrene-Tethered Hydroxamate Ligand for the Generation of Multichromophoric Supramolecular Systems. The Pyrene Excimer as Switch for Iron(III)-Driven Intramolecular Fluorescence Quenching." *J. Am. Chem. Soc.* **1998**, *120*, 7511-7519.
133. Jung, H. S.; Park, M.; Han, D. Y.; Kim, E.; Lee, C.; Ham, S.; Kim, J. S., "Cu<sup>2+</sup> Ion-Induced Self-Assembly of Pyrenylquinoline with a Pyrenyl Excimer Formation." *Org. Lett.* **2009**, *11*, 3378-3381.
134. Wang, R.; Wang, W.; Ren, H.; Chae, J., "Detection of copper ions in drinking water using the competitive adsorption of proteins." *Biosens. Bioelectron.* **2014**, *57*, 179-185.
135. Yang, Y.; Gou, X.; Blecha, J.; Cao, H., "A highly selective pyrene based fluorescent sensor toward Hg<sup>2+</sup> detection." *Tetrahedron Lett.* **2010**, *51*, 3422-3425.

136. Campbell-Verduyn, L.; Elsinga, P. H.; Mirfeizi, L.; Dierckx, R. A.; Feringa, B. L., "Copper-free click': 1,3-dipolar cycloaddition of azides and arynes." *Org. Biomol. Chem.* **2008**, *6*, 3461-3463.
137. Smanmoo, S.; Nasomphan, W.; Tangboriboonrat, P., "Highly selective fluorescent chemosensor for Fe<sup>3+</sup> imaging in living cells." *Inorg. Chem. Commun.* **2011**, *14*, 351-354.
138. Kumar, M.; Kumar, R.; Bhalla, V., "Optical chemosensor for Ag<sup>+</sup>, Fe<sup>3+</sup>, and cysteine: information processing at molecular level." *Org. Lett.* **2011**, *13*, 366-369.
139. Marcus, Y., "Ionic radii in aqueous solutions." *Chem. Rev.* **1988**, *88*, 1475-98.
140. Dudev, T.; Lim, C., "Tetrahedral vs Octahedral Zinc Complexes with Ligands of Biological Interest: A DFT/CDM Study." *J. Am. Chem. Soc.* **2000**, *122*, 11146-11153.
141. Gans, P. *HypNMR*, Protonic Software: Leeds, 2006.
142. Baeuml, E.; Tscheschlok, K.; Pock, R.; Mayr, H., "Synthesis of  $\gamma$ -lactones from alkenes employing p-methoxybenzyl chloride as a <sup>+</sup>CH<sub>2</sub>CO<sub>2</sub><sup>-</sup> equivalent." *Tetrahedron Lett.* **1988**, *29*, 6925-6926.
143. Xiao, Z.-P.; Shi, D.-H.; Li, H.-Q.; Zhang, L.-N.; Xu, C.; Zhu, H.-L., "Polyphenols based on isoflavones as inhibitors of Helicobacter pylori urease." *Bioorg. Med. Chem.* **2007**, *15*, 3703-3710.
144. Dike, S. Y.; Merchant, J. R.; Sapre, N. Y., "A new and efficient general method for the synthesis of 2-spirobenzopyrans: first synthesis of cyclic analogs of precocene I and related compounds." *Tetrahedron* **1991**, *47*, 4775-4786.

145. Wallace Karl, J.; Gray, M.; Zhong, Z.; Lynch Vincent, M.; Anslyn Eric, V., "An artificial siderophore for the detection of iron(III)." *Dalton Trans.* **2005**, 2436-41.
146. Campbell-Verduyn, L.; Eslinga, P. H.; Mirfeizi, L.; Dierckx, R. A.; Feringa, B. L., "Copper Free Click:1,3 Dipolar Cycloaddition of Azides and Arynes." *Org. Biomol. Chem.* **2008**, *6*, 3461-3463.
147. Mitra, A.; Ramanujam, B.; Rao, C. P., "1-(-Glucopyranosyl-2'-deoxy-2'-iminomethyl)-2-hydroxynaphthalene as chemo-sensor for Fe<sup>3+</sup> in aqueous HEPES buffer based on colour changes observable with the naked eye." *Tetrahedron Lett.* **2009**, *50*, 776-780.
148. Singhal, N. K.; Mitra, A.; Rajsekhar, G.; Shaikh, M. M.; Kumar, S.; Guionneau, P.; Rao, C. P., "Role of the orientation of -OH groups in the sensitivity and selectivity of the interaction of M<sup>2+</sup> with ribosyl- and galactosyl-imino-conjugates." *Dalton Trans.* **2009**, 8432-8442.
149. Chen, Y.-B.; Wang, Y.-J.; Lin, Y.-J.; Hu, C.-H.; Chen, S.-J.; Chir, J.-L.; Wu, A.-T., "A water-soluble ribosyl-based fluorescent sensor for Hg<sup>2+</sup> and Cu<sup>2+</sup> ions." *Carbohydr. Res.* **2010**, *345*, 956-959.
150. Song, Z.; He, X.-P.; Jin, X.-P.; Gao, L.-X.; Sheng, L.; Zhou, Y.-B.; Li, J.; Chen, G.-R., "'Click' to bidentate bis-triazolyl sugar derivatives with promising biological and optical features." *Tetrahedron Lett.* **2011**, *52*, 894-898.
151. Hsieh, Y.-C.; Chir, J.-L.; Wu, H.-H.; Chang, P.-S.; Wu, A.-T., "A sugar-aza-crown ether-based fluorescent sensor for Hg<sup>2+</sup> and Cu<sup>2+</sup>." *Carbohydr. Res.* **2009**, *344*, 2236-2239.

152. Hsieh, Y.-C.; Chir, J.-L.; Yang, S.-T.; Chen, S.-J.; Hu, C.-H.; Wu, A.-T., "A sugar-aza-crown ether-based fluorescent sensor for Cu<sup>2+</sup> and Hg<sup>2+</sup> ions." *Carbohydr. Res.* **2011**, *346*, 978-981.
153. Chen, K.-H.; Lu, C.-Y.; Cheng, H.-J.; Chen, S.-J.; Hu, C.-H.; Wu, A.-T., "A pyrenyl-appended triazole-based ribose as a fluorescent sensor for Hg<sup>2+</sup> ion." *Carbohydr. Res.* **2010**, *345*, 2557-2561.
154. Chinta, J. P.; Rao, C. P., "Triazole linked lower rim glycosyl appended 1,3-calix[4]arene conjugates: Synthesis, characterization, and their interaction with jacalin." *Carbohydr. Res.* **2013**, *369*, 58-62.
155. Mitra, A.; Mittal, A. K.; Rao, C. P., "Carbohydrate assisted fluorescence turn-on gluco-imino-anthracenyl conjugate as a Hg(II) sensor in milk and blood serum milieu." *Chem. Commun.* **2011**, *47*, 2565-2567.
156. Areti, S.; Khedkar, J. K.; Chilukula, R.; Rao, C. P., "Thiourea linked peracetylated glucopyranosyl-anthraquinone conjugate as reversible ON-OFF receptor for fluoride in acetonitrile." *Tetrahedron Lett.* **2013**, *54*, 5629-5634.
157. Jung, H. S.; Kim, H. J.; Vicens, J.; Kim, J. S., "A new fluorescent chemosensor for F<sup>-</sup> based on inhibition of excited-state intramolecular proton transfer." *Tetrahedron Lett.* **2009**, *50*, 983-987.
158. Kushwaha, D.; Singh, R. S.; Tiwari, V. K., "Fluorogenic dual click derived bis-glycoconjugated triazolocoumarins for selective recognition of Cu(II) ion." *Tetrahedron Lett.* **2014**, *55*, 4532-4536.



159. Gunther, K.; Schips, C.; Ziegler, T., "Preparation of Some Glycosyl Amino Acid Building Blocks via Click Reaction and Construction of a Glycotetrapeptide Library Using Spot Synthesis." *J. Carbohydr. Chem.* **2008**, *27*, 446-463.
160. Wang, P.; Shen, G. J.; Wang, Y. F.; Ichikawa, Y.; Wong, C. H., "Enzymes in oligosaccharide synthesis: active-domain overproduction, specificity study, and synthetic use of an  $\alpha$ -1,2-mannosyltransferase with regeneration of GDP-Man." *J. Org. Chem.* **1993**, *58*, 3985-3990.
161. Fazli, A.; Bradley, S. J.; Kiefel, M. J.; Jolly, C.; Holmes, I. H.; von Itzstein, M., "Synthesis and Biological Evaluation of Sialylmimetics as Rotavirus Inhibitors." *J. Med. Chem.* **2001**, *44*, 3292-3301.
162. Manandhar, E.; Broome, J. H.; Myrick, J.; Lagrone, W.; Cragg, P. J.; Wallace, K. J., "A pyrene-based fluorescent sensor for  $Zn^{2+}$  ions: a molecular butterfly." *Chem. Commun.* **2011**, *47*, 8796-8798.
163. Silverstein, R. M.; Webster, F. X.; Kiemie, D., *Spectrometric Identification of Organic Compounds, 7th Edition*. John Wiley & Sons Hoboken, New Jersey, 2002; p 1-502.
164. Hu, L.; Xu, G., "Applications and trends in electrochemiluminescence." *Chem. Soc. Rev.* **2010**, *39*, 3275-3304.
165. Miao, W., "Electrogenerated Chemiluminescence and Its Biorelated Applications." *Chem. Rev.* **2008**, *108*, 2506-2553.
166. Lee, Y. O.; Pradhan, T.; Choi, K.; Choi, D. H.; Lee, J. H.; Kim, J. S., "Electrogenerated chemiluminescence of N,N-dimethylamino functionalized tetrakis(phenylethynyl)pyrenes." *Tetrahedron* **2013**, *69*, 5908-5912.

167. Oh, J.-W.; Kim, T. H.; Yoo, S. W.; Lee, Y. O.; Lee, Y.; Kim, H.; Kim, J.; Kim, J. S., "Multisignaling metal sensor: Optical, electrochemical, and electrochemiluminescent responses of cruciform-shaped alkynylpyrene for selective recognition of Fe<sup>3+</sup>." *Sens. Actuators, B* **2013**, *177*, 813-817.
168. Lai, R. Y.; Fleming, J. J.; Merner, B. L.; Vermeij, R. J.; Bodwell, G. J.; Bard, A. J., "Electrogenerated Chemiluminescence. 74. Photophysical, Electrochemical, and Electrogenerated Chemiluminescent Studies of Selected Nonplanar Pyrenophanes." *J. Phys. Chem. A* **2004**, *108*, 376-383.
169. Oh, J.-W.; Lee, Y. O.; Kim, T. H.; Ko, K. C.; Lee, J. Y.; Kim, H.; Kim, J. S., "Enhancement of electrogenerated chemiluminescence and radical stability by peripheral multidonors on alkynylpyrene derivatives." *Angew. Chem., Int. Ed.* **2009**, *48*, 2522-2524.
170. Parajuli, S.; Miao, W., "Sensitive Determination of Hexamethylene Triperoxide Diamine Explosives, Using Electrogenerated Chemiluminescence Enhanced by Silver Nitrate." *Anal. Chem.* **2009**, *81*, 5267-5272.
171. Richter, M. M., "Electrochemiluminescence (ECL)." *Chem. Rev.* **2004**, *104*, 3003-3036.
172. Beideman, F. E.; Hercules, D. M., "Electrogenerated chemiluminescence from 9,10-diphenylanthracene cations reacting with radical anions." *J. Phys. Chem.* **1979**, *83*, 2203-2209.
173. Faulkner, L. R.; Tachikawa, H.; Bard, A. J., "Electrogenerated chemiluminescence. VII. Influence of an external magnetic field on luminescence intensity." *J. Am. Chem. Soc.* **1972**, *94*, 691-699.

174. Rubinstein, I.; Bard, A. J., "Electrogenerated chemiluminescence. Aqueous ecd systems based on tris(2,2'-bipyridine)ruthenium(2+) and oxalate or organic acids." *J. Am. Chem. Soc.* **1981**, *103*, 512-516.
175. Chang, M.-M.; Saji, T.; Bard, A. J., "Electrogenerated chemiluminescence. 30. Electrochemical oxidation of oxalate ion in the presence of luminescers in acetonitrile solutions." *J. Am. Chem. Soc.* **1977**, *99*, 5399-403.
176. Sun, Y.-Q.; Liu, J.; Lv, X.; Liu, Y.; Zhao, Y.; Guo, W., "Rhodamine-Inspired Far-Red to Near-Infrared Dyes and Their Application as Fluorescence Probes." *Angew. Chem., Int. Ed.* **2012**, *51*, 7634-7636.
177. Ma, Y.; Luo, W.; Quinn, P. J.; Liu, Z.; Hider, R. C., "Design, synthesis, physicochemical properties, and evaluation of novel iron chelators with fluorescent sensors." *J. Med. Chem.* **2004**, *47*, 6349-6362.
178. Chen, X.; Pradhan, T.; Wang, F.; Kim, J. S.; Yoon, J., "Fluorescent Chemosensors Based on Spiroring-Opening of Xanthenes and Related Derivatives." *Chem. Rev.* **2012**, *112*, 1910-1956.
179. Cherreddy, N. R.; Thennarasu, S.; Mandal, A. B., "Incorporation of triazole into a quinoline-rhodamine conjugate imparts iron(III) selective complexation permitting detection at nanomolar levels." *Dalton Trans.* **2012**, *41*, 11753-11759.
180. Maity, S. B.; Bharadwaj, P. K., "A Chemosensor Built with Rhodamine Derivatives Appended to an Aromatic Platform via 1,2,3-Triazoles: Dual Detection of Aluminum(III) and Fluoride/Acetate Ions." *Inorg. Chem.* **2013**, *52*, 1161-1163.

181. Chereddy, N. R.; Thennarasu, S.; Mandal, A. B., "A new triazole appended rhodamine chemosensor for selective detection of Cu<sup>2+</sup> ions and live-cell imaging." *Sens. Actuators, B* **2012**, 171-172, 294-301.
182. Barcelo, J.; Poschenrieder, C., "Fast root growth responses, root exudates, and internal detoxification as clues to the mechanisms of aluminum toxicity and resistance: a review." *Environ. Exp. Bot.* **2002**, 48, 75-92.
183. Berthon, G., "Aluminium speciation in relation to aluminium bioavailability, metabolism and toxicity." *Coord. Chem. Rev.* **2002**, 228, 319-341.
184. Kepp, K. P., "Bioinorganic Chemistry of Alzheimer's Disease." *Chem. Rev.* **2012**, 112, 5193-5239.
185. Perl, D. P.; Gajdusek, D. C.; Garruto, R. M.; Yanagihara, R. T.; Gibbs, C. J., Jr., "Intraneuronal aluminum accumulation in amyotrophic lateral sclerosis and parkinsonism-dementia of Guam." *Science* **1982**, 217, 1053-1055.
186. Faller, P.; Hureau, C., "A Bioinorganic view of Alzheimer's disease: When misplaced metal ions re-direct the electrons to the wrong target." *Chem.--Eur. J.* **2012**, 18, 15910-15920.
187. House, E.; Collingwood, J.; Khan, A.; Korchazkina, O.; Berthon, G.; Exley, C., "Aluminium, iron, zinc and copper influence the in vitro formation of amyloid fibrils of A $\beta$ 42 in a manner which may have consequences for metal chelation therapy in Alzheimer's disease." *J. Alzheimer's Dis.* **2004**, 6, 291-301.
188. Goswami, S.; Das, S.; Aich, K.; Sarkar, D.; Mondal, T. K.; Quah, C. K.; Fun, H.-K., "CHEF induced highly selective and sensitive turn-on fluorogenic and colorimetric sensor for Fe<sup>3+</sup>." *Dalton Trans.* **2013**, 42, 15113-15119.

189. Kalluri, R.; Zeisberg, M., "Fibroblasts in cancer." *Nat. Rev. Cancer* **2006**, *6*, 392-401.
190. Kim, H.; Lee, S.; Lee, J.; Tae, J., "Rhodamine Triazole-Based Fluorescent Probe for the Detection of  $\text{Pt}^{2+}$ ." *Org. Lett.* **2010**, *12*, 5342-5345.
191. Ma, X.; Tan, Z.; Wei, G.; Wei, D.; Du, Y., "Solvent controlled sugar-rhodamine fluorescence sensor for  $\text{Cu}^{2+}$  detection." *Analyst* **2012**, *137*, 1436-1439.
192. Diwan, U.; Kumar, A.; Kumar, V.; Upadhyay, K. K.; Roychowdhury, P. K., "A water compatible turn 'on' optical probe for  $\text{Cu}^{2+}$  based on a fluorescein-sugar conjugate." *Sens. Actuators, B* **2014**, *196*, 345-351.
193. Li, K.-B.; Zhang, H.-L.; Zhu, B.; He, X.-P.; Xie, J.; Chen, G.-R., "A per-acetyl glycosyl rhodamine as a novel fluorescent ratiometric probe for mercury (II)." *Dyes Pigm.* **2014**, *102*, 273-277.
194. Yin, J.; Ma, X.; Wei, G.; Wei, D.; Du, Y., "A highly selective and sensitive sugar-rhodamine "turn-on" fluorescent sensor for divalent copper ion detection in acetonitrile." *Sens. Actuators, B* **2013**, *177*, 213-217.
195. Yang, Y.-K.; Shim, S.; Tae, J., "Rhodamine-sugar based turn-on fluorescent probe for the detection of cysteine and homocysteine in water." *Chem. Commun.* **2010**, *46*, 7766-7768.
196. Galardon, E.; Tomas, A.; Roussel, P.; Artaud, I., "New fluorescent zinc complexes: Towards specific sensors for hydrogen sulfide in solution." *Dalton Trans.* **2009**, 9126-9130.

197. Hortala, M. A.; Fabbrizzi, L.; Marcotte, N.; Stomeo, F.; Taglietti, A., "Designing the selectivity of the fluorescent detection of amino acids: A chemosensing ensemble for histidine." *J. Am. Chem. Soc.* **2003**, *125*, 20-21.
198. Huang, W.; Zhou, P.; Yan, W.; He, C.; Xiong, L.; Li, F.; Duan, C., "A bright water-compatible sugar-rhodamine fluorescence sensor for selective detection of Hg<sup>2+</sup> in natural water and living cells." *J. Environ. Monit.* **2009**, *11*, 330-335.
199. Jana, A.; Kim, J. S.; Jung, H. S.; Bharadwaj, P. K., "A cryptand based chemodosimetric probe for naked-eye detection of mercury(II) ion in aqueous medium and its application in live cell imaging." *Chem. Commun.* **2009**, 4417-4419.
200. Yapici, N. B.; Jockusch, S.; Moscatelli, A.; Mandalapu, S. R.; Itagaki, Y.; Bates, D. K.; Wiseman, S.; Gibson, K. M.; Turro, N. J.; Bi, L., "New Rhodamine Nitroxide Based Fluorescent Probes for Intracellular Hydroxyl Radical Identification in Living Cells." *Org. Lett.* **2012**, *14*, 50-53.
201. Brotherton, W. S.; Clark, R. J.; Zhu, L., "Synthesis of 5-iodo-1,4-disubstituted-1,2,3-triazoles mediated by in situ generated copper(I) catalyst and electrophilic triiodide ion." *J. Org. Chem.* **2012**, *77*, 6443-6455.
202. Benesi, H. A.; Hildebrand, J. H., "A spectrophotometric investigation of the interaction of iodine with aromatic hydrocarbons." *J. Am. Chem. Soc.* **1949**, *71*, 2703-2707.
203. Exner, O., "Calculating equilibrium constants from spectral data: reliability of the Benesi-Hildebrand method and its modifications." *Chemom. Intell. Lab. Syst.* **1997**, *39*, 85-93.

204. Fielding, L., "Determination of Association Constants ( $K_a$ ) from Solution NMR Data." *Tetrahedron* **2000**, *56*, 6151-6170.
205. Scott, R. L., "Some comments on the Benesi-Hildebrand equation." *Recl. Trav. Chim. Pays-Bas Belg.* **1956**, *75*, 787-789.
206. Gans, P.; Sabatini, A.; Vacca, A., "Investigation of equilibria in solution. Determination of equilibrium constants with HYPERQUAD suite of programs." *Talanta* **1996**, *43*, 1739-1753.
207. Zeng, X.; Dong, L.; Wu, C.; Mu, L.; Xue, S.-F.; Tao, Z., "Highly sensitive chemosensor for Cu(II) and Hg(II) based on the tripodal rhodamine receptor." *Sens. Actuators, B* **2009**, *141*, 506-510.
208. Liu, W.; Chen, J.; Xu, L.; Wu, J.; Xu, H.; Zhang, H.; Wang, P., "Reversible "off-on" fluorescent chemosensor for  $Hg^{2+}$  based on rhodamine derivative." *Spectrochim. Acta, Part A* **2012**, *85*, 38-42.
209. Kumar, M.; Puri, A., "A review of permissible limits of drinking water." *Indian J. Occup. Environ. Med.* **2012**, *16*, 40-44.
210. Wang, J.; Li, Y.; Patel, N. G.; Zhang, G.; Zhou, D.; Pang, Y., "A single molecular probe for multi-analyte ( $Cr^{3+}$ ,  $Al^{3+}$  and  $Fe^{3+}$ ) detection in aqueous medium and its biological application." *Chem. Commun.* **2014**.
211. Goswami, S.; Aich, K.; Das, S.; Das, A. K.; Sarkar, D.; Panja, S.; Mondal, T. K.; Mukhopadhyay, S., "A red fluorescence 'off-on' molecular switch for selective detection of  $Al^{3+}$ ,  $Fe^{3+}$  and  $Cr^{3+}$ : experimental and theoretical studies along with living cell imaging." *Chem. Commun.* **2013**, *49*, 10739-10741.

212. Martell, A. E.; Hancock, R. D.; Smith, R. M.; Motekaitis, R. J., "Coordination of Al(III) in the environment and in biological systems." *Coord. Chem. Rev.* **1996**, *149*, 311-328.
213. Rubini, P.; Lakatos, A.; Champmartin, D.; Kiss, T., "Speciation and structural aspects of interactions of Al(III) with small biomolecules." *Coord. Chem. Rev.* **2002**, *228*, 137-152.
214. Yokel, R. A., "Aluminum chelation principles and recent advances." *Coord. Chem. Rev.* **2002**, *228*, 97-113.
215. Riemer, J.; Hoepken, H. H.; Czerwinska, H.; Robinson, S. R.; Dringen, R., "Colorimetric ferrozine-based assay for the quantitation of iron in cultured cells." *Anal. Biochem.* **2004**, *331*, 370-375.
216. Stookey, L. L., "Ferrozine-a new spectrophotometric reagent for iron." *Anal. Chem.* **1970**, *42*, 779-7881.
217. Viollier, E.; Inglett, P. W.; Hunter, K.; Roychoudhury, A. N.; Van Cappellen, P., "The ferrozine method revisited: Fe(II)/Fe(III) determination in natural waters." *Appl. Geochem.* **2000**, *15*, 785-790.
218. Vogler, A.; Kunkely, H., "Photochemistry induced by metal-to-ligand charge transfer excitation." *Coord. Chem. Rev.* **2000**, *208*, 321-329.
219. Gispert, J. R., *Cordination Chemistry*. Wiley-VCH: Weinheim, 2008; p 1-591.
220. Lee, T. S.; Kolthoff, I. M.; Leussing, D. L., "Reaction of ferrous and ferric ions with 1,10-phenanthroline. II. Kinetics of formation and dissociation of ferrous phenanthroline." *J. Am. Chem. Soc.* **1948**, *70*, 3596-600.



221. Dean, K. M.; Qin, Y.; Palmer, A. E., "Visualizing metal ions in cells: An overview of analytical techniques, approaches, and probes." *Biochim. Biophys. Acta, Mol. Cell Res.* **2012**, *1823*, 1406-1415.
222. Fernandez-Suarez, M.; Ting, A. Y., "Fluorescent probes for super-resolution imaging in living cells." *Nat. Rev. Mol. Cell Biol.* **2008**, *9*, 929-943.
223. Terai, T.; Nagano, T., "Fluorescent probes for bioimaging applications." *Curr. Opin. Chem. Biol.* **2008**, *12*, 515-521.
224. Fernandez-Moreira, V.; Thorp-Greenwood, F. L.; Coogan, M. P., "Application of d6 transition metal complexes in fluorescence cell imaging." *Chem. Commun.* **2010**, *46*, 186-202.
225. Pysz, M. A.; Gambhir, S. S.; Willmann, J. K., "Molecular imaging: current status and emerging strategies." *Clin. Radiol.* **2010**, *65*, 500-16.
226. Miller, J. C.; Thrall, J. H., "Clinical molecular imaging." *J. Am. Coll. Radiol.* **2004**, *1*, 4-23.
227. Domaille, D. W.; Que, E. L.; Chang, C. J., "Synthetic fluorescent sensors for studying the cell biology of metals." *Nat. Chem. Biol.* **2008**, *4*, 168-175.
228. Messenger, A. J. M.; Barclay, R., "Bacteria, iron and pathogenicity." *Biochem. Educ.* **1983**, *11*, 54-63.
229. Perkins-Balding, D.; Ratliff-Griffin, M.; Stojiljkovic, I., "Iron transport systems in *Neisseria meningitidis*." *Microbiol. Mol. Biol. Rev.* **2004**, *68*, 154-171.
230. Banin, E.; Vasil, M. L.; Greenberg, E. P., "Iron and *Pseudomonas aeruginosa* biofilm formation." *Proc. Natl. Acad. Sci.* **2005**, *102*, 11076-11081.

231. Kluytmans, J.; van, B. A.; Verbrugh, H., "Nasal carriage of *Staphylococcus aureus*: epidemiology, underlying mechanisms, and associated risks." *Clin Microbiol Rev* **1997**, *10*, 505-20.
232. Soh, J. H.; Swamy, K. M. K.; Kim, S. K.; Kim, S.; Lee, S.-H.; Yoon, J., "Rhodamine urea derivatives as fluorescent chemosensors for  $\text{Hg}^{2+}$ ." *Tetrahedron Lett.* **2007**, *48*, 5966-5969.
233. Weerasinghe, A. J.; Abebe, F. A.; Sinn, E., "Rhodamine based turn-ON dual sensor for  $\text{Fe}^{3+}$  and  $\text{Cu}^{2+}$ ." *Tetrahedron Lett.* **2011**, *52*, 5648-5651.
234. Selwyn, J. E.; Steinfeld, J. I., "Aggregation of equilibriums of xanthene dyes." *J. Phys. Chem.* **1972**, *76*, 762-774.
235. Valdes-Aguilera, O.; Neckers, D. C., "Aggregation phenomena in xanthene dyes." *Acc. Chem. Res.* **1989**, *22*, 171-177.
236. Yu, K.-K.; Li, K.; Hou, J.-T.; Yu, X.-Q., "Coumarin-TPA derivative: a reaction-based ratiometric fluorescent probe for Cu(I)." *Tetrahedron Lett.* **2013**, *54*, 5771-5774.